Maryland Sea Grant Research Fellows

Final Student Papers Summer 2012

Edited by
Mike Allen, Jenna Clark, and Fredrika Moser

Sponsored by
Maryland Sea Grant

Maryland Sea Grant College
Publication number UM-SG-TS-2012-01

Copies of this publication are available from:

Maryland Sea Grant College Program
4321 Hartwick Road, Suite 300
College Park, MD 20740

For more information, visit the Maryland Sea Grant web site:
http://www.mdsg.umd.edu/

This publication, produced by the Maryland Sea Grant College Program, is a compilation of the final REU student fellow papers produced for summer 2012.

This report was prepared under award NA10OAR4170072 from Maryland Sea Grant, National Oceanic and Atmospheric Administration, U.S. Department of Commerce. The statements, findings, conclusions and recommendations are those of the author(s) and do not necessarily reflect the views of Maryland Sea Grant, the National Oceanic and Atmospheric Administration or U.S. Department of Commerce.

Contents

UMCES Chesapeake Biological Laboratory

UMCES Horn Point Laboratory

UNIVERSITY OF MARYLAND
CENTER FOR ENVIRONMENTAL SCIENCE

Chesapeake Biological Laboratory

(Blank)

Comparing Methods to Quantify Sperm Storage in Female Blue Crab (*Callinectes sapidus*) Spermathecae

Joshua Epstein, REU Fellow
Maryland Sea Grant

Dr. Michael Wilberg, Associate Professor
Chesapeake Biological Laboratory, University of Maryland Center for Environmental Science

Abstract

Potential sperm limitation has become a concern for blue crabs *Callinectes sapidus* in Chesapeake Bay. However, methods to quantify sperm in blue crabs are time intensive, which limits the sample size that can be obtained for sperm limitation studies. Our goal was to develop an efficient method for rapidly preparing spermathecae samples that more quickly quantifies sperm in blue crabs. Ultimately such a method will help address questions of sperm limitation in the Chesapeake Bay. In this study, we tested two methods for grinding spermathecae, and we tested whether DNA fluorometry is an accurate method for determining sperm quantity in blue crabs. We processed spermathecae using a dounce homogenizer and a Polytron, and compared sperm counts using a paired t-test. We compared fluorometry with direct counting of sperm cells under a microscope, a more time consuming yet already tested process, to determine if the sperm quantities obtained from fluorometry correspond with sperm counts. Samples processed using the dounce homogenizer had significantly higher sperm counts ($p=0.007$). Fluorescence was negatively related to sperm count ($p=0.003$), which was opposite the expected pattern. Our results indicate that the dounce homogenizer should be used to process samples and that the fluorometry methods we tested should not be used to quantify sperm in blue crabs.

Keywords: Microscopy, DNA fluorometry, Sperm limitation, Chesapeake Bay

Introduction

While sperm limitation is not considered a problem for many species, many decapod crustaceans have a mating system that may be particularly prone to sperm limitation. For most species the number of eggs produced by females is thought to be the limiting factor for population growth because the lifetime production of eggs by a female is much less than the lifetime production of sperm by males. Sperm limitation is the opposite of egg limitation; low abundance of males in the population potentially hinders population growth. The sperm limitation hypothesis states that with fewer and smaller males present, the male to female ratio and the amount of sperm females receive during mating will decrease, which then limits the number of eggs a female can fertilize (Hines et al. 2003). For many crab species sperm limitation may become a concern under intense harvesting of males. For example, the Japanese population of the coconut crab, *Birgus latro,* has declined due to extreme male harvesting, leading to sperm limitation for female crabs (Sato et al. 2010).

Female blue crabs, *Callinectes sapidus*, like females of many other crab species, typically have only one mating opportunity during their lives (Hines et al. 2003). Female blue crabs reach sexual maturity following their pubertal molt (Jivof 2003). Shortly after the female molts she will be in her "soft shell" state, and copulation will occur, lasting for 5-12 hours (Jivof 2003). During this process males pass seminal fluid and sperm-containing spermatophores from the vas deferens to the female's pair of sperm storage organs or spermathecae (Jivof 2003). The female is capable of storing this sperm for more than a year and it can be used for multiple spawnings (Jivof 2003). Because a female can only mate once in her life, it is important that she receives adequate sperm. If a female does not receive enough sperm to fertilize all of her eggs, there is the possibility that her fitness will be reduced. In the extreme, a low number of males in the population could lead to females without mates (Hines et al. 2003) and Allee effects (Freckleton et al. 1999). Even in cases when females can find mates, males may not have enough time to replenish their sperm between copulations. When this happens it is possible that females will not receive an adequate amount of sperm for fertilization of all their eggs (Hines et al. 2003). Males, in contrast, can mate an indefinite number of times upon reaching maturity.

Blue crabs are important prey and scavengers in the Chesapeake Bay ecosystem (NOAA 2012). They are also one of the most important commercial and recreational species in the Chesapeake Bay. Thus, it will be important to determine whether a decrease in male blue crabs, in relation to females, will affect female sperm storage, and how this will ultimately affect the Chesapeake Bay ecology and blue crab fishery (NOAA 2012). Additionally, understanding blue crab sperm limitation will help in developing male specific fishery reference points for blue crabs in the Chesapeake Bay. These reference points would describe target and limit fishing mortality levels for males (M. Wilberg personal communication).

Recently concerns have been raised about potential sperm limitation in the Chesapeake Bay blue crab population because of the adoption of regulations limiting female harvest (Hines et. al 2003). Fisheries management also favors male harvesting by restricting the harvesting of females. In 2008 Virginia closed their winter dredge fishery, which primarily targeted female blue crabs during their winter dormancy. Also, Maryland implemented bushel limits on the amount of female blue crabs fishermen could harvest daily in 2008 (M. Wilberg personal communication). Additionally, males are typically more highly valued by the fishery than females due to their larger size (Jivoff 2003). As a result of these management measures, the ratio of male to female blue crabs has increased in catch, but has declined in the population (Figure 1) and adult female abundance was nearly five times higher than male abundance in 2010 (Miller et al. 2011).

To assess the prevalence of sperm limitation and its possible severity in the Chesapeake Bay methods are needed that can process many spermathecae samples quickly. Methods for counting sperm in blue crabs are very labor intensive making it difficult to obtain large sample sizes. The spermathecae need to be homogenized in order to count the sperm, and counting must be done using a high-powered microscope. Currently used homogenizing techniques involve hand grinding the spermathecae in a dounce homogenizer (Hines et al. 2003); it can take more than an hour to prepare one sample. To determine the possibility of sperm limitation, a technique that will enable the analysis of many samples in an efficient manner will be necessary. DNA fluorometry is a technique that uses fluorescent dyes, which bind to DNA, to quantify the amount of DNA in a sample (Reichardt and Wheller 1995). The DNA in sperm cells could be quantified in this manner through the staining of sperm cells in the spermathecae, as was done in the estimation of sperm numbers in the desert leaf-cutter ant, *Acromyrmex versicolor* (Reichardt and Wheller 1995). Our main objective was to develop an efficient method for counting sperm in blue crabs to address whether sperm limitation is

occurring in the Chesapeake Bay. We compared DNA fluorescence to total sperm counts to determine whether fluorometry could be used as a more rapid method to estimate sperm quantity in female blue crabs.

Materials and Methods

Commercial fishermen collected female blue crabs from six tributary rivers of the Chesapeake Bay: the Chester, Choptank, Patuxent, Potomac, York, and James rivers (Figure 2). Each tributary was sampled 2-6 times during the months of September, October, and November of 2011, in order to obtain mature females that had already mated and were migrating to the mouth of the bay. Once brought back to the lab, the crabs were frozen and labeled by river and date caught.

Analysis 1: Dounce Homogenizer vs. Polytron Grinding

For our initial analysis we compared spermathecae tissue grinding using a Brinkmann Instruments Polytron and dounce homogenizer to determine whether the faster Polytron could provide the same results as using the dounce homogenizer. The Polytron only takes 15 seconds to process a sample, whereas the dounce homogenizer takes 30-60 minutes. To compare the two methods, we homogenized 22 spermathecae (both spermathecae from 11 crabs, 2 spermathecae from the 6 river systems). One of the crab's spermathecae was ground with the Polytron while the other was ground with the dounce homogenizer. We alternated between grinding the left or right spermathecae with the dounce homogenizer and homogenized the remaining spermathecae using the Polytron.

We dissected the crabs to remove the spermathecae for sperm quantity analysis. To prepare for dissection, a crab was thawed in cold water for an hour. River system, carapace length (measured from lateral spine to lateral spine in millimeters), and molt status of each female (intermolt, premolt, molt, or post molt) were recorded prior to dissection and removal of the spermathecae. The cleanliness of the shell was also noted. We lifted the carapace and removed the spermathecae with tweezers and a scalpel to cut the spermathecae from the surrounding tissue. We measured the wet weight of each spermathecae after drying each side of the sample with a kim wipe to remove excess liquid, and recorded the fullness of the spermathecae.

The dissected spermathecae was minced in 5 mL of artificial seawater, in a weigh boat, until the pieces were 2-5 mm in size. Thirty-five µL of crystal violet stain was added to the weigh boat to stain the tissue. The contents of the weigh boat, were transferred to the dounce homogenizer and ground for 60 minutes, or placed in a plastic container to be ground by the Polytron. When using the Polytron we ground our samples on setting 6 (setting ranges from 1 to 11) for 15 seconds. After completing the grinding we poured an additional 5 mL of artificial seawater into either the dounce homogenizer or the container used for the Polytron to pick up any extra sperm that may have remained on the wall of the container. We then poured the contents into a scintillation vial. Ten µL of the solution was pipetted onto both sides of a hemacytometer. Four subsamples were taken from each spermathecae sample (i.e., two complete spermathecae samples). We viewed the sperm cells under 400X magnification on a compound microscope outfitted with a digital camera, so the image could be viewed on a desktop computer screen. We took a picture of each image and archived it on the computer. For each sample we directly counted the sperm cells from the image. We counted the number of sperm cells in the four corners and center squares on the main grid of the hemacytometer and averaged the counts to get a mean sperm quantity per square.

After finding the average number of sperm per square we scaled up from the sample to the total volume used to get an estimate of the total number of sperm in the spermathecae. We divided the average number of sperm per square by .00025 µL (the volume of one square) to get the count per µL. We then multiplied by 1000 to convert to mL. Lastly, we multiplied by the total volume of our sample (approximately 10mL) to obtain an estimate of total sperm in our total sample. We used a paired t-test to determine whether sperm counts differed between homogenization methods.

Analysis 2: Sperm Count vs. DNA Fluorometry

We analyzed 24 female crabs for sperm quantity, 4 crabs from each tributary. The crabs from each tributary were chosen to obtain a wide range of female sizes in our analysis. We dissected the crabs to remove the spermathecae for sperm quantity analysis. The dissection was identical to that in the previous experiment. Only one spermathecae from each crab was used in this study. We froze the unused spermathecae from each crab in a scintillation vial for storage. We alternated between using the left and right spermathecae of each crab.

After removal, we placed the spermathecae into a dounce homogenizer with 5 mL of artificial seawater, bringing the total volume to approximately 5.4 mL. We did not mince the spermathecae prior to grinding in this analysis, due to possible sperm loss from cutting in the weigh boat. The spermathecae was ground for 30 minutes because there was no significant difference between counts with 30 and 60 minute grinding times. After homogenization, ten 50 µL subsamples of the solution were pipetted out to be used for DNA fluorometry. We placed the spermathecae subsamples in microcentrifuge vials with 150 µL 1% N-lauroylsarcosine and vortexed vigorously for 60 minutes to separate the proteins. Next, we diluted the samples with 1350 µL TRIS-EDTA buffer and centrifuged for 15 minutes at 14,000 x gravity to separate the solids and liquids in the sample. Following centrifugation, the samples, RNA and DNA standards, blanks, and control homogenate were pipetted into a 96 well plate. After shaking the plate for 15 minutes, we added 75 µL ethidium bromide to each well as a fluorescent tag and shook on the lowest setting for 15 minutes. We then inserted the plate into the fluorometer to obtain an initial fluorescence reading. Next, we added 7.5 µL RNase to each well, for RNA degradation, and took a final fluorescence reading in the fluorometer after shaking the plate for an additional 20 minutes. We ran two spermathecae samples (10 wells per spermathecae equaling 20 wells) per plate.

The remaining sample was used for direct sperm counting. We added 17 µL of crystal violet stain to the ground sample and mixed it into the solution. Next, we pipetted 10 µL of the solution onto both sides of a hemacytometer. We viewed the samples under 400X magnification and counted the sperm cells as we did in our previous analysis. We conducted counts on four replicate subsamples for each spermathecae. We saved the remaining sample in a scintillation vial and labeled it for possible further analysis. After finding the average number of sperm per square we scaled up from the sample to the total volume used to get an estimate of the total number of sperm in the spermathecae. We divided the average number of sperm per square by .00025 µL (the volume of one square) to get the count per µL. We then multiplied by 1000 to convert to mL. Lastly we multiplied by the total volume of our sample (approximately 5.4 mL) to obtain an estimate of total sperm in our total sample.

Results

Samples from the dounce homogenizer had 72% higher sperm counts than samples from

the Polytron (paired t-test; p=0.007). These results are consistent with how the samples looked; the Polytron samples appeared to have larger pieces of tissue intact and lower numbers of sperm under the microscope. Although longer run times might result in more complete homogenization, we did not run the Polytron for longer than 15 seconds because the spermathecae solution was foaming and pieces were getting caught in the drill.

We found a large range of sperm counts and fluorescence values among the six tributaries that we analyzed. Our total sperm count ranged from 2.09×10^7 per spermathecae for the highest sample in the York River to 6.69×10^6 per spermathecae for the lowest in the Potomac River. A sample from the James River had the highest fluorescence with 1317.3 relative fluorescence units (RFUs). The sample with the lowest fluorescence was observed from a sample in the Choptank River with a value of 518.1 RFUs. Fluorescence was negatively related to total sperm count (intercept 1362, standard error (SE) 159; slope -4.27×10^{-5}, SE 1.26×10^{-5}, p = 0.003; Figure 3). There was a substantial amount of variability about the relationship, and the regression line only explained 31% of the variation.

Discussion

We found a negative relationship between DNA fluorescence and total sperm count in blue crab spermathecae. We expected to find a positive relationship similar to a study on quantifying sperm in the desert leaf-cutter ant (Reichardt and Wheeler 1995). If a spermathecae contains more sperm, it is expected that it will have more DNA and therefore should fluoresce at a higher RFU than a sample with less sperm. There are two possible reasons our results differed from our expectations. Compared to Reichardt and Wheeler's study, the fluorescence values that we determined were much higher (0-100 compared to 500-1400). It is possible that because our samples are not very diluted, the intensity of the fluorescence was too high for our fluorometer. This is known as quenching; i.e., collisions between the molecules in the sample result in the loss of excitation energy due to creation of heat in place of light (Turner Designs 2012). Our values may have reached peak fluorescence, which our machine could no longer detect and therefore gave a negative trend. In order to test this we will need to dilute our sample in different amounts of artificial seawater to see if it shows an effect of saturation. If this hypothesis is correct, we expect to see our fluorescence increase initially and then decrease as the sample becomes more diluted. Another possibility for this negative trend could be a problem with our fluorometer. Our fluorometer was not providing consistent readings across columns on the microplate before column 8. Therefore, we only used columns after 8 for our analysis. It is possible that there could also be error in rows 8 through 12, which could have affected our results. When there is error in the fluorometer that could interfere with fluorescence values there is often a problem with the DNA and RNA standards. We reviewed the standards and they produced consistent fluorescence values throughout all of our trials therefore we concluded that this was not our problem. To rule out any fluorometer error we would need to run this test with another fluorometer.

In our initial study on examining whether the Polytron or dounce homogenizer is better for sperm counts, our goal was to isolate the effects of using these grinding methods by controlling for all factors except the variation of grinding method. We ran this analysis in order to determine if using a Polytron, a much faster and easier method for grinding spermathecae, is the same as using a dounce homogenizer. From conducting a paired t-test relating the dounce homogenizer and the Polytron, our results suggest that the dounce homogenizer was better because it ground our sample completely and produced higher sperm counts. Although the dounce homogenizer is more labor intensive and time consuming, we now know that it is more precise at counting spermathecae samples and should be used over the Polytron. We also do not

recommend the Polytron because the machine captures some of spermathecae material inside the unit, which we believe is one of the causes of lower sperm counts. The Polytron also produces more foam than the dounce homogenizer when grinding the spermathecae sample, which makes it difficult to transfer the entire sample into a scintillation vial.

An additional problem that we discovered during the Polytron-dounce homogenizer comparisons was losing sperm on the weigh boat. Although we halved our total sample volume between our first analysis and our second one, we still counted more than double the number of sperm in analysis 2 than in analysis 1. We believe that this was due to losing sperm in the weigh boat when mincing the spermathecae before homogenization. We also transferred the sample between containers more often in our first analysis, possibly leaving sperm in each one as it moved from container to container. For these reasons, we did not mince the spermathecae at all in our second analysis but directly put it into a dounce homogenizer to be ground whole. We also used half of the amount of liquid to dilute samples in analysis 2 compared to analysis 1 to count more sperm in the hemacytometer, which should lead to more precise counts. In our second analysis, we also began waiting two minutes after the subsamples were put on the hemacytometer to allow the cells to settle.

In our second analysis the volume we used as the total volume of our sample was an estimated volume. To more accurately measure the volume, we measured the volume of three separate spermathecae in a graduated cylinder with 5 mL of artificial seawater. The total volume of each sample was 5.4 mL. Because most of the spermathecae were very small (under 0.25 grams), they did not contribute significantly to the volume of our sample. There was one larger spermathecae from the Potomac River (0.42 grams). For this sample we used the left spermathecae to get an accurate volume for calculating total sperm count and homogenized the right spermathecae for actual analysis. Even with this larger spermathecae the volume only increased to 5.45 mL, less than a 1% difference.

Another outcome of our study was the realization that recently fertilized crab spermathecae do not work with our methods. The spermathecae of just fertilized crabs are filled with seminal fluid and are very swollen and delicate. These spermathecae weigh significantly more (1 to 2 grams) as opposed to spermathecae that have lost their seminal fluid (under 0.25 grams). While it is easy to burst these spermathecae, they are also too thick to be ground in the dounce homogenizer. We would need more artificial seawater for the grinding process, but our dounce homogenizer does not have a large enough volume to hold the needed amount. Because of this we would need to modify our homogenization methods.

Conclusions

While these results are only preliminary, we were able to make some significant conclusions for future sperm quantification in blue crabs. We first conclude that using a dounce homogenizer is a better way to grind the spermathecae than using a Polytron. We found a negative correlation between sperm count and DNA fluorescence, although our results are opposite of what we expected and what was concluded in the counting of sperm in the desert leaf-cutter ant spermathecae (Reichardt and Wheeler 1995). Because of this trend, we cannot recommend that DNA fluorescence can be used to quantity sperm in blue crab spermathecae, and more analysis needs to be done.

Acknowledgements

I thank the Maryland Department of Natural Resources for the funding to collect our crabs and analyze our samples. I also thank Dr. Michael Wilberg and Sarah Rains for all of their support and assistance with this project, and Dr. Thomas Miller and Danielle Zaveta for assistance with the fluorometer. Lastly, I thank Maryland Sea Grant and the National Science Foundation for funding the REU program and allowing me to partake in this research experience.

References

Caldarone, E.M., M. Wagner, J. St. Onge-Burns, and L.J. Buckley. 2001. Protocol and guide for estimating nucleic acids in larval fish using fluorescence microplate reader. Northeast Fisheries Science Center Reference Document 01-11, 22p.

Chesapeake Bay Foundation. 2012. Major Tributaries of the Chesapeake Bay. http://www.cbf.org/page.aspx?pid=589.

Freckleton, R.P., P.A. Stephens, and W.J. Sutherland. 1999. What is the Allee effect? Oikos 87:185-190.

NOAA Chesapeake Bay Office. 2012. Blue Crab. http://chesapeakebay.noaa.gov/fish-facts/blue-crab.

Hines, A. H., P.R. Jivoff, P.J. Bushmann, J. van Montfrans, S.A. Reed, D.L. Wolcott, and T.G. Wolcott. 2003. Evidence for sperm limitation in the blue crab, *Callinectes sapidus.* Bulletin of Marine Science 72:287-310.

Jivof, P. 2003. A review of male mating success in the blue crab, *Callinectes sapidus,* in reference to the potential for fisheries induced sperm limitation. Bulletin of Marine Science 72:273–286.

Jivof, P. 2003. Summary Session Paper. Blue Crab Symposium 2000. Reproduction and Embryonic Development. Bulletin of Marine Science 72:265-272.

Miller, T., M.J. Wilberg, A.R. Colton, G.R. Davis, A. Sharov, R.N. Lipcius, G.M. Ralph, E.G. Johnson, and A.G. Kaufman. 2011. Assessment of Blue Crab in Chesapeake Bay. http://hjort.cbl.umces.edu/crabs/Assessment.html

Reichardt, A.K. and D.E. Wheeler. 1995. Estimation of sperm numbers in insects by fluorometry. Insectes Sociaux 42:449-452.

Sato, T., K. Yoseda, K. Okuzawa, and N. Suzaki. 2010. Sperm limitation: Possible impacts of large male-selective harvesting on reproduction of the coconut crab *Birgus latro*. Aquatic Biology 10: 23-32.

Turner Designs. 2012. Technical note: An introduction to fluorescence measurements, Revision A. Accessed on August 9, 2012 from http://www.turnerdesigns.com/t2/doc/appnotes/998-0050.pdf

Figures

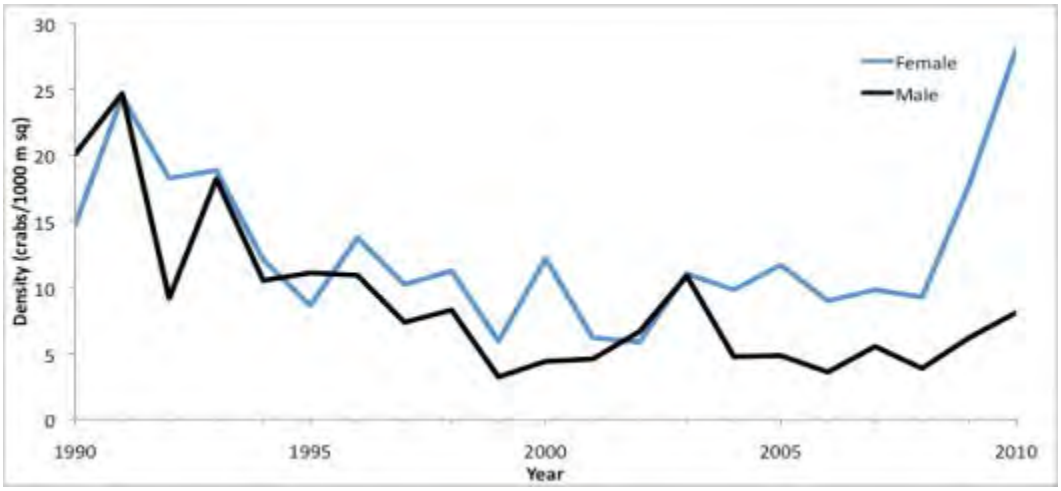

Figure 1. Mean blue crab density during 1990-2010 from the blue crab winter dredge survey.

Figure 2. Sampling locations in the Chesapeake Bay of blue crabs used in this study (map from Chesapeake Bay Foundation 2012).

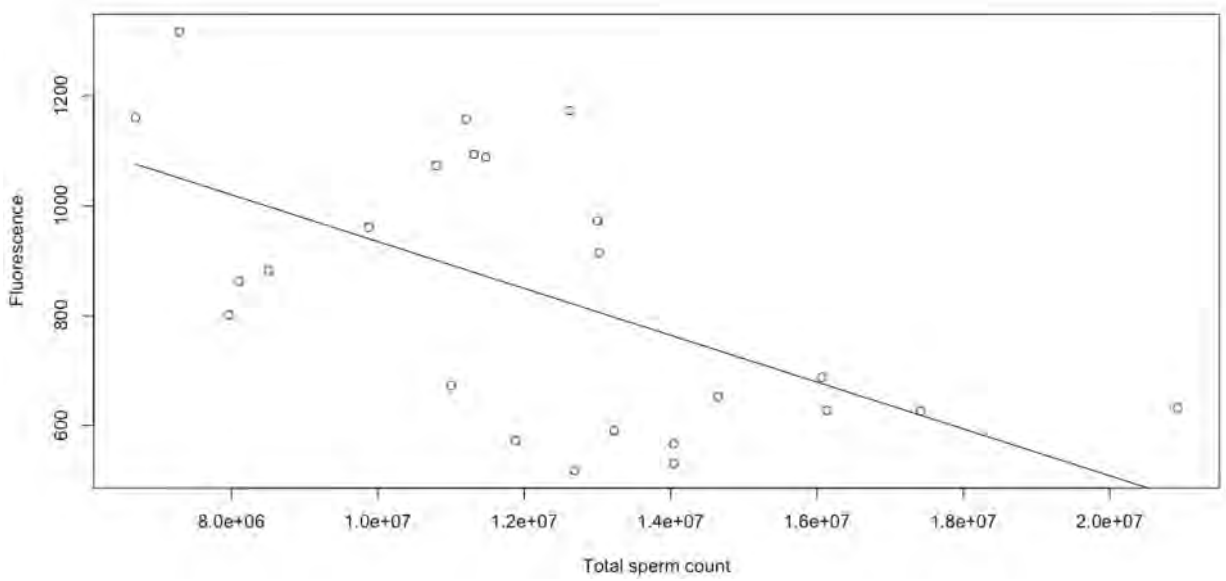

Figure 3. Total sperm count (total count per spermathecae) vs. fluorescence (RFUs) for our 24 spermathecae from six river systems.

Migration Routes and Corridors of the Eastern North Pacific Stock of the Blue Whale Along the U.S. West Coast

Michelle Ferraro, REU Fellow
Maryland Sea Grant

Dr. Helen Bailey, Research Assistant Professor
Chesapeake Biological Laboratory, University of Maryland Center for Environmental Science

Abstract

The Eastern North Pacific Stock of the blue whale (*Balaenoptera musculus*) which occurs along the Western Coast of the United States, has been considered endangered since 1966 and despite concerted efforts to protect this species through whaling restrictions, their population is currently not increasing. It has been suggested that ship strikes are potentially hindering the recovery of these animals, so it is important to study their migration patterns to identify where they are at risk in order to improve protection for this species. This study analyzes daily state-space modeled positions from satellite telemetry data for 104 whales tagged from 1994 to 2008 in order to determine the migration pathways and areas of high-use for these animals that might overlap with shipping traffic lanes. This analysis revealed that high-use areas of blue whales occurred off the coast of Santa Barbara and San Francisco at latitudes 34^{o}N and 37-38^{o}N and coincided with major shipping lanes. This overlap suggests that adjustments to the shipping lanes in the Santa Barbara Channel and San Francisco Bay region could reduce the risk of ship strikes for these whales and potentially help this population grow in numbers.

Keywords: Blue whales, Migration, California Coast, Ship strikes

Introduction

Baleen whales spend a large portion of their time migrating from high latitude feeding grounds to their low latitude breeding grounds (Corkeron and Connor 1999). This large spatial separation seems to be characteristic of this group and although there is some interspecies variation in length of migration, scientists suggest that there is an important evolutionary driver that induces these large mammals to expend the energy to migrate (Corkeron and Connor 1999). The drivers that have been suggested include that calves born in warm water have less thermoregulatory demands than those born in the polar waters and thereby can put that energy towards growth, that the calmer waters of the lower latitudes require less energy expended on the part of the calves to navigate them and that breeding in the lower latitudes might reduce the risk of killer whale predation on their young within a critical vulnerable growing period (Corkeron and Connor 1999). Regardless of these drivers, migration is an important part of the ecology of these species.

A series of developments in technology has occurred over the years in order to track whales along their migration routes. The first effort to tag whales was with Discovery tags which solely recorded two locations: the location at which the animal was tagged and the location where the animal died and the tag was retrieved (Mate et al. 2007). This tag provided limited information on the range of specific whale species (Mate et al. 2007). The VHF (Very High Frequency) and HF (High Frequency) radio tags that came afterwards gave more detailed information as they could be implanted and transmit information from the whale, but the problem with these was that radio signals could only be detected for a short distance and required extensive close range tracking of the animals to have relayed information (Mate et al. 2007). These radio tags were only effective for short periods of time and in limited inshore areas and therefore more useful for pinniped studies than those of whales who have a larger range (Mate et al. 2007). The invention and further modification of the satellite tag so that it was small and implantable revolutionized the field of migration studies as these tags could transmit information long distance and be implanted for fairly long periods depending on the design of the tag (Mate et al. 2007). The ARGOS satellite tags provide global locations and have proved useful for designating cetacean hotspots and receiving locations of the animals in real time (Block et al. 2011). In addition to the development of the tag, deployment and implantation on the animal has also proved a struggle over the years in order to ensure the tag remains in place for an extended period of time. Attachment strategies varied from pole applicators, shotguns, crossbows, helicopters and air powered applicators all with varying success (Mate et al. 2007). The predominant method used over the past 10 years has been the Air Rocket Transmitter System (ARTS), an air powered applicator method (Mate et al. 2007).

Additional methods have been used other than telemetry, which include photo identification surveys and line-transect surveys (Calambokidis and Barlow 2004). Some drawbacks of the photo-identification surveys include that they can be geographically biased toward whales that are in closer to shore, they may provide skewed results if there is little mixing among whales and stay in specific groupings, and they require a large amount of effort to survey the population (Calambokidis and Barlow 2004). Line-transect surveys have a similar problem with requiring a large sustained effort to survey the transects (Calambokidis and Barlow 2004). One study showed that remotely sensed data paired with a predictive model had high explanatory power and thereby the use of this remotely sensed data could majorly reduce daily effort needed to obtain appropriate real time densities of baleen whales (Becker et al. 2010). The recent shift towards telemetry is due to its ability to track cetacean movements and behavior, and because it provides real time data with less daily human effort to survey the entire cetacean habitat (Block et al. 2011).

The data collected from satellite tags track the progression of a single animal and allows the speed and turning angle of the animal to be determined for each of its locations based on the horizontal movement derived from latitude and longitude coordinates over time (McConnell et al. 2010). The problem with these tags is that often the whales do not surface long enough or enough times to transmit a sufficient number of signals to the satellite to ensure a high degree of accuracy (Costa et al. 2010). Studies done with GPS comparisons of satellite tagging locations on elephant seals, which spend similar amounts of time underwater as whales, can have errors up to 101 km (Costa et al. 2010). This large range of error necessitates the use of a predictive model that can estimate the most likely course of the animal within the probable range determined from the error in the satellite positions in order to interpret the data. Some methods that have been used for this purpose have been heuristic approaches, curvilinear smoothing, and state-space models (McConnell et al. 2010). The approach used in this paper is space-state modeling because it does not exclude relevant data and generates a track that has biological significance unlike curvilinear smoothing (McConnell et al. 2010).

The state-space model uses the known error distribution for the locations determined by satellite with a behavior based model to predict the best possible track that the animal was likely to follow (Patterson et al. 2008). The behavioral model used to analyze the movement of whales switches between two modes: migration and area restricted search (ARS) (Bailey et al. 2009). Migration is where the whale moves from one location directly to another (Bailey et al. 2009). This is characterized by higher speeds, very low turning angles and a high autocorrelation in speed and direction that indicates that the whale is moving in a relatively straight and direct path (Bailey et al. 2009). The ARS behavior indicates the animal stays within a certain area for an extended period of time (Bailey et al. 2009). This type of behavior is characterized by lower speed, higher turning angles, and lower autocorrelation in speed and direction, which indicates that the whale is remaining in a certain area either to breed or to feed on an abundant patch of food (Bailey et al. 2009). The state space model uses these parameters to not only determine where the whale is but also determines its most likely behavior at each point along the track supplying very important biological information on feeding grounds and cetacean hotspots (Bailey et al. 2009).

Blue whales (*Balaenoptera musculus*) are the largest known mammals to have existed on Earth reaching lengths of over 30 m and are considered one of the top predators of the oceans (Branch et al 2007). These majestic creatures belong to the order Cetacea and the suborder Mysteceti and primarily feed on krill by a process known as filter feeding (Branch et al 2007). These animals appear blue underwater but more grayish at the surface and they have a lighter ventral color that is often a pale yellow (NOAA 2012). They are found throughout the world's oceans but this specific study focuses on the Eastern North Pacific blue whale.

The blue whale in the Pacific Ocean feeds primarily on *Euphausia pacifica* and *Thysanoessa spinifera (Fiedler et al. 1998) and like all baleen whales,* feed via baleen plates that extend down from the roof of their mouth and filter krill out of the water column. As krill are very small organisms, it is energetically costly to filter them through these baleen plates when they are not in dense patches and thereby blue whales only feed on krill when they are congregating so they can compensate for the energy losses of feeding (Branch et al 2007). Abundances in these krill tend to peak during the summer over the continental shelf where high primary productivity occurs due to increased nutrients from upwelling events and increased sunlight (Branch et al. 2007). The largest species of krill are most abundant in the more polar regions while the more midsized krill appear at the mid-latitudes. This gradient in food size may account for the Eastern North Pacific blue whale migrations along the U.S. West Coast (Branch et al. 2007). From previous studies, it has been determined that Eastern North Pacific blue whales are migratory animals that travel to the far sub-polar region of the Gulf of Alaska along the western coast of California in order to feed during the summer and travel back down to the Costa Rica Dome and Baja California to breed in the winter (Bailey et al. 2009; Caretta et al. 2011). Since the Costa Rica Dome and Baja California are considered highly productive areas during the winter and spring, it has been suggested that these blue whales feed throughout the entire year (Carretta et al. 2011). The Western U.S. Coast is also considered an important feeding ground for this stock in the summer and fall months (Carretta et al. 2011).

Scientists estimate that 9,500 North Pacific blue whales were taken by commercial whalers from 1910 to 1965, 3,000 of which were taken along the West Coast of the US and Canada (Carretta et al. 2011). The current stock is estimated as a minimum of 2,046 individuals and they are still considered "endangered" under the Endangered Species Act (Carretta et al. 2011). The blue whale was originally put under protection by the IWC and they are also protected under the Endangered Species Act as of 1973 (Carretta et al. 2011). However, ship strikes have recorded a large number of whale mortalities as five were killed between 2004 and

2008, four of which were in 2007. This exceeded the yearly Potential Biological Removal (PBR) assigned to the US which is 3.1 whales per year (Carretta et al. 2011). These confirmed deaths do not include major injuries and non-reported strikes which can occur (Carretta et al. 2011). Currently there is no evidence to support that this blue whale stock is increasing in numbers (Carretta et al. 2011). This indicates that more information on their migration routes and high-use areas is needed to better protect and preserve this species along the U.S. West Coast.

The objective of this study is to examine the variation of coastal migration routes of the Eastern North Pacific stock of blue whales using Argos satellite tracking data (Figure 1). The goal of this project is to identify whether there are any migratory corridors along the U.S. West Coast, and specifically within the Santa Barbara and San Francisco Bay region in order to further inform management and the shipping industry on how to avoid potential ship strikes of this endangered species. This involved:

- Determining how the migration patterns and width of migration routes varied along the U.S. West Coast,
- Using these migration patterns to identify specific migration corridors and high-use areas,
- Comparing the migration routes to known shipping routes and large shipping ports to identify potential threat zones.

Materials and Methods

Satellite Tagging

In this study, 141 whales were tagged with ARGOS satellite tags in four locations including the western portion of the Santa Barbara Channel, the Gulf of Farallones, Cape Mendocino and the Gulf of California, Mexico (Bailey et al. 2009). Most deployments took place in the Santa Barbara Channel and the tags were deployed during August to October from 1993 to 2008 excluding 1996, 1997 and 2003 (Bailey et al. 2009). These Telonics ST-6 or ST-10 tags were contained in stainless steel cylinders and attached with sub dermal anchors via 68kg Barnett compound crossbows until 1996. In subsequent years, Telonics ST-15 tags were used and placed in stainless-steel cylinders that could be implanted subdermally with a slow release antibiotic coating to reduce infection (Mate et al. 2007). After 2002, the tags were deployed with the ARTS air powered applicator system (Mate et al. 2007). All tags were attached from 1 to 4m in front of the whale's dorsal fin.

State-space Modeling

After the data was collected via satellite, the ARGOS satellite positions, composed of latitudinal and longitudinal locations, were analyzed using a state-space model to obtain daily position estimates with 95% credible limits to incorporate the uncertainty of ARGOS measurements due to short or low quality class transmissions from the tags (Bailey et al. 2009). The state-space model is a time-series model that combines positional information gathered from the tags and their known accuracy ranges based on their ARGOS quality class ranking (3, 2, 1, 0, A, B, and Z) with a behavioral model (Jonsen et al. 2003). The ARGOS quality class ranking of 3 is regarded as the best class while Z is the worst class transmission (Costa et al. 2010). The error in location class Z is so high that location class B is the lowest class considered in this study. The majority of transmissions for this experiment were in the 1, 0, A, and B classes. The behavioral model is based on a correlated random walk that examines the mean turning angle and the autocorrelation in speed and direction between consecutive locations to determine if the animal is in an ARS or migration mode (Jonsen et al. 2005, 2007). The model is fit using a Bayesian approach and the parameters are estimated based on a total

of 1,000 independent samples (Bailey et el. 2009). The outputs from the model include a tag identifier for each individual whale, the date of each daily position, the mean latitude of the position, the mean longitude of the position, the upper and lower 95% credible limits for the longitude and latitude of each position, and the mean and median of the behavioral mode from the 1,000 samples. The behavioral mode has two classifications: 1 which equates to a migration behavioral mode and 2 which corresponds to the ARS behavioral mode. The mean behavioral mode (bmode) provides a value between 1 and 2. The last position in the track is assigned a behavioral mode of 0 since there is no subsequent location to determine the behavior. In this study, the designation of migration behavior is when $0 < b\ mode < 1.5$ and the whale is considered in ARS behavior when $b\ mode \geq 1.5$. A detailed description of the state-space model can be found in Bailey et al. (2009). In this analysis, the mean latitude and longitude position values from the state-space model will be used.

Data Analysis

The data analysis consisted of 3 components:

- Data exploration and identifying any biases and confounds
- Determination of common population-level migration routes that can be identified from the individual tracks
- Identifying high-use areas from the time spent within a location and the foraging ARS mode

First, data exploration was done to further organize the data outputted from the state-space model and to account for the limitations of the data such as uncertainty in location estimates, the development of a population-level route network from individual based data, unequal track lengths and unequal samples sizes among years and seasons. Tables were created to summarize how the mean and maximum lengths of the tracks vary in each calendar year and deployment year (Table 1). For each degree of latitude the total number of positions, the number of positions in migration mode, the number of positions in ARS behavior, the number of tags deployed at that latitude, the average width of the 95% credible limits in latitude and longitude, the years for which there are positions, and the months of the year for which there are positions were calculated. This gave important information on the data available along the U.S. West Coast as well as on the behaviors. In addition, a frequency distribution was created of the number of individuals that had location estimates for the same relative day of their tracks to see how the number of individual positions decreased as the number of days since deployment increased. This determined the amount of bias from unequal track lengths due to tag loss or malfunction. The latitude of the positions were plotted in relation to the date to determine if and when the individuals changed their movement from northward to southward. This enabled the data to be separated into northbound and southbound migrations so the data could be analyzed based on the migration direction.

The data were then analyzed to see if there were any apparent common population-level migration routes along the coast. The U.S. West Coast is primarily oriented in the North-South direction so we examined the longitudinal width of the whales' migrations to determine if there are any common routes or corridors along the coast. The mean, 1st quartile, 3rd quartile, and interquartile range of the longitude were calculated based on sorting by 1^{o} latitude intervals, where all latitude values were rounded down to the nearest 1^{o} latitude. This latitudinal separation gave a fine scale view of the migration routes of the whales and the use of the 95% credible limit positions gave a measure of uncertainty in the position estimates. These calculations supplied the information to plot a graph that showed the interquartile range in longitude as a measure of the width and variation in migration routes over 1^{o} latitude intervals

for all of the data. This approach is similar to a study done on North American Pronghorn where width and range were calculated for their migration routes to determine important areas for habitat management to maintain the species (Berger et al. 2006). These comparisons will show how the spread of locations vary with latitude and identify any narrow ranges that would indicate a migratory corridor. The mean, upper, and lower credible limits for the interquartile longitude values for each latitudinal degree were then divided by the total number of tags in that latitude and then plotted against latitude to account for variation in the number of tags at each latitude.

Then an analysis of the longitude of the whale positions was performed to determine if there are any relationships between the whales' route and the variables latitude, year, month, behavioral mode and individual using a similar approach to Vardanis et al. (2011). The latitudes chosen were off California at 33^{o}N, 35^{o}N, 37^{o}N, 39^{o}N, and 41^{o}N. The relationships were tested using a linear mixed effect model. The fixed factors were latitude, year, behavioral mode, and month. The reference levels for the factors were set to year 2005, month September, and behavioral mode of transit because these were the values which contained the most observations. In order to increase the sample size for certain month values because there few observations, the months March, April, and May were grouped together, January was grouped with December, and July was grouped with June. The random effect was the individual and the response variable was the longitude (based on the mean position estimate from the state-space model) at which the whale crossed each of the latitudes. Any observations that crossed multiple latitudinal lines or crossed any of the aforementioned latitudes twice were included in this analysis. There were a total of 384 observations. A linear regression model was also run on the same data with the same fixed factors but without the random effect of the individual in order to determine the significance of this random effect.

The next analysis performed was an analysis of the timing of whale movements which sought to examine the relationship between relative dates of all positions crossing latitude 41^{o}N and the direction of migration of the whale. The relative date is defined as the deviation of the actual date the individual crossed the 41^{o}N latitude from the average date of the entire group of positions examined in this analysis. Mean date was calculated for the latitude 41^{o}N crossing positions for both northbound and southbound tracks together to examine synchrony of timing of movements between individuals. The direction is defined with two directions: northbound and southbound. Northbound is the track length the animal pursued up to its most northerly point while it is foraging in the summer and autumn. Southbound is the track the animal takes after it reaches its most northerly point as it moves south to its wintering grounds. Three tracks were excluded because they crossed this latitude during the winter. These tracks went more northward in the winter months and proved outliers to the data in this analysis of summer/autumn movements. Only individuals that crossed the latitude 41^{o}N twice were considered because without a minimum of two observations the linear mixed effects model does not have enough observations for each tagged individual in order to make a comparison. 41^{o}N was the only latitude considered because it was least likely to be biased by the tagging location that occurred at the lower latitudes but had a sufficient number observations to run a linear mixed effects model, which was done in the program R (R Development Core Team 2008). There were a total of 58 observations used in this analysis. In the model, the relative date was the response variable; the direction was set as a fixed factor and the individual was set as a random effect to account for the variation between and within individuals as a random sample of the population. The direction was treated as a categorical factor with the reference level as the northbound direction. A linear regression model was then run on the same data for the latitude 41^{o}N with direction and individual as fixed factors in order to determine if there were any significantly different individuals. The reference levels were set at direction northbound and individual 404175. A second linear regression was run on this same data with direction and

year as fixed factors to discern if there was any significant difference in the relative dates of crossing between distinct years. Both direction and year were categorical factors with the reference levels set as northbound for direction and 2008 for year.

We then identified high-use areas based on the amount of time animals spent in different areas and the amount of time they spent in ARS behavior off the U.S. West Coast, which is indicative of foraging. We calculated in quarter degree grid cells the total number of positions (giving the number of days the animals spent there) and the proportion of positions classified as ARS behavior. To account for variation in track duration, a weighting scheme was implemented as used by Block et al. (2011) in their study on the migration of top oceanic predators. The following formula was used (adapted from Block et al. 2011):

$$W = 1/n_t \quad (1)$$

where W, the weighting, is determined by the inverse of n_t, the number of individuals with the t^{th} day location estimate. This reduced bias from the tagging location because it allows for the later locations to be weighted more heavily than the initial deployment locations. In order to make sure the later locations are not too heavily weighted, a threshold time weighting was used where beyond the 85% percentile of the track lengths, the weights were set equal to the weight set on the threshold day as determined appropriate by Block et al. (2011). These weights were summed for each grid cell to determine the relative amount of use of different areas. In addition, the proportion of positions that were classified as ARS behavior in each grid cell were used to determine important feeding areas.

Finally, we compared visually the locations of the migration routes and high-use areas with known shipping routes and large shipping ports to identify potential threat zones.

Results

The organization of the data by deployment year (Table 1) demonstrated how the number of tags and mean track length were much higher after the year 1998. There were a total of 104 state-space modeled tracks with the longest track spanning 504 days and the mean length of all tracks was 106 days. In addition to these results, once the tracks were plotted there was a discovery of a third wintering strategy that was different from the two previously described (Bailey et al. 2009). The two common wintering strategies consisted of whales migrating south for the winter months either to the Gulf of California or the Costa Rica Dome which served as feeding and breeding grounds. This third wintering strategy takes a different approach, where the whales go southwest off the tip of Baja and then move northwesterly far offshore. These whales remained offshore until they return to the coast for summer feeding. Three tracks demonstrated this third wintering strategy.

The plotting of the width of the longitudinal interquartile ranges by 1^o latitude allowed for the identification of narrow migratory corridors. These corridors occurred at 33^oN to 34^oN, 37^oN to 38^oN, and 40^oN to 42^oN (values <0.02 for interquartile range/number of individuals) as seen in Figures 2.1 and 2.2. These trends were visible when purely interquartile ranges were taken into account as seen in Figure 2.1 but also when the interquartile ranges were adjusted for the number of individuals with positions in that latitude.

In the analysis of the whales' route which looked at the relationship between longitude and the factors latitude, month, year, and behavioral mode, each of the latitudes (35^oN, 37^oN, 39^oN, and 41^oN) had a significantly different mean longitude value from the reference level of

33°N as seen in Table 2. The results indicate that at the more northerly latitudes the animals move further west. In regards to months, August, November, and the December-January grouping were significantly different from the reference level month of September. The animals were further east during August than in September and further west in November to January. There was no significant difference between September and October indicating that the routes were similar during these months. The year 2008 was found to be significantly different from the reference level of year 2005. These animals in 2008 crossed on average 3 degrees of longitude west of the animals in year 2005. Otherwise none of the other years which included 1995, 1998, 1999, 2004, 2006, and 2007 were significantly different from the reference level year of 2005. There was also no significant difference in longitude between the behavioral modes ARS and transiting. The random effect for individual in the model had an intercept of 1.697 and a residual of 3.254 which indicated that there was more within individual variation than between individual variation in the longitude at which these animals crossed each of the latitudes.

The linear mixed effect model run on the timing of the whales' movement, which looked at the relationship between relative date and direction of the whale migration, demonstrated that there was some similarity in the timing of movement between whales with the northbound migration occurring significantly earlier than the southbound migration. The northbound tracks were on average 12 days earlier than the calculated mean date which was October 4th and it was 43 days earlier than the mean of the southbound tracks as seen in Table 3.1. Although there is a significant difference in the means of these two directions there is a high amount of overlap which can be seen in Figure 3. An intercept of 23.909 and a residual of 18.095 for the individual random effect term indicated that there was greater between individual variation than within individual variation although the within individual variation was still high. The linear regression model was performed on the same data because it provided a look at individual variation as a fixed factor in order to identify which individuals were migrating at different times. Significantly different individuals from the reference individual 404175 from year 1998 were 3800834, 3800845, 3810823, each from year 2005, and 4904176 from year 2008. This model explained almost 60% of the variation in the data with individual and direction as fixed factors. The adjusted R^2 value was 0.591. A second linear regression model with year as a fixed factor was performed because the results from the first linear regression model with just individual and direction as a fixed factor indicated that three out of five individuals who had tracks in the year 2005 had significantly different values from the reference level individual 404175. These individuals had larger negative coefficient values which means that these animals were crossing the 41^{0}N latitude at an earlier date than the whales in other years. One out of two tracks that occurred in 2008 had a more positive relative date which indicated that this whale crossed 41°N at a later date than the other whales. The results for each individual whale of this test can be seen in Table 3.2. The second linear regression with year as a fixed factor showed that the relative date for year 2005 was significantly earlier by 38 days from the reference level year of 2008 (Table 3.3). The reference year of 2008 was not significantly different from the remaining years of 1998, 2000, 2004, and 2007. This may be due to the fact that the sample size in this year was very small and only one individual from 2008 was significantly different from the reference individual 404175. The variation and the medians of the relative dates for each year can be seen in Figure 3.2.

The map created that shows the amount of time spent in days in each quarter degree cell can be seen in Figure 4.1. Figures 4.2 and 4.3 demonstrate, on different scales, the amount of time spent in each quarter degree cell weighted up to the 85th percentile. It can be seen in Figure 4.3 that more time is spent in areas such as in the west portion of the Santa Barbara Channel at 34°N latitude and northwest off the coast of San Francisco at 37 to 38°N.

Both of these areas can be considered hotspots for the blue whale and should be avoided by ship traffic. In Figure 4.4, which show the proportion of positions classified as ARS behavior along the U.S. west coast, there are some grid cells with a high proportion of ARS behavior that only had a few positions overall in that cell (Figure 4.3), so Figure 4.3 is generally a better reflection of high-use areas. According to a current map of the Santa Barbara Channel shipping lanes as seen in Figure 5, the traffic lanes in the Santa Barbara Channel have the greatest overlap with high-use areas between the Channel Islands and the mainland on the continental shelf in the northwest portion of the Santa Barbara Channel. Similarly, a map of shipping traffic of the coast of San Francisco seen in Figure 6 taken from a Vessel Strike and Acoustic Report on the Gulf of Farallones (Abramson 2012) shows that of the three traffic lanes depicted in Figure 6, the traffic lanes that proceeds northwest along the coast has the most overlap with blue whale high-use areas. The southbound traffic lane in Figure 6 also has some overlap with high-use areas, although not to the extent of the northwest traffic lane, and the purely westward traffic lane has the least overlap in this San Francisco region. It is also important to note that Figure 5 is a map of the Santa Barbara region's shipping lanes while Figure 6 shows the vessel density within and beyond the shipping lanes in the San Francisco Bay.

Discussion

The results from this study have identified migration corridors and distinct high-use areas of blue whales off the U.S. West Coast, that coincide with shipping channels, which has important management implications. This study also identified that there was seasonal and interannual variation in the route and timing of the whales' movement along the coast.

The analysis of the whales' route indicated that as whales move northward up along the coast, they tend to move west in longitude. Although some of the westerly movement can be attributed to the coastline, which is generally further westward in the northern regions, in order to tell if these animals are moving farther offshore an analysis of the distance of these positions from the coastline must be performed. Studies have shown that krill mostly gather on the continental shelf and would thereby suggest that these animals are still staying close to the continental shelf to feed in the north (Ressler et al. 2005). There was a significant difference in the route between months. August was significantly different than September in that more of the positions were further east and thereby closer to the coastline. November to January was significantly different from September but the tracks were farther out to the west. November was on average 3 degrees of longitude further west and in December-January the whales were more than 7 degrees west of the longitude in September. This may be due to the fact that by the winter months most of the upwelling has been advected away from the coastline and thereby the whales have to search further offshore to look for food (Garcia-Reyes and Largier 2012). September and October are not significantly different which indicates that these months may be similar in traveling pattern offshore. Only the year 2008 had a significantly different mean longitude from the reference level year of 2005. In the year 2008, the whales were about 3 degrees to the west of that in the reference level year of 2005, indicating that these whales were further offshore during this year. Due to the fact that 2008 was an La Niña year (L'Heureux 2008) which increased primary productivity and thereby increased the food source of these whales, there was likely to have been more food early in the season and as a result whales would have migrated further off the coast, where congregations of krill could have been advected by currents. The results also indicate that there is no significant difference between ARS and the transiting behavioral mode in regards to mean longitude which suggests that these mammals may continue to search for food while they are migrating.

The analysis of the timing of whales' movements along the coast demonstrated that there are significantly different mean dates for northbound migration and southbound migration, but since there is a lot of overlap between individuals as seen in Figure 3, it is hard to define northbound and southbound as separate and distinct time periods. Figure 3 shows that at the same location one whale might be migrating north while another whale might be moving south. The migration of these animals depends on the individual and these whales do not necessarily move in one mass along the coast at one time. Normally in the summer feeding season, the whales tend to move northwards, but this analysis indicates that some whales move back and forth, which is why there is a temporal overlap in the northbound and southbound dates. The population on average will move in a northbound direction 43 days earlier than when they move in a southbound direction towards their breeding grounds for the winter. Since there seemed to be an effect of individual, a linear mixed model was implemented to see which individuals were significantly different using individual as a fixed factor. Some patterns have emerged from the data including that those individuals who were tracked in the year 2005 tended to cross the 41^{o}N latitude significantly earlier than in other years. In 2005, there were anomalous changes in atmospheric pressure, not quite like El Niño but with similar effects, which caused an intrusion of warm water along the coast of the Pacific suppressing upwelling and thereby suppressing primary production along the coast during that year (Schwing et al. 2006). Primary production, or phytoplankton, acts as the main food source for krill and other zooplankton on which the blue whales feed (Ressler et al. 2005). If there was little primary production, then there were likely to be fewer krill present and thereby the whales in this year did not find much food. If there was little food available then our results indicate that these whales continued directly northward in search of a better food source. This is similar to what happened to gray whales (*Eschrichtius robustus*) in Oregon during the same year, where they did little feeding in the upwelling deprived area and tended to move right past it although it had been seen in previous years that the whales would often stay as residents of the area (Newell et al. 2006). The gray whales that did stay in the area during this year showed signs of diminished health and less blubber indicating a lack of substantial food source (Newell et al. 2006). More evidence that this was a poor year for top predators can be seen in the effect it had on the California sea lion (*Zalophus californianus*) that had to search for a longer duration and over a wider distance in order to find food during the year 2005 (Weise et al. 2006). This explains why the blue whales in 2005 occurred further north at an earlier time than other individuals because they did not spend as much of their time in ARS behavior further south because there was little food to be found. This may mean that in years that experience El Niño type events that negatively affect upwelling, it may be more likely that these whales will migrate northward sooner in the year than they would in normal years. In complete reverse, an individual in year 2008 was significantly later than the other individuals although overall the timing of individuals from that year was not significantly different than in other years (except 2005), but that may be because there were few observations in that year. The later date for individual 4904176 from year 2008 might be due to the fact that in 2008 the Pacific had La Niña conditions in which upwelling was enhanced and thereby considerably increased the primary production in the region (L'Heureux 2008). This whale moved north later because it spent more time in the lower latitudes off the west coast of Baja and Southern California which might be due to the fact that it found more food there and thereby spent more time in ARS behavior rather than in direct transit. Both of these examples show how the varying climate in each year can affect the timing of the migration and movements of these animals. Another important finding in the linear regression was that this particular model, which took into account solely individual and direction as fixed factors, was able to account for almost 60% of the variation in timing of the migration which means that direction and individual variation are important factors in explaining the timing of movements in this population.

As determined by both the analysis of the interquartile ranges by 1° latitude intervals, as seen in Figures 2.1 and 2.2, and by the plots of time spent and proportion of time spent in ARS behavior in quarter degree sections as seen in Figures 4.3 and 4.4, the latitudes 34°N, 37 to 38°N and 40°N on the edge of the continental shelf are important areas for blue whales. These areas are important for feeding as the proportion of ARS behavior in these areas are high as seen in Figure 4.4. These regions correspond to the Santa Barbara Channel, the Gulf of Farallones off of San Francisco, and the coast off of Humboldt County respectively. All three of these narrow migratory corridors, which are also high-use areas, are located around headlands. This may indicate that there are increased feeding opportunities around headlands which would make them important feeding grounds for top predators like the blue whale. There has been a study that shows that in areas of shallow continental shelf and near headlands, the bathymetry and topography tend to change current circulation and concentrate chlorophyll in their surrounding area increasing standing stocks of krill (Ressler et al. 2005). These observations explain why these headlands are hotspots for these cetaceans as there is a larger concentration of food making it an important feeding area. The corridors and high-use areas in the Santa Barbara Channel and off San Francisco are also areas in which shipping traffic lanes pass through as seen in Figures 5 and 6. This could potentially be a zone for ship strikes and thereby there should be some changes made to the shipping routes in order to protect this endangered species. In regards to the Santa Barbara Channel, it can be seen from Figure 5 in combination with Figure 4.3 and 4.4 that the ends of the shipping lanes coincide with areas where high amounts of time are spent and large amount of feeding is occurring, making the animals considerably more susceptible to ship strikes (Parks et al 2012). Based on this overlap, it is advisable that the shipping lanes along the coast next to the Channel Islands Marine Sanctuary be rerouted so that the traffic lanes go southwest at Oxnard and then travel south of the larger Channel Islands in the Marine Sanctuary to reduce possible ship impacts to these whales. In a Channel Island report created for the Channel Islands National Marine Advisory council, authors suggest amendments to traffic lanes in order to reduce ship strikes based on whale data and they also suggest that a reduction in speed might reduce these risks (Abramson et al. 2009). In regards to the San Francisco region, it can be seen by comparing Figures 4.3 and 4.4 to Figure 6 of the shipping lanes that there is also a high area of overlap in the route that remains close to the coast and proceeds northward. It is more advisable that ships take the western route over the continental shelf to reduce the amount of time spent in blue whale dense areas and if they wish to proceed north, they do so farther offshore away from the continental shelf, this is a similar recommendation to that advised in a report on the Gulf of the Farallones created for the Gulf of the Farallones and Cordell Bank National Marine Sanctuaries Advisory Council (Abramson 2012).

These changes to the major traffic lanes in Santa Barbara and San Francisco will benefit other whales such as the humpback whale (*Megaptera novaeangliae*), Baird's beaked whale (*Berardius bairdii*), and fin whales (*Balaenoptera physalus*) because they are also found in high densities near the coast in these areas (Forney et al. 2012). Unfortunately, according to previous research, other animals such as the small beaked whales (whales from the genus *Mesoplodon*) and sperm whales (*Physeter macrocephalus*) might be more at risk from by ship strikes if the shipping lanes were moved further offshore because these species occur in higher densities more offshore past the continental shelf (Forney et al. 2012). However, the densities of these species are lower than the species that would benefit from these changes in shipping routes and thereby overall this recommendation is still likely to benefit cetaceans as a whole (Forney et al. 2012). When considering any management changes, it is important to weigh the cost and benefits on an ecosystem-wide scale instead based solely on one organism.

In addition to changing traffic lanes, another important discovery is the third wintering strategy of these animals that go further off the coast in search of food instead of going south to the wintering ground in the Gulf of California or the Costa Rica Dome. These animals are still at risk for ship strikes this far offshore but unfortunately their bodies are unlikely to be found as they sink to the ocean floor and thereby are not reported and go unnoticed. This may be the reason that the blue whale population is not growing in numbers because their population is reduced by these ship strikes that are not even reported. Further investigation into this third wintering strategy may be warranted to discover the true explanation of what is happening to this population of blue whales. In order to better inform the decision on the exact changes to shipping lanes that should take place, more research that includes how the migration of these animals relate to other variables such as distance from the coast and season and other environmental variables that could influence foraging such as upwelling and water temperature should be looked at in more detail.

Conclusions

Research on blue whales is warranted due to the fact that these whales are considered "endangered" by the Endangered Species Act and not enough is known about their biology to adequately protect them (Carretta et al. 2011). In addition to reducing biodiversity if the blue whale goes extinct as a top predator, it also might lead to a trophic cascade affecting lower trophic levels and disrupting the ocean ecosystem as a whole which could have negative impacts on fisheries and other endangered species (Block et al. 2011).

Numerous studies have identified various sources of danger to the Eastern North Pacific blue whale stock such as ship strikes and disturbance due to anthropogenic noise (Cassoff et al. 2011; Laist et al. 2001). Ship strikes in particular have been shown to have devastating effects on whales such as inflict broken ribs and flippers, cranial, jaw and vertebrae fractures, large lacerations, and slash cuts which can lead to system-wide infections and eventual stranding and death (Berman-Kowalewski et al. 2010). Also whales that have been tagged outside shipping lanes have been reported to spend a portion of their migration transiting or feeding in these shipping lanes which puts them at risk for strikes (Berman-Kowalewski et al. 2010). As seen in this study, the shipping lanes in the Santa Barbara Channel and the Gulf of Farallones go straight though high-use areas for blue whales. Often whales that are reported stranded and dead are found in large shipping areas such as the San Francisco Bay, Port of Los Angeles and the Santa Barbara Channel (Berman-Kowalewski et al. 2010). This is why our study of the high-use areas and specific migration patterns and corridors of these animals in these port regions is important because there is high boat traffic and thereby more likelihood for ship strikes. Blue whales may also be hit further out in the ocean and are never found, so our current estimates of their impacts can be sorely underestimated (Cassoff et al. 2011) especially the whales that have adopted the third wintering strategy where the whale travels further offshore during the winter months. Even if only a few ship strikes with unfound whale bodies occur each year, since the population is of such a small size it can have a detrimental impact on their recovery.

As the population PBR is set at 3.1 whales and the number of ship strikes has exceeded this in some years, it is crucial to reduce ship strikes for the Eastern North Pacific blue whale population to recover (Carretta et al. 2011). This is especially imperative as juveniles have proven more vulnerable to ship strikes and we need to protect the whales as they migrate with their young because otherwise the population will not grow and eventually recover (Laist et al. 2001). It is also essential to identify and safeguard various feeding grounds along the coast in order to protect the whales because it has been shown that whales are more vulnerable to ship

strike when feeding because they cannot hear as well near the surface, a phenomenon known as the Lloyd Mirror Effect (Laist et al. 2001), and that is why the feeding zones in the Santa Barbara Channel and the Gulf of Farallones should have priority protection in order to save this species from extinction.

Acknowledgements

Thank you to Dr. Helen Bailey for her advice and support, and to Maryland Sea Grant and Chesapeake Biological Laboratory for making this experience possible.

References

Abramson, L. 2012. Vessel strikes and acoustic impacts: Gulf of the Farallones and Cordell Bank National Marine Sanctuaries. Gulf of Farallones and Cordell Bank National Marine Sanctuaries Advisory Councils.

Abramson, L., S. Polefka, S. Hastings, and K. Bor. 2009. Reducing the threat of ship strikes on large cetacean in the Santa Barbara Channel region and Channel Islands National Marine Sanctuary: Recommendations and case studies. Channel Islands National Marine Sanctuary Advisory Council.

Amante, C., and B. W. Eakins. 2009. ETOPO1 1 Arc-Minute global relief model: Procedures, data sources and analysis. NOAA Technical Memorandum NESDIS NGDC 24: 19.

Bailey, H., B.R. Mate, D.M.Palacios, L. Irvine, S.J. Bograd, and D.P. Costa. 2009. Behavioural estimation of blue whale movements in the Northeast Pacific from state-space model analysis of satellite tracks. Endangered Species Research 10:93-106. doi: 10.3354/esr00239.

Becker, E.A., K.A. Forney, M.C. Ferguson, D.G. Foley, R.C. Smith, J. Barlow, and J.V. Redfern. 2010. Comparing California Current cetacean-habitat models developed using *in situ* and remotely sensed sea surface temperature data. Marine Ecology Progress Series 413:163-183. doi: 10.3354/meps08696.

Berger, J., S.L. Cain, and K.M. Berger. 2006. Connecting the dots: An invariant migration corridor links the Holocene to the present. Biology Letters 2:528-531. doi: 10.1098/rsbl.2006.0508.

Berman-Kowalewski, M., F.M.D. Gulland, S. Wilkin, J. Calambokidis, B. Mate, J. Cordaro, D. Rotstein, J.S. Leger, P. Collins, K. Fahy, and S. Dover. 2010. Association between blue whale (*Balaenoptera musculus*) mortality and ship strikes along the California Coast. Aquatic Mammals 36:59-66. doi: 10.1578/AM.36.1.2010.59.

Block, B.A., I.D. Jonsen, S.J. Jorgensen, A.J. Winship, S.A. Shaffer, S.J. Bograd, E.L. Hazen, D.G. Foley, G.A. Breed, A.L. Harrison, J.E. Ganong, A. Swithenbank, M. Castleton, H. Dewar, B.R. Mate, G.L. Shillinger, K.M. Schaefer, S.R. Benson, M.J. Weise, R.W. Henry, and D.P. Costa. 2011. Tracking apex marine predator movements in a dynamic ocean. Nature. doi: 10.1038/nature10082.

Branch, T.A., K.M. Stafford, D.M. Palacios, C. Allison, J.L. Bannister, C.L.K Burton, E. Cabrera, C.A. Carlson, B.G. Vernazzani, P.C. Gill, R. Hucke-Gaete, K.C.S Jenner, K. Matsuoka, Y.A. Mikhalev, T. Miyashita, M.G. Morrice, S. Nishiwaki, V.J. Sturrock, D. Tormosov, R.C. Anderson, A.N Baker, P.B. Best, P. Borsa, R.L. Brownell Jr., S. Childerhouse, K.P. Findlay, T. Gerrodette, A.D. Ilangakoon, M. Joergensen, B. Kahn, D.K., Ljungblad, B. Maughan, R.D. Mccauley, S. Mckay, T.F. Norris, Oman Whale and Dolphin Research Group, R.M. Warneke, S. Rankin, F. Samaran, D. Thiele, and K. Van Waerebeek. 2007. Past and present distribution, densities and movements of blue whales *Balaenoptera musculus* in the Southern Hemisphere and Northern Indian Ocean. Mammal Review 37:116-175. doi: 10.1111/j.1365-2907.2007.00106.x.

Calambokidis, J., and J. Barlow. 2004. Abundance of blue and humpback whales in the Eastern North Pacific estimated by capture-recapture and line-transect methods. Marine Mammal Science 20:63-85.

Carretta, J.V., K.A. Forney, E. Oleson, K. Martien, M.M. Muto, M.S. Lowry, J. Barlow, J. Baker, B. Hanson, D. Lynch, L. Carswell, R.L. Brownell, J. Robbins, D.K. Mattila, K. Ralls, and M.C. Hill. 2011. U.S. Pacific marine mammal stock assessments: 2010. U.S. Department of Commerce, NOAA Technical Memorandum NOAA-TM-NMFS-SWFSC-476, 352pp.

Cassoff, R.M., K.M. Moore, W.A. McLellan, S.G. Barco, D.S. Rotstein, and M.J. Moore. 2011. Lethal entanglement in baleen whales. Diseases of Aquatic Organisms 96:175-185. doi: 10.3354/dao02385.

Corkeron, P.J., and R.C. Connor. 1999. Why do baleen whales migrate? Marine Mammal Science 15:1228-1245.

Costa, D.P., P.W. Robinson, J.P.Y. Arnould, A. Harrison, S.E. Simmons, J.L. Hassrick, A.J. Hoskins, S.P. Kirkman, H. Oosthuizen, S. Villegas-Amtmann, and D.E. Crocker. 2010. Accuracy of ARGOS locations of pinnipeds at sea estimated using Fastloc GPS. PLoS ONE doi:10.1371/journal.pone.0008677.

Fiedler, P.C., S.B. Reilly, R.P. Hewitt, D. Demer, V.A. Philbrick, S. Smith, W. Armstrong, D.A. Croll, B.R. Tershy, and B.R. Mate. 1998. Blue whale habitat and prey in the California Channel Islands. Deep-Sea Research II 45:1781-1801.

Garcia-Reyes, M., and J.L. Largier. 2012. Seasonality of coastal upwelling off central and northern California: New insights, including temporal and spatial variability. Journal of Geophysical Research 117. doi: 10.1029/2011JC007629.

Forney, K.A., M.C. Ferguson, E.A. Becker, P.C. Fiedler, J.V. Redfern, J. Barlow, I.L. Vilchis, and L.T. Balance. 2012. Predictive modeling of marine mammal density from existing survey data and model validation using upcoming surveys. NOAA Technical Memorandum NOAA-TM-NMFS-SWFSC-444.

Jonsen, I.D., R.A. Myers, and M.C. James. 2007. Identifying leatherback turtle foraging behavior from satellite telemetry using a switching state-space model. Marine Ecology Progress Series 337:255-264. Habitat-based spatial models of cetacean density in the eastern Pacific Ocean. Endangered Species Research 16:113-133. doi: 10.3354/esr00393.

Jonsen, I.D., J.M. Flemming, and R.A. Myers. 2005. Robust state-space modeling of animal movement data. Ecology 86:2874-2880.

Jonsen, I.D., R.A. Myers, and J.M. Flemming. 2003. Meta-analysis of animal movement using state-space models. Ecology 84:3055-3063.

Laist, D.W., A.R. Knowlton, J.G. Mead, A.S. Collet, and M. Podesta. 2001. Collision between ships and whales. Marine Mammal Science 17:35-75.

L'Heureux, M. 2008. An overview of the 2007-08 La Niña and boreal wintertime variability. Science and Technology Infusion Climate Bulletin. 8pp.

Mate, B.R., R. Mesecar, and B. Lagerquist. 2007. The evolution of satellite-monitored radio tags for large whales: One laboratory's experience. Deep-Sea Research 54:224-247. doi: 10.1016/j.dsr2.2006.11.021.

McConnell, B., M. Fedak, S. Hooker, and T. Patterson. 2010. Telemetry. In: Marine mammal ecology and conservation, eds. I.L. Boyd, W.D. Bowen, and S.J. Iverson, 222-242. New York: Oxford University Press.

Newell, C.L., and T.J. Cowles. 2006. Unusual gray whale *Eschrichtius robustus* feeing in the summer of 2005 off the central Oregon Coast. Geophysical Research Letters 33. doi: 10.1029/2006GL027189.

NOAA Fisheries Office of Protected Resources. 2012. Blue Whale *(Balaenoptera musculus).* http://www.nmfs.noaa.gov/pr/species/mammals/cetaceans/bluewhale.htm Accessed 30 Mar 2012.

Parks, S.E., J.D. Warren, Karen Stamieszkin, C.A. Mayo, and D. Wiley. 2012. Dangerous dining: Surface foraging of North Atlantic right whales increases risk of vessel collisions. Biology Letters 8:57-60. doi: 10.1098/rsbl.2011.0578.

Patterson, T.A., L. Thomas, C. Wilcox, O. Ovaskainen, and J.Matthiopoulos. 2008. State-space models of individual animal movement. Trends in Ecology and Evolution 23:87-94. doi: 10.1016/j.tree.2007.10.009.

R Development Core Team. 2008. R: A language and environment for statistical computing. R Foundation for Statistical Computing, Vienna, Austria. http://www.R-project.org.

Ressler, P.H., R.D. Brodeur, W.T. Peterson, S.D. Peirce, P.M. Vance, A. Røstad, and J.A. Barth. 2005. The spatial distribution of euphasiid aggregations in the Northern California Current during August 2000. Deep-Sea Research II 52:89-108. doi: 10.1016/j.dsr2.2004.09.032.

Schwing, F.B, N.A. Bond, S.J. Bograd, T. Mitchell, M.A. Alexander, and N. Mantus. 2006. Delayed coastal upwelling along the U.S. West Coast in 2005: A historical perspective. Geophysical Research Letters. doi: 10.1029/2006GL026911.

Segee, B.P. 2010. Whale of an opportunity: Coast guard study of Los Angeles/Long Beach Port Access routes holds great potential for reducing ship strikes within Santa Barbara Channel. Ecology Law Currents 37: 58-67.

Vardanis, Y., R.H.G. Klassen, R. Strandberg, and T. Alerstam. 2011. Individuality in bird migration: Routes and timing. Biology Letters. doi: 10.1098/rsbl.2010.1180.

Weise, M.J., D.P. Costa, and R.M. Kudela. 2006. Movement and diving behavior of male California sea lion (*Zalophus californianus*) during the anomalous oceanographic conditions of 2005 compared to those of 2004. Geophysical Research Letters 33. doi: 10.1029/2006GL027113.

Figures and Tables

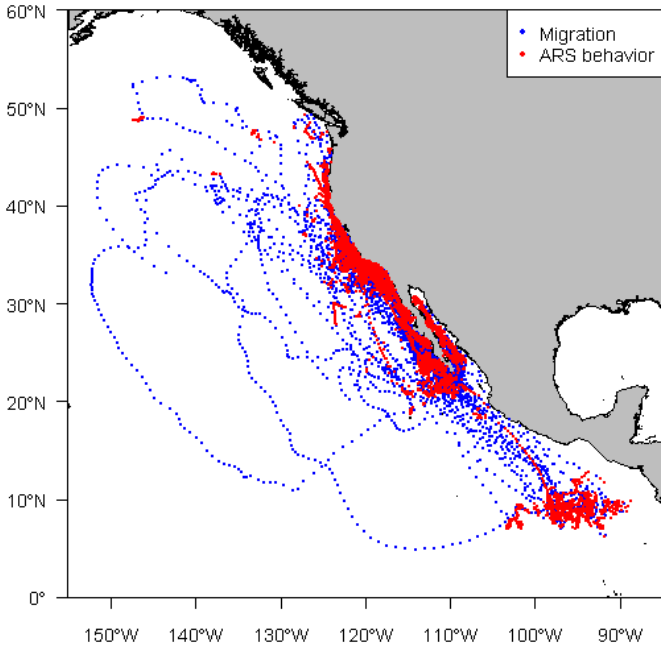

Figure 1.1. Map of all blue whale tracks along the US West coast color-coded by behavioral mode.

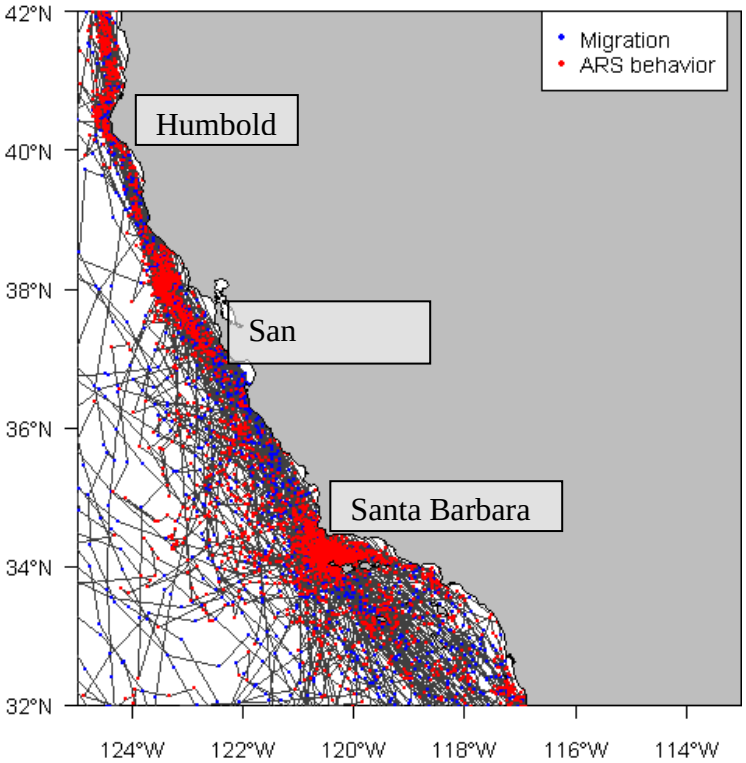

Figure 1.2. Map of tracks for the California region color-coded by behavioral mode.

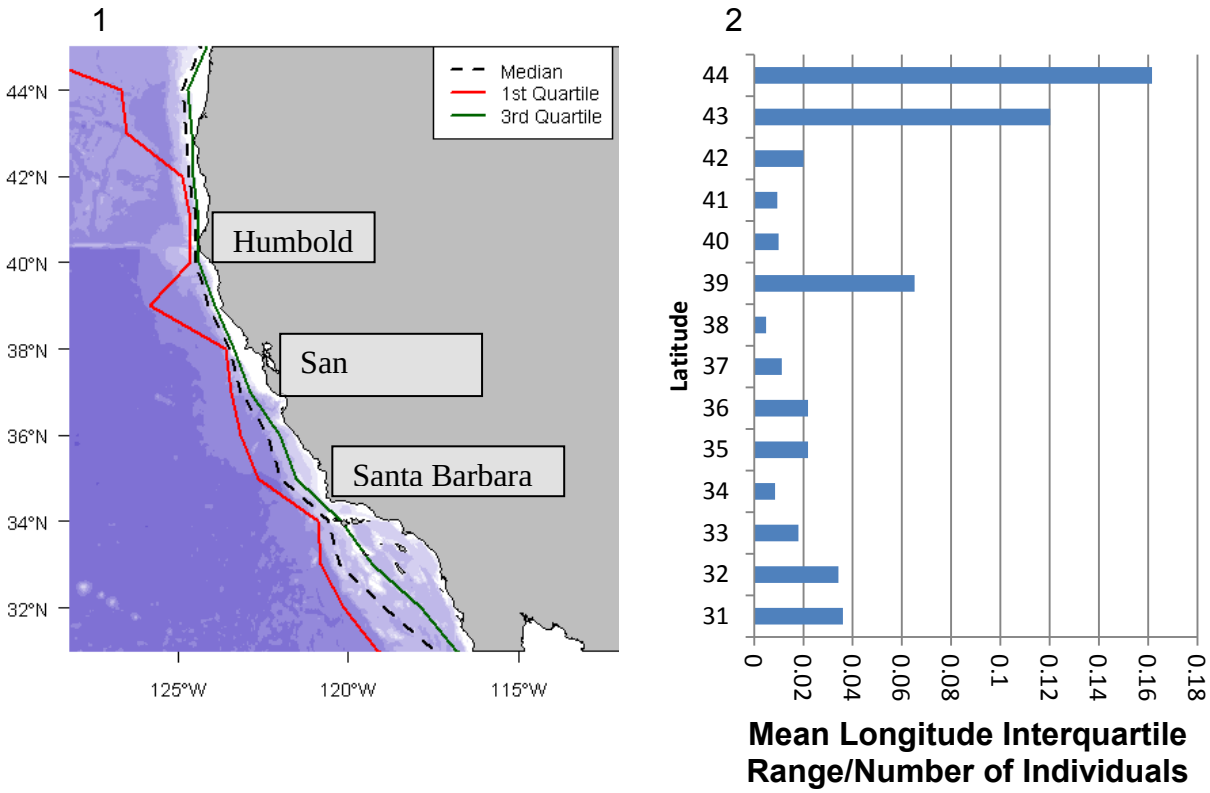

Figure 2.1. Map with the first and third quartile lines of longitude at 1° latitudinal intervals overlaid on bathymetry where depths <200 m are shown in white. Bathymetry provided by Amante and Eakins (2009).

Figure 2.2. Bar chart of longitude interquartile range/number of individuals at 1° latitudinal intervals.

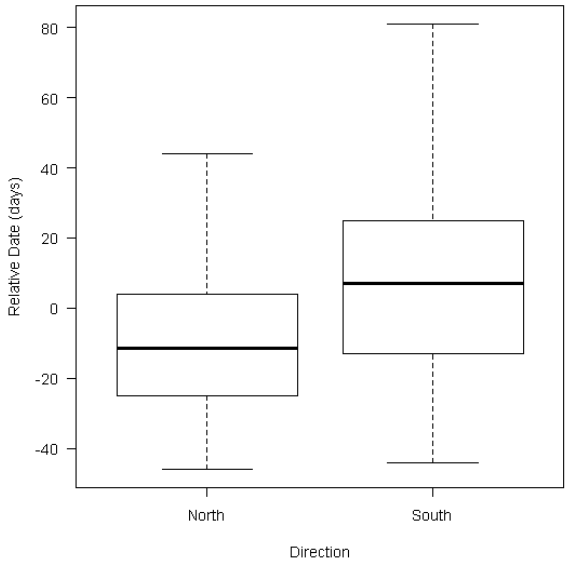

Figure 3.1. Box plot of the relative date at which the latitude 41°N was crossed that shows the variation and median (bold line) of the relative dates for each direction.

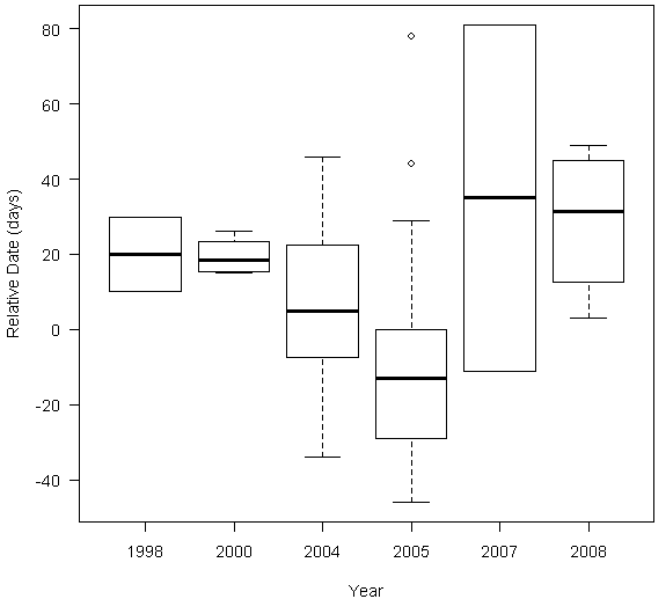

Figure 3.2. Box plot of the relative date that shows the variation and median (bold line) of the relative dates for each year.

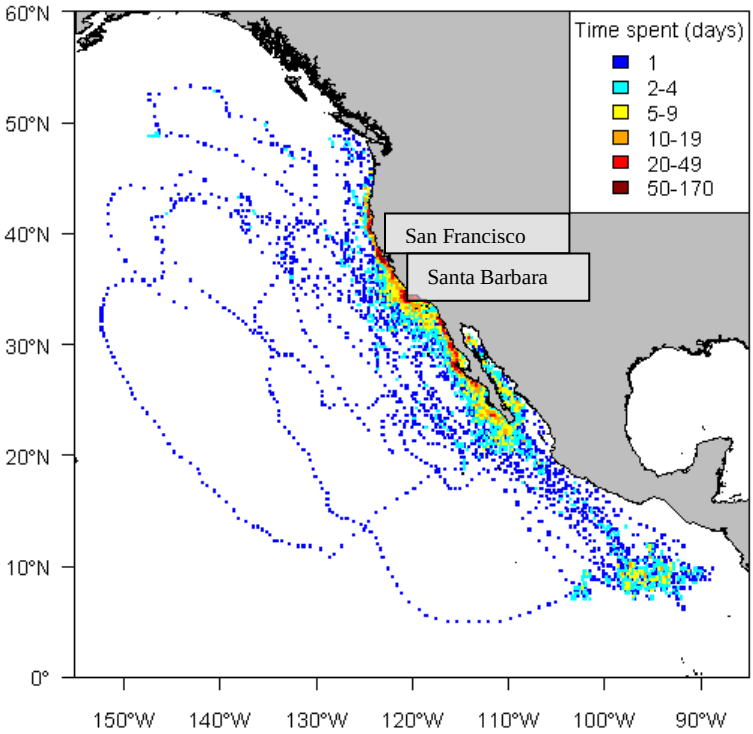

Figure 4.1. Map of entire U.S. West Coast color-coded by time spent in days by all whales on grid with 0.25^0 latitude by 0.25^0 longitude sections.

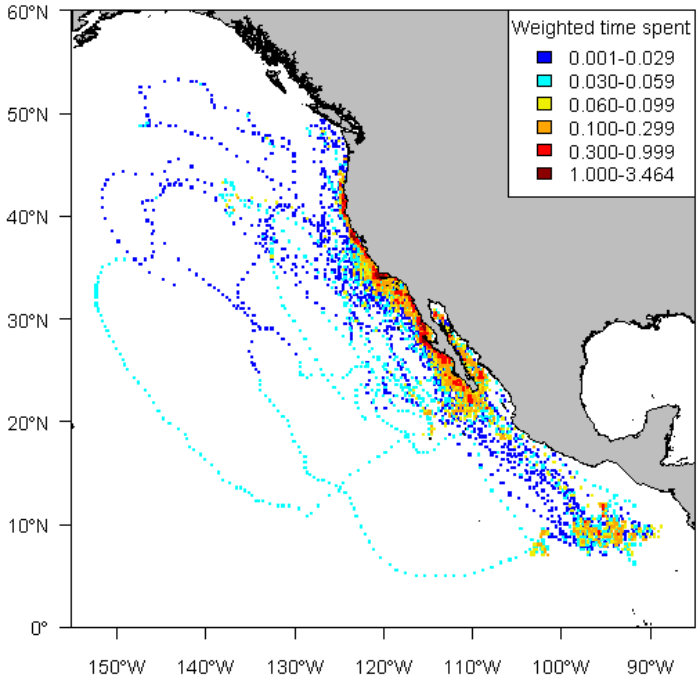

Figure 4.2. Color-coded map of entire U.S. West Coast showing the amount of time spent in days of all whales in 0.25° latitude by 0.25° longitude sections adjusted using weighting scheme where later dates in the track are more heavily weighted up to the 85th percentile.

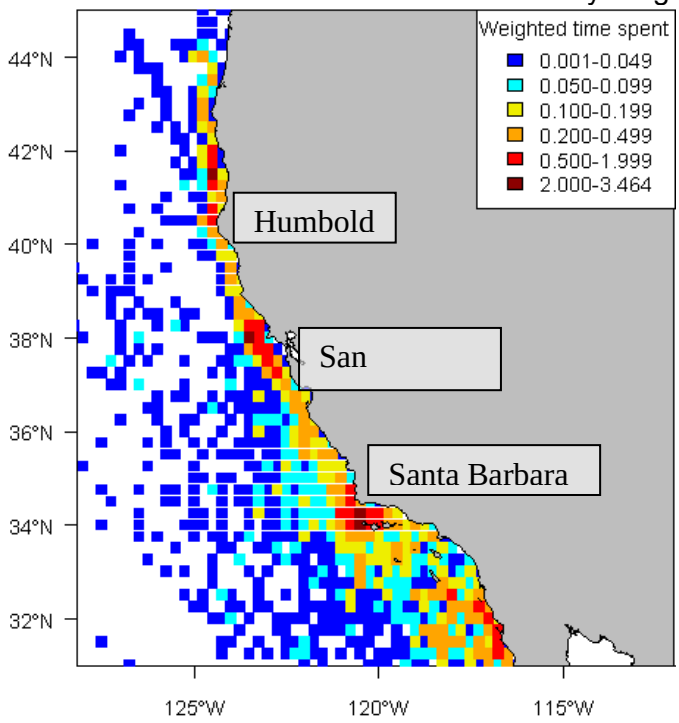

Figure 4.3. Amount of time spent in days of all whales in 0.25° latitude by 0.25° longitude sections adjusted using weighting scheme where later dates in the track are more heavily weighted up to the 85th percentile, off the California Coast.

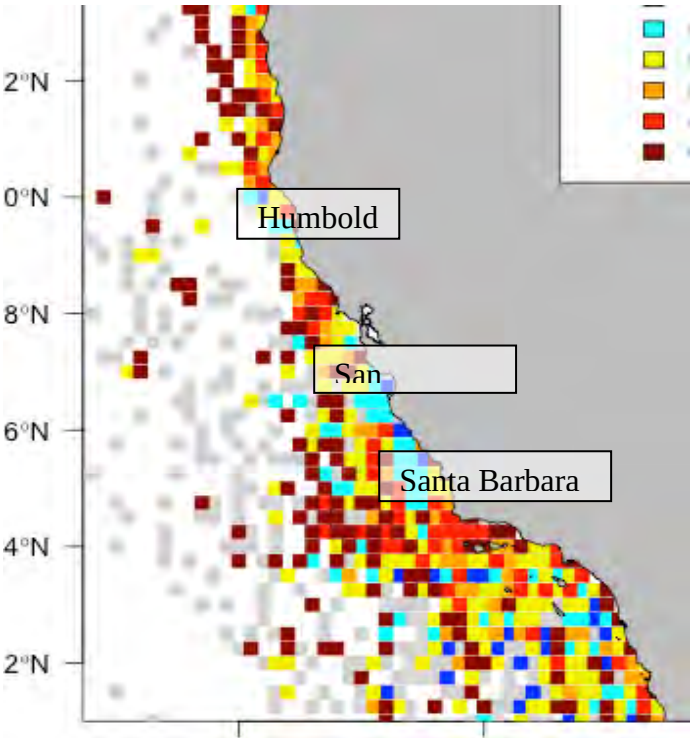

Figure 4.4. Color-coded map of U.S West Coast showing the proportion of ARS behavior in quarter degree sections.

Figure 5. Map of shipping lanes along the Los Angeles, Long Beach and Santa Barbara coast (Segee 2010).

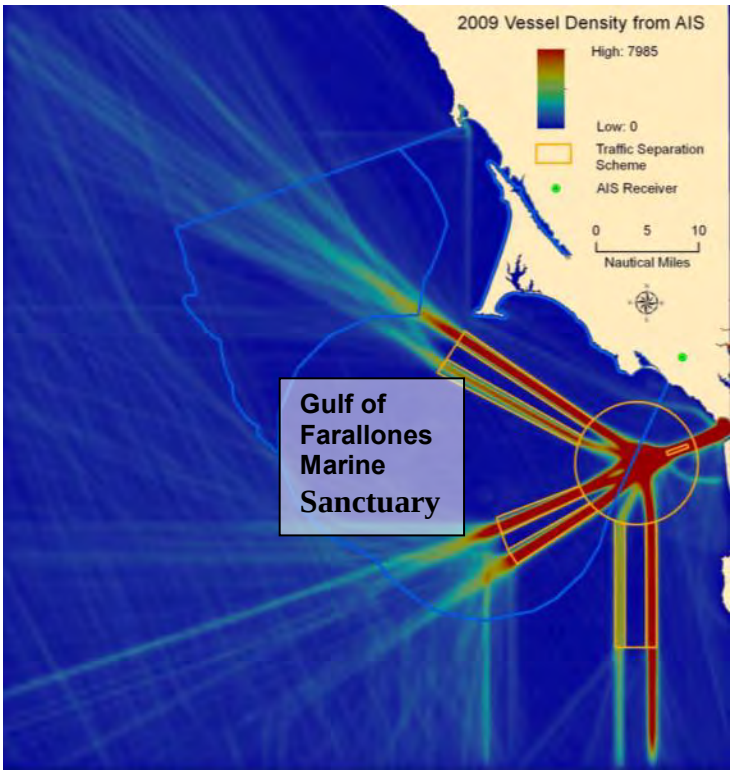

Figure 6. Map of shipping traffic of the coast of San Francisco color-coded by vessel density (Abramson 2012).

Table 1. Summarizing tag data by deployment year.

Deployment year	Number of Tags	Mean Track Length (days)	Maximum Track Length (days)
1994	2	11	13
1995	8	26	80
1998	7	57	126
1999	15	98	228
2000	6	121	248
2001	1	213	213
2002	2	138	193
2004	16	105	504
2005	14	93	235
2006	7	168	287
2007	14	109	221
2008	12	131	259

Table 2. Linear Mixed Effects Model results for longitude analysis with individual as a random effect. Reference levels are latitude 33°N, month September, year 2005, and transiting behavior.

Factor		Coefficient Estimate	SE	DF	p-value
Intercept		-119.2772	0.75836	318	0.0000*
Latitude in °N:	35	-2.8074	0.55078	318	0.0000*
	37	-3.88757	0.57282	318	0.0000*
	39	-5.00081	0.64853	318	0.0000*
	41	-6.60144	0.65794	318	0.0000*
Month:	March, April, May	-2.07789	1.27628	318	0.1045
	June, July	-0.58294	1.31346	318	0.6575
	August	1.65045	0.51825	318	0.0016*
	October	-1.04371	0.57393	318	0.0699
	November	-3.46633	0.68109	318	0.0000*
	December, January	-7.78019	0.8813	318	0.0000*
Year:	1995	-0.11171	1.50335	46	0.9411
	1998	0.04354	1.14261	46	0.9698
	1999	-0.21075	1.21052	46	0.8626
	2000	1.4384	1.72303	46	0.4081
	2004	0.21462	0.74291	318	0.7728
	2006	0.7885	1.57006	318	0.6159
	2007	-1.02002	1.19478	318	0.3939
	2008	-3.21428	0.90741	318	0.0005*
Behavior:	ARS	0.44047	0.43643	318	0.3136

*Denotes statistical significance at p-value<0.05

Table 3.1. Linear Mixed Effect Model results for relative date analysis with individual as a random effect. Reference level is north for direction.

Factor	Coefficient Estimate	SE	DF	p-value
Intercept	-12.7059	7.615259	43	0.1025
Direction: South	31.56065	5.613821	43	0.0000*

*Denotes statistical significance at p-value<0.05

Table 3.2. Linear regression model results for relative date analysis with the direction and individual as fixed factors. Reference levels are for direction north and for individual 404175.

Factor		Coefficient Estimate	SE	p-value
Intercept		-12.849	13.981	0.3632
Direction:	South	32.849	5.692	7.86e-07*
Tag ID:	701386	24.137	16.212	0.1438
	3300840	-12.325	14.083	0.3863
	3304175	-1.075	18.282	0.9534
	3310821	11.925	18.282	0.5177
	3310843	11.925	18.282	0.5177
	3800834	-29.615	14.000	0.0402*
	3800845	-39.075	18.282	0.0383*
	3810820	-22.075	18.282	0.2338
	3810823	-48.575	18.282	0.0110*
	3810829	17.529	14.747	0.2411
	4501385	31.425	18.282	0.0928
	4900825	8.925	18.282	0.6279
	4904176	41.425	18.282	0.0285*

*Denotes statistical significance at p-value<0.05

Table 3.3. Linear Regression model results for relative date analysis with direction and year as fixed factors. Reference levels are north for direction and 2008 for year.

Factor		Coefficient Estimate	SE	p-value
Intercept		20.828	12.528	0.10256
Direction:	South	15.844	6.569	0.01951*
Year:	1998	-16.672	21.197	0.43519
	2000	-5.289	17.177	0.75941
	2004	-23.57	13.971	0.0977
	2005	-38.23	12.788	0.00429*
	2007	6.25	20.941	0.76657

*Denotes statistical significance at p-value<0.05

The Effects of Plant Density on the Morphological and Biomechanical Properties of a Tidal Wetland Macrophyte: *Zizania aquatica*

Yasiel A. Figueroa, REU Fellow
Maryland Sea Grant

Dr. Lora Harris, Assistant Professor
Chesapeake Biological Laboratory, University of Maryland Center for Environmental Science

Abstract

Tidal freshwater wetlands provide a variety of ecological and social benefits such as habitat and protection of shorelines from storm surges. Unfortunately, sea level rise and development pressures have greatly impacted these ecosystems. Widespread historical wetland losses and ongoing vulnerability underscore the importance of understanding tidal wetland responses and resilience to stressors in order to achieve successful management of these resources. Recently reported accelerated rates of sea level rise are of particular concern. The role of wetland macrophytes in responding to sea level rise by changing stem density and morphology to create feedbacks with sediment capture has been well documented in tidal salt marshes. In some cases, the plasticity of these morphological responses results in changed structural characteristics of the plants. However, these processes have been less well studied in freshwater tidal systems. This study carried out field manipulations of *Zizania aquatica,* a dominant species in tidal freshwater marshes of the Chesapeake Bay. Morphological and biomechanical measurements were documented in control and experimentally thinned, lower density plots. The plants growing at a lower density were structurally stronger as demonstrated by computing a "factor of safety" that relates the biomechanical load capability of the stems to ambient forces. This study concludes that plant density influences the morphological and biomechanical characteristics of *Z. aquatica*.

Keywords: Tidal freshwater wetlands, Factor of safety, Biomechanics

Introduction

Wetland ecological services valuation is a relatively recent phenomenon; historically these systems have been viewed as a waste of valuable land and were often destroyed (Woodward and Wui 2001). Fortunately, we now recognize that wetlands provide numerous ecological and social benefits as wildlife habitat and nurseries, recreation opportunities, water purification, groundwater recharge, flood control, nutrient cycling, carbon sequestration, and protection of urban areas, among others (Mitsch and Gosselink 2000). While this appreciation has been translated into protection laws, regulations, and management plans, wetlands are threatened by both natural and anthropogenic effects such as sea level rise and urban encroachment. The risks to wetlands underline the importance of understanding the system's

vulnerability, responses, and resilience to stressors in order to successfully manage these ecosystems.

Vegetation plays an important role in the long term sustainability and ecological services of tidal wetlands. As sea level rises, Morris et al. (2002) hypothesize that maintenance of tidal salt marsh platform elevation is dependent upon the interaction between vegetation, sedimentation rates, and sea level rise via a dynamic equilibrium. This conceptual model describes a system where macrophytes maintain the elevation of their respective habitats within a relatively narrow portion of the intertidal zone by increasing aboveground production, and altering the amount of sediment captured and belowground biomass, thereby playing an important role in the system's equilibrium with sea level rise (Morris et al. 2002). Because the productivity and response of wetland vegetation may be critical to how these ecosystems respond to changes in inundation brought about by sea level rise, questions arise regarding more specific mechanisms and feedbacks between tidal wetland morphology, sediment inputs, and inundation from tidal waters.

In order to carry their own weight and resist external wind and tide forces, plants must be mechanically reliable, they must not only invest energy and resources in stem, branches and roots for support and anchorage (Anten et al. 2005), but also deal with mechanical stressors. The morphological properties, such as shape and size, and mechanical properties of a structure or system (e.g. plant, bridge and/or building) play an important role in its structural support and load capabilities, while extrinsic forces (e.g. tides, winds) determine actual loads. This engineering perspective has been applied to plant stems by exploring mechanical reliability with the concept of critical height; this is the maximum height a structure can support before collapsing under its own weight (Greenhill 1881). Complementary to the computation of critical heights is the determination of a structure's "factor of safety", a term that describes the structural capacity of a structure or system beyond the typical loads it supports (Niklas and Spatz 1999). The factor of safety is the extent to which the critical height exceeds the actual height (Niklas and Spatz 1999). Structures (in this case plants) that grow close to their critical height have a lower factor of safety and are more vulnerable to physical stress than plants whose actual height is not close to their critical height, they have a higher factor of safety.

Organisms living in dense aggregations face mechanical, biological and ecological consequences as a result of both competitive and cooperative relationships among species (Harley and Bertness 1996; Holbrook et al. 1991). Allometry is the study of the relationship of an organism's size with its parts. Changes in the allometry of a plant and its leaves, roots, or stems in response to environmental conditions can be characterized as morphological plasticity. Morphological plasticity is a typical response of vascular plants to high densities. A study focused on salt marsh plants (*Spartina alterniflora, Juncus gerardi, Iva frutescens* and *Salicornia europae*) concluded that plants growing at high densities tend to be taller and thinner than plants growing at lower densities (Harley and Bertness 1996). In a similar way, when submitted to prolonged inundation events we expect plants to put more energy into above ground biomass becoming taller and thinner as has been documented by Morris et al. (2002). Taller plants are more vulnerable to mechanical stress due to their greater weight and because they will experience a greater effect caused by wind force (or fluid forces in aquatic systems) generated bending moments in comparison with smaller plants (Anten et al. 2005). Thigmomorphogenesis, the response of plants to breaking stimuli (i.e. wind, touching, rubbing) leads to plants producing shorter and thicker stems and allocating more mass to roots in order to increase their resistance to mechanical failure (Anten et al. 2005). In contrast, other studies (Henry and Thomas 2002; Ashby et al. 1979) suggest that thigmomorphogenesis at high densities is partially suppressed since outcompeting neighbors for sunlight becomes a more critical limiting resource. Harley and

Bertness (1996) also concluded that the presence of neighbors causes biomechanical differences in plants. Their study shows that isolated plants (i.e. plants whose neighbors were eliminated) increased resistance to breaking by increasing stem diameter. Moreover, Bertness and Callaway (1994) have shown that the presence of neighbors in plant communities may reduce the effects of physical stress and provide physical support. Several studies (Bertness and Leonard 1997; Harley and Bertness 1996; Holbrook et al. 1991) highlight the importance and effects of natural plant density for biological, biomechanical and ecological features in aquatic vegetation. Sea level rise, urban encroachment and other anthropogenic pressures negatively affecting tidal wetlands have the potential of altering wetland vegetation natural densities and composition. For example, van der Putten (1997) suggest that eutrophication may be responsible for a large scale dieback of *Phragmites australis* in European wetlands during the 1990's that occurred due to reduced structural vigor and consequent stem lodging (e. g. failure). These effects and potential stressors raise questions about the possible feedback reactions that could occur as a result of changes in plant density and also encourage further study of the biomechanics of wetland vegetation.

Harley and Bertness (1996) examined the morphological and biomechanical effects of crowding (i.e. plants living in dense aggregations) on salt-marsh plants species, however no significant study has addressed this question for tidal freshwater marsh plant species. Thus, this pilot study focused on studying the effects of plant density on the morphological and biomechanical properties of wild rice (*Zizania aquatica*), a tidal freshwater marsh plant. *Zizania aquatica* is an annual, highly productive grass usually growing in shallow waters along the shores of rivers and streams in the central and eastern U.S. and Canada, often forming dense continuous stands (Whigham and Simpson 1977). Tidal freshwater marshes exist between non-tidal freshwater marshes and tidal saline wetlands (i.e. salt marshes). This ecosystem usually occurs in association with large estuarine/river systems and is characterized by an average annual salinity of 0.5 ppt. and high macrophyte diversity in comparison with salt marshes (Odum 1984). Tidal range may be greater in tidal freshwater systems than in salt marshes. For example, along the Potomac River, tidal range in typical salt marsh areas is approximately 70 cm, while the tidal freshwater marshes 100 km upstream experience a tidal range in excess of one meter (Odum 1988). In comparison to salt marshes, there has never been a broad research interest in tidal freshwater marshes. Limnologists ignore this ecosystem because of the presence of ocean tidal influence and marine scientists disregard them for the dominance of freshwater and freshwater species (Odum 1988). One of the major highlights of this ecosystem is its high productivity. Studies on salt marsh vegetation not only have shown that higher salinities lower primary production, photosynthesis and biomass in salt tolerant species, but also that vascular plants have to invest more energy to exclude salts and sulfides, therefore tidal freshwater marshes are likely to support a higher net primary production (Odum 1988).

Zizania aquatica is a dominant species in tidal freshwater marshes, especially in the low marsh zones. This plant has been the focus of various restoration efforts. Since the 1990's *Z. aquatica* has been under management at Jug Bay Wetlands Sanctuary in the Patuxent River, MD, USA because of population decreases attributed to grazing pressures of Canadian Geese (*Branta canadensis*). In terms of ecological services, wild rice (*Z. aquatica*) serves as an important source of food to wildlife such as birds, muskrats and other animals, and its decomposition is very important for the marsh's platform composition (Haramis and Kearns 2007). Seasonal variation in net production rates are present in this plant, seedling and flowering phenophases are characterized by relatively low net production (Whigham and Simpson 1977). The greatest net production rates occur in the growing season and studies suggest that approximately 65% of the biomass is allocated to the shoot system in this phenophase. Only during the seedling phenophase the highest percentage of biomass is

allocated below ground (Whigham and Simpson 1977). As an annual plant, wild rice depends on its flowering phenophase for survival. As a result in this phenophase most of the energy is used for inflorescence development leading to a decline in net production (Whigham and Simpson 1977). Plant density is the highest during seedling phenophase, but natural self thinning is experienced, as adult plants develop in the growing season populations can experience as much as a thirty-fold decrease in density (Weiner and Whigham 1988).

This study approached the importance of plant density on tidal freshwater wetlands vegetation with a focus on *Z. aquatica*. The major objective was to determine the effects of plant density on the morphological and biomechanical properties of *Z. aquatica*. A transect within wild rice populations of the Jug Bay Wetland Sanctuary was set for the purpose of manipulating plant density in order to explore the proposed objectives, directing all efforts to achieve a better understanding of tidal freshwater marsh's auto-ecology and possible feedback interactions brought about by sea level rise and associated changes in inundation.

Materials and Methods

To address the objectives of this study, a *Z. aquatica* population of the Jug Bay Wetlands Sanctuary component of the Maryland Chesapeake Bay National Estuarine Research Reserve was identified for experimental manipulation. In this tidal freshwater reserve *Z. aquatica* is known to be a dominant species in the low marsh zone (Weiner and Whigham 1988). With that in mind, in collaboration with a graduate student who is currently developing her Master's thesis project at Jug Bay, a transect was delineated in the low marsh zone through a stand dominated by *Z. aquatica*. For the purpose of this study, six (0.25 m^2) plots equally distributed between control and thinned plots (i.e. three control plots and three thinned plots) were established (Figure 1). To manipulate plant density the three treatment plots were thinned to 50% (~80 m^2) of the average of the control plot's plant density (160 m^2). In order to determine values for the biomechanical properties we studied in this project (i.e. modulus of elasticity, critical height, factor of safety), we estimated morphological and biomechanical characteristics that were used to parameterize the following equations.

The modulus of elasticity, a measure of the stiffness or resistance to deformation of a structure (Holbrook et al.1990) (i.e. plant stem) is defined as:

$$E = FL^3/(3DI), \quad (1)$$

where *E* is the modulus of elasticity, *F* is the bending stress, *D* is the stem deflection and *I* is the second moment of area. The bending stress (*F*) is the force, measured in Newtons (N), applied to deflect the stem. The bending stress (*D*) is the distance the stem deflects from a starting point and the length (*L*) is the plant's overall height. The second moment of area (*I*) is the contribution of the stem's shape to the structural support of the plant (Harley and Bertness 1996) and is defined as:

$$I = \pi\left[\mathrm{ab}^3 - \mathrm{cd}^3\right]/4, \quad (2)$$

where *a* and *b* are respectively the larger and smaller external radii of a hollow elliptical stem and *c* and *d* are the larger and smaller internal radii, respectively as shown in Figure 2 (Harley and Bertness 1996). Variables c and d are not considered in the equation if the cross-section of the stem is a solid surface.

The modulus of elasticity is required to calculate the critical height (H_{crit}), which is defined as the theoretical maximum height a structure can reach before collapsing under its own weight:

$$Hcrit = \mathrm{C\ x}\ \left(\frac{\mathrm{E}}{\rho \mathrm{g}}\right) \mathrm{X}\ (\mathrm{R}^{\frac{2}{3}}) \tag{3}$$

The critical height (H_{crit}), is determined by the following parameters: modulus of elasticity (*E*), the density of the stem material (ρ), the constant of gravitational acceleration (g), the stem's basal radius (R), and a constant relating to the taper of the column, the constant of proportionality (*C*). To incorporate a point load (e. g. crown or seed head) at the top of the stem the constant of proportionality (C) was defined as the ratio of crown to trunk weight determined empirically by fitting the following polynomial equation to the function C(k) (Harley and Bertnees 1996):

$$C\ (k) = \frac{0.007601 + 0.08655\ k + 0.334\ k^2}{0.001427 + 0.02907\ k + 0.1695\ k^2 + 0.6125\ k^3}^{1/3} \tag{4}$$

Given these values, we were able to calculate the factor of safety for control and thinned plots. The factor of safety describes the structural capacity of a system beyond actual or typical loads and is defined by:

$$Factor\ of\ safety = \frac{H\ actual}{H\ crit} \tag{5}$$

This provides a quantitative description of the difference between plants actual height and its theoretical critical height. Plants whose actual height is close to their critical height have a low factor of safety making them more vulnerable to physical stress.

Morphological Measurements

Laboratory measurements were done to determine morphology. These include plant height (cm) (*L*), crown height (cm) (C), stem basal radius (mm) (*R*), second moment of area (cm) (*I*), and tissue density (g/m^3) (ρ). A caliper was used to measure stem basal radius (R). For plants that had a crown the crown's dry weight was measured to obtain the constant of proportionality (C). To determine tissue density (ρ) a piece of stem was collected and its volume and dry weight was measured. Parameters to obtain the second moment of area (*I*) were estimated measuring the larger and smaller external and internal radii of the stem with a ruler. All these parameters were used in the calculation of the modulus of elasticity (1) and the critical height (2).

Biomechanical Measurements

Biomechanical measurements included the bending stress (F from (1)) and stem deflection (D from (1)), five plants from each plot (a total of 30 plants) were subjected to these measurements. Efforts made to measure these parameters in the field and to repeat protocols done in previous studies (Harley and Bertness 1996; Holbrook 1991) were unsuccessful and a new protocol was developed. Figures 3 and 4 provide a photo and drawing of the apparatus used to make these measurements in the laboratory. Using a spring scale attached to the stem at a distance of 5 cm from the sediment surface the plant stem was pulled to measure the bending stress (F from (1)) in Newtons (N). The average tidal depth at the study site where plants were collected was 15 cm. The stem deflection (D from (1)) was measured with the ruler

as pictured in Figures 3 and 4. Both parameters were measured at different bending angles. Measurements were done with the plant on a vertical position as shown in Figure 4. Paired t-tests were used to test differences in morphological variables and derived biomechanical characteristics. A significance level of $P < 0.05$ was used to determine significance.

Results

Our results report differences between the morphological and biomechanical characteristics of control and thinned *Z. aquatica* plots. Figure 5 shows that plants within the control plots grew taller than plants within the thinned plots. Figure 6 shows that the plants within the control plots developed thicker stems than plants that experience the thinning of their neighbors. The modulus of elasticity was higher for the plants in the thinned plots implying that the plants within this population were stiffer than the control plants, as shown in Figure 7. Figure 8 displays that control plants grew closer to their theoretical critical height, making them more vulnerable than thinned plants to physical stress. As a result plants from the thinned plots had a higher factor of safety as Figure 9 displays. Differences between control and thinned plots were significantly different ($P < 0.05$) for overall plant height, basal diameter and modulus of elasticity comparisons, while critical height and factor of safety comparisons were not found to be significantly different.

Discussion

Our results show that plant density plays a role in the way *Z. aquatica* develops throughout the growing season and that *Z. aquatica* populations growing at lower plant densities are structurally more reliable. However, we want to emphasize that the results from this study are preliminary. Our sampling intensity was lower than would be needed to statistically determine significant differences in a population with such high inherent variability. This lack of statistical power is likely responsible for the high variability evident in our results. Future studies would benefit from more intensive sampling.

Despite these limitations, there were several interesting findings regarding Harley and Bertness (1996) study. Plants within the control population grew significantly more than the thinned population plants but also developed significantly thicker stems. As in Harley and Bertness (1996) study, we were expecting the control plants to have taller heights but also thinner stems. This is because a short height, thicker stem morphology is more appropriate if the neighbor's structural support is lost. It seems like *Z. aquatica* responded to the lost of neighbors by limiting its height. If this assumption is correct, a question arises: Why did the plants not develop thicker stems as a response to losing structural support?

Overall, the modulus of elasticity values reported in this study are approximately double the values reported by Harley and Bertness (1996). If we compare *Z. aquatica's* morphology with the plants studied by Harley and Bertness (1996) (*Spartina alterniflora, Juncus gerardi, Iva frutescens* and *Salicornia europaea*) this makes sense: with a naked eye the morphological difference between *Z. aquatica* and these group of plants can be distinguished. *Zizania aquatica* is much more robust and taller, and has a thicker stem. Opposite to what Harley and Bertness (1996) found, for this study, plants within the thinned population had a significant higher modulus of elasticity. Having a stiffer stem increases the critical height (Harley and Bertness 1996) making it a positive characteristic for plants who have less structural support from neighbors. The *Z. aquatica* thinned plots in general were more mechanically reliable than the control plots, the plants from the control plots grew closer to their critical height. As a result, plants within the thinned population had a bigger factor of safety. This coincides with Harley and

Bertness (1996) assumption that isolated plants have to invest more heavily in structural support, because they lost structural support provided by their neighbors.

As discussed before, future studies have to be done to further explore these questions. Various modifications should be done to enhance the quality of our results. Since the biomechanical measurements were done in a laboratory setting, I suggest developing a field-friendly protocol to estimate these parameters, since this will provide more realistic measurements. Monitoring the natural forces (e.g. wind forces, tidal forces) within the study site will also be a way of getting a higher quality data.

Conclusion

While this study had several limitations, I believe we can still conclude that plant density influences *Z. aquatica* morphologically and biomechanically. This study also suggests that removing neighbors from *Z. aquatica* makes it invest more heavily in structural support, enhancing mechanical reliability of the stems. Our results give a clue of the response of this species to a scenario which they may grow under lower plant densities, but future studies have to be done to confirm our findings. A decrease in plant density could force *Z. aquatica* to invest more energy in structural support, thereby negatively affecting functions such as reproduction and sedimentation rates that are vital for the sustainability of its population and habitat.

Acknowledgements

First of all, I thank the National Science Foundation for funding this excellent REU program for so many years. I also acknowledge Maryland Sea Grant and Chesapeake Biological Laboratory for all the facilities and resources. To my mentor Dr. Lora Harris, thanks for all your support, assistance and tips throughout all this process. I thank Jennifer Bryan for all the comments, support, tips and field assistance. Last but not least, I thank all the folks who provided field assistance, lab assistance, comments and support.

References

Anten, N.P.R., R. Casado-Garcia, and H. Nagashima. 2005. Effects of mechanical stress and plant density on mechanical characteristics, growth, and lifetime reproduction of tobacco plants. The American Naturalist 166:650-660.

Ashby, W.C., C.A. Kolar, T.R. Hendricks, and R.E. Phares. 1979. Effects of shaking and shading on growth of three hardwood species. Forest Science 25:212–216.

Bertness, M.D., and R. Callaway. 1994. Positive interactions in communities. Trends in Ecology and Evolution 9:191-193.

Greenhill, A.G. 1881. Determination of the greatest height consistent with stability that a vertical pole or mast can be made, and the greatest height to which a tree of given proportions can grow. Proceedings of the Cambridge Philosophical Society 4:65-73.

Haramis, G., and G.D. Kearns. 2007. Herbivory by resident geese: The loss and recovery of wild rice along the tidal Patuxent River. The Journal of Wildlife Management. 71:788-794.

Harley, C.D.G., and M.D. Bertness. 1996. Structural interdependence: an ecological consequence of morphological responses to crowding in marsh plants. Functional Ecology 10: 654-661.

Henry, H.A.L., and S.C. Thomas. 2002. Interactive effects of lateral shade and wind on stem allometry, biomass allocation and mechanical stability in *Abutilon theophrasti* (Malvaceae). American Journal of Botany 89:1609–1615.

Holbrook, N. M., M.W. Denny, and M.A.R. Koehl. 1991. Intertidal “trees”: consequences of aggregation on the mechanical and photosynthetic properties of sea-palms *Postelsia palmaeformis* Ruprecht. Journal of Experimental Marine Biology 146:39-67.

Mitsch and Gosselink. 2000. Wetlands, 3rd edition. New York: John Wiley & Sons, Inc.

Morris, J.T., P.V. Sundareshwar, C.T. Nietch, B. Kjerfve, and D.R. Cahoon. 2002. Responses of coastal wetlands to rising sea level. Ecology 83:2869-2877.

Niklas, K.J., and H. Spatz. 1999. Methods for calculating factors of safety for plant stems. The Journal of Experimental Biology 202:3273-3280.

Odum, W.E., T.J. Smith III, J.K. Hoover, and C.C. McIvor. 1984. The ecology of tidal freshwater marshes of the United States east coast: A community profile. U.S. Fish and Wildlife Service FWS/0BS-83/17. 177pp.

Odum, W.E. 1988. Comparative ecology of tidal freshwater and salt marshes. Annual Review of Ecology and Systematics 19:147-176.

van der Putten, W.H. 1997. Die-back of *Phragmites australis* in European wetlands: An overview of the European Research Programme on Reed Die-back and Progression (1993-1994). Aquatic botany 59:263-275.

Weiner, J., and D.F. Whigham. 1988. Size variability and self-thinning in wild-rice (*Zizania aquatica)*. American Journal of Botany 175:445-448.

Whigham, D., and R. Simpson. 1977. Growth, mortality, and biomass partitioning in freshwater tidal wetland populations of wild rice (*Zizania Aquatica var. aquatica)*. Bulletin of the Torrey Botanical Club 104:347-351.

Woodward, R.T., and Y. Wui. 2001. The economic value of wetland services: A meta-analysis. Ecological Economics 37:257-270.

Figures and Tables

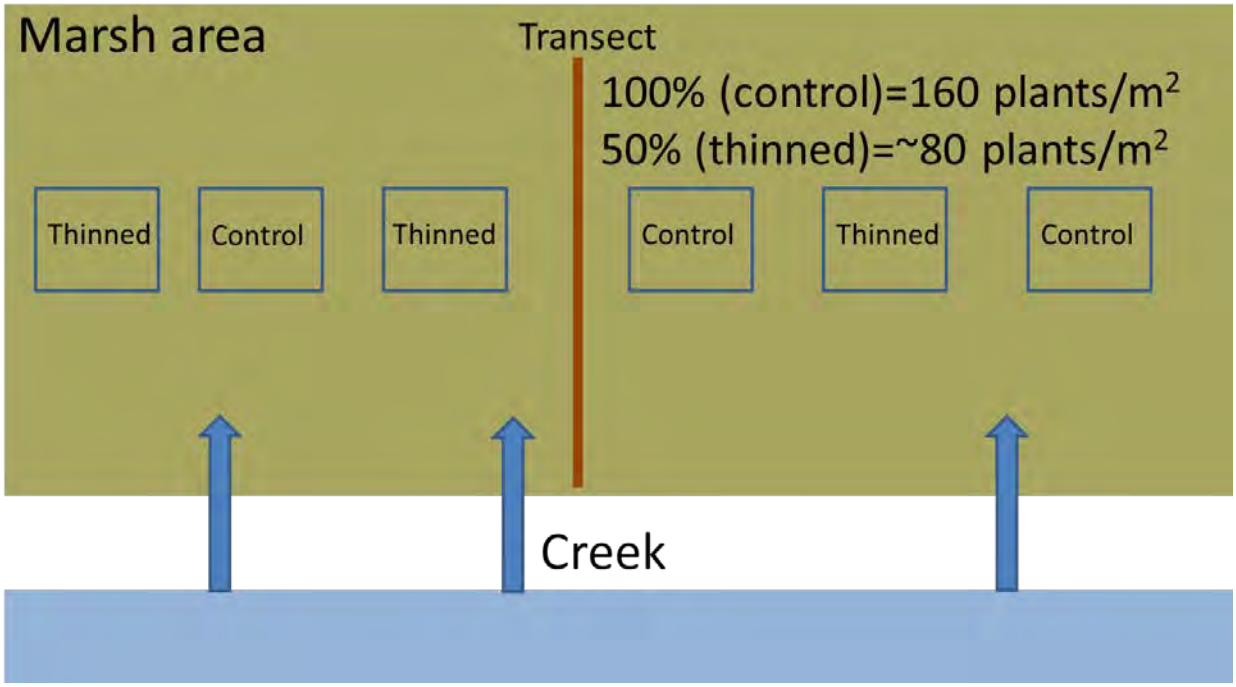

Figure 1. A diagram of the transect established at the study site. The squares with the blue borders represent the plots.

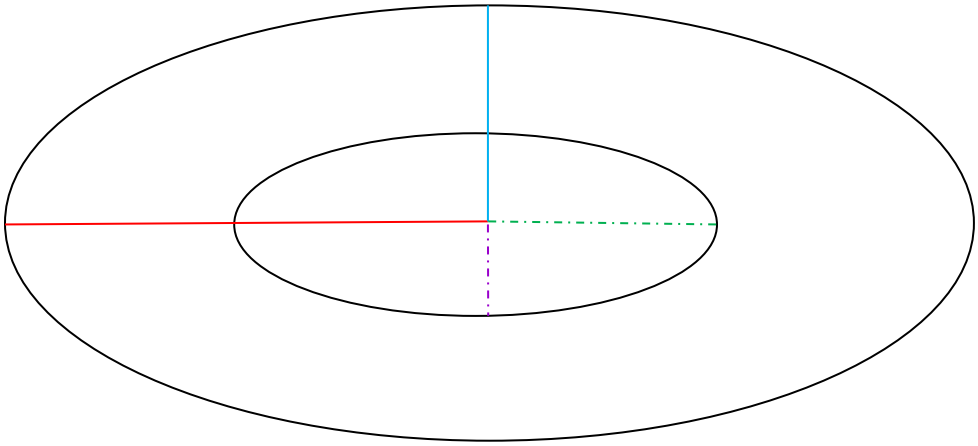

Figure 2. Diagram of a hollow elliptical stem where the red line is *a*: the larger external radii, the blue line *b*: the smaller external radii. The green dashed line is *c*: the larger internal radii and the purple dashed line is *d*: the smaller internal radii.

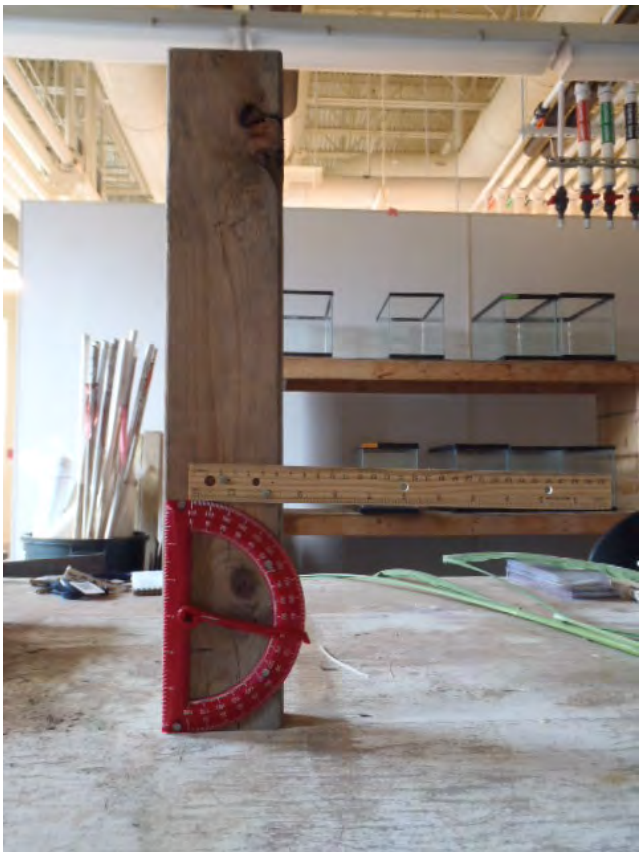

Figure 3. Stand constructed to measure bending stress and stem deflection at different angles.

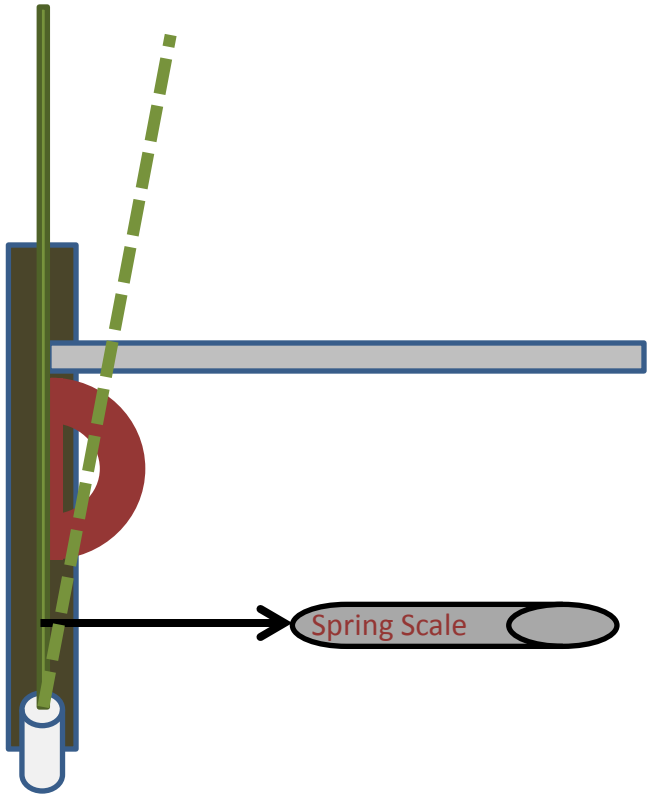

Figure 4. Diagram representing the protocol developed to measure bending stress and stem deflection.

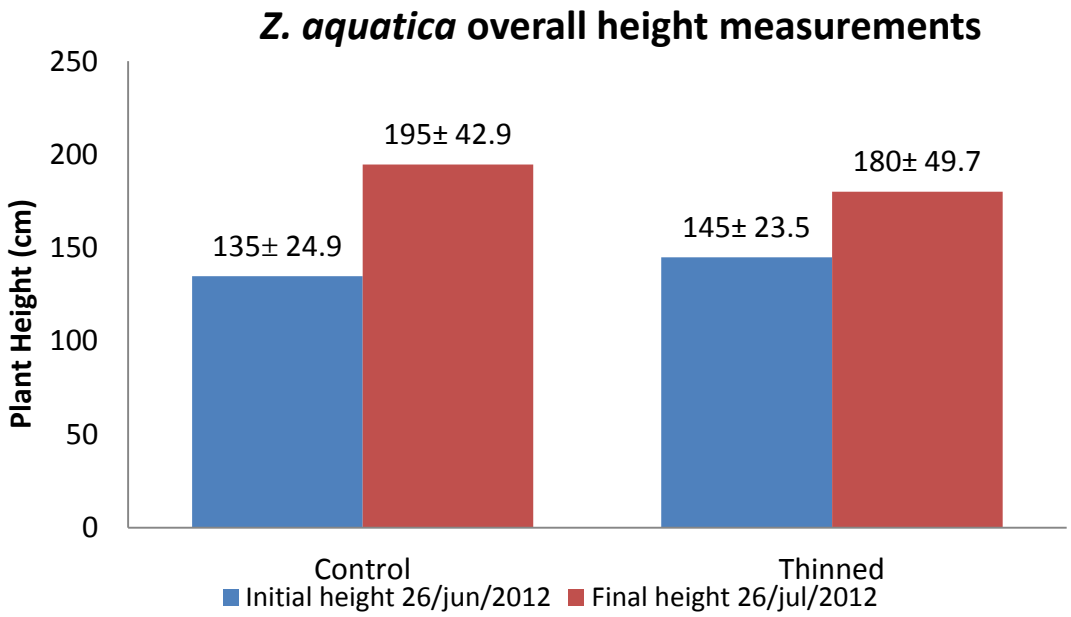

Figure 5. Initial and final mean height for control and thinned plots. Data is the mean of all harvested plants (n=158). Both datasets are statistically different $P < 0.05$. Numbers are for mean ± standard deviation.

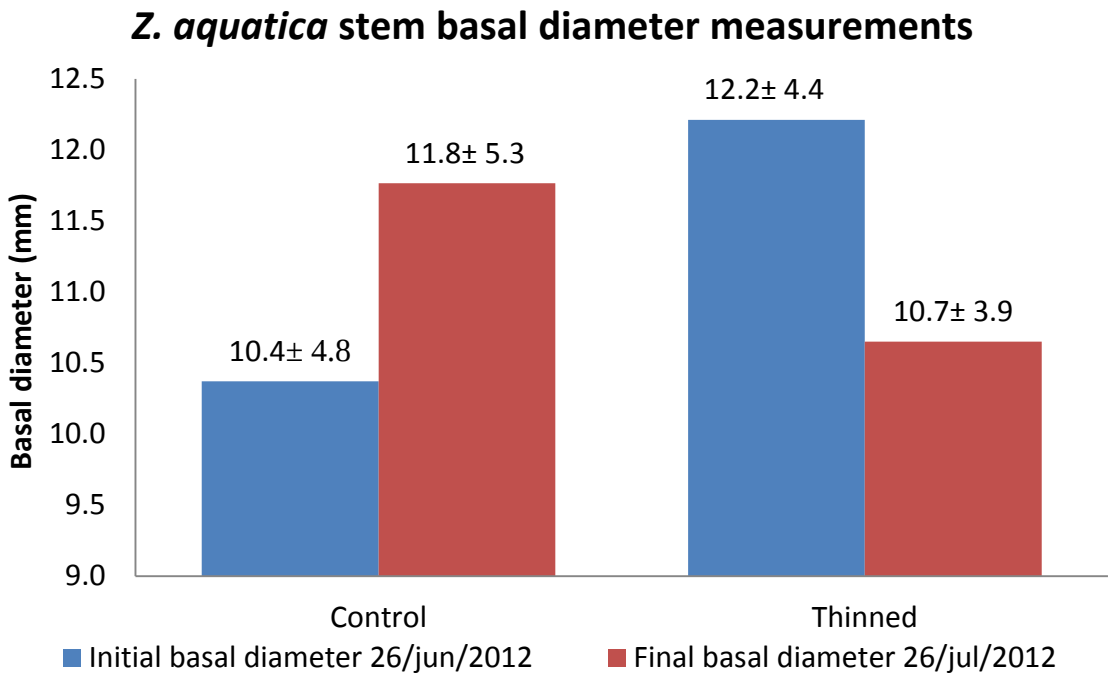

Figure 6. Initial and final mean basal diameter for control and thinned populations. Data are the mean of all harvested plants (n=158). Both datasets are statistically different P < 0.05. Numbers are for mean ± standard deviation.

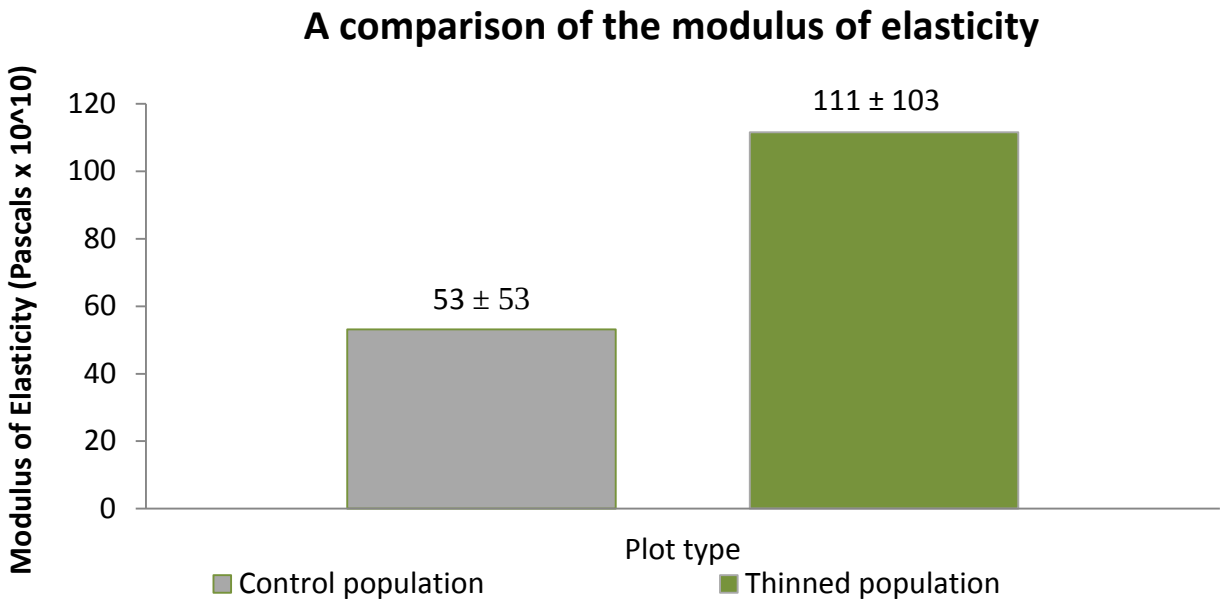

Figure 7. The modulus of elasticity for control and thinned plots. The data is the mean of a subsample (n=29). Both datasets are statistically different P < 0.05. Numbers are for mean ± standard deviation.

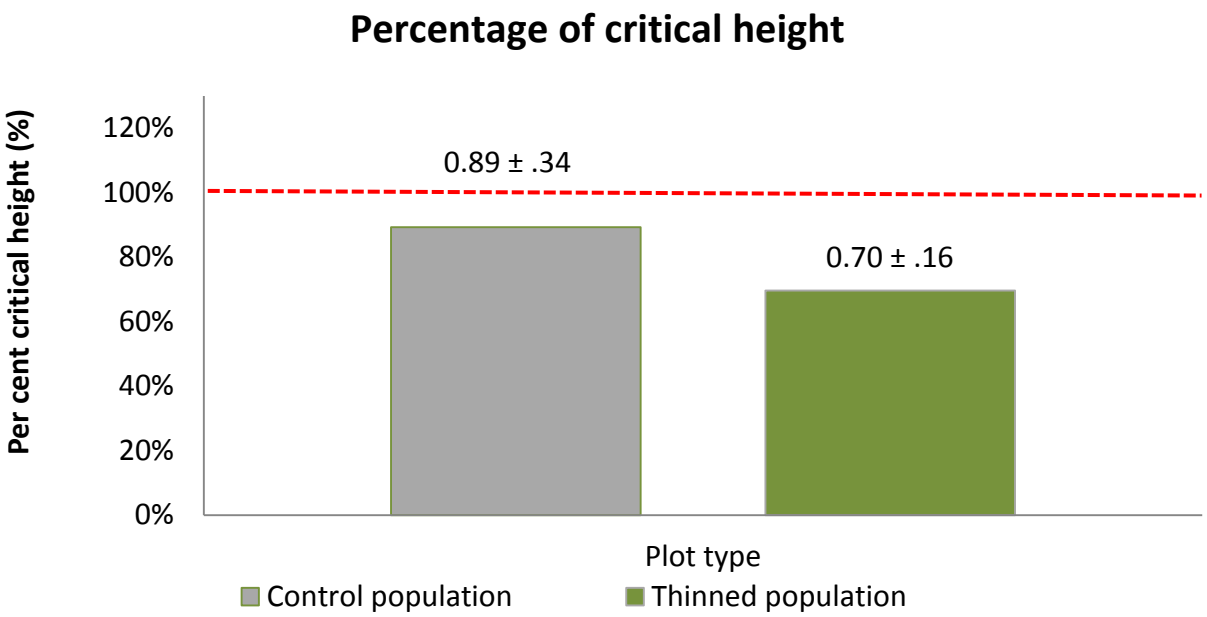

Figure 8. Percent of critical height for control and thinned plots. The data is the mean of a subsample (n=29). Datasets are not statistically different P > 0.05. Numbers are for mean ± standard deviation.

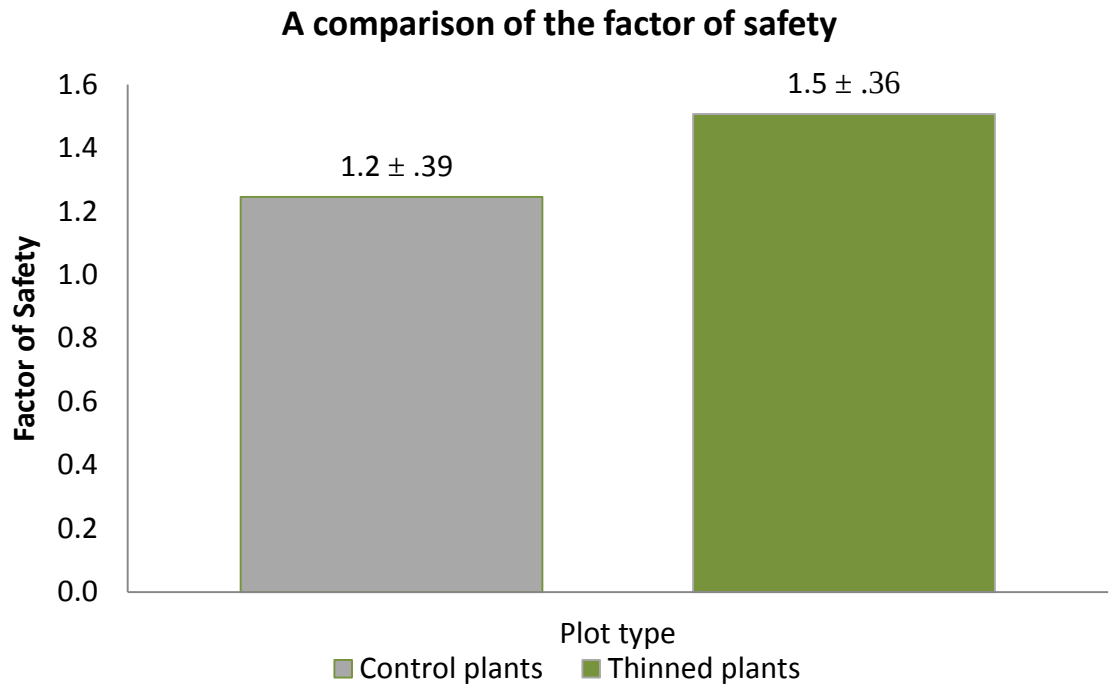

Figure 9. Factor of safety for control and thinned plots. The data is the mean of a subsample (n=29). Datasets are not statistically different P > 0.05. Numbers are for mean ± standard deviation.

Stability of Ni(II) and Cu(II) Complexes with Desferrioxamine B at Seawater Ionic Strength

Kailee Potter, REU Fellow
Maryland Sea Grant

Dr. Johan Schijf, Associate Professor
Chesapeake Biological Laboratory, University of Maryland Center for Environmental Science

Emily Christenson, Graduate Research Assistant
Chesapeake Biological Laboratory, University of Maryland Center for Environmental Science

Abstract

In oceanic systems, microorganisms secrete siderophores to facilitate the uptake of Fe(III) which is a scarce and essential nutrient. Siderophores are capable of binding to metal ions other than Fe^{3+}. In this research, desferrioxamine B was used as a representative siderophore and the stability constants for its complexation with Cu^{2+} and Ni^{2+} were determined at seawater ionic strength (0.7 M). Stability constants, log β_1, log β_2, and log β_3 for the Ni–DFOB complex were found to be 4.65±0.04, 7.72±0.03, and 9.76±0.07, respectively. Stability constants for Cu(II), log β_1 and log β_2, were determined to be 7.86±0.06 and 13.09±0.04, respectively, but log β_3 could not be resolved from titration data in the presence of excess DFOB, indicating that Cu^{2+} does not form a bond with the third hydroxamate group of the siderophore.

Keywords: Desferrioxamine B, Copper, Nickel, Stability constants.

Introduction

Iron is important in the metabolic processes of all bacteria (Butler and Theisen 2010). It is typically present in seawater in minute concentrations, due in part to the low solubility of Fe(III). To facilitate the uptake of iron, microorganisms secrete chelating organic molecules called siderophores. The siderophores bind tightly to Fe(III) and the microorganisms recover the complex and extract the metal. Although siderophores complex strongly with Fe(III), they can bind to other metals as well. This property may enable the use of siderophores in metal remediation, recovery and waste reduction (Hernlem et al. 1996). Siderophores are a large group of molecules about which relatively little is known. An exception to this is desferrioxamine B (DFOB).

DFOB is a naturally occurring molecule that has been synthesized and utilized as a treatment for human iron overload disorders (Bernhardt 2007). It is currently the only siderophore commercially available in macroscopic quantities. As such, it is commonly used in research experiments as a representative siderophore molecule (Christenson and Schijf 2011). DFOB (Figure 1) has three hydroxamate groups. When a proton is displaced from the

hydroxamate group, its oxygen atoms become negatively charged and form a bidentate bond with the metal, as is shown in Figure 2.

Bruland (1980) determined metal concentration profiles for Cu and Ni as a function of depth in the northern Pacific Ocean. Graphs of these Cu and Ni profiles can be seen in Figure 3 and Figure 4, respectively. Nickel has a concentration profile that resembles that of phosphate at shallow depths and shifts to more closely resemble the silicate profile below 800 m. This indicates that Ni may go through similar cycling processes as phosphate and silicate. Copper has a rather unique profile since its concentration increases almost linearly with depth. These distribution profiles are determined not only by physical processes such as mixing and sedimentation but also by speciation. Speciation refers to what chemical form the metal is in i.e., if it is complexed and what it is complexed with. The speciation of metals determines their bioavailability. In the surface water, above 200 m, it was determined that greater than 99.7% of Cu is complexed with organic ligands (Coale and Bruland 1988). They reported stability constants of 11.5 and 8.5 for two separate organic ligands. However the identity of these organic compounds remains unknown. The values reported by Coale and Bruland (1988) are similar to the stability constants determined by Hernlem et al. (1996) for the Cu–DFOB complex which suggests that the unknown ligand might be siderophore-like. However, the constants determined by Hernlem et al. (1996) were not measured at seawater ionic strength. If Cu is complexed with siderophore-like molecules it may increase its bioavailability.

Copper–DFOB complexes are of particular interest because while Cu is a micronutrient it can also be toxic. For instance, it is required for several enzymes including cytochrome oxidase and plastocyanin. However, studies done by Brand et al. (1986) show that high levels of Cu inhibit the growth of algae. This is thought to occur by Cu acting as a competitive inhibitor of enzymes which typically bind to other metals such as Fe and Mn (Coale and Bruland 1988). Hernlem et al. (1996) reported a stability constant for Cu–DFOB complex formation of 13.73, corresponding to the fully complexed metal (i.e., all three hydroxamate groups are bound to the metal). Although this constant was determined in a 0.1 M $NaClO_4$ solution and our experiments were done in a 0.7 M $NaClO_4$ solution, the constants were expected to be similar.
Nickel is an understudied metal especially as a constituent of marine systems. Farkas et al. (1997) reported values of the Ni–DFOB complex stability constants, but due to inconsistencies in their reported metal–DFOB speciation model, their stability constants for Cu–DFOB are different from those of Hernlem et al. (1996) and their values for Ni–DFOB are therefore similarly unreliable.

The two objectives of this research are as follows:

1) Determine the stability constant of the Cu–DFOB complex at seawater ionic strength.
2) Determine the stability constant of the Ni–DFOB complex at seawater ionic strength.

Materials and Methods

A specific methodology for the determination of stability constants of DFOB–YREE complexes was described by Christenson and Schijf (2011). Their method was employed for this research. Christenson and Schijf furthermore determined pK_a values for the three hydroxamate protons of DFOB which were also utilized. The pK_as are the dissociation constants i.e. the average pH at which protons are added or removed from the hydroxamate groups of DFOB. When the metal of interest is added, based on the affinity of DFOB for the metal, the titration curve will shift with respect to the initial titration curve of pure DFOB due to a proton being ejected sooner than it typically would be, because it is being forced off by the metal. Examples of this can be seen in Figure 5. For each metal, titrations were performed at three

different M–DFOB ratios (1:2, 1:4, and 0.7:1) and each titration was performed twice. Desferrioxamine B was purchased as the mesylate salt ($C_{25}H_{48}N_6O_8 \cdot CH_3SO_2OH$, ~95%) from Sigma-Aldrich and was used without further purification (stored at –32°C). Stock solutions of 40 mM DFOB were prepared daily in 0.7 M $NaClO_4$ ($NaClO_4 \cdot xH_2O$, 99.99%, Sigma-Aldrich) in acid-washed Teflon vials. Titrant reagents of NaOH (0.1001 M or 1.0005 M, certified) were obtained from Brinkmann and stored in polypropylene bottles. Background electrolyte solutions (1 L) of 0.7 M $NaClO_4$ ($NaClO_4 \cdot xH_2O$, 99.99%, Sigma-Aldrich) were prepared by determining the molar concentration from the density using the equation of Janz et al. (1970). The pH standard for calibrating the glass electrode of the autotitrator was made by dissolving sodium chloride (NaCl, 99.999%, Sigma-Aldrich) in Milli-Q water to obtain a solution of 0.70 M and its pH was set to 3.000 by the addition of certified hydrochloric acid (HCl, 1.0011 M, Brinkmann). Stock solutions of 40 mM copper(II) perchlorate hexahydrate ($Cu(ClO_4)_2 \cdot 6H_2O$ 99.999%, Alfa Aesar) and 40 mM nickel(II) perchlorate hydrate ($Ni(ClO_4)_2 \cdot xH_2O$, 99.998%, Alfa Aesar) were prepared in 0.7 M $NaClO_4$ and analyzed via ICP-MS (Agilent 7500cx) to determine exact concentrations.

A Brinkmann Metrohm 809 Titrando autotitrator and accompanying Tiamo software were utilized to perform all potentiometric titrations. The DFOB and Cu or Ni solution started at a pH of 3 and were titrated with 0.1001 M NaOH until a pH of 10 was reached. The base was added using a Metrohm 800 Dosino precision syringe drive in combination with a 2 mL (1.0005 NaOH) gas-tight burette. Titrations were performed in jacketed glass reactors with a circulating water bath (LAUDA-Brinkmann RE-106) to maintain a constant temperature of 25.0°C (± 0.1°C). During the titration the reaction vessel was sealed and sparged with N_2 gas to prevent the formation of carbonate from the dissolution of CO_2. The N_2 gas was continuously bubbled into the solution throughout the titration. A glass combination electrode (Metrohm) was used to measure the pH of the solution. Prior to each titration the electrode was calibrated and the internal electrolyte (3 M NaCl) was replaced daily. To make the experiments more closely conform to metal behavior in the ocean, titrations were conducted in a 0.7 M $NaClO_4$ solution which has the same ionic strength as seawater. Perchlorate, which is inert, was used instead of Cl^- because metals form complexes with Cl^- which would complicate the data regression. The final titration data consisted of a list of incremental titrant volumes and mV readings, which was exported into Excel format. Titration data were analyzed using the computer program FITEQL 4.0 to determine the final stability constants of the Cu–DFOB and Ni–DFOB complexes.

Results

The stability constants (log β) for Ni–DFOB complex were found to be 4.65±0.04, 7.72± 0.03, and 9.76±0.07. The stability constants (log β) for Cu–DFOB complex were determined to be 7.86±0.06, and 13.09±0.04. A value of log β_3 could not be determined from the regressions. The data are summarized in Table 1.

Figure 5 shows the titration data for both Cu and Ni and pure DFOB. Early in the titration the Cu curve deviates more from the DFOB than the Ni does. Nearer the end of the titration the curves cross over. The deviation in the curves corresponds to the metals' abilities to eject protons from the DFOB.

Discussion

For the Cu–DFOB complexes, the titration data were initially fit assuming that the Cu would bind with all three hydroxamate groups yielding three log β values. Using this model, the titration data for the smallest ratio of Cu–DFOB did not converge even when the number of iterations was increased from 100 to 150. Also, the log β_2 and log β_3 values were unrealistically

close together. All of the Cu–DFOB data were refit omitting the fully coordinated $CuHDFOB^0$ species. With the new model all of the data converged with fewer iterations. Hernlem et al. (1996) reported three log β values for Cu and the log β_2 and β_3 values are close to one another. The log β_2 determined in this work lies between the log β_2 and β_3 reported by Hernlem et al. (1996). The log β_1 value found in this work agrees closely with the value reported by Hernlem et al. (1996).

The study done by Coale and Bruland (1988) described two classes of Cu binding ligands in the ocean. One of the classes is present in surface waters in nanomolar concentrations and decreases as a function of depth. This class binds strongly to Cu and has a stability constant of 11.5. The stability constant determined in this work for the Cu–DFOB complex was 13.09. These values are relatively close and coupled with the aforementioned characteristics suggest that this class of ligands may be siderophores or siderophore-like molecules.

In the classic paper by Anderegg et al. (1963) the stability constants for Ni were determined to be 4.36, 7.70, and 10.90. The constants determined in this work agree with the constants determined by Anderegg et al. (1963) with the largest deviation being between the log β_3 values. As was explained by Hernlem et al. (1996), the latter is likely due to the fact that Anderegg et al. (1996) were unable to determine the value of pK_{a4}, which made it impossible for them to properly account for all proton release.

As shown in Figure 5, the early and significant deviation in the Cu curve from the DFOB curve indicates a strong complexation of Cu with the first hydroxamate group. Ni also deviates early in the titration although not as significantly, indicating a less strong complex. Nearer the end of the titration, Ni exhibits greater deviation than Cu. Although Ni does not bind as tightly to DFOB it displaces all three hydroxamate protons. Cu binds tighter, but the data suggest that it is unable to eject the third proton.

Conclusions (Anticipated Benefits)

Siderophores are ubiquitous in the surface waters of the ocean and yet relatively little is known about them. The Cu–DFOB stability constants determined in this study suggest that siderophores may be part of a class of previously unidentified organic ligands that complex strongly with Cu in the surface waters of the ocean. It is becoming more apparent that trace metals have a strong influence on the productivity of phytoplankton and vice versa. Phytoplankton plays a major role in the exchange of CO_2 between the atmosphere and the ocean which has important implications for global warming.

The next step in the research is to input the stability constants determined in this work into a metal speciation model such as MINEQL. These data could be useful in developing better metal speciation models and in the explanation of the profiles observed for dissolved metals in the oceans. Cu is more reactive as evidenced by its low free metal concentration in the surface waters and its gradual increase in concentration as it moves down the water column. The higher reactivity increases the probability that Cu will react with siderophores. This is supported by the relatively high stability constant determined for Cu. Understanding the bioavailability of these metals may also add clarity to the movement of metals within the ocean.

References

Anderegg, G., F. l'Eplattenier, and G. Schwarzenbach. 1963. Hydroxamatkomplexe II. Die Anwendung der pH-Methode. Helvetica Chimica Acta 46:1400-1408.

Christenson, E.A., J. Schijf. 2011. Stability of YREE complexes with the trihydroxamate siderophore desferrioxamine B at sea water ionic strength. Geochimica Cosmochimica Acta 75:7047-7062.

Bernhardt, P.V. 2007. Coordination chemistry and biology of chelators for the treatment of iron overload disorders. Dalton Transactions 3214-3220.

Bruland, K.W. 1980. Oceanographic distributions of cadmium, zinc, nickel, and copper in the North Pacific. Earth and Planetary Science Letters 47:176-198.

Butler, A. and R.M. Theisen. 2010. Iron(III)–siderophore coordination chemistry: reactivity of marine siderophores. Coordination Chemistry Reviews 254:288-296.

Coale, K.H. and K.W. Bruland. 1988. Copper complexation in the Northeast Pacific. Limnology and Oceanography 33:1084–1101.

Farkas, E., H. Csóka, G. Micera, and A. Dessi. 1997. Copper(II), Nickel(II), Zinc(II), and Molybdenum(VI) complexes of desferrioxamine B in aqueous solution. Journal of Inorganic Biochemistry 65:281-286.

Gould, B.L., and N. Langerman. 1982. A thermodynamic description of the binding of iron to ferrioxamine b in aqueous solutions. Archives of Biochemistry and Biophysics 215:148-156.

Hernlem, B.J., L.M. Vane, and G.D. Sayles. 1996. Stability constants for complexes of the siderophore desferrioxamine B with selected heavy metal cations. Inorganica Chimica Acta 244:179-184.

Janz, G. J., B.G. Oliver, G.R. Lakshminarayanan, and G.E. Mayer. 1970. Electrical conductance, diffusion, viscosity, and density of sodium nitrate, sodium perchlorate, and sodium thiocyanate in concentrated aqueous solutions. Jounal of Physical Chemistry 74:1285-1289.

Figures and Tables

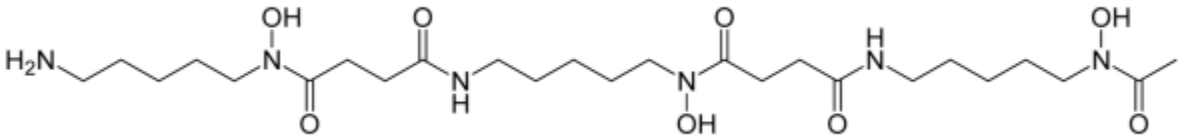

Figure 1. Desferrioxamine B skeletal structure.

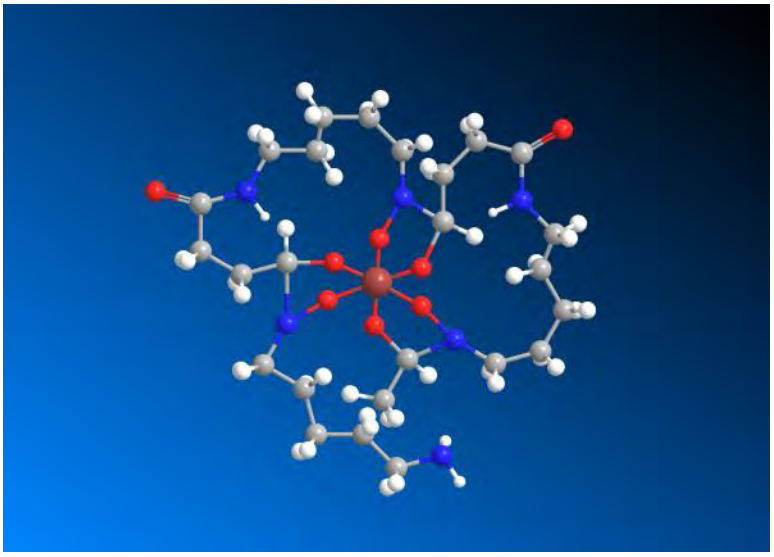

Figure 2. Desferrioxamine B complexed with iron.

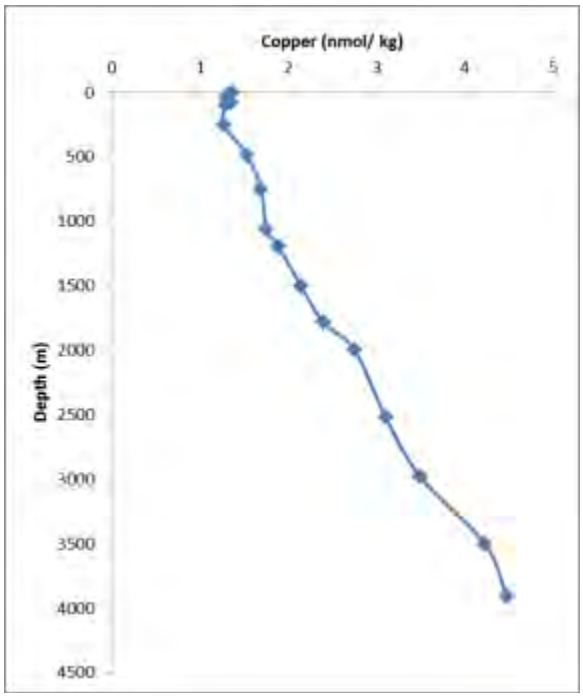

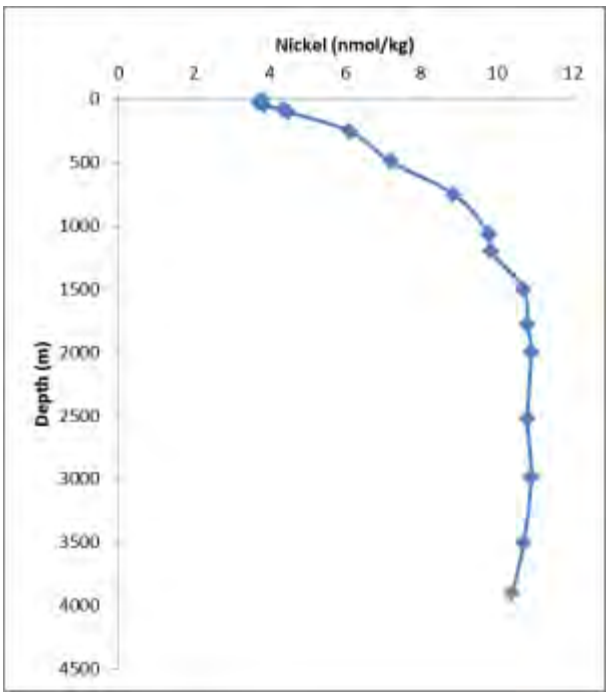

Figure 3 and 4. Ocean profiles of Cu and Ni. The data were taken from Bruland (1980).

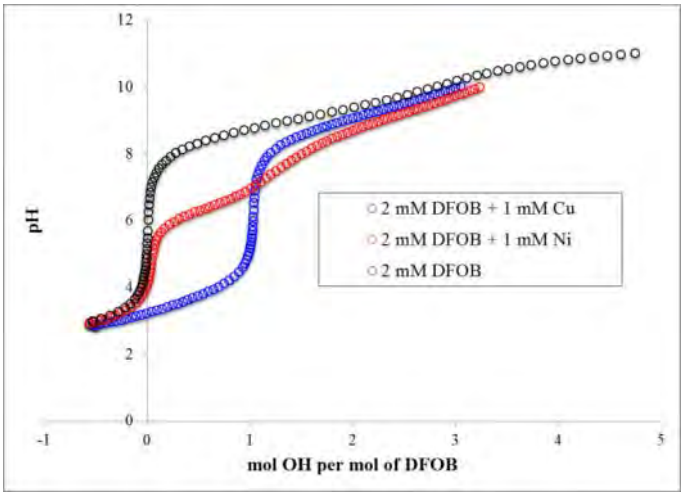

Figure 5. Titration curves for DFOB in the presence and absence of a metal. The data from the DFOB only curve were taken from Christenson and Schijf (2011).

Table 1. Summary of stability constants

Metal ion	log β_1	log β_2	log β_3
Fe (Gould and Langerman 1982)	10.5	21.84	30.60
Cu (This work)	7.86±0.06	13.09±0.04	–
Cu (Hernlem et al. 1996)	7.66	12.94	13.54
Ni (This work)	4.65±0.04	7.72±0.03	9.76±0.07
Ni (Anderegg et al. 1963)	4.36	7.70	10.90

Characterizing the Distribution of Methane Flux from Sediment to the Water Column in the Chesapeake Bay

Steven Sheets, REU Fellow
Maryland Sea Grant

Dr. Laura Lapham, Assistant Professor
Chesapeake Bay Laboratory, University of Maryland Center for Environmental Science

Abstract

Methane production is the last stage of organic matter decay. Several microorganisms take part in organic matter decomposition, including aerobic bacteria, sulfate-reducing bacteria, and the methane-producing methanogens themselves. Another group of microorganisms, the methanotrophs, reverses this process of methanogenesis with methanotrophy, where sulfate is reduced and the methane is oxidized back into carbon dioxide. Methanotrophic activity determines methane flux, and sulfate availability determines methanotrophic activity. It was originally hypothesized that the Chesapeake Bay's salinity gradient should therefore control methane flux. The flux-salinity data did not support this idea, however; it actually showed flux increasing as salinity increased. Another possible hypothesis was developed: dissolved oxygen content may serve as a control over methane flux, rather than salinity. While methanotrophs oxidize methane anaerobically in the sediment, methane can also be oxidized aerobically by bacteria both in the top layer of the sediment or in the water column, provided there are oxic conditions. The Chesapeake Bay undergoes hypoxic conditions seasonally, during which times there should be increased methane flux. We did not acquire sufficient data to explore this possibility, so further study must be devoted to tracing methane's movement after it passes from the sediment into the water column.

Introduction

The simplest of the alkanes, methane is colorless and odorless, and it is the main component of natural gas. Methane is also a greenhouse gas, and it is almost 21 times more effective than CO_2 when it comes to trapping heat in the atmosphere. Records from the Energy Information Administration show that, although methane emissions make up only 1.1 percent of total U.S. greenhouse gas emissions, they are responsible for 8.5 percent of the greenhouse gas emissions based on global warming potential (http://www.naturalgas.org/environment/naturalgas.asp).

Common anthropogenic sources of methane emissions include landfills, coal mining, wastewater treatment and rice cultivation (http://www.epa.gov/methane/sources.html). Further sources include the waste management industry, the agricultural industry, as well as leaks and emissions from the oil and gas industry. There are natural sources as well, with wetlands, bogs, and swamps playing a significant role in the methane cycle. The process by which the methane is formed in these water bodies also applies to the Chesapeake Bay, which served as the area

of interest for this study. This study attempted to characterize the distribution of methane flux from the sediments to the water column in the bay and also to determine what factors played a role in the distribution.

The prevalent methane-forming process in the bay is known as methanogenesis, and it involves the production of methane by archaea microbes called methanogens. Methanogenesis is the final phase of organic matter decay and, being purely an anaerobic process, it can only occur in the parts of the seafloor sediment where oxygen has been depleted. Organic matter is essentially any material that can decay – typically the remains of once-living organisms. Plants, for example, play a vital role in the carbon cycle, converting solar energy and carbon dioxide (CO_2) into an organic carbon source that the plant can then use for food and energy. This carbon source becomes part of the plant and, when the plant dies, it is buried and becomes part of the soil sediment.

Methanogenesis can occur using both competitive and non-competitive substrates – a substrate being the reactant utilized by the bacteria that are breaking down the organic matter. This means that methanogenesis is a reduction-oxidation (REDOX) reaction; in order for organic matter to be oxidized, something else must be reduced (i.e. sulfate). Competitive substrates are of particular interest in this process, and in this case the competition is between the CO_2-consuming methanogens and sulfate reducing bacteria (SRB), which consume sulfate in addition to carbon-based compounds. Salt water is rich in sulfate due to oceanic weathering processes, so there is a higher concentration of sulfate available to SRB in marine sediments when compared to low-sulfate freshwater sediments.

As seen in Figure 1, organic matter (shown empirically as CH_2O) drifts to the sea floor, where it enters the sediment and goes through aerobic decomposition, releasing CO_2:

$$CH_2O + O_2 \rightarrow CO_2 + H_2O \quad (1)$$

When the oxygen in the sediment is depleted, aerobic decomposition stops and SRB begin to decompose the organic matter anaerobically through sulphate reduction, producing hydrogen sulfide (H_2S):

$$2\ CH_2O + SO_4^{2-} \rightarrow H_2S + 2HCO_3^- \quad (2)$$

Methanogens are outcompeted by the SRB – who also utilize hydrogen and carbon-based compounds in addition to sulfate – until the amount of dissolved sulfate available starts to become depleted (Oremland and Polcin 1982). When this happens, the SRB become inactive and the methanogens are free to take over, turning CO_2 into methane (CH_4) through the process of carbonate reduction (Whiticar 1999):

$$CO_2 + 4H_2 \rightarrow CH_4 + 2H_2O \quad (3)$$

A study conducted by Reeburgh (1969) found that, while there was no methane present in the upper 10-20cm of Chesapeake Bay sediments, the methane concentration increased with depth up to 150ml/liter – an increase no doubt due to the presence of methanogens. While the methanogens are busy producing methane through carbonate reduction, another group of microbes, known as the methanotrophs, are using methane oxidation to remove methane from the sediment. Methanotrophs are prokaryotes and can be found in aerobic or anaerobic conditions. In the deepest area of the sulfate-reduction zone, there is a window of opportunity

for the methanotrophs to become active. When active, they are able to oxidize the methane, using it as their only source of carbon in the following reaction:

$$CH_4 + SO_4 \rightarrow HS^- + HCO_3^{2-} + H_2O \quad (4)$$

Both SRB and methanotrophs occupy this part of the sulfate-reduction zone, which is shown as the shaded region of Figure 2. It should be noted that there is a much larger window for methanotrophs to become active in marine sediments than in freshwater sediments. This is once again due to the presence of sulfate, which is required for both SRB and the methanotrophs. The importance of this difference is that the anaerobic consumption of methane by methanotrophs controls the methane concentrations in oceanic sediments; it essentially controls the methane flux, or the flowing of methane out of the sediment, into the water column, and eventually into the atmosphere. For this reason, methanotrophs are sometimes said to act as a biofilter, due to their ability to capture and filter the methane. It is possible that freshwater sediments are not as effective as marine sediments when it comes to curtailing the release of methane into the water column, due to having a much smaller window for methanotrophs to consume the methane; this has not been proven, however.

Water in the Chesapeake Bay lies somewhere between freshwater and saltwater, meaning it contains a salinity gradient. Parts of the bay will therefore be high in sulfate, while others will not (Figure 3). I hypothesize that methane flux will vary according to the salt concentrations, with the highest methane fluxes being found in areas where salinities are lowest. For this project, I sought to collect sediment samples from several salinity regimes, measure the methane concentrations present in these areas, and use the data to calculate methane flux. I could then compare the methane flux data to salinity measurements from the water column and see if there was a trend. Given the geography of the bay area, the expectation was that that methane flux would be low in the southern parts of the bay, where the bay meets the ocean and there is an abundance of sulfate for methane oxidation. Moving north, methane flux was expected to get progressively higher as sulfate concentrations decreased, resulting in less methane oxidation in the sediment.

Objective

The primary objective of the study was to quantify the spatial distribution of methane flux from sediments to the water column within the Chesapeake Bay. In order to achieve this objective, sediment core samples were collected within the main stem of the bay. The samples were then used to measure methane and sulfate concentrations, which were then used to create depth profiles. Using the profiles, methane fluxes were calculated for each station using a combination of the gradients created from the stations' methane profiles, data acquired from porosity samples, and data acquired from CTD casts.

Hypothesis

Since sulfate availability determines methanotrophic activity, and methanotrophic activity determines methane flux, the salinity gradient present in the Chesapeake Bay should serve as a control over methane flux.

Methods

Field Work

A research cruise was utilized to collect 21 sediment box core and gravity core samples at various locations in the Chesapeake Bay (Figure 4). Sediment cores were taken for methane at all stations, with the exception of stations 9 and 10. Cores were taken for sulfate at stations 1, 2, 5, 6, and 7.

The sediment core liners had holes pre-cut into the sides, through which syringes were placed to take 3-mL sediment plugs (Figure 5). Using 3mL syringes with the tips cut off, 3mL mud samples were taken from the cores designated for methane testing and then stored in glass vials. For the other cores, 3mL pore water samples were extracted using syringes with rhizome filter attachments (Figure 6). These samples were also stored in vials.

Salinity, temperature and water depth information were collected for each station using a conductivity-temperature-depth (CTD) device. The device was lowered over the side of the research vessel and continuously measured these parameters down through the water column. The data were downloaded from the CTD computer and graphed for visual display (Figure 7).

Laboratory work

When preparing the samples for the methane concentration measurements, the sediment plugs were preserved with base (1M potassium hydroxide); the base effectively “killed” the sediment samples, causing all microbial activity to cease. When preparing the samples for sulfate concentration measurements, a 500uL subsample of the filtered pore water was taken and pipetted into a 2mL centrifuge tube pre-loaded with 50uL 1M H_3PO_4. The acid was used to degas any sulfide present in the sample, since sulfide could easily oxidize to form sulfate when being transferred to a vial for storage. If the sulfide had not been degassed, it might have contaminated the sample by artificially increasing the sulfate concentration.

To determine sulfate concentrations, 40uL of the preserved pore water samples were diluted with 5mL milli-Q water and then run on a Dionex ICS-1000 ion chromatograph. Concentrations were determined by comparing the area under the curves to areas obtained from various dilutions of seven-anion standard; dilutions included 1:1000, 1:500, 1:100, 1:10, 1:5, 1:4, 1:2, 3:4, and 1:1. An example of a standard curve obtained for sulfate measurements can be seen in Figure 8.

To determine methane concentrations, an SRI multi-gas gas chromatograph was used to run methane standards to obtain a standard curve; both 99.51ppm and 980.5ppm methane standards were utilized. The preserved sample vials were first injected with 10mL helium, which was then allowed to equilibrate with the samples. Once equilibrated, the headspace from the sample vials could be injected into the gas chromatograph. The injection volume varied based on the resulting methane concentrations. If the methane peaks were too high for the gas chromatograph to properly measure, a double-peak (shaped similarly to the letter “M”) would appear, but it would be representing a lower concentration than was actually present and was therefore inaccurate. Due to an abundance of these instances while sampling the cores from the first station, only the top four samples from each core were run for the subsequent stations. 3mL injections were typically used for the surface layer samples, while 1mL injections were used for the deeper, more concentrated layers. The areas of the unknown methane peaks were then

compared to those obtained from the methane standard injections in order to calculate the methane concentrations of the samples.

Calculations

Methane concentrations in parts per million (ppm) were calculated using the average peak areas of methane standards run at various injection volumes (3mL, 1mL, 0.5mL, or 0.25mL). Using both the 99.51ppm and 980.5ppm methane standards allowed the unknown methane concentrations to be calculated using a proportion to a methane standard of similar concentration.

The concentrations then had to be converted from parts per million to micromoles per liter (μmol/L, or μM). This was done with the following equation:

$\mu M\ CH_4 = (HS\ CH_4 + Water\ CH_4) / 0.0825 / 298 / (SedInj * \Phi) * 1000$, where
- $HS\ CH_4$ = amount of CH_4 in headspace in μL
- $Water\ CH_4$ = amount of CH_4 in water in μL
- 0.08205 = gas constant in L atm/mol K
- 298 = lab temperature in Kelvin
- SedInj = original volume of sediment stored in vial in mL
- Φ = Porosity

In order to calculate the amount of methane in the headspace and in the water, the following equations were used:

$HS\ CH_4 = ppm\ CH_4 * DF * (V_{vial} – V_{base}) / 1000$, where
- DF = headspace dilution factor
- V_{vial} = max volume of vials used for methane sample storage
- V_{base} = volume base added to sediment sample

$Water\ CH_4 = ppm\ CH_4 * (V_{vial} – V_{base}) / 1000 * 0.025$, where
- 0.025 = Bunsen solubility constant, corrected for salinity and temperature
  - *measurement of the volume of methane per volume of air
- V_{vial} = max volume of vials used for methane sample storage
- V_{base} = volume base added to sediment sample

The headspace dilution factor utilized in the first equation was calculated as follows:

$DF = (V_{vial} – V_{base} + V_{He}) / (V_{vial} – V_{mud})$, where
- V_{He} = volume helium added to closed methane sample vial
- V_{vial} = max volume of vials used for methane sample storage
- V_{base} = volume base added to sediment sample
- V_{mud} = volume mud sample taken from sediment core

In order to calculate porosity for the conversion from parts per million to micromolar for methane, separate porosity samples were taken periodically throughout the sediment core sampling process, and their depths were recorded along with the rest of the methane samples. The final porosity equation was as follows:

$\Phi = (R * 2.65) / ((R * 2.65) + ((1 – R) * 1.024))$
- R = ratio of seawater to wet sediment
- 2.65 = sediment density in g/cm

1.024 = saltwater density in g/mL

The porosity samples were weighed in their vials (the vials themselves were weighed prior to collecting the samples), dried in an oven for two days at 100°C and then weighed again. The weights of the sediment samples and the water were obtained by subtracting the vial weights from either the dry weights or the wet weights. The weight of the water and sediment combined was also recorded.

Seawater weight was calculated by multiplying the original water weight by a saltwater density of 1.024. The weight in grams of the salt in the seawater was then calculated as follows:

Salt = (seawater * salinity) / 1000

Salinity data was obtained from the CTD casts at each station, with the exception of stations 1 and 10; in these cases, the salinities of the succeeding stations were used. The data utilized from the CTD casts can be found in Table 1. The weight of the sediment was calculated by subtracting the weight of the salt by the weight of the dry sample.

Finally, the ratio of seawater to wet sediment was calculated as follows:

R = seawater / (wet mud – vial – salt), where all weights are in grams

Once the methane concentrations in micromolar were determined, profiles were made comparing methane and sulfate concentrations as they varied with depth; similar calculations did not have to be made for sulfate, since the sulfate peaks were already recorded in millimolar by the ion chromatograph.

Diffusion coefficients for methane and sulfate at 25°C, 1atm and 0psu were solved for using an equation developed by Millero (1974). These measurements (in cm^2/s) were then transformed to reflect in-situ temperatures, pressures and salinities.

Flux calculations were then made for methane using the following equation:

$J = D_o * \Phi * (dc/dx)$, where
- J = Flux across sediment-water interface
- D_o = Diffusion coefficient of sediment
- Φ = Porosity
- dc/dx = concentration-depth gradient

This calculates flux in units of $\mu mol/cm^2/s$; they were then converted into units of $mmol/m^2/d$. The differences in concentration and depth were calculated from the methane profiles that were generated, with the fraction (dc/dx) representing the inverse of the slope between the top two samples of the cores at each given station.

Results

Sulfate Concentrations

In each of the sulfate concentration-depth profiles (Figure 9), sulfate concentrations generally decreased with sediment depth. Station 1's box core show a sulfate concentration of 13mM at the surface of the sediment rising to 14mM (1.5cm) and then down throughout the rest

of the core, ending at 0.9mM (16.5cm); the gravity core shows a concentration of 14mM at the surface, dropping to 0.3mM (71.5cm). Station 2's box core shows a concentration of 10mM at the surface, dropping to 5mM (15cm). Station 5's box core shows a concentration of 9mM at the surface, rising to 10mM (2.5cm) and then dropping to 0.6mM (17.5cm). Station 6's box core shows a concentration of 9mM at the surface, rising to 10mM (1cm) and then dropping down to 6.4mM (18.5cm). Station 7's box core shows a concentration of 9mM at the surface, dropping to 5mM (14.5cm); the gravity core shows a concentration of 11mM (1cm) dropping to 0.2mM (126cm).

Methane Concentrations

In each of methane concentration-depth profiles (Figure 10), methane concentrations generally increased with sediment depth, with the exception of station 1's first box core, station 4's box core, and station 6's box core. It should be noted that the sediment in the first methane box core that was collected at station 1 was disturbed (it appeared to have been shaken up a bit), which was why a second box core was taken. There were no specific disturbances noticed while taking the cores at stations 4 or 6.

Station 1's first box core shows a concentration of 112uM (1cm) rising to 802uM (2.5cm) and then dropping to 603uM (10cm); the second box core shows a concentration of 9uM (1cm) rising to 104uM (5cm), dropping to 93uM (7.5cm), and rising to 264uM (17.5cm); the gravity core shows a concentration of 75uM (2cm) rising to 589uM (7cm). Station 3's box core shows a concentration of 0.5uM 91cm) rising to 6uM (7.5cm). Station 4's box core shows a concentration of 0.6uM (1cm) rising to 1.4uM (6cm) and dropping to 1.2uM (8.5cm). Station 5's box core shows a concentration of 1.1uM (0.5cm) rising to 22uM (8cm); the gravity core shows a concentration of 2.3uM (1cm) dropping to 1.7uM (3.5cm) and rising to 110uM (11cm). Station 6's box core shows a concentration of 0.79uM (2cm) rising to 0.85uM (2.5cm), dropping to 0.27uM (5cm), and rising back up to 0.34uM (7.5cm); the gravity core shows a concentration of 0.7uM (1cm) rising to 2uM (8.5cm). Station 7's gravity core shows a concentration of 12uM (0.5cm) rising to 82uM (8cm). Station 8's gravity core shows a concentration of 24uM (3cm) rising to 1895uM (18cm). Station 11's gravity core shows a concentration of 45uM (92cm) rising to 424uM (9.5cm). Station 12's gravity core shows a concentration of 220uM (1cm) rising to 2781uM (85cm).

Methane-Sulfate Profiles

Figure 11 shows a collection of profiles comparing the concentration-depth data for methane and sulfate; these comparisons could only be made for stations 1, 2, 5, 6, and 7, as these were the only stations at which samples were taken for both methane and sulfate. As was mentioned in the discussion of the study's sampling methods, only samples from the top four layers of each methane core were analyzed (with the exception of station 1). Due to the inability of the gas chromatograph to record higher concentrations, it is uncertain how much higher the methane concentrations would have increased with depth. In comparison, all of the sulfate samples that were collected were analyzed – there was no concern in regard to the sulfate concentrations being too high for the ion chromatograph to accurately measure. Each of the profiles show sulfate concentrations quickly approaching 0mM as depth increased; this can be seen particularly well in the gravity cores for stations 1 and 7. As the sulfate concentrations decreased at each station, the methane concentrations would simultaneously increase. Of each of the methane-sulfate profiles, station 1's box core includes the highest sulfate concentration (13.7mM at 1.5cm depth) and station 7's gravity core includes the lowest sulfate concentration (0.14mM at 86cm depth). Similarly, station 1's first box core includes the highest methane

concentration (802μM at 2.5cm depth) while station 6's box core includes the lowest methane concentration (0.34μM at 7.5cm depth).

Discussion

Sediment Cores

An interesting pattern was noticed in regard to the data obtained from the box and gravity cores. In most cases, the methane concentrations from the gravity core data would be offset above those from the box core data, particularly for the sediment plugs taken from the tops of the cores (Figure 12a). This offset is believed to be due to inaccuracies caused by the nature of the gravity cores. Although the gravity cores hold longer core liners and can therefore reach deeper parts of the sediment, it was noted during the sampling process that some sediment would always be lost from the tops of the gravity cores. Compaction of the sediment was also noted for the gravity cores, whereas there was no compaction in the box cores. For these reasons, it is recommended that box cores be used for methane samples at all sampling stations. Also, for instances where gravity cores are taken for methane as well, taking both box and gravity cores for sulfate samples would make it easy to correct for the offsets seen in the methane profiles. An exception to this issue can be seen in the data from station 5, where the gravity core data lines up almost directly on top of the box core data (Figure 12b); it is recommended that box cores always be used as a backup however, since this appears to be a rare occurrence. Unfortunately for this study, it was unknown that there would be an offset, so box cores were not taken at every station, leaving some of the stations with only gravity core data.

Methane Flux vs. Salinity

The methane flux measurements from the research cruise conducted in June are shown in Table 2. It was originally expected that methane flux would increase with decreasing sulfate availability as we moved from the southern marine sediments to the less-saline northern sediments. Methane fluxes at stations 1 and 12 were relatively much higher than the fluxes at each of the other stations. While the more southern stations do not seem to follow a progressive trend, it can be noted that they – with the exception of station 1 – had significantly lower fluxes when compared to the four northernmost stations.

The flux-salinity comparisons (Figure 13a) indicate that methane flux generally increases with an increasing salinity. This trend becomes more visible when the box and gravity core data are separated. The linear regressions (Figure 13b) show that there is a fairly strong correlation for the box core data and somewhat of a correlation for the gravity core data. If the data from station 12 were removed, the correlation coefficient would increase from 0.4575 to 0.8206, indicating a fairly strong correlation for the rest of the gravity core samples, which had much lower fluxes than the sample from station 12. This trend does not support the original hypothesis, which had stated that methane flux would increase with a decreasing salinity. The salinity data acquired ranged from 11psu (station 4) to 17psu (station 11), so it is uncertain how salinities outside of this range would have affected flux. In any case, the flux-salinity trend seen here is not yet understood and requires further study.

Methane Flux vs. Dissolved Oxygen

Since salinity did not seem to be controlling methane flux in the manner that was anticipated, dissolved oxygen was considered as another potential factor that would influence

flux in the bay. It was considered that control over methane flux might not be a question of salt vs. freshwater environments, but rather of oxic and hypoxic conditions. In the presence of oxic conditions in the deep water, methane can be broken down by bacteria aerobically, either in the top layer of the sediment or in the water column itself. This would mean that methane flux would be lower in regions experiencing oxic conditions and higher in regions experiencing hypoxic conditions. To test this new possibility, methane flux was plotted against the dissolved oxygen readings taken by the CTD casts (Figure 14a). The trends showed what was expected – that methane flux increased as dissolved oxygen decreased. The linear regression for the box core data (Figure 14b) showed a fairly strong correlation coefficient of 0.7849, and if the outlier (station 11) is removed from the gravity core data, its correlation coefficient would increase from 0.3744 to 0.7967, which would also indicate a fairly strong correlation for the gravity core data.

Supplemental Material

Several other figures were compiled to check for trends, including methane flux vs. water depth, flux vs. temperature, salinity vs. water depth, and salinity vs. temperature. These comparisons can be found in the supplemental material.

Conclusion

Box cores proved to be more reliable than gravity cores when it came to taking sediment core samples. The gravity core data were usually offset above the box core data; this offset is believed to have been a result of disturbances in the cores as a result of compaction and loss of sediment from the top layers of the core. It was discovered that methane concentrations were heterogeneous in the Chesapeake Bay, with concentrations ranging from 0.34μM (station 6) to 2781μM (station 12). It was originally hypothesized that the salinity gradient present in the Chesapeake Bay acts as a control over methane flux, where methane flux should increase as salinity decreases. The methane flux and salinity data obtained from the bay does not support this, however, and actually shows the opposite trend. It is uncertain what caused the trend, but more data would have to be obtained that encompass the entire salinity spectrum; the data acquired from this study only include a salinity range of 11-17psu, so it is unknown what the data would look like for salinities outside of this range. Another possible hypothesis considers hypoxic conditions to be the control of methane flux, due to the possibility that methane is being oxidized aerobically either in the top layer of the sediment or in the water column. This would mean that hypoxia – which occurs seasonally in the Chesapeake Bay – could be a key source of atmospheric methane. More water column data would need to be acquired in order to investigate this possibility, however. Another thing to investigate would be the amount of organic carbon present at each station sampled. The amount of organic matter that enters the sediment would be a limiting factor of methane production and therefore a limiting factor of methane flux.

Acknowledgements

I would like to thank my mentor, Dr. Laura Lapham, both for her guidance and for the many hours of her time that she dedicated throughout the course of the REU program to ensure my success. I would like to acknowledge Cédric Magen and Kathleen Marshall for their help in the lab; their patience with me in the early stages of research helped to make me more comfortable in the lab setting and running the machinery. I would also like to acknowledge Captain Michael Hulme of the R/V Rachel Carson, as well as Bruce Cornwell, for ensuring that everything went smoothly during our research cruise and that it was a safe environment in which to work. I would like to thank Mike Allen and Fredrika Moser for the time and energy they put into ensuring that the REU program was a fun and exciting experience for all of the REU

students. I would like to thank Maryland Sea Grant and Chesapeake Biological Laboratory for the opportunity to take part in such a wonderful program. The research experience and knowledge I gained through the program will prove to be invaluable, and it is an experience that will not be forgotten.

References

Bernard, B. B., J. M. Brooks, and W. M. Sackett. 1976. Natural gas seepage in the Gulf of Mexico. Earth and Planetary Science Letters 31:48-54.

Boetius, A., K. Ravenschlag, C.J. Schubert, D. Rickert, F. Widdel, A. Gleseke, R. Amann, B.B. Jorgensen, U. Witte, and O. Pfannkuche. 2000. A marine microbial consortium apparently mediating anaerobic oxidation of methane. Nature 407:623-626.

Riley, J.P., and R. Chester. 1975. Chemical Oceanography, Vol. 4, 2nd edition. London: Academic Press, Inc. Table 25, p 338, developed by Millero, 1974, with pressure corrections by Matthäus, 1972.

Froelich, P. N., G. P. Klinkhammer, M.L. Bender, N.A. Luedtke, G.R. Heath, D. Cullen, and P. Dauphin. 1979. Early oxidation of organic matter in pelagic sediments of the eastern equatorial Atlantic: suboxic diagenesis. Geochemica et Cosmochimica Acta 43:1075-1090.

Hoehler, T.M., M.J. Alperin, D.B. Albert, and C.S. Martens. 1994. Field and laboratory studies of methane oxidation in an anoxic marine sediment: Evidence for a methanogens-sulfate reducer consortium. Global Biogeochemical Cycles 8:451-463.

Jorgensen, B.B., and A. Boetius. 2007. Feast and famine – microbial life in the deep-sea bed. Nature Reviews Microbiology 5:770-781.

Kvenvolden, K.A. 1995. A review of the geochemistry of methane in natural gas hydrate. Organic Geochemistry 23:997-1008.

Mason, R.P., E. Kim, J. Cornwell, and D. Heyes. 2006. An examination of the factors influencing the flux of mercury, methylmercury and other constituents from estuarine sediment. Marine Chemistry 102:96-110.

Oremland, R.S., and S. Polcin. 1982. Methanogenesis and sulfate reduction: Competitive and noncompetitive substrates in estuarine sediments. Applied and Environmental Microbiology 44:1270-1276.

Reeburgh, W.S. 1969. Observations of gases in Chesapeake Bay sediments. Limnology and Oceanography 14:368-375.

Whiticar, M.J. 1999. Carbon and hydrogen isotope systematics of bacterial formation and oxidation of methane. Chemical Geology 161:291-314.

Figures and Tables

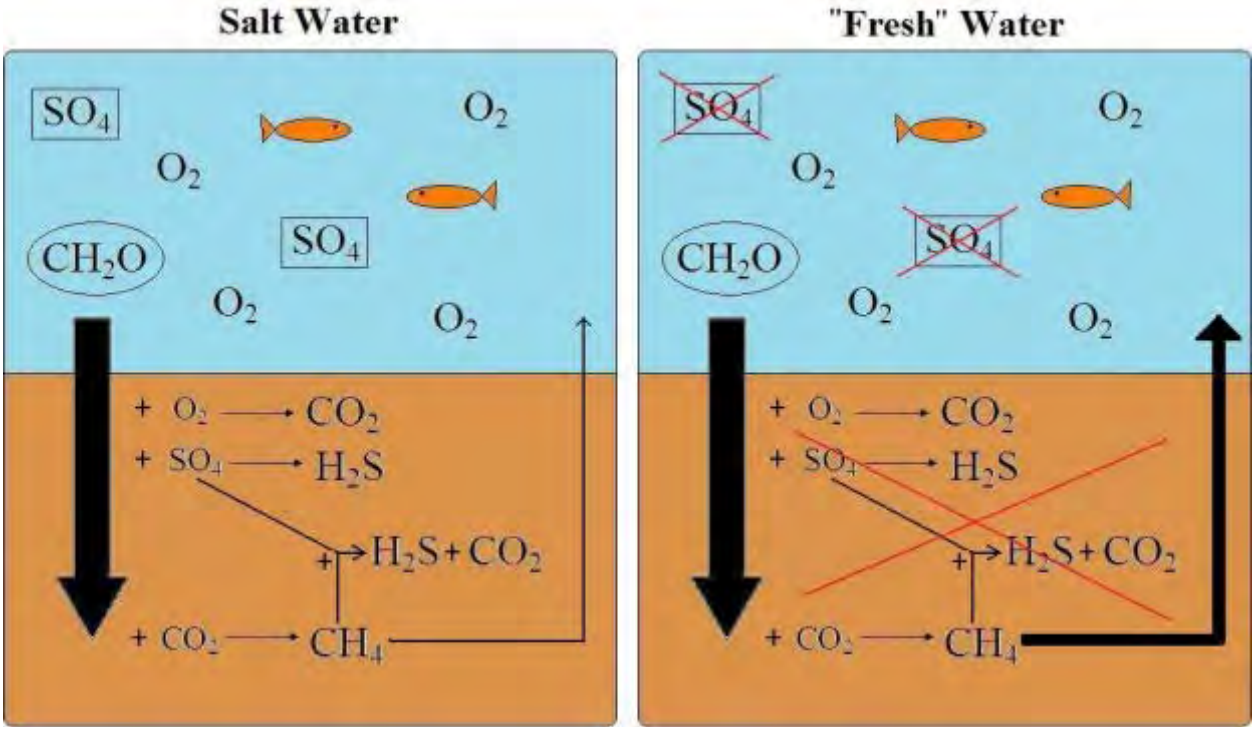

Figure 1. Comparison of organic matter decay in fresh water and salt water systems.

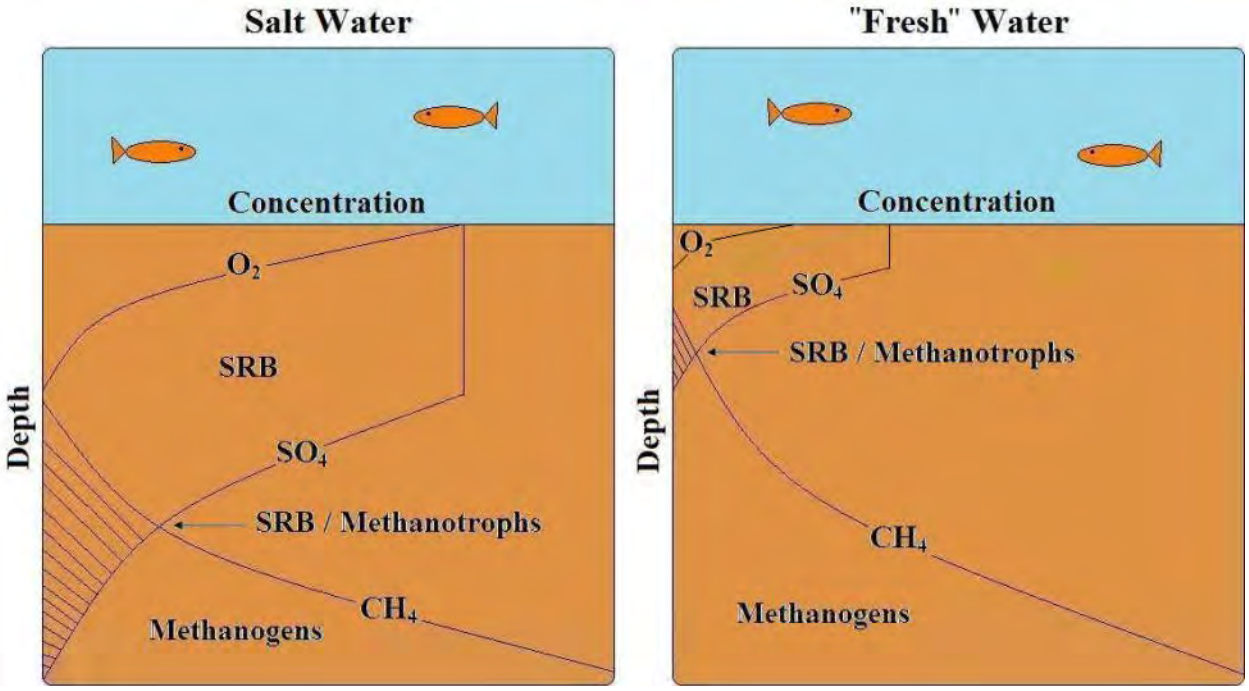

Figure 2. Comparison of the ranges of sulfate reduction and methanogenesis in fresh water and salt water systems.

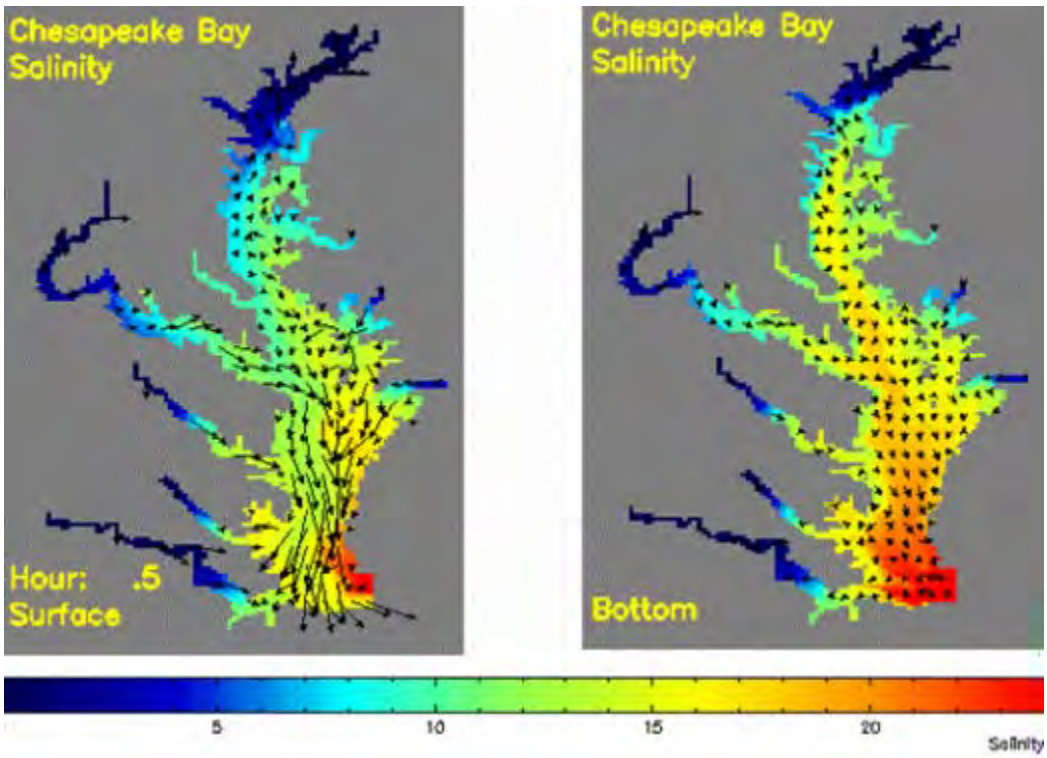

Figure 3. Salinity distribution in the Chesapeake Bay (http://web.vims.edu/physical/WEB/PRESNT/bsalt.htm).

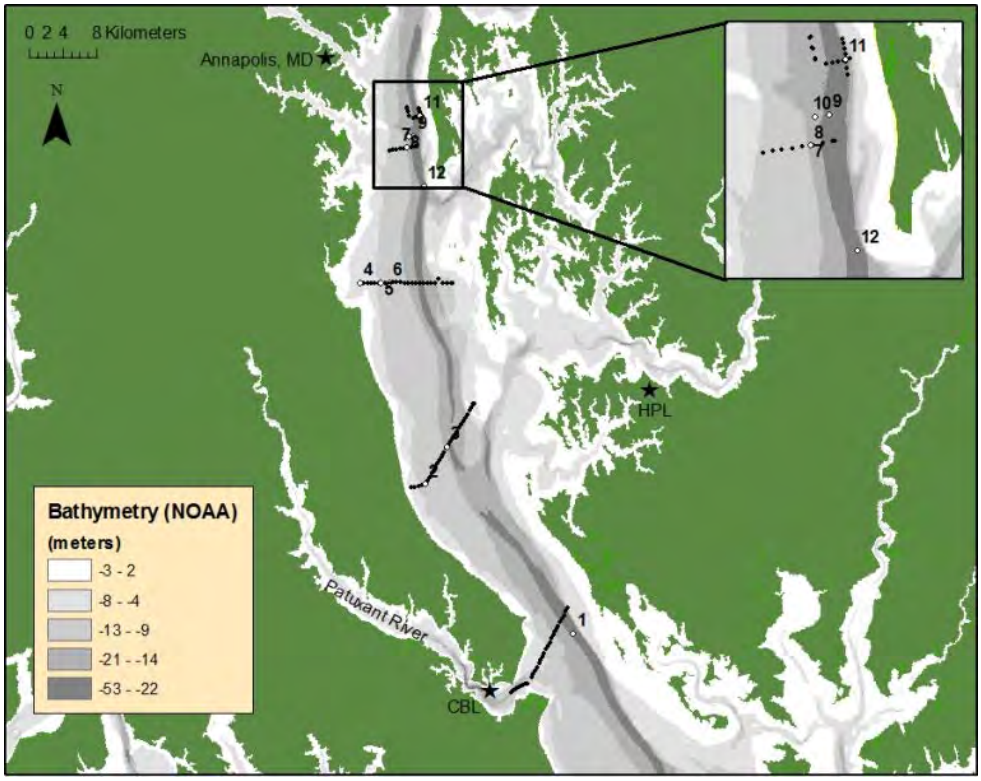

Figure 4. Chesapeake Bay: Research Cruise Plan.

Figure 5. Sediment plug being taken from a box core sample.

Figure 6. Rhizome filter attachment being used to take pore water samples for sulfate concentration analysis.

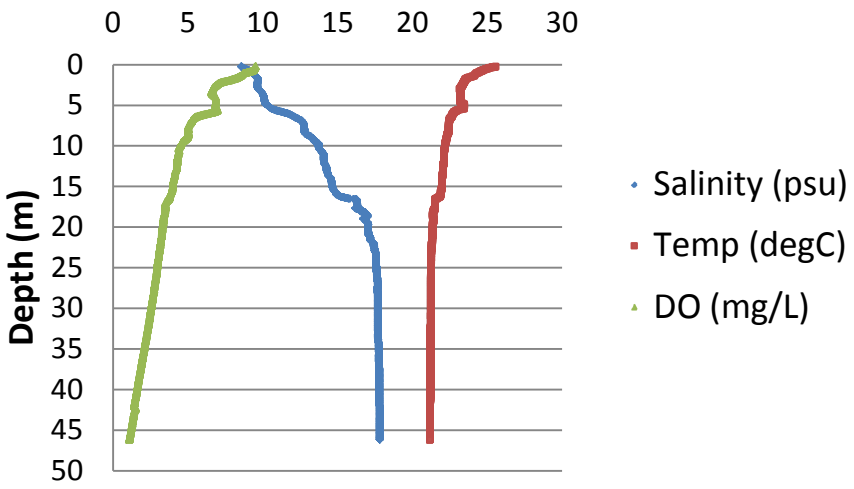

Figure 7. Example of CTD data acquired at station 12.

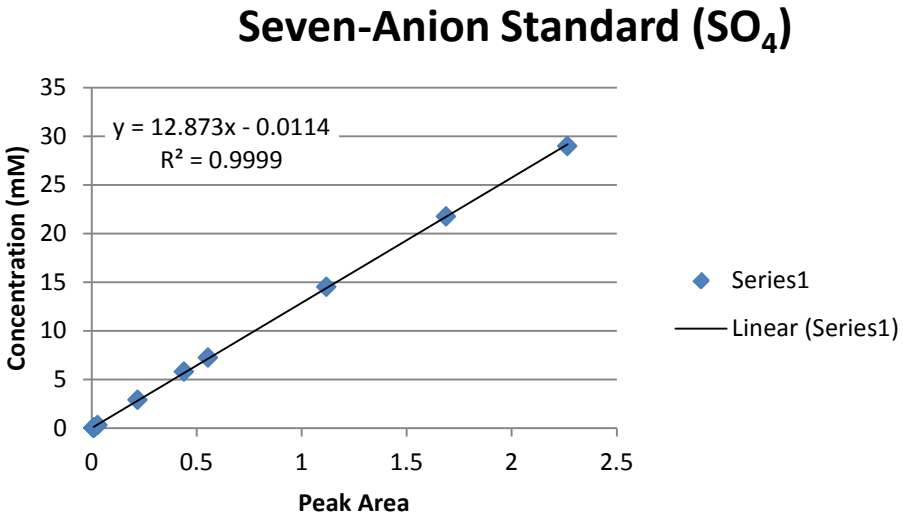

Figure 8. Example of a standard curve obtained to determine unknown sulfate concentrations.

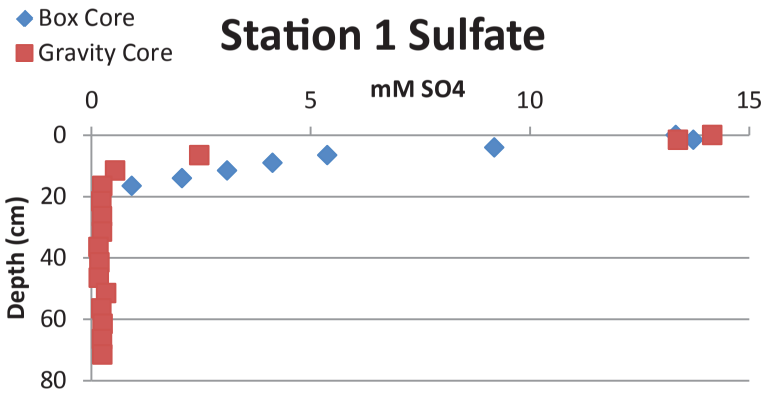

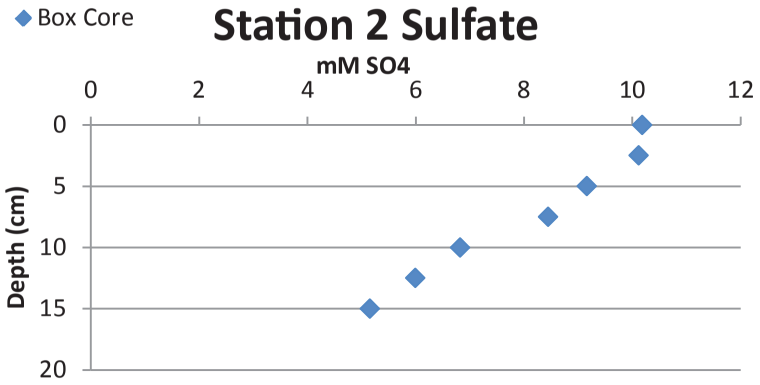

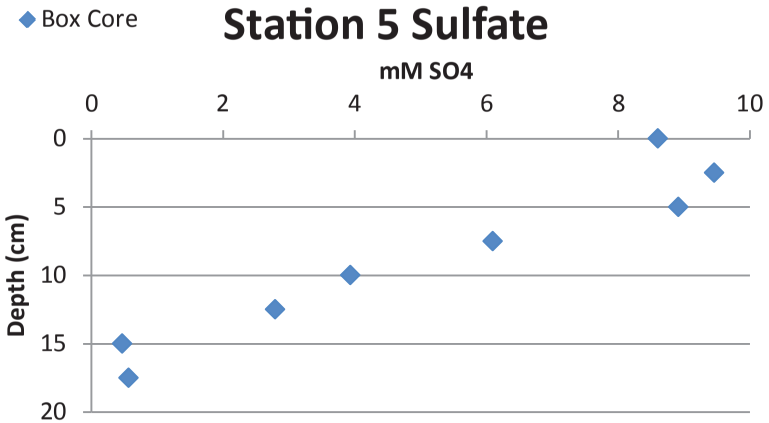

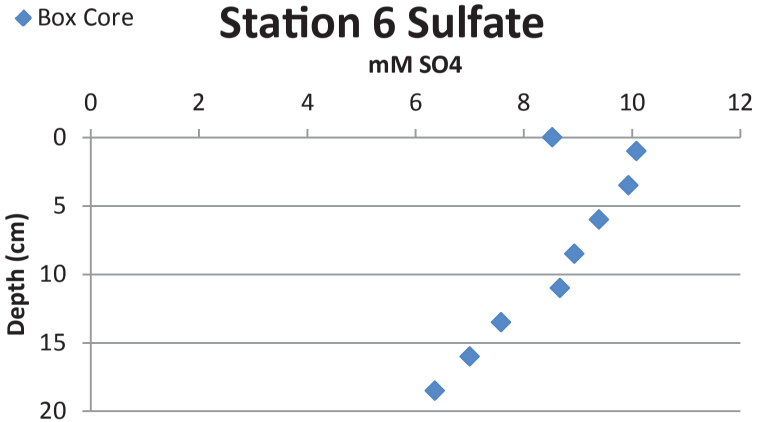

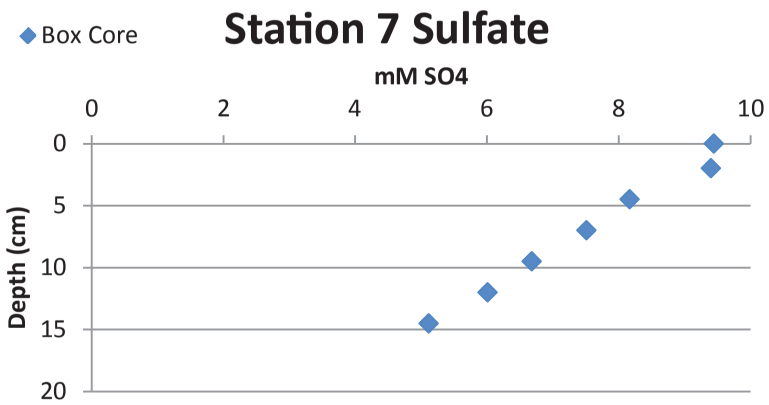

Figure 9. Sulfate concentration-depth profiles (June research cruise).

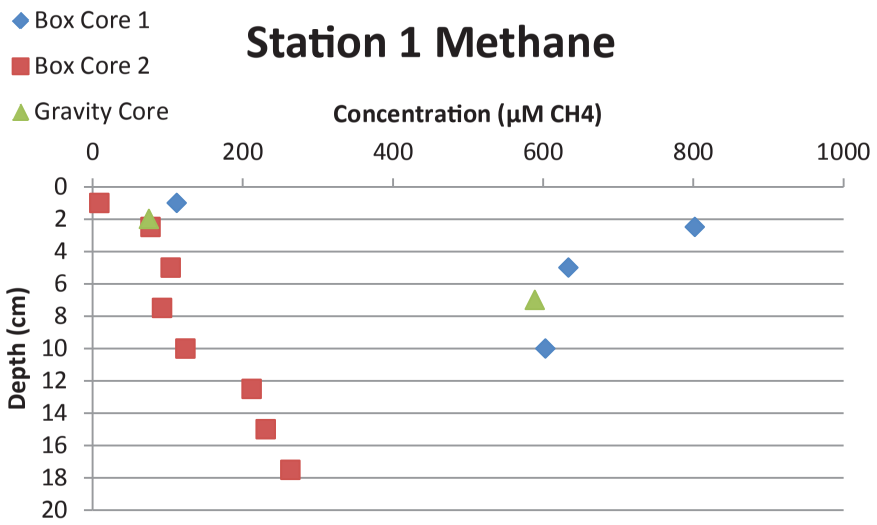

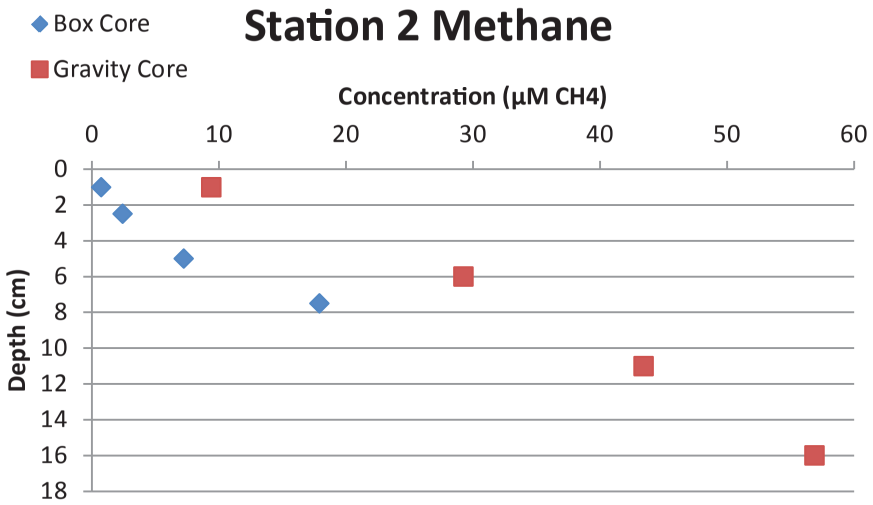

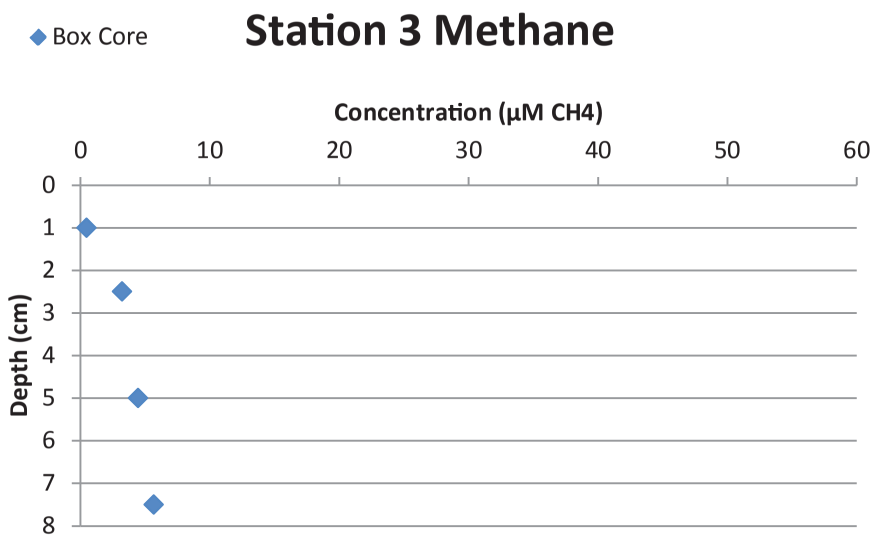

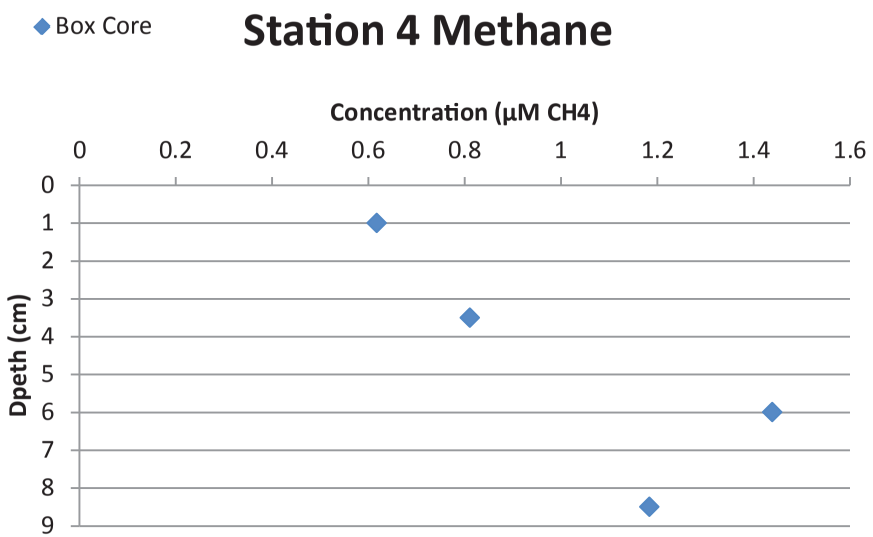

Figure 10. Methane concentration-depth profiles compiled from samples (June research Cruise).

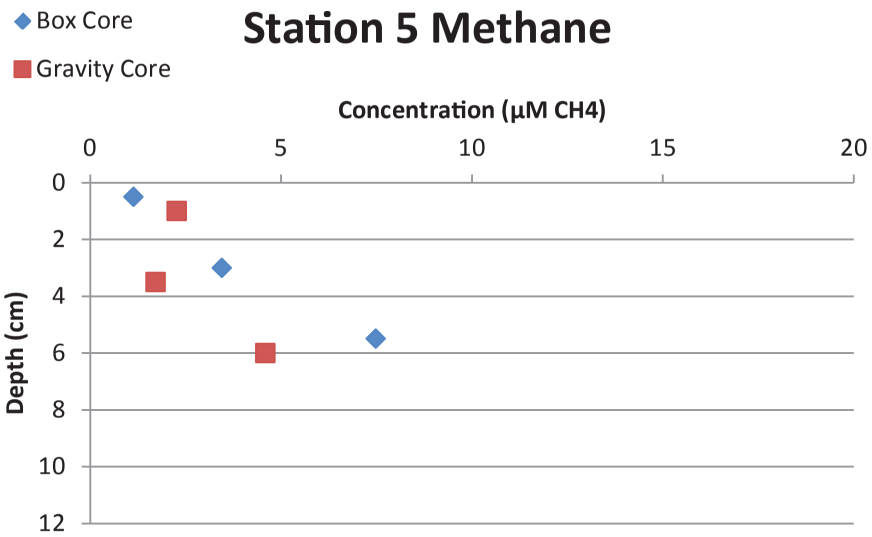

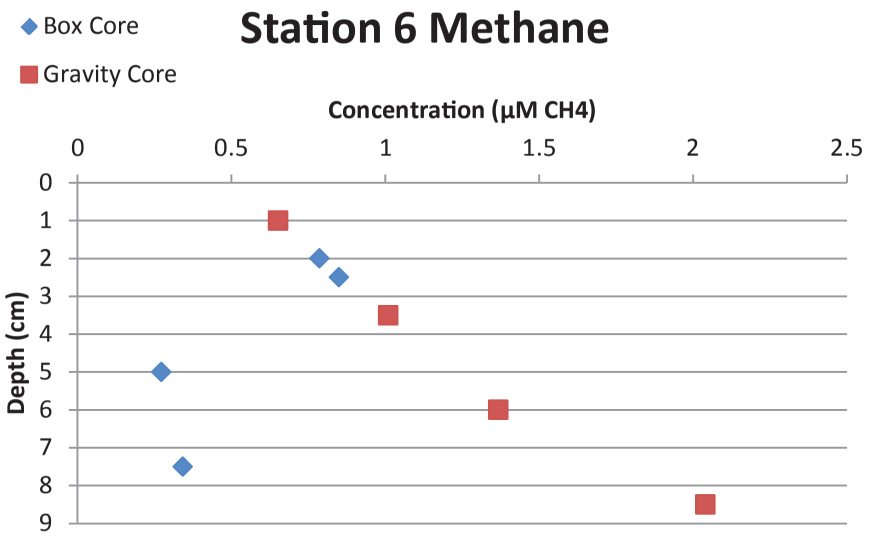

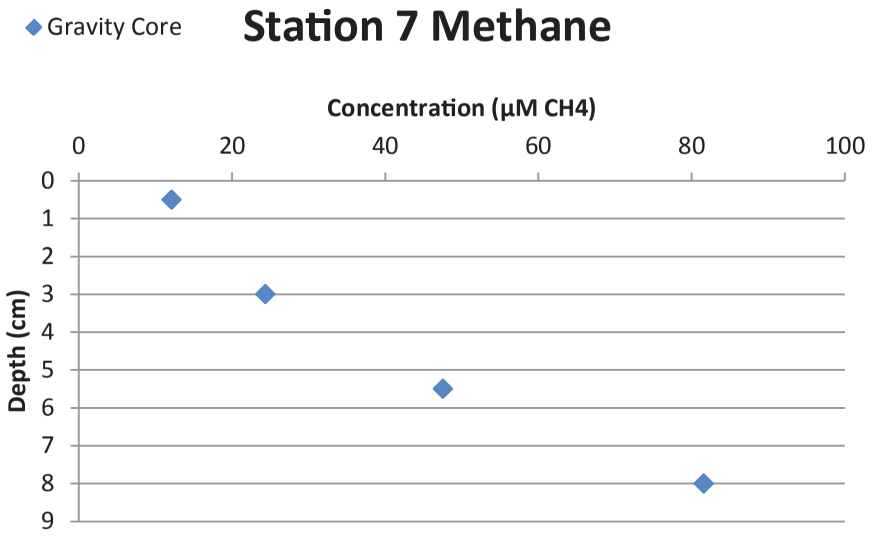

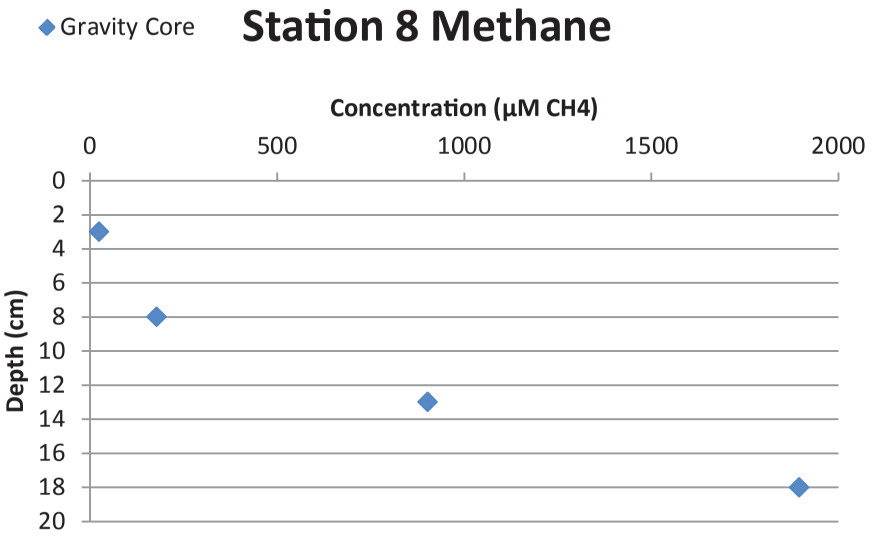

Figure 10 (continued). Methane concentration-depth profiles.

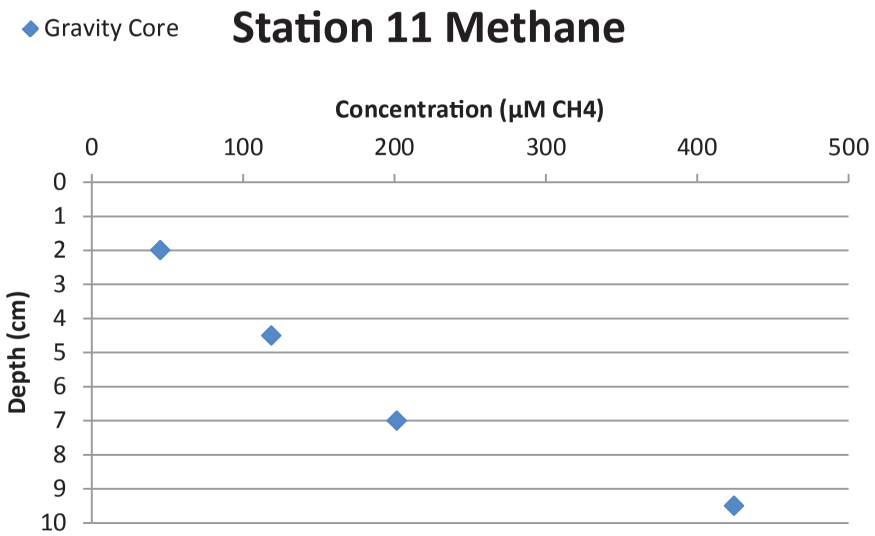

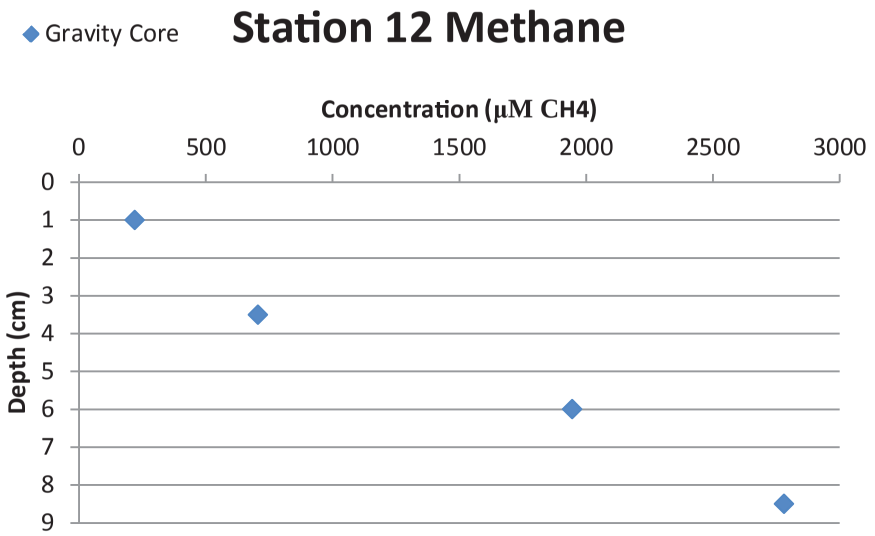

Figure 10 (continued). Methane concentration-depth profiles.

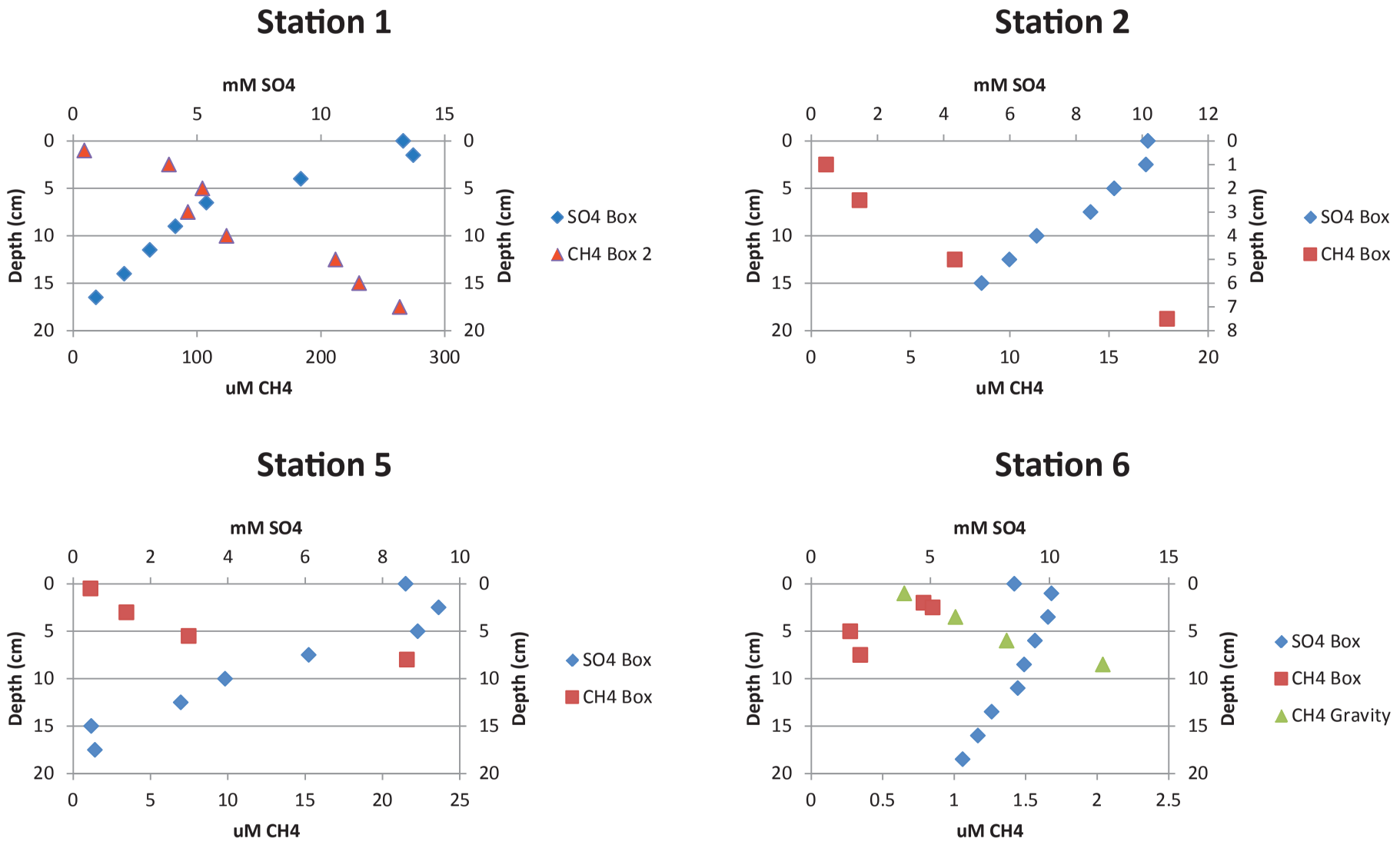

Figure 11. Concentration-depth comparison for methane and sulfate.

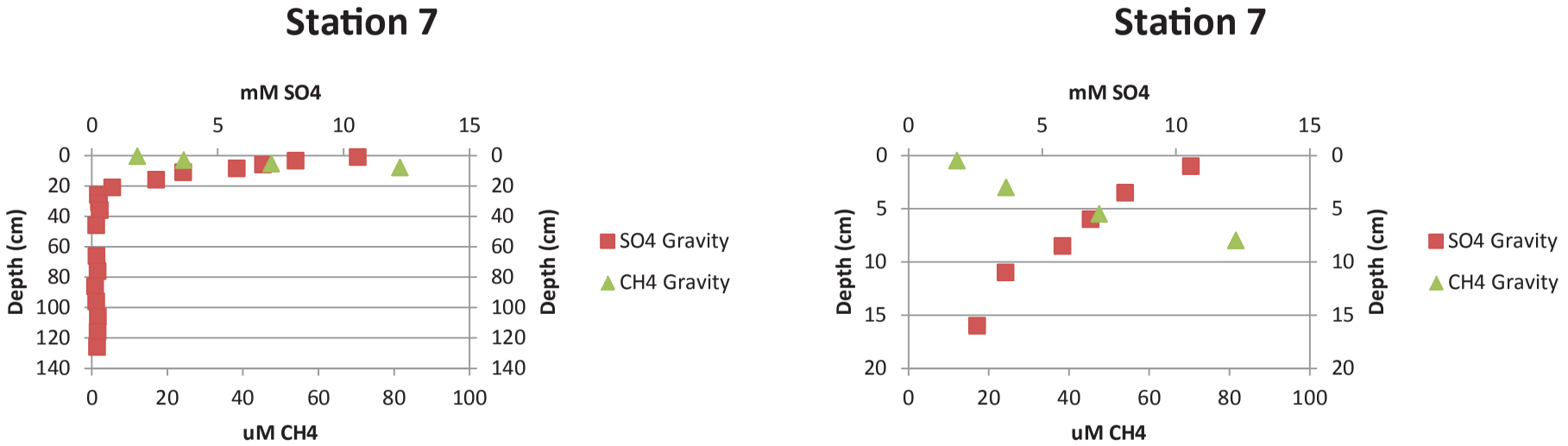

Figure 11 (continued). Concentration-depth comparison for methane and sulfate.

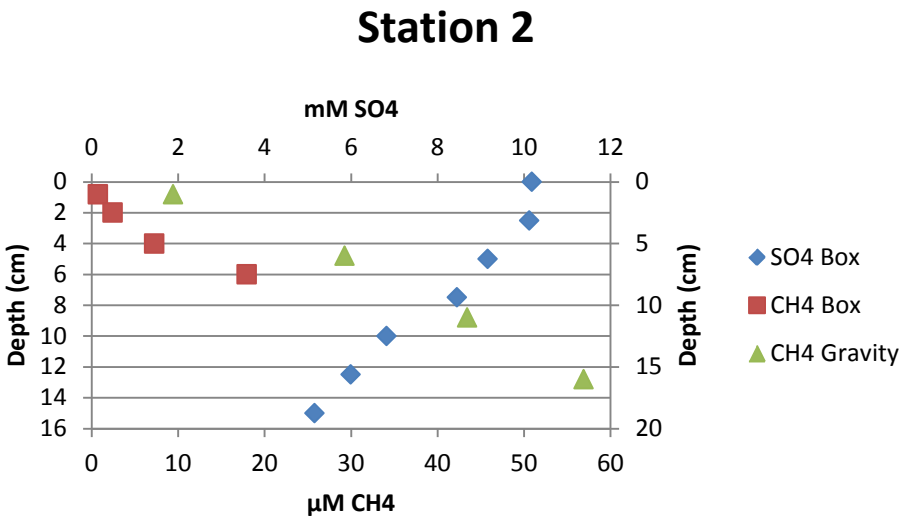

Figure 12a. Example of gravity core data being offset above box core data.

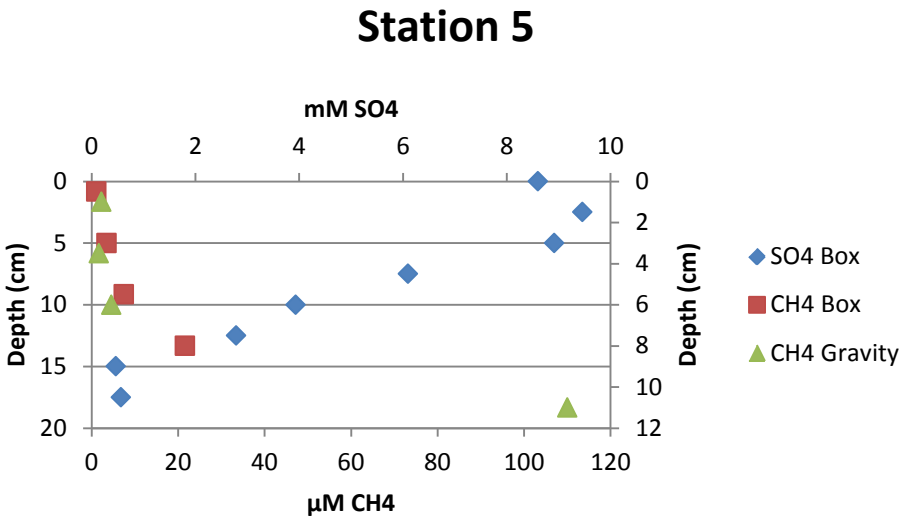

Figure 12b. Example of gravity core data matching up with box core data.

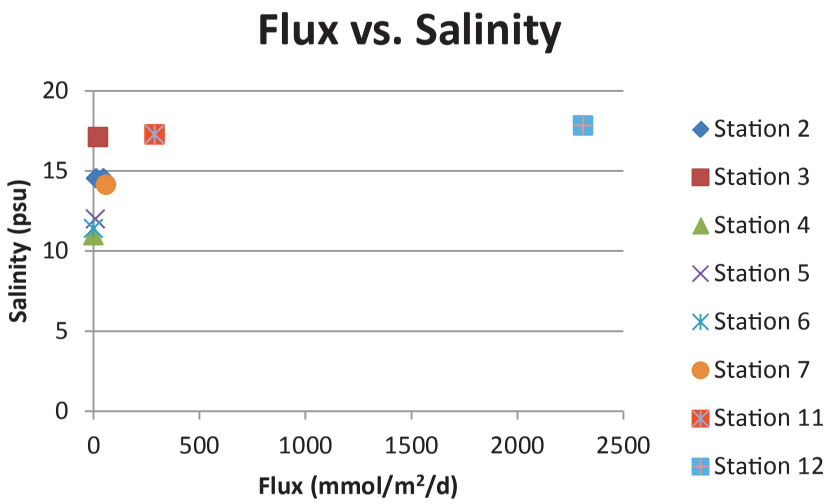

Box and gravity core data included for all stations with CTD data

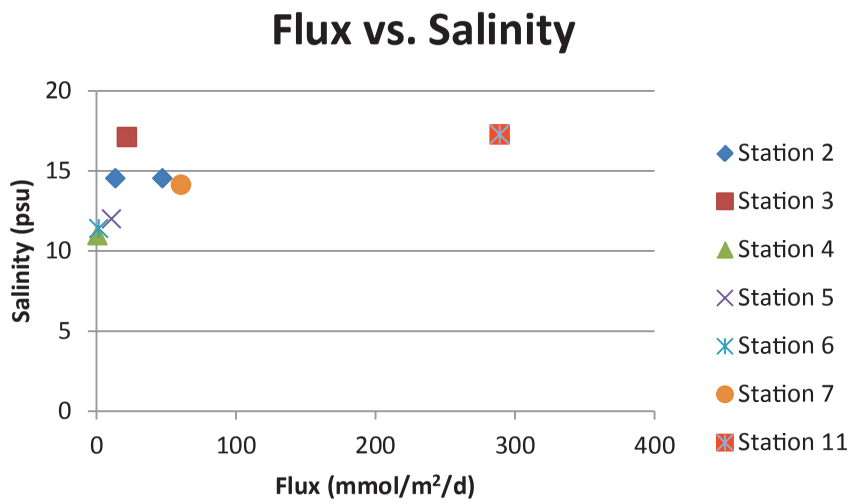

Station 12 removed to enhance stations with lower flux

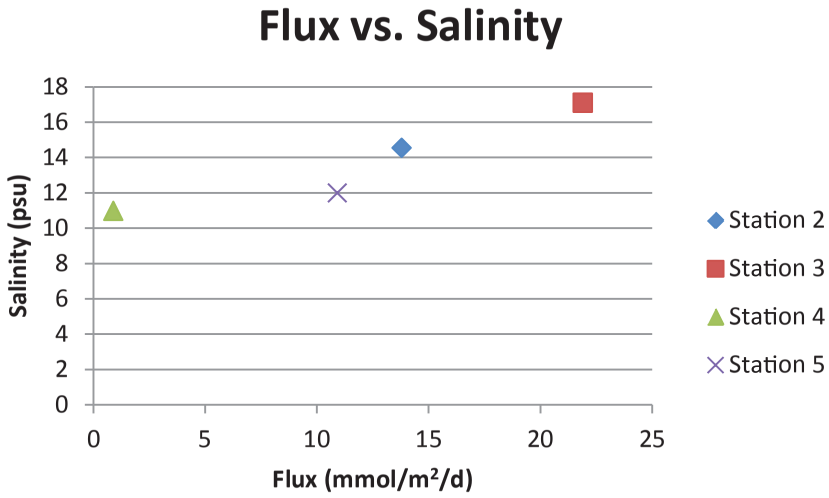

Box cores only

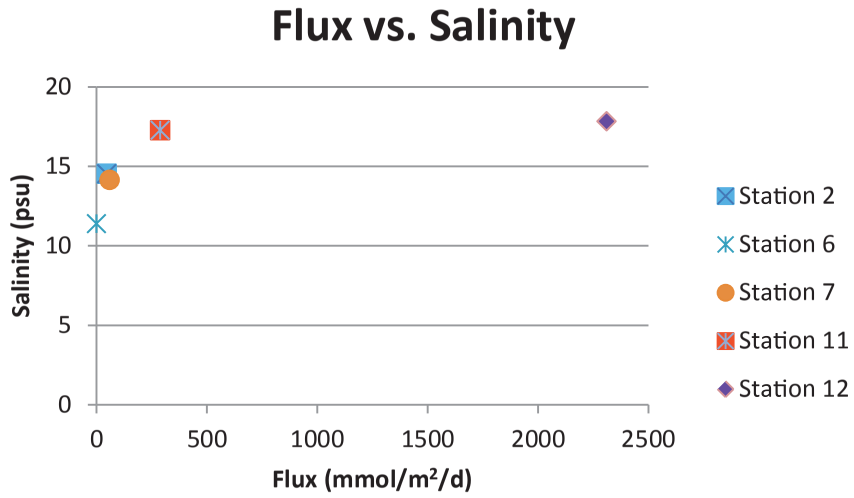

Gravity cores only

Figure 13a. Flux-salinity trends; salinity measurements recorded by CTD device.

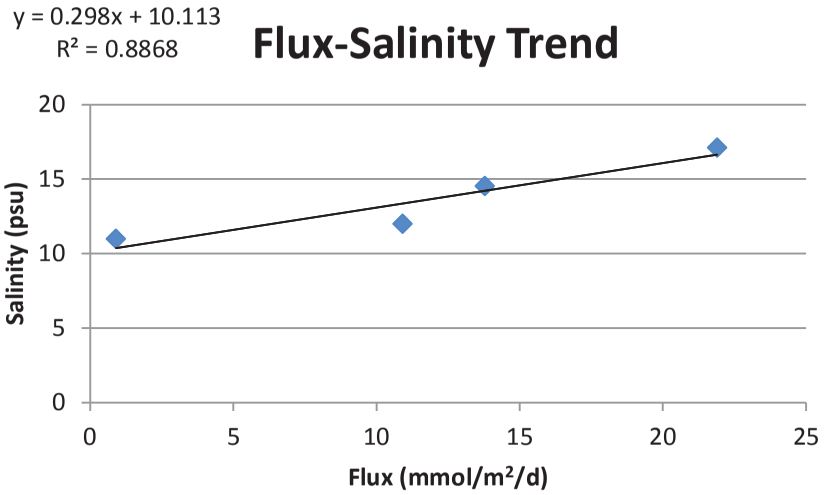

Flux-salinity relationship for box core

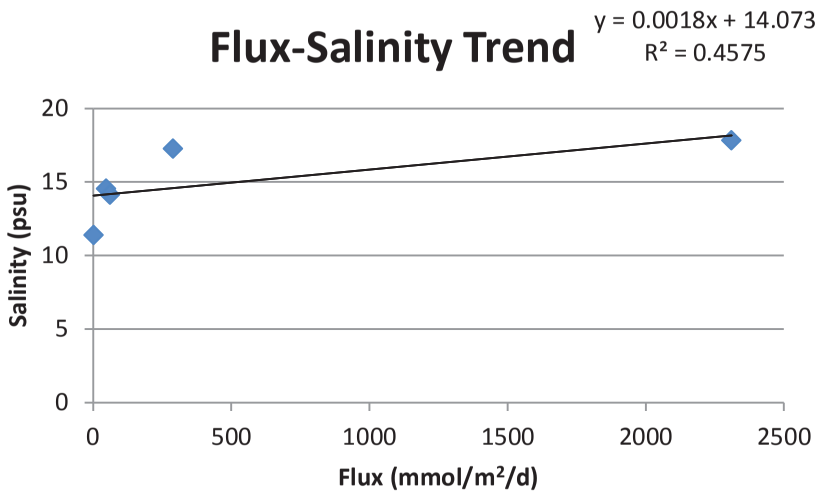

Flux-salinity relationship for gravity cores

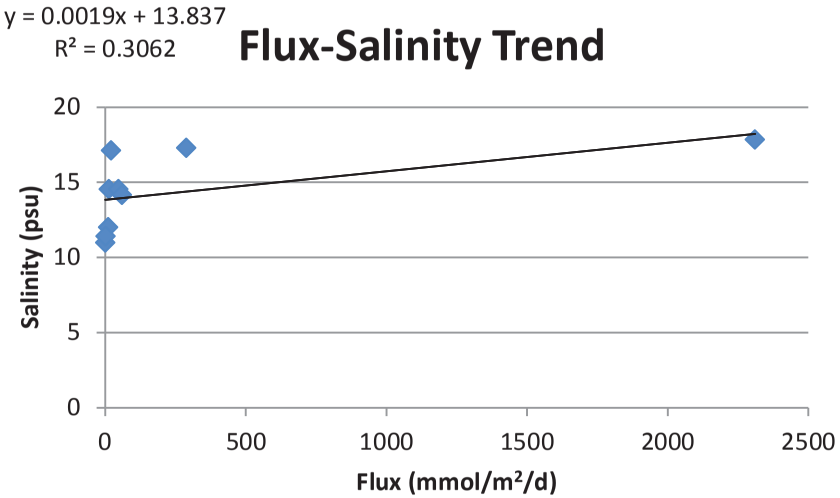

Box and gravity core curve shown as one data series

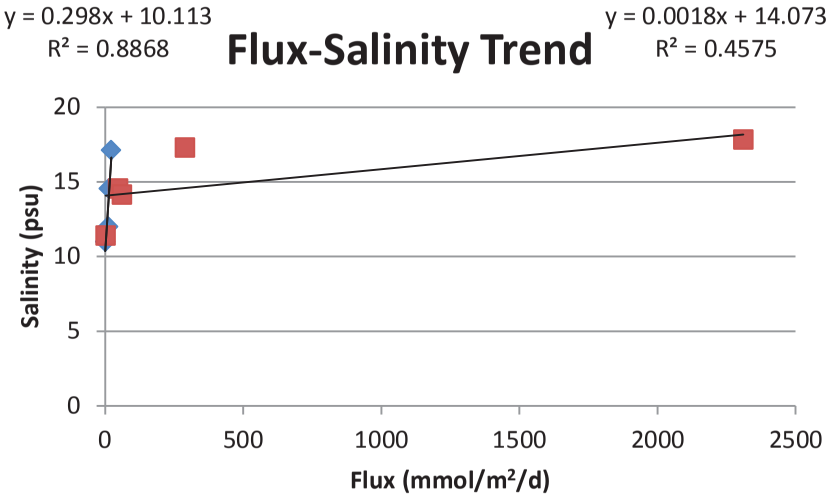

Box and gravity core curves shown as two data series

Figure 13b. Flux-salinity linear relationships. Linear equations for the box core data are shown in the top left corner of each graph, while the gravity core equations are shown in the top right corner.

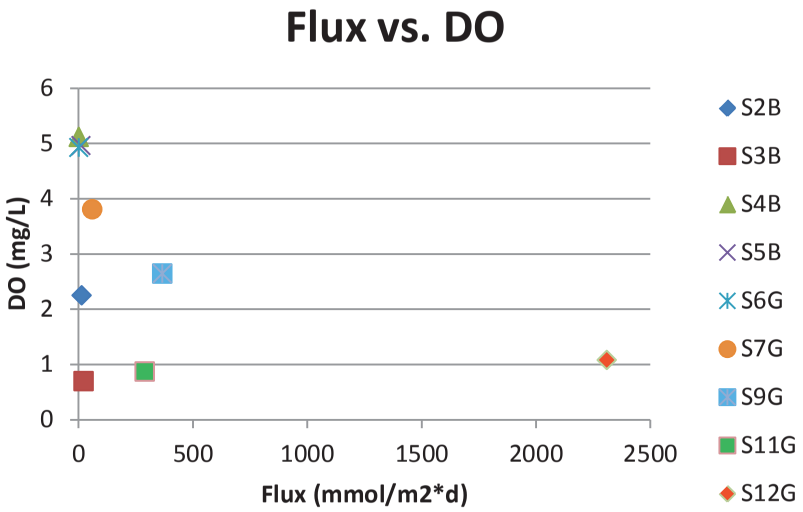

Box and gravity cores included for all stations with CTD data

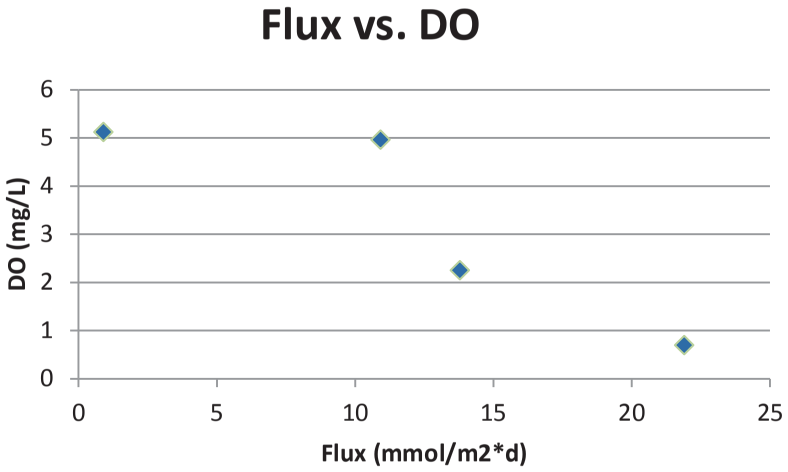

Box cores only

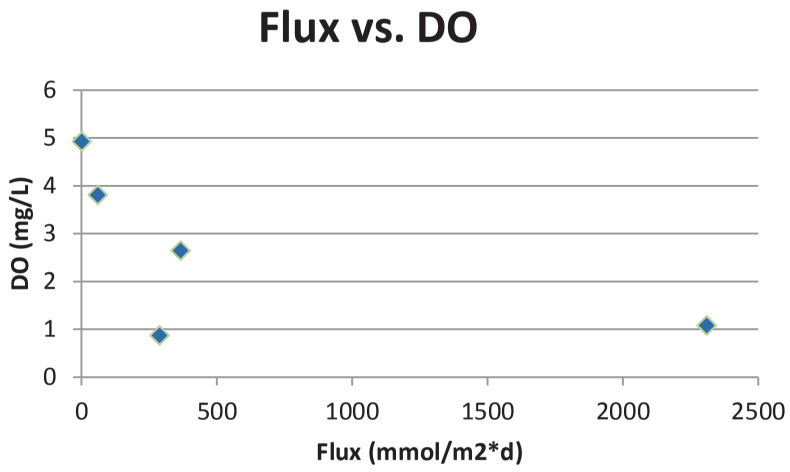

Gravity cores only

Figure 14a. Flux-DO trends; dissolved oxygen measurements recorded by CTD device.

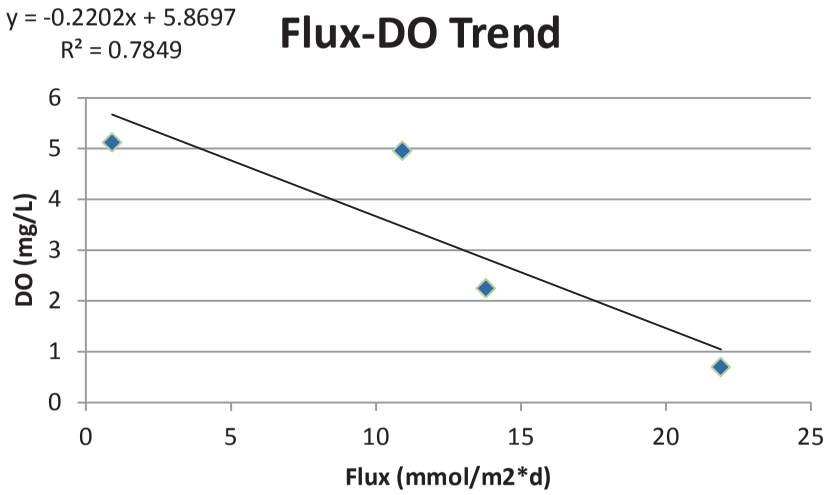

Box cores only

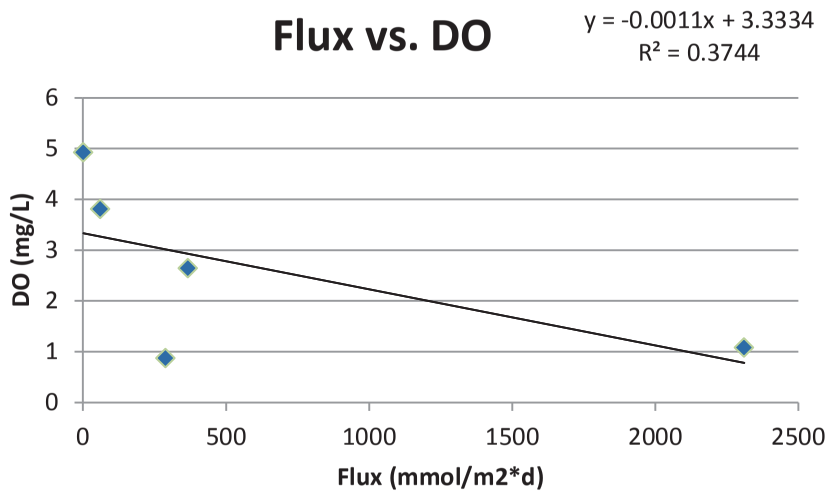

Gravity cores only

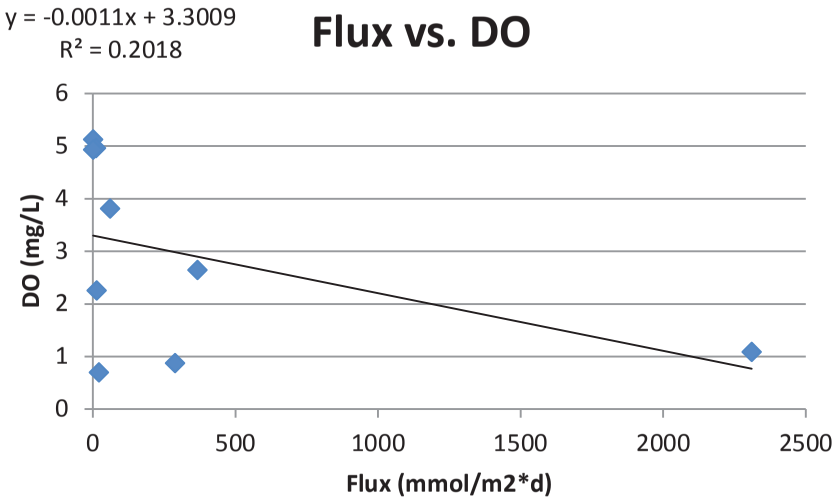

Box and gravity core curve shown as one series

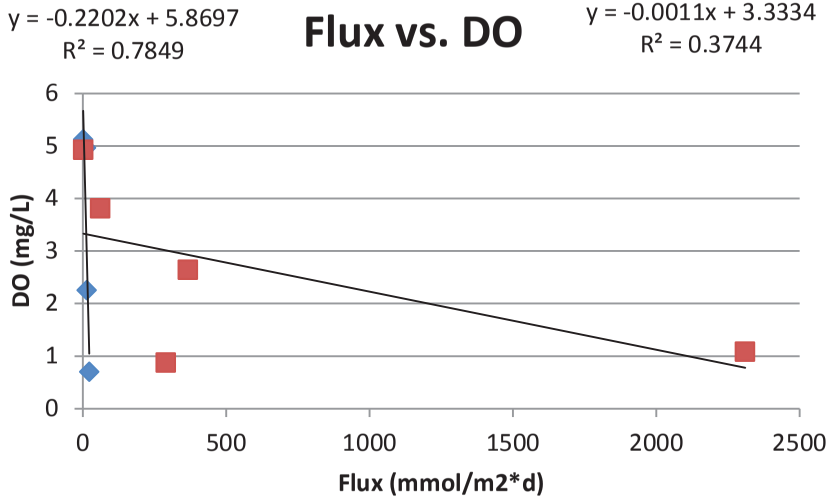

Box and gravity core curves shown as two series

Figure 14b. Flux-DO linear relationships. Linear equations for the box core data are shown in the top left corner of each graph, while the gravity core equations are shown in the top right corner.

Table 1. CTD cast data; this data reflects the measured parameters in the bottom water at each station.

Station	Time (s)	Depth (m)	Salinity (psu)	Temp (°C)	DO (mg/L)	% O_2 Sat	% Transmittance	Fluorescence (mg/m^3)
2	247	8.7	14.5	22.4	2.2	28.2	13.1	3.0
3	373	16.8	17.1	21.6	0.7	8.7	19.6	4.4
4	223	5.5	11.0	22.8	5.1	63.4	14.7	4.2
5	264	8.5	12.0	22.6	5.0	61.6	13.7	2.7
6	226	9.2	11.4	22.6	4.9	61.0	16.4	4.1
7	342	12.4	14.1	21.8	3.8	47.2	17.3	3.8
9	366	22.3	17.7	21.0	2.6	32.9	17.9	3.7
11	382	22.8	17.3	21.1	0.9	10.8	21.1	5.8
12	4209	46.2	17.8	21.1	1.0	13.5	23.0	4.5

Table 2. Methane flux data from June research cruise; no porosity samples were taken at station 1, so an estimated porosity of 0.9 was used. A CTD cast was not completed at stations 1 or 8, so temperatures were estimated to be 298.15 K and 294.01 K (station 9's temperature) in these cases. Core names are formatted as follows: "S1B1" designates Station 1, Box core 1.

Core	Porosity	In-Situ Do (cm^2/s)	Slope (cm/µM)	Slope (µM/cm)	Flux (µmol/cm^2/s)	Flux (mmol/m^2/d)
S1B1	0.90	1.68 E-05	0.0022	454.55	6.86 E-03	5930.4
S1B2	0.90	1.68 E-05	0.0219	45.66	6.90 E-04	595.8
S1G	0.92	1.68 E-05	0.0097	103.09	1.60 E-03	1378.4
S2B	0.90	1.56 E-05	0.8846	1.13	1.60 E-05	13.8
S2G	0.89	1.56 E-05	0.2521	3.97	5.50 E-05	47.5
S3B	0.91	1.52 E-05	0.5468	1.83	2.53 E-05	21.9
S4B	0.85	1.59 E-05	12.916	0.08	1.05 E-06	0.9
S5B	0.86	1.58 E-05	1.079	0.93	1.26 E-05	10.9
S6G	0.87	1.58 E-05	6.9908	0.14	1.96 E-06	1.7
S7G	0.93	1.54 E-05	0.2048	4.88	7.02 E-05	60.6
S8G	0.92	1.50 E-05	0.0324	30.86	4.24 E-04	366.7
S11G	0.76	1.50 E-05	0.0341	29.33	3.35 E-04	289.0
S12G	0.91	1.50 E-05	0.0051	196.08	2.67 E-03	2310.6

SUPPLEMENTAL MATERIAL

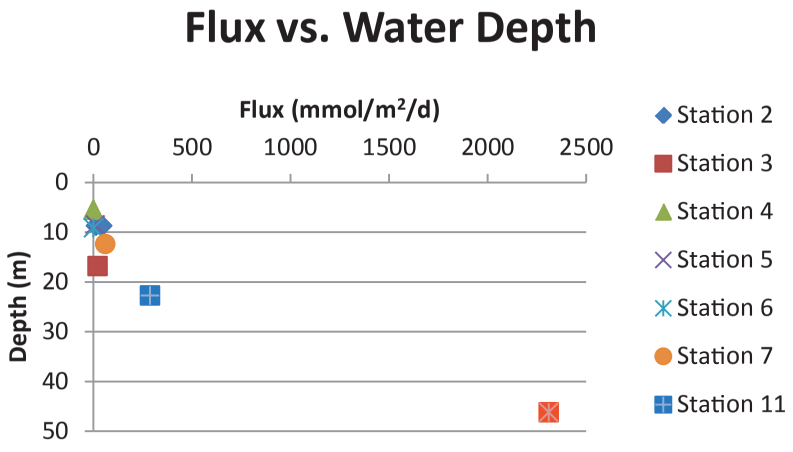

Box and gravity cores included for all stations with CTD data

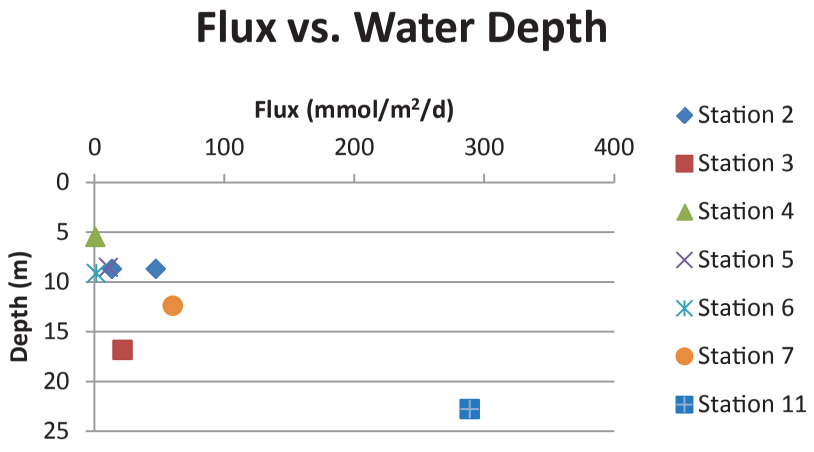

Station 12 removed to show stations with lower flux

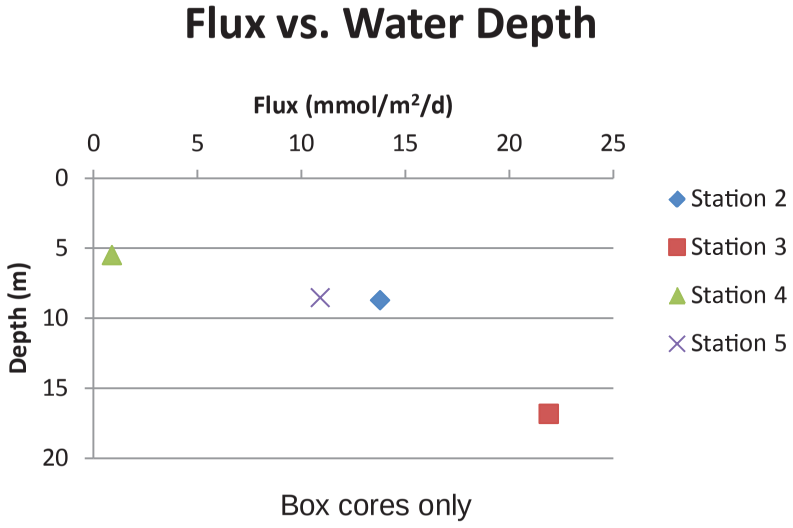

Box cores only

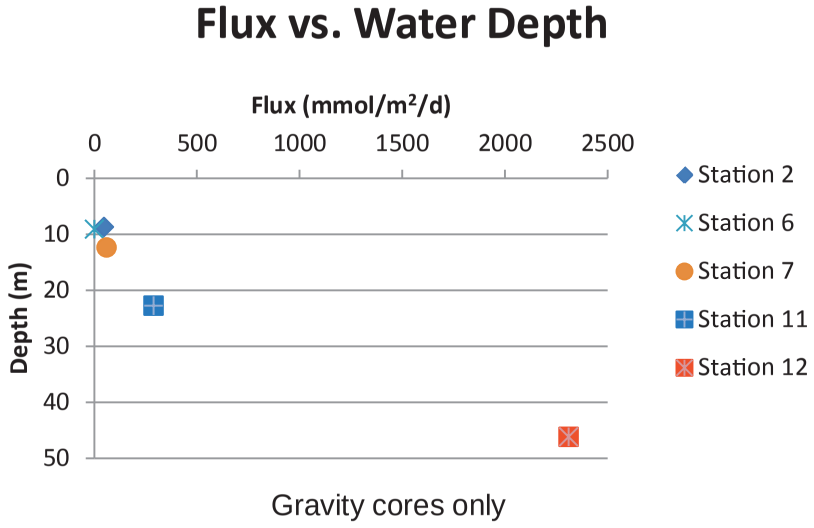

Gravity cores only

S1a. Flux-depth trends; water depth measurements recorded by CTD device.

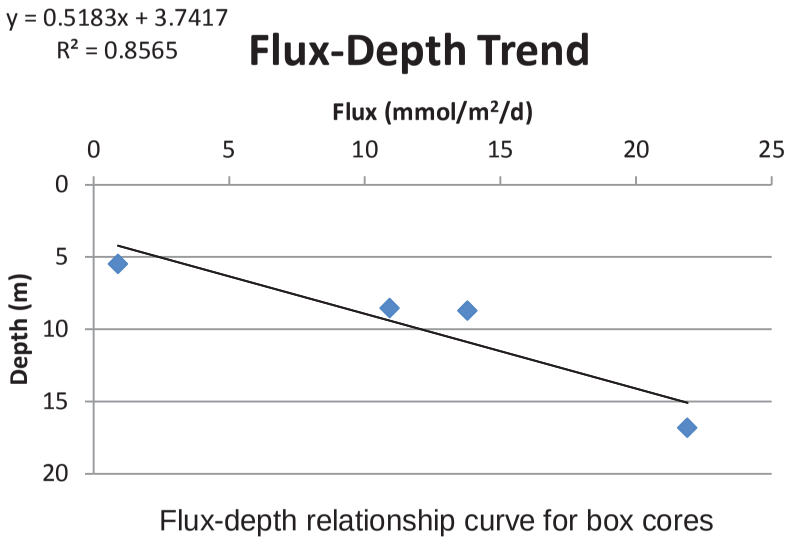

Flux-depth relationship curve for box cores

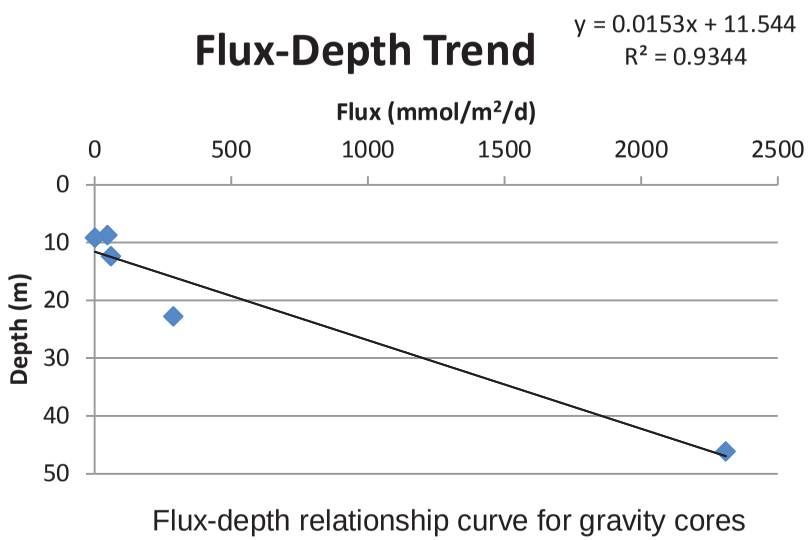

Flux-depth relationship curve for gravity cores

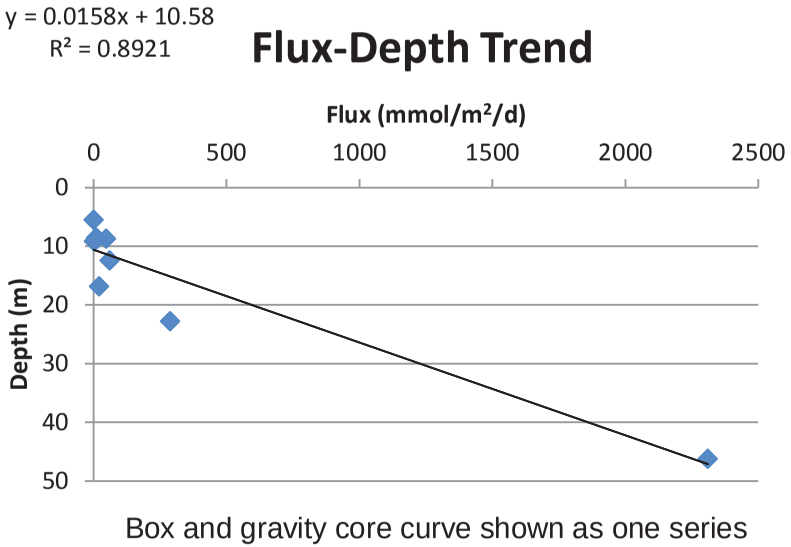

Box and gravity core curve shown as one series

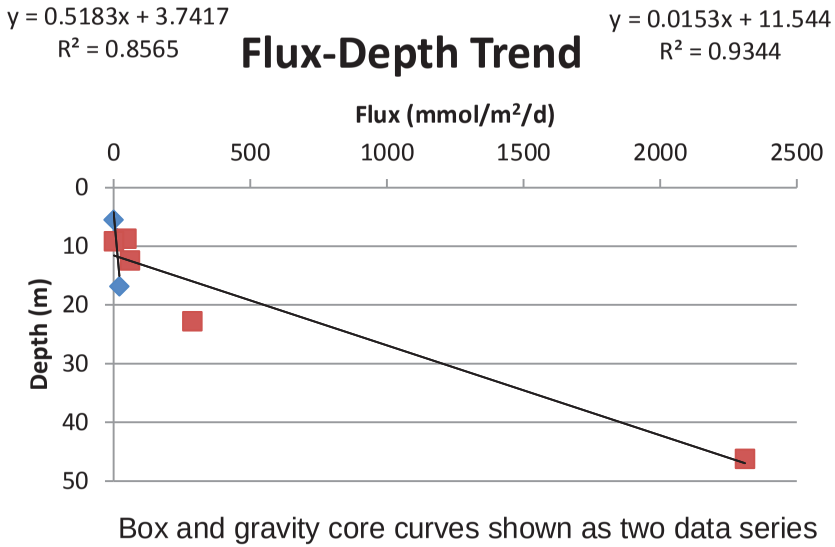

Box and gravity core curves shown as two data series

S1b. Flux-depth linear relationships. Linear equations for the box core data are shown in the top left corner of each graph, while the gravity core equations are shown in the top right corner.

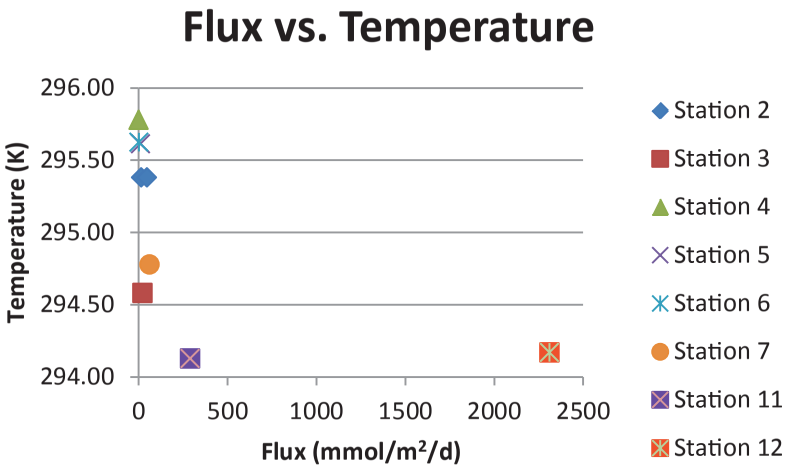

Box and gravity cores included for all stations with CTD data

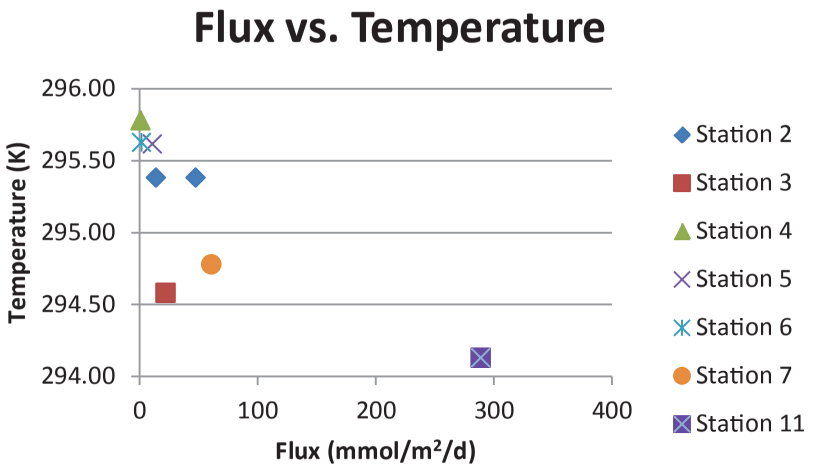

Station 12 removed to enhance stations with lower flux

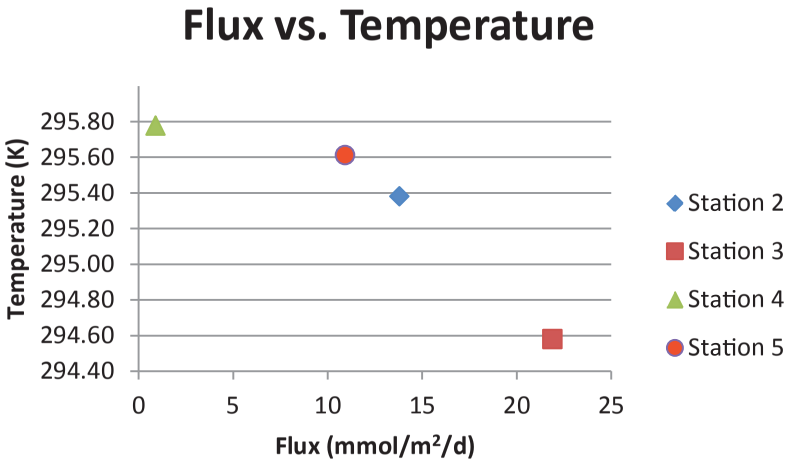

Box cores only

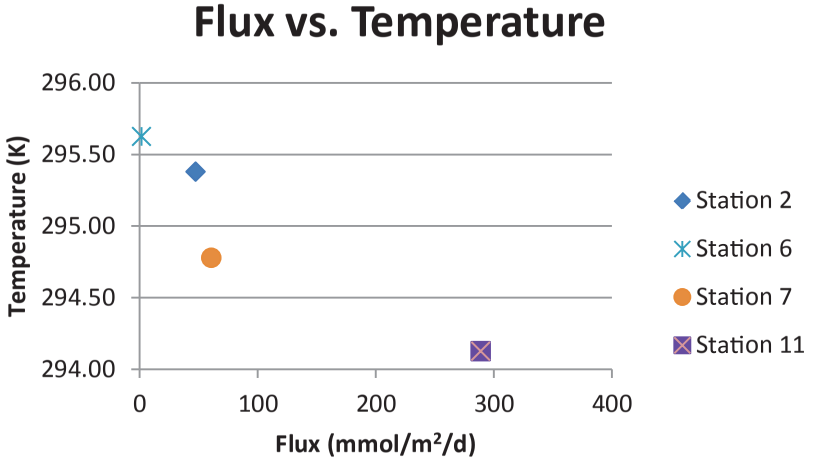

Gravity cores only, not including station 12

S2a. Flux-temperature trends; temperature measurements recorded by CTD device.

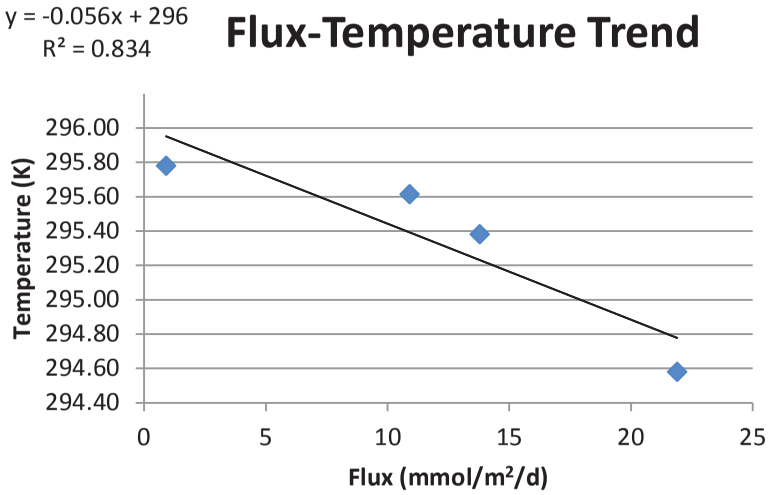

Flux-temperature relationship for box cores

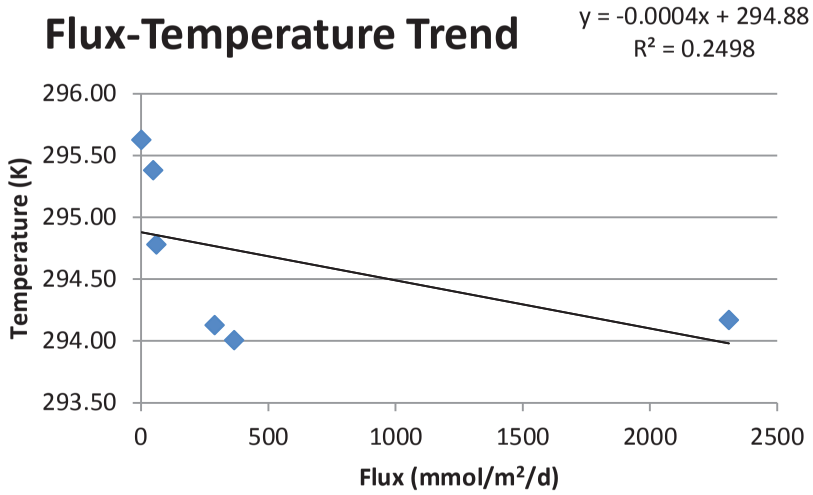

Flux-temperature relationship for gravity cores

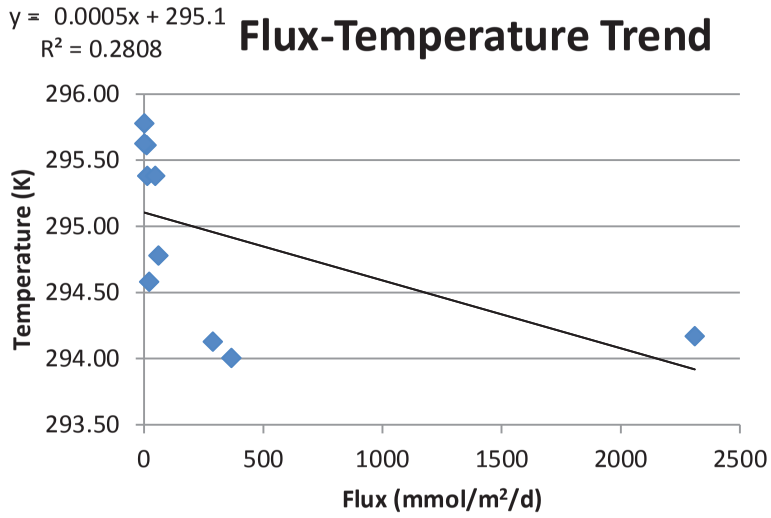

Box and gravity core curve shown as one series

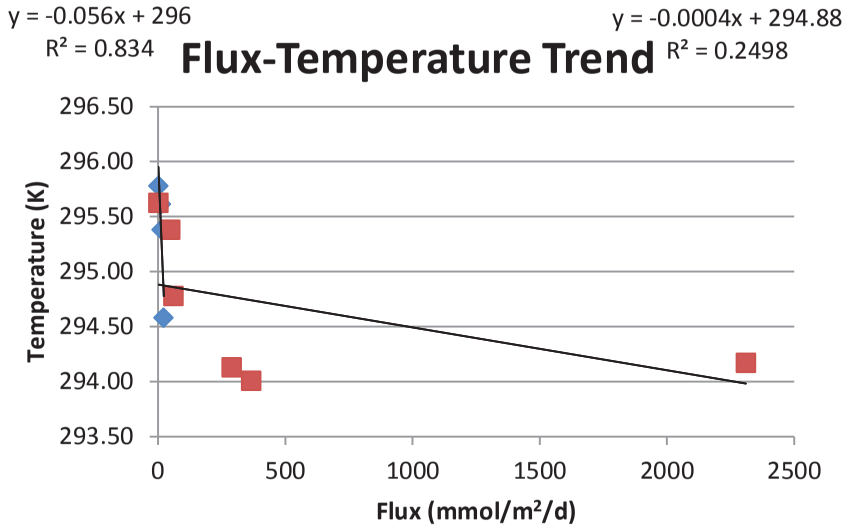

Box and gravity core curves shown as two data series

S2b. Flux-temperature linear relationships. Linear equations for the box core data are shown in the top left corner of each graph, while the gravity core equations are shown in the top right corner.

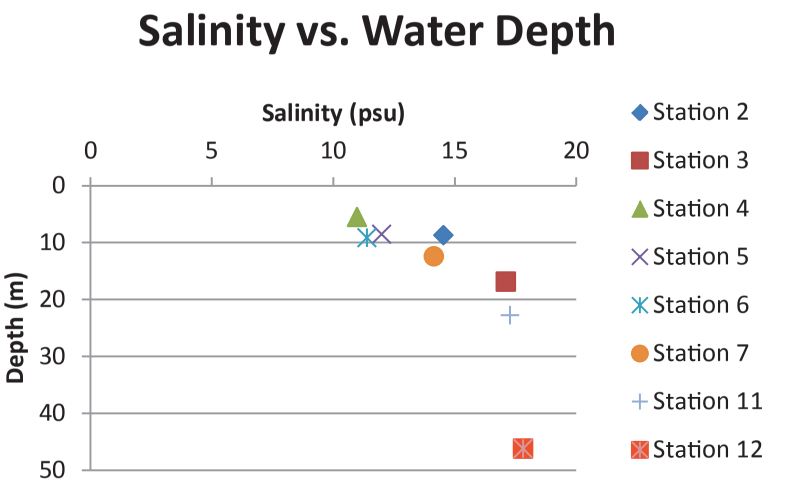

Box and gravity cores included for all stations with CTD data

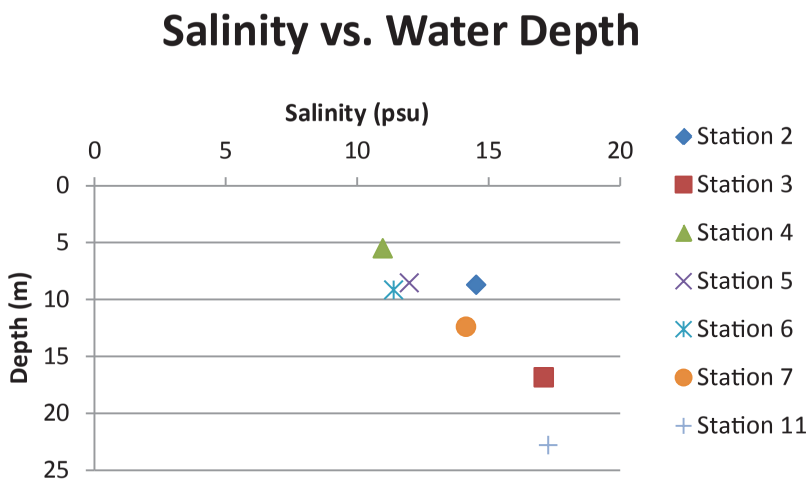

Station 12 removed

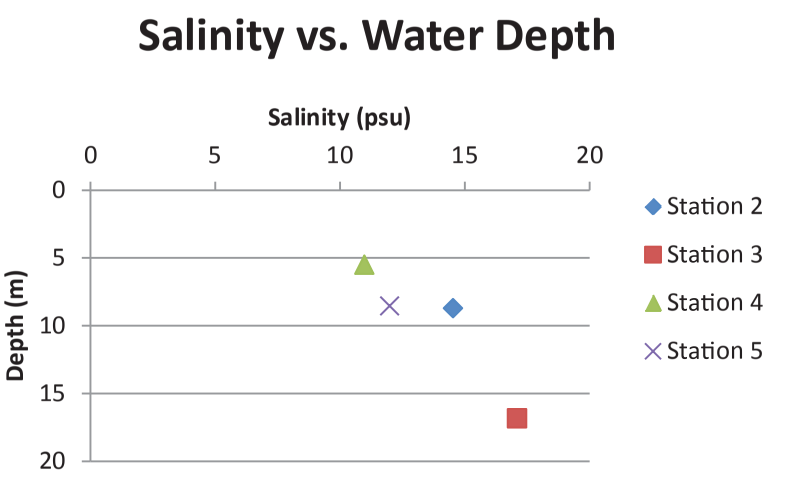

Box cores only

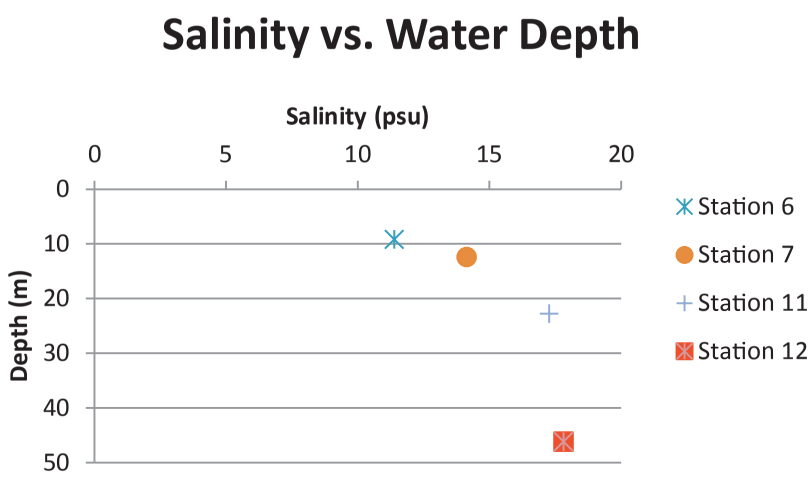

Gravity cores only

Figure S3a. Salinity-depth trends; water depth and salinity measurements recorded by CTD device.

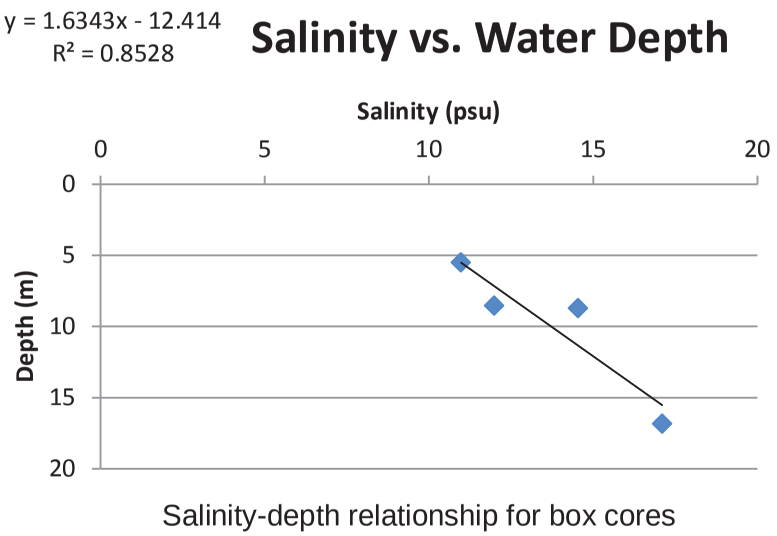

Salinity-depth relationship for box cores

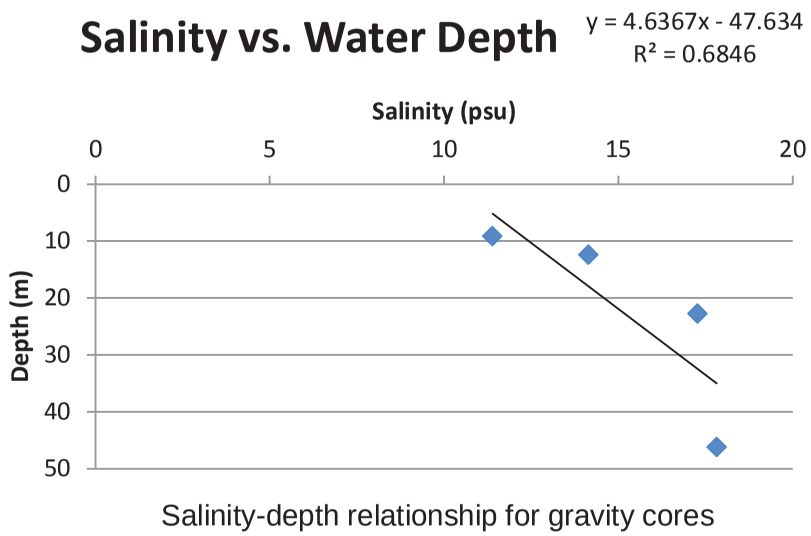

Salinity-depth relationship for gravity cores

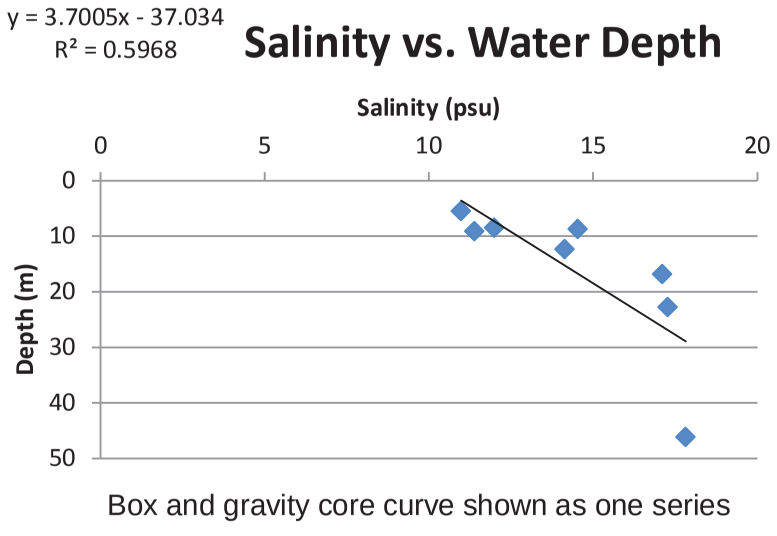

Box and gravity core curve shown as one series

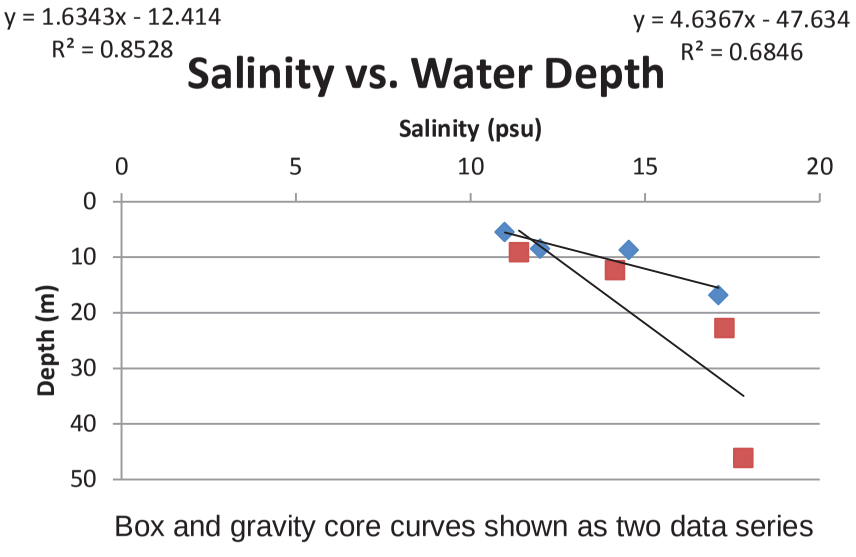

Box and gravity core curves shown as two data series

Figure S3b. Salinity-depth linear relationships. Linear equations for the box core data are shown in the top left corner of each graph, while the gravity core equations are shown in the top right corner.

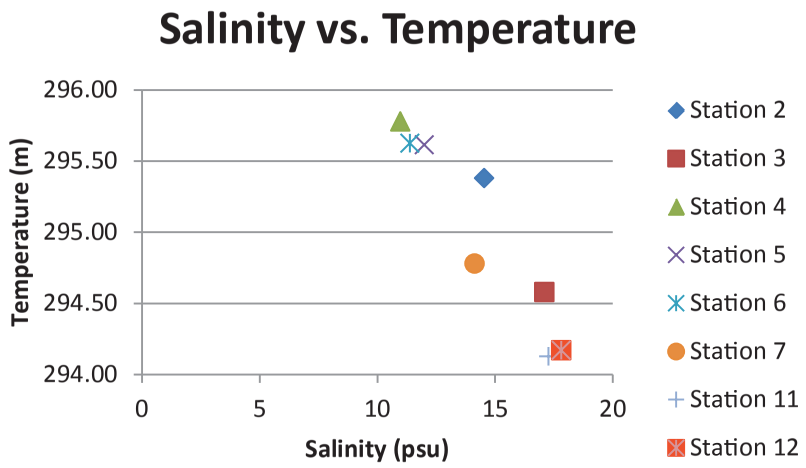

Box and gravity cores included for all stations with CTD data

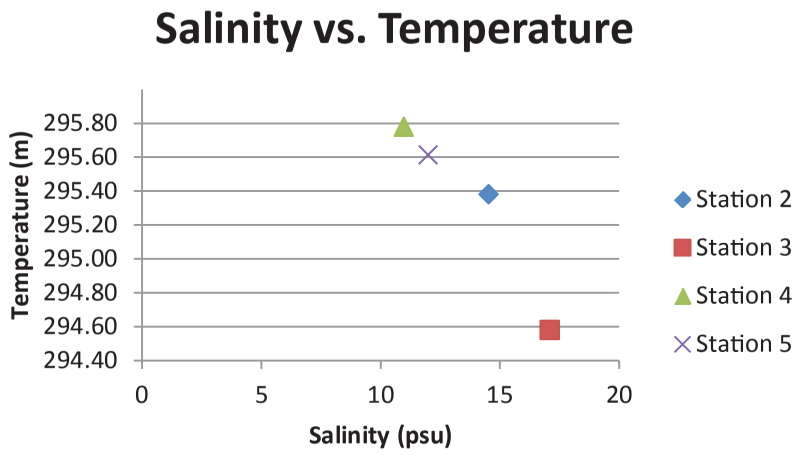

Box cores only

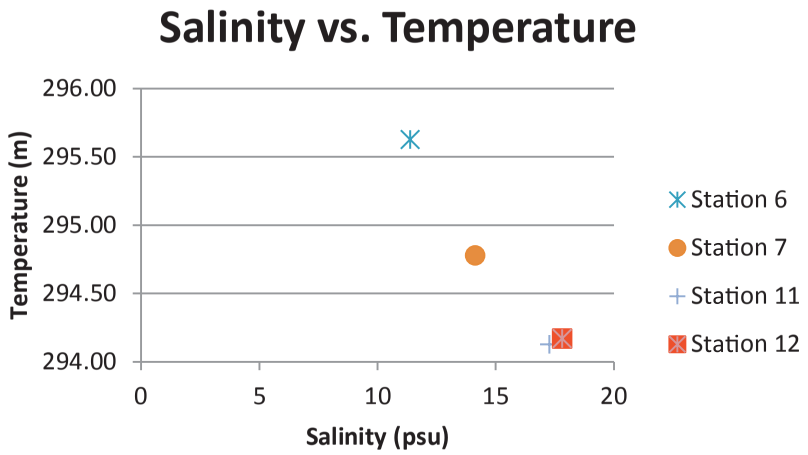

Gravity cores only

Figure S4a. Salinity-temperature trends; water temperature and salinity measurements recorded by CTD device.

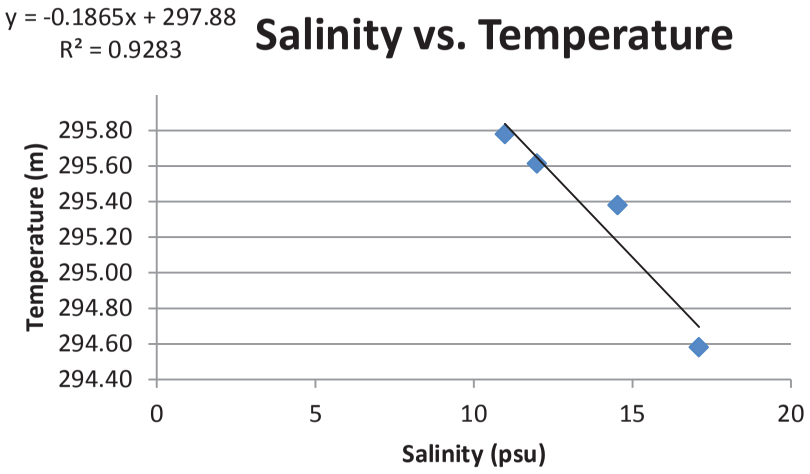

Box cores only

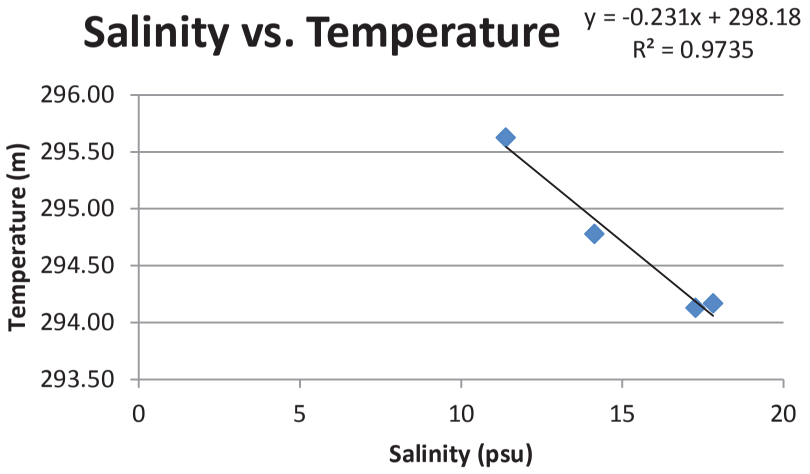

Gravity cores only

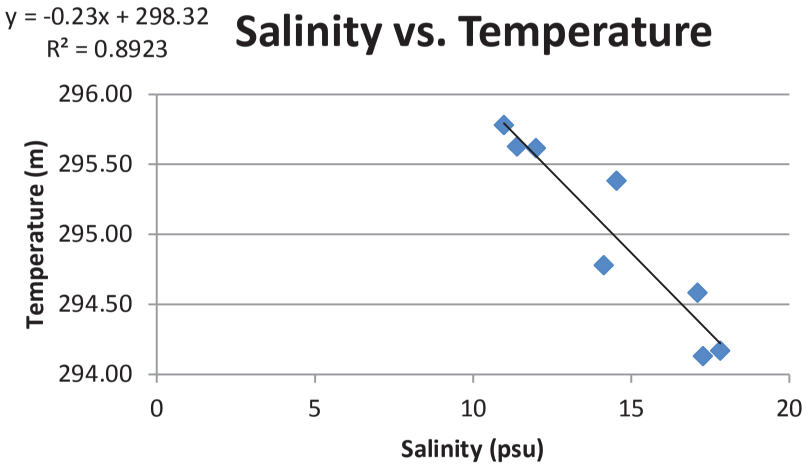

Box and gravity core curve shown as one series

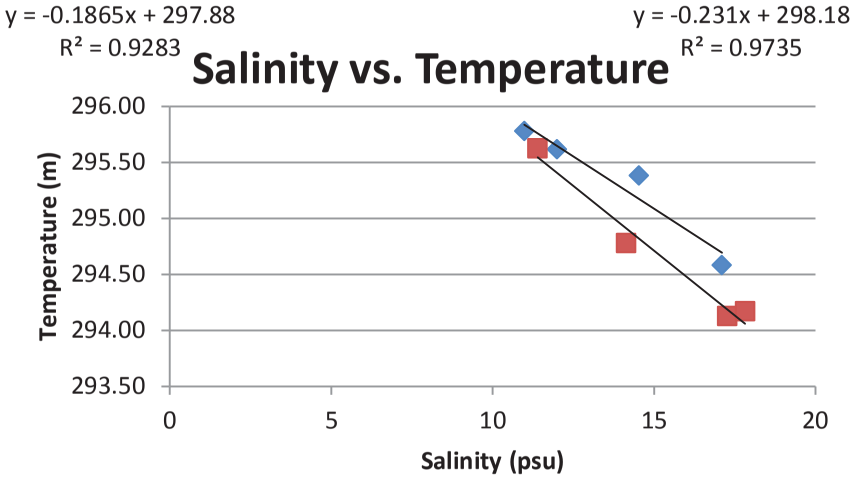

Box and gravity core curves shown as two data series

Figure S4b. Salinity-temperature linear relationships. Linear equations for the box core data are shown in the top left corner of each graph, while the gravity core equations are shown in the top right corner.

(Blank)

Evaluating the Nutrient and Major Anion Composition of Urban and Forested Catchment Streams in the Coastal Plain of Chesapeake Bay

Caroline Tapscott, REU Fellow
Maryland Sea Grant

Dr. Michael Williams, Research Assistant Professor
Chesapeake Biological Laboratory, University of Maryland Center for Environmental Science

Abstract

Eutrophication of the Chesapeake Bay has been a concern of environmentalists for several decades. A major source of nutrients that lead to eutrophication is from small streams and tributaries running throughout the Chesapeake Bay watershed. Studies show that degradation of water quality is prevalent in urbanized areas, and efforts are being made to help prevent pollution caused by decreased water quality from reaching the Bay. The purpose of this study was to examine the nutrient retention effectiveness of a stream restoration site in Anne Arundel County, Maryland during base- and storm-flow conditions. Concentrations of major anions (chloride (Cl^-) and sulfate (SO_4^{2-})) and nutrients (nitrate (NO_3^-), total dissolved nitrogen (TDN), and total dissolved phosphorus (TDP)) in precipitation and the stream water of both a partially suburban and a predominately forested catchment were determined. We found that nitrogen (N) and phosphorus (P) are being processed (uptake or loss) during base-flow periods but not during storm-flow periods. Additionally, anion and nutrient concentrations were generally higher in the urban catchment stream than in the forested catchment stream. The results of this study indicate that restoration sites can be effective at removing some N and P in stream water thereby reducing nutrient loads to tributaries of the Chesapeake Bay.

Keywords: Land use, Nutrients, Precipitation, Stream restoration, Water quality

Introduction

Nutrient cycling and nutrient enrichment in the Chesapeake Bay has led to eutrophication of the estuary (Kemp et al. 2005; Paerl et al. 2006). Eutrophication is the ecosystem's response to inputs of excess nutrients, such as nitrogen (N) and phosphorus (P) through fertilizers or sewage, to an aquatic system (Conley et al. 2002). Often hypoxia (low oxygen) or anoxia (no oxygen) is a response of aquatic systems to elevated nutrient loading (Diaz 2001). Nutrient enrichment has caused wide-spread changes in coastal habitats including more frequent algae blooms, decreased biodiversity, increased turbidity, and a reduction in the distribution of submerged aquatic vegetation — SAV (Cloern 2001; Testa et al. 2008; Orth et al. 2010; Williams et al. 2010). The deterioration of estuarine environments that would naturally process increased nutrient loading is occurring at an accelerated rate (Paerl et al. 2006). Thus, human population growth in coastal watersheds greatly contributes to increased amounts of nutrients in estuaries around the world. Increasing watershed development is especially

relevant to the Chesapeake Bay system, because the ratio of the Chesapeake's watershed area to its estuarine water area is relatively large when compared to this ratio for other estuaries (Kemp et al. 2005).

Degradation of the water quality of streams is common in urbanized areas. For example, Williams et al. (2005) found that nitrate (NO_3^-), chloride (Cl^-), and sulfate (SO_4^{2-}) concentrations are generally higher in urban and agricultural areas than in forested areas. All of these chemicals can come from a variety of sources, including road deicing salts, fertilizer use, animal wastes, and septic effluents (Herlihy et al. 1998; Williams et al. 2005). Cl^- in particular is a good indicator of human disturbance in the watershed because of its wide range of sources, most of which come from human activities within a watershed. The degradation of water quality in urban and agricultural areas is especially common because storm water is able to pick up oil, pesticides, and other chemicals as it flows across fields and streets, making its way to streams and storm drains. According to the Chesapeake Bay Program's website (www.chesapeakebay.net), increased development across the Bay's watershed has made storm water runoff the fastest growing source of pollution to the Bay. In urbanized areas, storm water runoff is unable to penetrate the surfaces of roads, parking lots, and roofs (i.e., impervious surfaces); instead, the runoff mobilizes chemicals, eventually dumping them into streams, and the increased velocity of runoff leads to the erosion of stream banks, causing more sediment fluxes to the Bay.

In addition to N entering streams via stormwater runoff, it is estimated that up to one third of the nitrogen that pollutes the Bay watershed comes from the air (www.chesapeake.org/stac/Pubs/atmosphericnitrogen.report.pdf). Sources of atmospheric pollution include exhaust from vehicles, industries, power plants, gas-powered lawn tools, and farm operations. Thus, in a heavily urbanized and agricultural area such as the Chesapeake Bay watershed, atmospheric N deposition is now the second major contributor to the worsening water quality of the Bay (www.chesapeakebay.net).

Efforts are being made to reduce the amount of pollution that is reaching the Bay. For instance, improving water quality is in part being done by implementing best management practices (BMPs) in streams (i.e., stream restoration) in the Chesapeake Bay watershed. BMPs work to keep chemicals contained in storm water runoff from reaching tributaries through a variety of means, such as promoting spillover of stream flow during high-flow periods (storm-flow events) onto adjacent floodplains and wetlands (Filoso and Palmer 2011). Other methods include reforestation or the use of cover crops to prevent erosion of stream banks as well as the export of excess nutrients and chemicals downstream.

The overall goal of this project was to evaluate how efficient a stream restoration BMP is at preventing pollutants from reaching the estuary. The restoration site used in this project, named Howard's Branch, is located in the Coastal Plain physiographic province of the Chesapeake Bay watershed and has two sub-catchments, one that has a substantial amount of low-density residential land use (henceforth referred to as urban) and one that is predominately forested; their streams join at the upstream end of the restored stream reach. Thus, this site is ideal for investigating the differences in the water quality of a forested versus a more urban setting. In order to do this, we evaluated how the chemicals of N, P, and major ions (Cl^- and SO_4^{2-}) change in concentration as they enter these catchments as rainfall and exit in the form of stream water runoff. The potential effectiveness of the stream restoration BMP was also examined by measuring the chemical concentrations of the same constituents in stream water, both up and downstream of the restoration reach and during base- and storm-flow periods.

Hypotheses and Objectives

According to Herlihy et al. (1998), elevated Cl^- concentrations in water are indicative of human activities in a watershed. Therefore, the Cl^- concentration in the stream water in the urban catchment should be higher than that of the forested catchment. In addition to a higher Cl^- concentration, the urban catchment stream should have higher NO_3^- and SO_4^{2-} concentrations than that of the forested catchment, as these chemicals are common pollutants found in urbanized areas. Previous studies suggest that restored streams with low gradient and adjacent wetland floodplains, such as at Howard's Branch, have lower concentrations of some forms of N in stream water during storm-flow periods (Filoso and Palmer 2011). Similarly, the restoration reach at Howard's Branch may be effective at filtering some forms of N (i.e., ammonium (NH_4^+) and NO_3^-) during base-flow periods. By contrast, if concentrations of N are not reduced along the restoration reach, this suggests that it is relatively ineffective removing forms of N and may actually be a source of some forms of N. Compared to N and P concentrations during base-flow periods, the respective concentrations of each chemical should be higher during storm-flow periods in the urban catchment due to storm water runoff and a reduction in the amount of time water is able to be processed (i.e., denitrified) in the restoration reach due to increased water velocity.

The primary objectives for this project were to:

- Determine if there is a significant difference in NO_3^-, SO_4^{2-}, Cl^-, total dissolved nitrogen (TDN), and total dissolved phosphorus (TDP) concentrations in the stream water draining the forested and urban catchments of the Howard's Branch study site.
- Use flow data to estimate potential differences in the solute fluxes (i.e., loads) of each site.
- Evaluate the relationship between the solute concentrations of the constituents mentioned previously in rainwater of the study site area and the stream water at the outflow of each stream during base-flow and one storm-flow event.
- Use a mixing analysis (conservative versus non-conservative solutes) to determine if the restoration reach is effective at filtering N (uptake or loss) and P during base-flow and a storm-flow event.

Study Site

The stream that was studied, Howard's Branch, flows into the Severn River, which is a tributary of the Chesapeake Bay. Anne Arundel County, in which the stream is located, is one of the most urbanized regions in the United States. The Howard's Branch watershed had a degraded lowland stream that was transformed into a stream-wetland complex in 2001 (Filoso and Palmer 2011). The stream was restored by establishing vegetated floodplains which create shallow wetlands adjacent to the restored reach, allowing excess water during storm-flow periods to spill over into the wetlands.

Land cover statistics for the area were determined by doing a Geographic Information System (GIS) analysis with National Land Cover Data (NLCD) of the Howard's Branch watershed from 2006 (Figure 2). Satellite images (Google) and ground truthing were also used to distinguish between forested and developed areas with some tree cover.

Materials and Methods

Water samples were collected from the Howard's Branch restoration site during base- and storm-flow periods using methods adapted from those used by Filoso and Palmer (2011). The samples taken during a base-flow period (defined as an antecedent period of 48 hours with no rainfall) provided a set of solute concentrations during normal conditions against which to compare the chemical concentrations found during a storm-flow period. Samples were taken in both the urban and forested catchment as well as downstream of the restored reach (i.e., at the restoration reach outflow) for a period of 24 hours. Hourly samples taken over this diel period were subsampled (by using every other sample) to determine their chemical composition. Water samples were collected using an automated pump sampler (Teledyne ISCO model 6712) with a 24-bottle carousel. Similar to base-flow samples, storm-flow was subsampled by using every other sample. Water samples were collected in 1-L polyethylene bottles that had been acid washed and rinsed several times with deionized water to prevent contamination. Through the use of an actuator, the autosampler was triggered when stream water levels increased 1 cm above normal base-flow levels. The Isco sample bottle carousel was filled with ice during sampling periods to help preserve solute concentrations of the samples before they were filtered. Water samples were transported to the Chesapeake Biological Laboratory (CBL) in an ice-filled container and were filtered within 24 hours of the storm event. At the laboratory, the samples were filtered and subsequently analyzed for NO_3^-, SO_4^{2-}, and Cl^- using a Dionex ion chromatograph (IC 2010). Filtration was done using pre-ashed Whatman glass-fiber filters (0.7 µm nominal pore size) and aliquots were stored in acid-washed bottles that had been rinsed several times with deionized water to avoid any contamination problems. A subset of samples was also analyzed for TDN and TDP using the methods identified on the Nutrient Analytical Services Laboratory (NASL) website (nasl.cbl.umces.edu).

Rainwater samples were collected in two buckets from one location at the restoration site. Acid washed buckets rinsed with deionized water (until rinse water had a conductivity of < 1 µS/cm) were installed in a forest clearing close to the restored stream reach and high enough (about 1 m above ground) so that no water splashing off the ground or stream surface would contaminate the bucket of rainwater. Moreover, the buckets were covered with acid-washed netting (mesh size approximately 2 mm^3) that had been rinsed with deionized water to prevent debris and bugs from contaminating the rainwater. Similar to the stream water samples, the rainwater samples were collected within 12 hours after the storm event and transported to the laboratory while being kept cool by ice packs. This water was also filtered and analyzed with the Dionex ion chromatograph for the same suite of anions and analyzed for TDN and TDP at NASL.

Results

Land Use

Using ground truthed data to refine the NLCD image analysis, it was determined that the mixed-forest pixels represented low-intensity urban landscape. Moreover, all of the mixed forest pixels in the predominately forested catchment and the northern portion of the restoration reach area (i.e., north of the stream) are forest. Accordingly, the entire watershed of the Howard's Branch study site consists of 72.0 ha (76.6%) forested land and 14.9 ha (15.9%) suburban or developed land out of a total of 94 ha. The remaining 7.1 ha (7.6%) is attributed to wetland. The urban sub-watershed of the study site is 58 ha of which 42.8 ha (73.8%) is forested, 11.2 ha (19.4%) is suburban/developed, and 4.0 ha (6.8%) is wetland. All houses in the residential area of this watershed are on a septic system. The forested sub-watershed is considerably

smaller than the urban sub-watershed that is 19 ha. This sub-watershed has 18.5 ha (97.2%) of forested land and 0.5 ha (2.8%) of wetland. The remaining 17.0 ha is accounted for by the restoration reach. Of this, 10.7 ha (62.9%) is forested land, 3.2 ha (18.8%) is suburban/developed, and 2.6 ha (15.3%) is wetland.

Stream Flow

Using modified pressure transducer data from the three sites, it was possible to compare the hydrographs for each site during base- and storm-flow conditions. For example, the forested stream had the lowest flow rate, as evidenced by the smaller peak height of the hydrograph, while the restored stream had the highest (Figure 3). Additionally, the wider base of the restored catchment hydrograph indicates that it was less flashy than the urban and forested catchments that had narrow hydrograph bases. Lastly, in contrast to the restoration reach, the baselines of the urban and forested sites were slightly higher after the storm-flow event.

Precipitation and Stream Water Chemistry

Base-flow samples for this study were taken on 20 June 2012, starting at 13:00, and subsequent samples were taken at 1 hour intervals for 24 hours. The storm event studied occurred overnight, 10 July to 11 July 2012. The sampler in the urban catchment was triggered at 19:18, while the sampler in the forested catchment was triggered at 20:30. The sampler for the restoration reach was triggered at 05:00 on the morning of July 10. The last twelve samples from this set were discarded, and new, clean bottles were added in order to obtain twelve storm-flow samples from the restoration site that coincided with those from the urban and forested catchment sites. The first sample of these was taken at 20:14 on July 10. Storm-flow samples were collected every 15 minutes, one sample per bottle, until all bottles were filled.

The average concentrations for Cl^-, SO_4^{2-}, NO_3^- (recorded as nitrate nitrogen—NO_3-N), TDP, and TDN during base- and storm-flow events for the three study sites, as well as for the rain sample, are included in Table 1. The rainwater collected during the storm event had considerably lower Cl^- and SO_4^{2-} concentrations than in stream water collected during both base- and storm-flow events. For example, Cl^- concentrations were 0.8 mg/L in rainwater compared to the means 67.0 mg/L in the urban catchment, 6.3 mg/L in the forested catchment, and 57.5 mg/L in the restored catchment during base-flow and 33.0 mg/L in the urban catchment, 4.8 mg/L in the forested catchment, and 33.2 mg/L in the restored catchment during storm-flow. By contrast, NO_3^-, TDN, and TDP concentrations in rainwater were closer their respective concentrations during both base- and storm-flow events than Cl^- or SO_4^{2-}. For instance, the NO_3^- concentration in rainwater was 0.33 mg/L compared to 0.36 mg/L in the urban catchment, 0.10 mg/L in the forested catchment, and 0.24 mg/L in the restored stream during base-flow and 0.41 mg/L in the urban catchment, 0.12 mg/L in the forested catchment, and 0.42 mg/L in the restored catchment during storm-flow. As stated, TDN and TDP followed this same general trend, which can be seen in Table 1.

During base-flow conditions, the average Cl^- concentration in the urban reach was nearly ten times higher than in the forested, while it was only about 1.2 times higher than the restored reach. The average NO_3^- concentration in the urban stream was 3.6 times higher than the forested, but only 1.5 times higher than the restored stream. TDN concentrations were on average higher in the urban reach than in the forested by a factor of about 2.5, whereas they were only greater than in the restored reach by a factor of about 1.5. Conversely, SO_4^{2-} and TDP concentrations were higher in the forested reach than in the other two reaches. SO_4^{2-} was

about 1.2 times more abundant in the forested stream than in the urban and nearly 1.5 times higher in the forested stream than the restored stream. Average concentrations for TDP in the forested stream were nearly twice as high as in the urban stream and 2.5 times higher than in the restored stream. Concentrations of all anions and nutrients were relatively invariant during the 24-hour base-flow sampling period (Figures 4-8).

During storm-flow conditions, concentrations of the major anions and nutrients in the urban and restored sites were similar. However, the automated sampler at the restored site was triggered to start sampling earlier than at the other two sites, giving a base-flow signature for the first six samples, followed by a storm-flow signature for the last six. Accordingly, Cl^-, NO_3^-, and TDN concentrations were all about equal in the urban and restored reaches and lower in the forested reach. Cl^- concentrations were almost seven times higher in the urban and restored sites than in the forested site. NO_3^- was about 3.5 times higher in the urban and restored reaches than in the forested, while TDN was 2.5 times greater in the urban and restored sites than in the forested. In addition, as during base-flow conditions, SO_4^{2-} and TDP concentrations were higher in the forested site than in the urban or restored site (the latter only briefly compared to the restored site), although it is unclear what the concentrations at the restored site were during the falling limb of the hydrograph. During storm-flow conditions at the restored site, NO_3^- (Figure 6), TDP (Figure 7), and TDN (Figure 8) concentrations all increased dramatically to a maximum before abruptly decreasing again, whereas Cl^- (Figure 4) concentrations decreased dramatically before abruptly increasing again. In contrast, SO_4^{2-} (Figure 5) concentrations increased slowly before decreasing towards the end of the sampling period. Storm-flow concentrations at the forested site for Cl^- were more stable than at the other two sites (Figure 4), but varied for all other nutrients and anions.

Discussion

Solute Dynamics

When water enters the atmosphere through evapotranspiration, it is almost completely pure, but immediately begins to interact with other substances in the air. The substances rainwater can interact with come from a variety of different sources. As part of the nitrogen cycle, molecular nitrogen in the atmosphere (N_2) fixed in order to be biologically available. In this process, N_2 is converted into nitric oxide (NO) or nitrogen dioxide (NO_2) (together referred to as NO_x gases) through reaction with oxygen at high temperatures through combustion. NO_x emissions are higher in urban areas where there is a large amount of vehicle traffic. These NO_x gases subsequently form nitric acid (HNO_3) in the atmosphere. HNO_3 then becomes dissolved in rainwater and falls back to the earth as NO_3^- (Vitousek et al. 1997). During the storm event, as the rainwater moved progressively through the forest canopy to soils and eventually the streams, some of the NO_3^- in rainwater was either utilized or denitrified. This is especially evident in the forested catchment where the NO_3^- concentration is less than half that of rainwater. Similarly, sulfur dioxide (SO_2) is emitted to the atmosphere through the combustion of coal or fossil fuels (as in vehicles). SO_2 reacts with water molecules in the air to form sulfuric acid (H_2SO_4), which is the major contributor to acid rain, and is probably the source of SO_4^{2-} in rainwater (Spiro et al. 2012). A common source of Cl^- in rainwater is aerosols originating from oceans or other bodies of salt water, such as the Chesapeake Bay; as water from the Bay is evaporated, some of the Cl^- ions travel with the water vapor (Avery et al. 2001). Finally, P in rainwater can also be contributed through air pollution (such as vehicle exhaust). P is much less mobile than N and, accordingly, it is just over 70 times less concentrated in rainwater than N (Spiro et al. 2012).

In examining Figure 3, it is evident that the restoration site hydrograph has a fatter base than the other two hydrographs. This indicates that the restoration site is helping to calm the flashy runoff from the urban site. Hence, the restoration site is reducing the energy of the water moving through the two upstream catchments, which helps to reduce the erosive power of the stream. Moreover, the baselines of the urban and forested streams are slightly higher after the storm, which is likely due to groundwater recharge depleting the streams during dry periods. When it rains, stormwater runoff fills the streams, increasing their volume (creating the hydrographs), and eventually the stream levels return to normal conditions. Stream water continually seeps into the groundwater reservoir, causing groundwater recharge. During periods with no precipitation (i.e., base-flow conditions), this leads to decreased amounts of flow in the streams. Therefore stream levels are slightly less during base-flow (above, defined as an antecedent period of 48 hours with no rainfall).

Using a basic two-sample t-test, it was determined that there was a significant difference in anion and nutrient concentrations in the urban and forested catchments (all p-values were well below 0.05). As predicted, Cl^- and NO_3^- were both significantly higher in the urban stream than the forested stream during both base- and storm-flow conditions. Sources of Cl^- and NO_3^- are often anthropogenic. Septic effluent is a common source of both Cl^- and NO_3^- in developed areas (Williams et al. 2005). As the entire low-density residential area is on a septic system, it is probable that septic effluent is being leached into the urban and restored catchments, causing increased concentrations of these constituents. Additionally, another common source of NO_3^- is lawn fertilizers; the increased concentrations of NO_3^- in the urban catchment towards the beginning of the storm-flow period (Figure 6) could be caused by stormwater picking up fertilizer as it runs over the lawns in the residential area. Like NO_3^-, TDN is also higher in the urban stream than the forested in base- and storm-flow conditions. There are likely similar causes of increased TDN in the urban stream (such as septic effluent and fertilizer contamination). Also, another source of Cl^- in the urban stream may come from road deicing salts used on the roads located in the urban watershed. Although these salts are only used in the winter, some of the chemicals (i.e., Cl^-) from them are transported to the ground and are slowly leached into groundwater and subsequently stream water throughout the year.

SO_4^{2-} concentrations were higher in the forested stream than in the urban stream or below the restored reach, unlike what was predicted. This could be because the higher loads of N and P have caused areas of hypoxia or anoxia in the urban and restored reaches. Hypoxia or anoxia could also be caused by the wetland areas in each watershed, which have strong reducing environments. In hypoxic and anoxic regions, oxygen is unable to be reduced which decreases the oxidation-reduction potential and changes the sediment chemistry in the streams (Kemp et al. 2005). This causes SO_4^{2-} to become preferred electron acceptor in these regions of low oxygen. Therefore, there is less SO_4^{2-} in the urban and restored reaches (where there is low oxygen) than in the forested stream. Another possible cause of higher SO_4^{2-} concentrations in the forested catchment is the mineralization of organic matter. There is probably more organic matter caught in the forested catchment than in the urban or restored catchments due to the suburban areas where leaf litter is removed. Mineralization of this organic matter results in SO_4^{2-} as a first step. In the restored catchment there is a greater amount of wetland area that is able to convert SO_4^{2-} into H_2S, thereby lowering the concentration of SO_4^{2-} in this catchment. During storm events, water moves more rapidly through the urban catchment (and the restored catchment as a result) than the forested catchment. This means that there is less time for the water to sit in the wetland areas to process SO_4^{2-}, resulting in a smaller distribution of SO_4^{2-} concentrations among the three catchments. TDP also has a higher average concentration at the forested site than at the urban or restored sites. This could be because there is more

organic matter from leaf litter in the forested catchment than in the urban or restored catchments.

Restoration Effectiveness

The most accurate way to determine if the restoration reach is effective at filtering N and P would be to use a mass balance approach, in which chemical loads entering and leaving the restoration reach need to be calculated. Solute loads are calculated as the product of solute concentration and discharge. Thus, it would be necessary to have stream flow data for each of the catchments in order to calculate the mass of solutes entering the restoration reach. Although pressure transducer data can be converted into flow data with the use of a flow rating curve at each sampling station, rating curves take many flow measurements at a wide range of stage heights to be accurate. Because the two upstream catchments are relatively new, there is not a sufficient amount of data to create accurate calibration curves for these sites. Thus, instead of using a mass balance approach to determine restoration effectiveness, we used a conservative versus non-conservative solute mixing analysis. Chloride is a conservative ion, meaning it is not utilized or processed (i.e., no uptake or loss) by plants or bacteria in the restoration reach. By analyzing the change in Cl^- concentration from the urban and forested sites to the restored site, it is possible to determine whether the restoration reach is losing more N and P than what would be expected if they were not being biologically utilized (i.e., uptake) or lost (e.g., denitrification). This can be done assuming that a certain percentage of the Cl^- concentrations from the urban and forested sites will be equal to 100% of the Cl^- concentration at the restored site and by using the following the equation

$$x[Cl^-]_U + y[Cl^-]_F = [Cl^-]_R \qquad (1)$$
$$x + y = 1$$

where x is the percentage contributed by the urban catchment, $[Cl^-]_U$ is the average Cl^- concentration at the urban site, y is the percentage contributed by the urban catchment, $[Cl^-]_F$ is the average Cl^- concentration at the forested site, and $[Cl^-]_R$ is the average Cl^- concentration at the restored site. We found that the urban site contributes approximately 84% (x) of the end-member mixing Cl^- concentration during base-flow conditions. This leaves about 16% (y) to be contributed by the forested site. These percentages approximate the estimated discharge from the two upstream catchments, therefore these values are realistic. Using these percentages along with the above equation to calculate the expected NO_3^- concentration for the restored site (replacing Cl^- concentrations with NO_3^- concentrations), we estimate that the actual NO_3^- concentration is approximately 24% less than the expected value if NO_3^- were acting conservatively. Similarly, doing the same calculations for TDN and TDP, we estimate that TDN and TDP are both about 34% less than the expected conservative mixing values during base-flow conditions. These decreases in concentration suggest that the restoration reach is effective in retaining or processing (uptake) N and P during base-flow conditions.

Although according to Table 1, Cl^- concentrations in the urban and restored catchments during the storm event are very similar, when comparing samples from the urban site to those of the restoration site with similar corresponding times, Cl^- concentrations in the restored catchment are greater than those in the urban catchment (Figure 4). Thus, performing a mixing analysis for the storm-flow event is not meaningful due to these higher average Cl^- concentrations in the restored reach than in either the urban or forested reaches (Table 1). For instance, when a mixing analysis for the storm-flow event is attempted, using equation (1) shows that the urban stream accounts for 100.6% of the Cl^- concentration entering the restoration catchment. While much of the water in the restoration site during the storm event is

contributed by the urban stream, it is not possible that it is contributing more than 100%. The higher Cl^- concentration in the restored reach indicates that there is likely a source of Cl^- entering the stream along the restoration reach. An example of a possible source of Cl^- downstream of the urban and forested sites during storm events is a storm drain which fills with stormwater runoff from the neighborhood adjacent to the urban stream. Because of lateral inputs to the stream between the upstream and downstream catchments, it is impossible to determine how much of the water at the restoration catchment is contributed by the two upstream sites and by various possible lateral inputs. Moreover, storm-flow concentrations for all constituents are generally higher than base-flow concentrations for each catchment (Figures 4-8). Although it is difficult to determine whether there is little or no processing of N or P during storm-flow events using this technique, we speculate that there is little nutrient processing because as rainwater and runoff combine with stream water, stream water velocity increases, causing the water to move through the restoration reach quickly. With the increase in storm size, there is likely a corresponding decrease in the amount of processing that occurs due to the shortened residence time of water in the restoration reach.

Conclusions

Eutrophication of the Chesapeake Bay is a problem that worsens with the increase flow of nutrients and other chemicals into the Bay. As many of these excess nutrients stem from human activities within the watershed, it is becoming increasingly important to monitor the levels of these chemicals in tributaries in developing and urbanized areas. The implementation of BMPs, such as stream restoration projects, need to be part of a larger plan, such as reducing fertilizer use, driving cars less, or moving away from using septic systems, to help restore the Bay to a healthy state. However, in order to determine if these BMPs are effective it is necessary to test the water quality in the streams draining restoration reaches, which was the goal of this study. Results from this project suggest that the restoration site at Howard's Branch is effective at processing N and P during base-flow conditions. However, it is unlikely that there is much processing of nutrients occurring during storm-slow conditions due to the short residence time of the stream water in restored areas. The results of this study suggest that the type of stream restoration implemented in Howard's Branch is a potentially effective BMP that could be used to reduce nutrient runoff from other degraded streams in the Coastal Plain region of the Chesapeake Bay watershed, and this information will be particularly useful for water resources managers.

Acknowledgements

I would like to thank Maryland Sea Grant and the National Science Foundation for providing me with the opportunity and funding to do this research. Also, I would like to thank Jen Li and Jenna Briscoe for their help with lab and field work, as well as Rosemary Fanelli for helping to compile the GIS data.

References

Avery, G.B. Jr., J.D. Willey, R.J. Kieber. 2001. Diurnal variations in major rainwater components at a coastal site in North Carolina. Atmospheric Environment 35: 3927-3933.

Chesapeake Bay Program. 2012. http://www.chesapeakebay.net. Accessed 6 June 2012.

Chesapeake Bay Program. 2009. Workshop on Atmospheric Deposition of Nitrogen. www.chesapeake.org/stac/Pubs/atmosphericnitrogen.report.pdf. Accessed 7 June 2012.

Cloern, J.E. 2001. Our evolving conceptual model of the coastal eutrophication problem. Marine Ecology Progress Series 210: 223–253. doi:10.3354/meps210223.

Conley, D.J., S. Markager, J. Andersen, T. Ellermann, and L.M. Svendsen. 2002. Coastal eutrophication and the Danish National Aquatic Monitoring and Assessment Program. Estuaries 25: 848–861.

Diaz, R.J. 2001. Overview of hypoxia around the world. Journal of Environmental Quality 30: 275–281.

Filoso, S., M.A. Palmer. 2011. Assessing stream restoration effectiveness at reducing nitrogen export to downstream waters. Ecological Applications 21: 1989-2006.

Herlihy, A. T., J.L. Stoddard, and C.B. Johnson. 1998. The relationship between stream chemistry and watershed land cover data in the mid-Atlantic region, US. Water Air and Soil Pollution 105: 377-386.

Kemp, W.M., W.R. Boynton, J.E. Adolf, D.F. Boesch, W.C. Boicourt, G. Brush, J.C. Cornwell, T.R. Fisher, P.M. Glibert, J.D. Hagy, L.W. Harding, E.D. Houde, D.G. Kimmel, W.D. Miller, R.I.E. Newell, M.R. Roman, E.M. Smith, and J.C. Stevenson. 2005. Eutrophication of Chesapeake Bay: Historical trends and ecological interactions. Marine Ecology Progress Series 303: 1-29. doi:10.3354/meps303001.

Nutrient Analytical Services Laboratory. http://nasl.cbl.umces.edu. Accessed 10 June 2012.

Orth, R.J., M.R. Williams, S.R. Marion, D.J. Wilcox, K.A. Moore, W.M. Kemp, R.A. Batiuk, P. Bergstrom, T.J.B. Carruthers, N. Rybicki, and W.C. Dennison. 2010. Annual and decadal patterns in distribution and abundance of submersed aquatic vegetation (SAV) in Chesapeake Bay and tributaries. Estuaries and Coasts: 1984–2006.

Paerl, H.W. 1988. Nuisance phytoplankton blooms in coastal, estuarine, and inland waters. Limnology and Oceanography 33: 823-847.

Paerl, H.W., L.M. Valdes, B.L. Peierls, J.E. Adolf, and L.W. Harding Jr. 2006. Anthropogenic and climatic influences on the eutrophication of large estuarine systems. Limnology and Oceanography 51:448-462.

Spiro, T.G., K.L. Purvis-Roberts, W.M. Stigliani. 2012. Chemistry of the environment, 3rd edition. University Science Books.

Vitousek, P.M., J. Aber, R. Howarth, G.E. Likens, P. Matson, D. Schindler, W. Schlesinger, and G.D. Tilman. 1997. Human Alteration of the global nitrogen cycle: causes and consequences. Ecological Applications 7: 737-750.

Williams M., C. Hopkinson, J. Vallino, and E. Rastetter. 2005. Relationships of land use and stream water solute concentrations in the Ipswich River basin, northeastern Massachusetts. Water, Air, and Soil Pollution 161:55-74.

Williams, M.R., S. Filoso, B.J. Longstaff, and W.C. Dennison. 2010. Long-term trends of water quality and biotic metrics in Chesapeake Bay: 1986 to 2008. Estuaries and Coasts 33: 1279–1299.

Figures and Tables

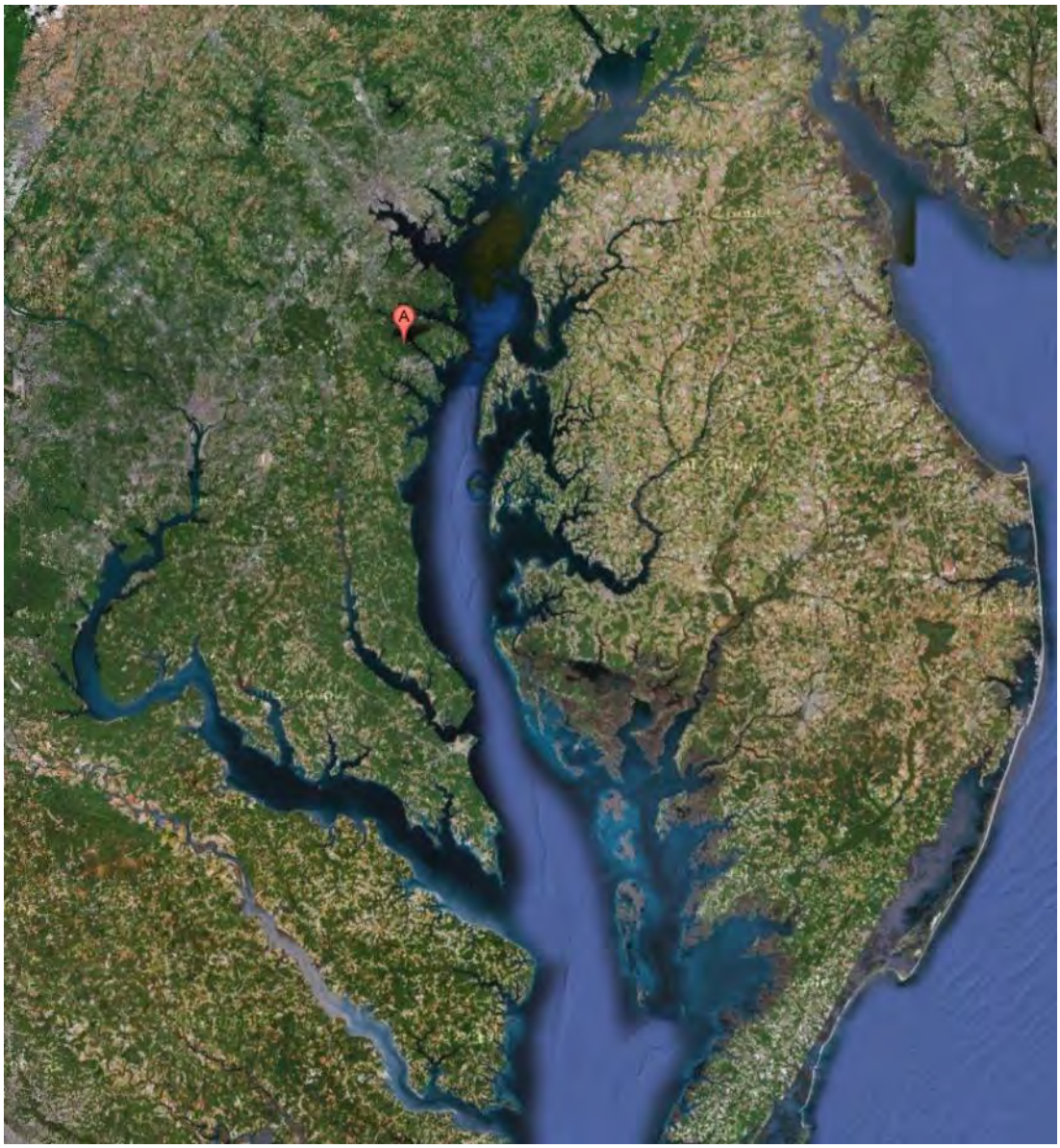

Figure 1. Howard's Branch study site location within the Chesapeake Bay Watershed.

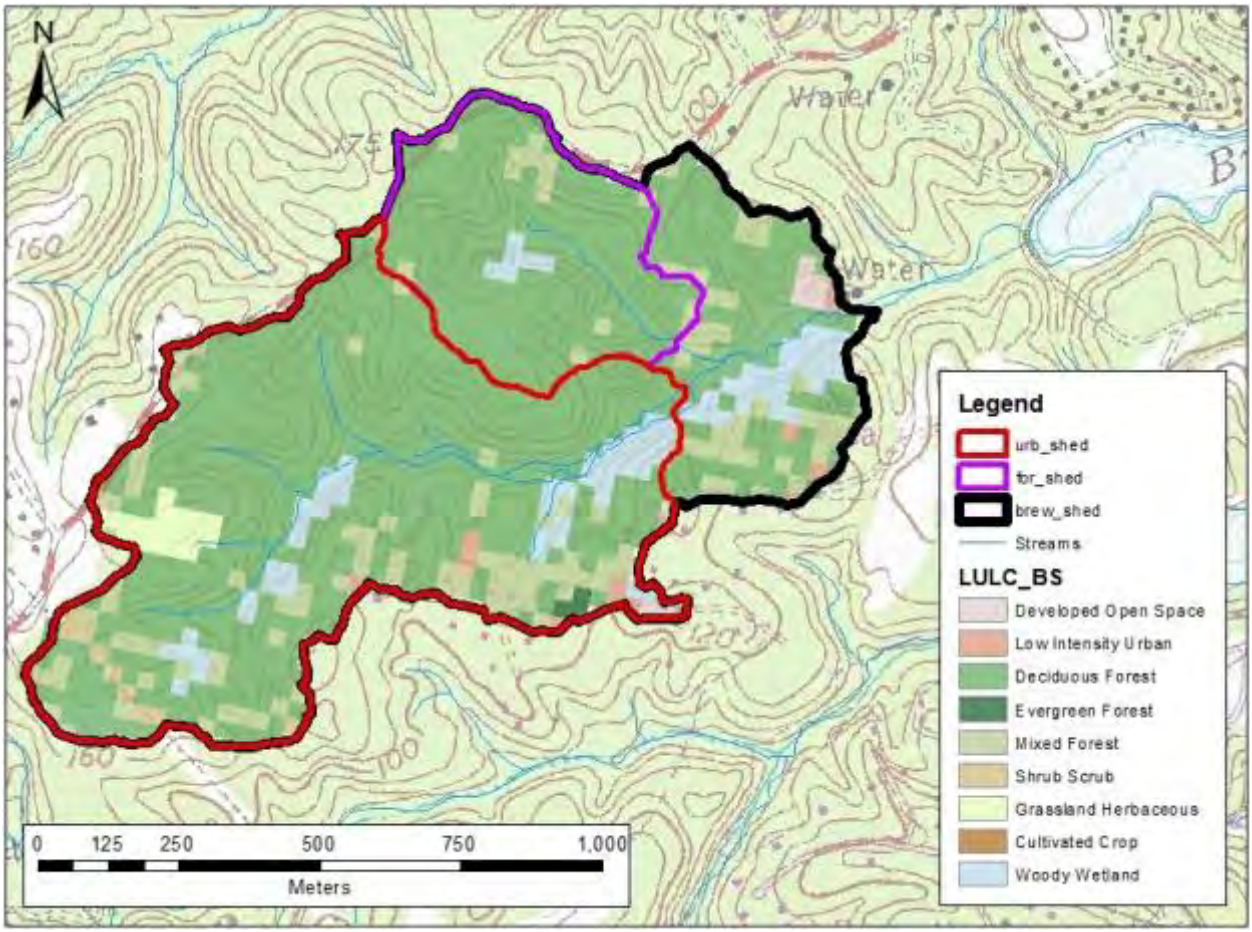

Figure 2. Land use and study site catchments in the Howard's Branch watershed. The urban watershed is outlined in red, the forested watershed is outlined in purple, and the restored watershed is outlined in black.

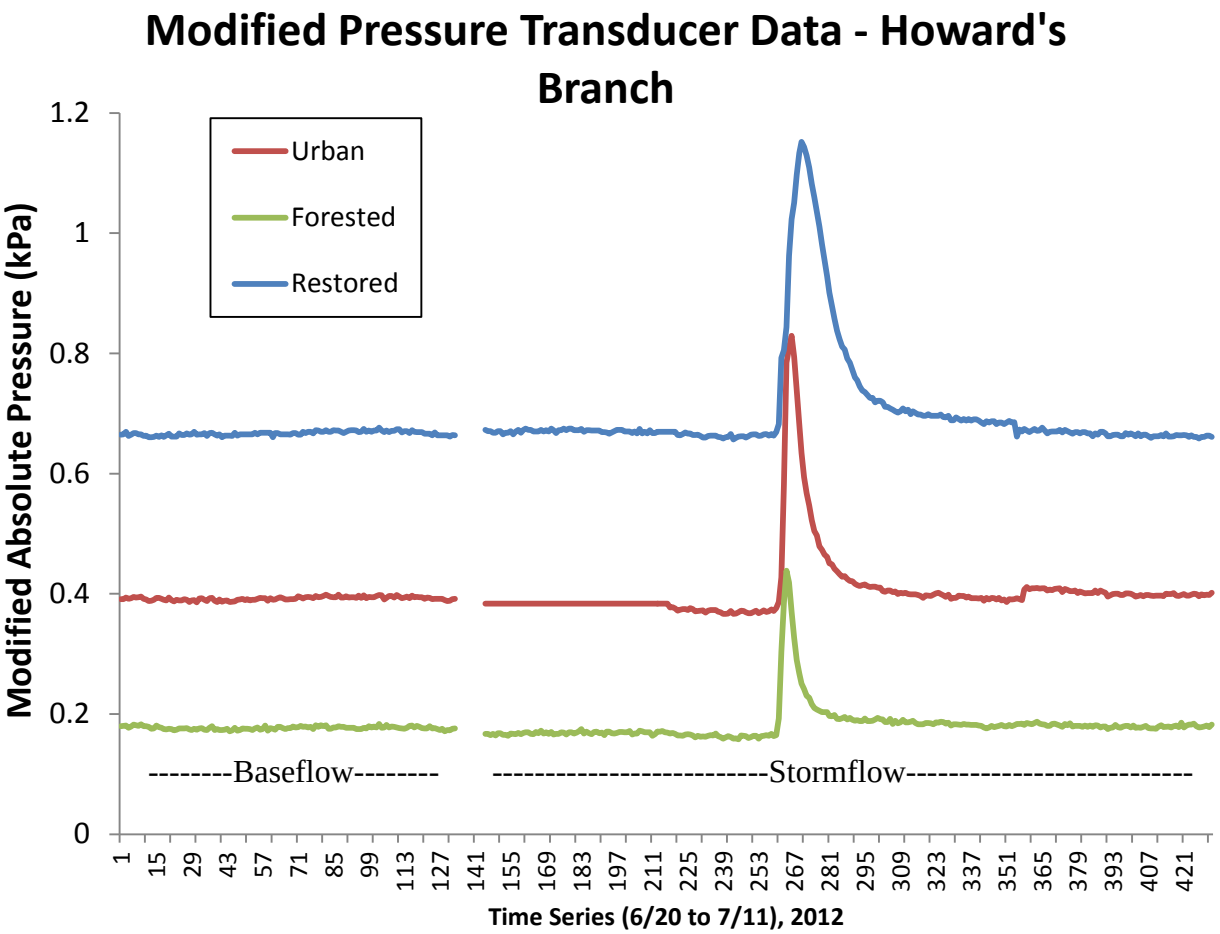

Figure 3. Modified pressure transducer data during base- and storm-flow condition. Actual kPa readings were found by subtracting the barometric pressure (air) from the stream pressure transducer data, giving readings of around 0.1 to 0.3 kPa for each catchment. The baselines have been modified so they are easier to visually compare by stacking.

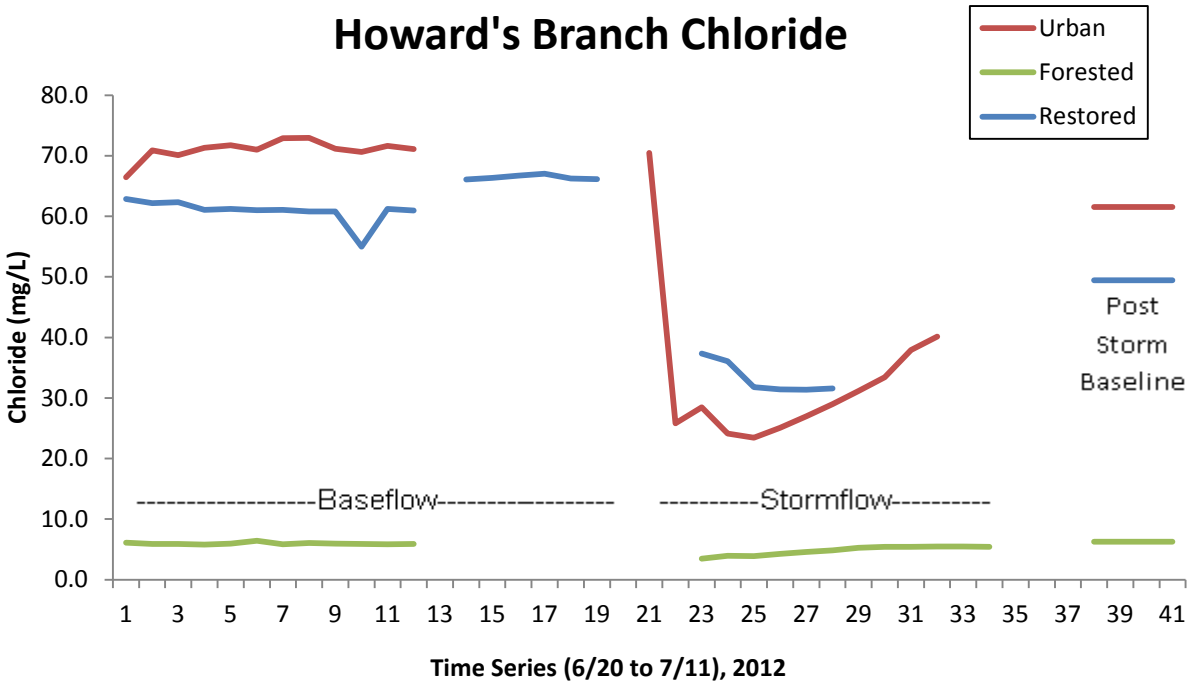

Figure 4. Cl^- concentrations (mg/L) in both base- and storm-flow conditions. Baseflow samples (6/20) were taken every 2 hours over a 24 hour period. Stormflow samples (7/11) were taken every 15 minutes over 6 hours.

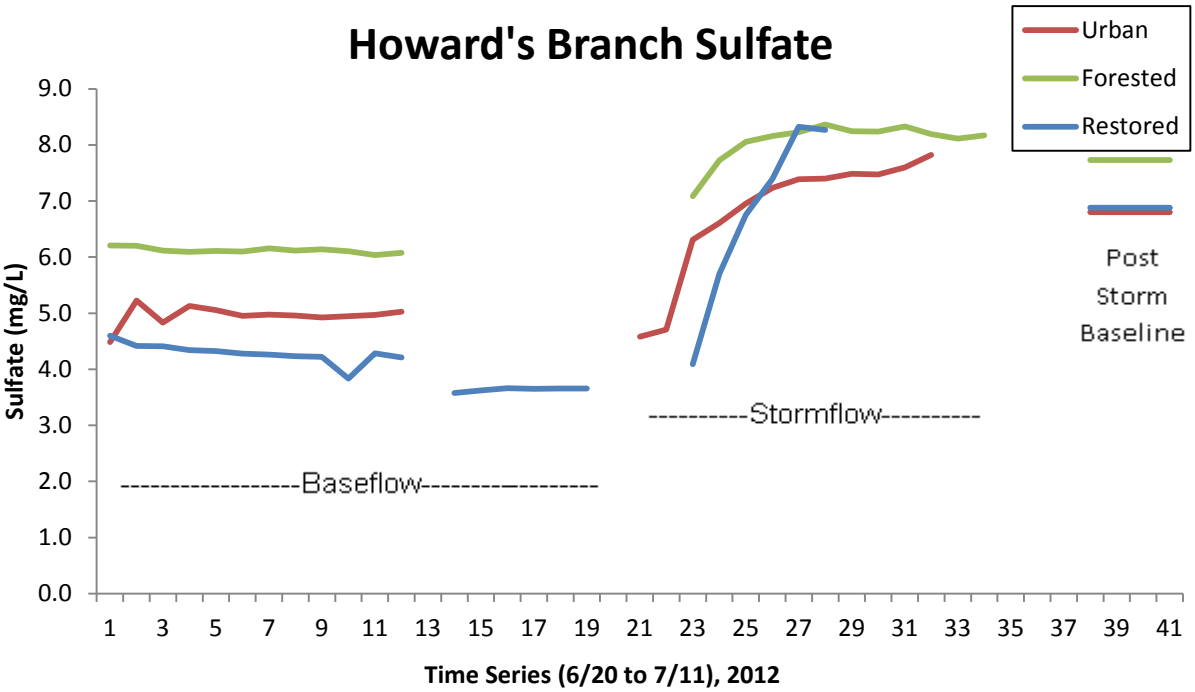

Figure 5. SO_4^{2-} concentrations (mg/L) in both base- and storm-flow conditions. Baseflow samples (6/20) were taken every 2 hours over a 24 hour period. Stormflow samples (7/11) were taken every 15 minutes over 6 hours.

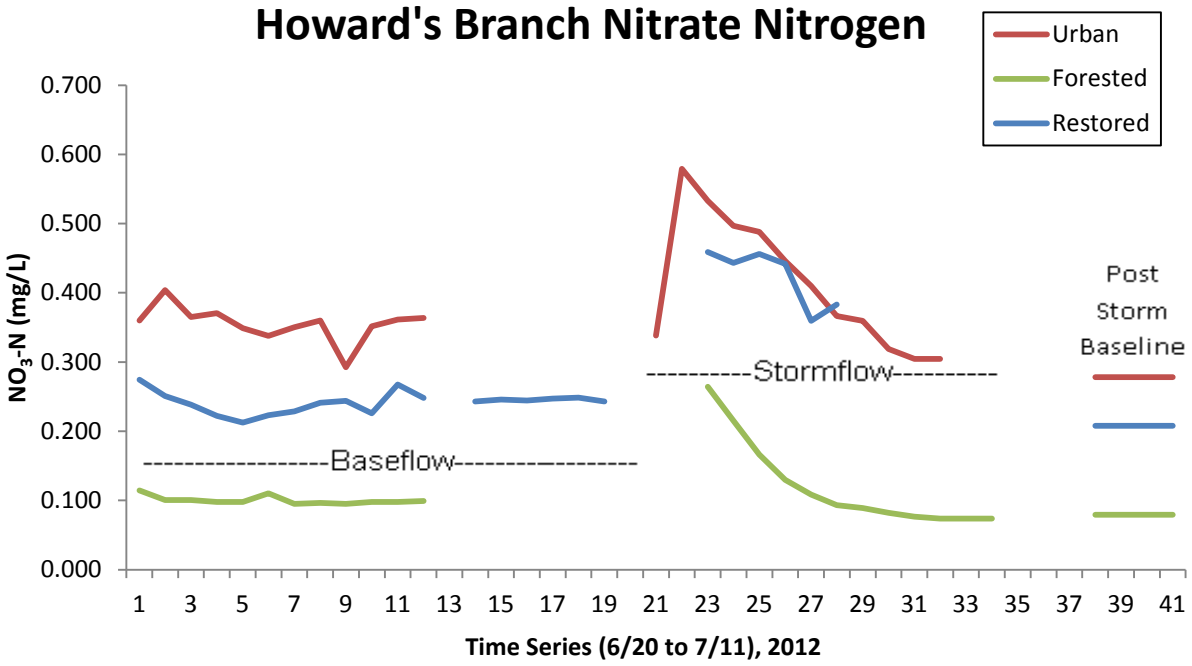

Figure 6. NO_3-N concentrations (mg/L) in both base- and storm-flow conditions. Baseflow samples (6/20) were taken every 2 hours over a 24 hour period. Stormflow samples (7/11) were taken every 15 minutes over 6 hours.

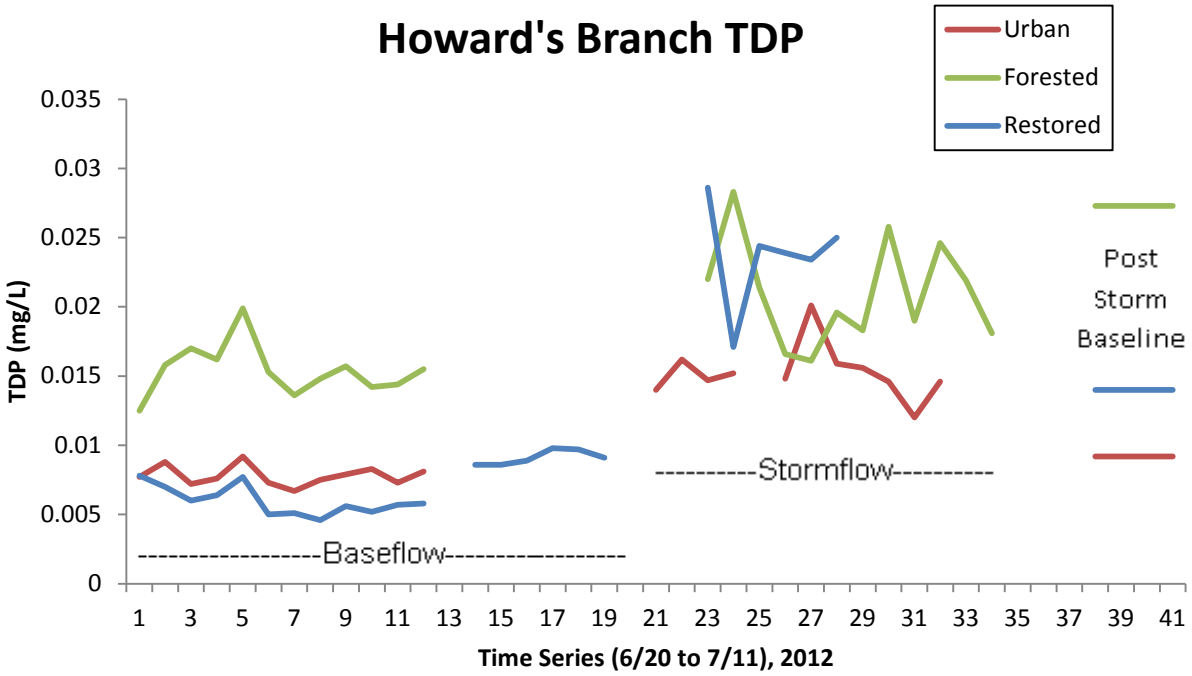

Figure 7. TDP concentrations (mg/L) in both base- and storm-flow conditions. Baseflow samples (6/20) were taken every 2 hours over a 24 hour period. Stormflow samples (7/11) were taken every 15 minutes over 6 hours.

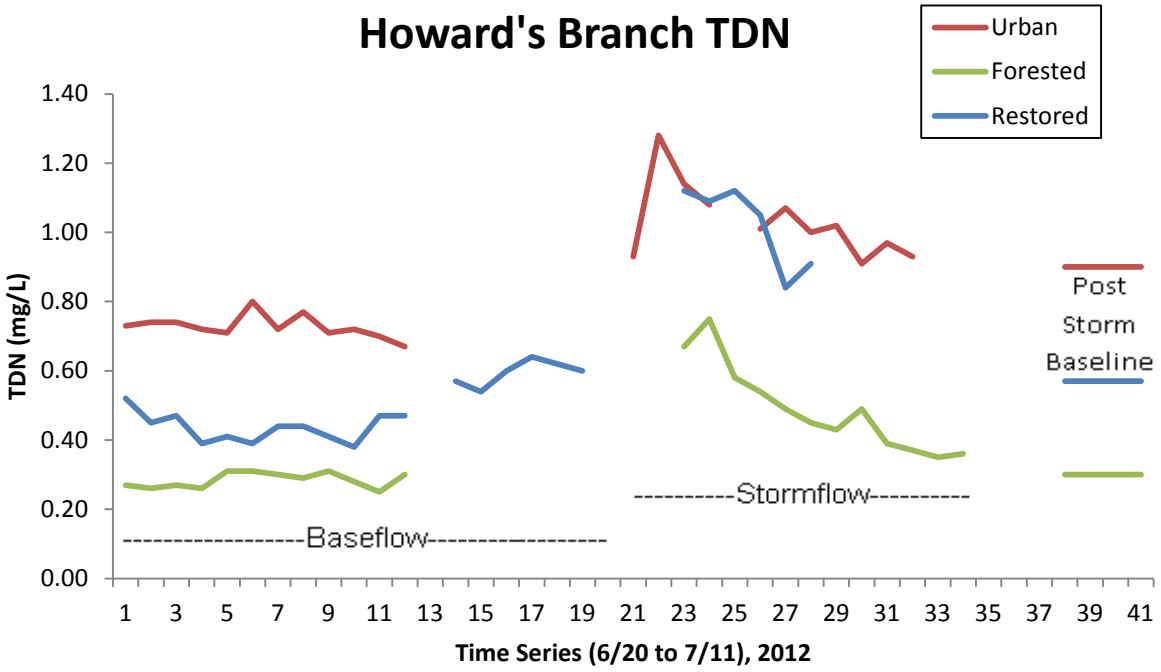

Figure 8. TDN concentrations (mg/L) in both base- and storm-flow conditions. Baseflow samples (6/20) were taken every 2 hours over a 24 hour period. Stormflow samples (7/11) were taken every 15 minutes over 6 hours.

Table 1. Average anion and nutrient concentration (mg/L) during base- and storm-flow events.

	Site	Cl^-	SO_4^-	NO_3-N	TDN	TDP
Baseflow	Urban	67.0±1.7	5.0±0.2	0.36±0.03	0.73±0.03	0.008±0.001
	Forested	6.3±0.2	6.1±0.0	0.10±0.01	0.28±0.02	0.015±0.002
	Restored	57.5±2.0	4.3±0.2	0.24±0.02	0.44±0.04	0.006±0.001
Stormflow	Urban	33.0±12.9	6.8±1.1	0.41±0.09	0.98±0.06	0.016±0.003
	Forested	4.8±0.7	8.1±0.4	0.12±0.06	0.40±0.05	0.021±0.003
	Restored	33.2±2.7	6.8±1.6	0.42±0.04	1.02±0.12	0.024±0.004
Rain		0.8	1.0	0.33	0.80	0.011

(Blank)

UNIVERSITY OF MARYLAND
CENTER FOR ENVIRONMENTAL SCIENCE

Horn Point Laboratory

(Blank)

Investigating the Effects of Unusual Weather Patterns on Water Quality, Sediment Composition, and Submersed Aquatic Vegetation Biomass at the Susquehanna Flats

Steven DiFalco, REU Fellow
Maryland Sea Grant

Cassie Gurbisz, MEES Ph.D. Student
Horn Point Laboratory, University of Maryland Center for Environmental Science

Dr. W. Michael Kemp, Professor
Horn Point Laboratory, University of Maryland Center for Environmental Science

Abstract

Our data have quantified and characterized the composition of sediment and water quality parameters at the Susquehanna Flats. These variables are important factors in determining the rate of growth of submersed aquatic vegetation (SAV) for a given year. This summer, the SAV has had a much weaker growth than previous years. An unusual year of weather, with heavy fall storms and warm winter temperature, appears to have contributed to lower SAV growth and abundance. During the summer of 2012, we found that there were higher concentrations of suspended solids and phytoplankton chlorophyll inside the bed and down-bay from the bed than would be expected (based on conditions measured in previous years). The suspended solids are mostly made up of inorganic materials, suggesting that input of these materials into the water column from the fall storms discharge was more important than the eutrophication effects from nutrient inputs. Elevated levels of sediment down-bay are attributed to continual resuspension and deposition of bottom sediments inside the bed. It is likely that this increase in suspended particles caused decreased water clarity which in turn caused reduced SAV growth. Biomass samples collected in this study revealed lower SAV growth associated with increased epiphyte levels. Understanding how environmental changes influence the growth and abundance of SAV can help to explain both disappearance and resurgence of SAV in the Susquehanna Flats.

Keywords: Submersed Aquatic Vegetation, Susquehanna Flats, Water quality, Sediment composition

Introduction

Seagrass and related submersed aquatic vegetation (SAV) are rooted vascular plants found in shallow freshwater, estuarine, and marine environments. The plants create dense beds that provide a habitat for many species, including juvenile fish, crustaceans, mollusks, and echinoderms (Barbier et al. 2011; Heck et al. 1995). Historically, SAV covered vast coastal

areas around the world. In recent years SAV abundance has declined globally as well as locally in the Chesapeake Bay, largely due to decreasing water clarity associated with eutrophication (Orth et al. 2010). However, in the upper Chesapeake Bay one bed, Susquehanna Flats, experienced a sudden resurgence in the early 2000's, where SAV abundance increased dramatically over a 5 year period (Figure 1). Dr. Michael Kemp and his research group at Horn Point Laboratory are investigating potential causes of the resurgence. Preliminary analyses reveal that feedback processes, where plants impact their environment in ways that improve their own growth, may play an important role in the resurgence. However, this year after several field trips to the site, we have realized that the state of the bed is much different than previous years.

Prior to this year, the abundance of plants in the bed had been consistent for about four years. Continuous water quality monitoring data from 2007-2011 at Harve de Grace and inside the SAV bed suggested that positive feedback processes have led to better water clarity inside the bed. However this year, it appeared that turbidity was greater inside the bed and that plant biomass was less than expected. Recent extreme weather, including heavy floods (Figure 2) in the fall and an unusually warm winter (Figure 3), are potential causes of these unexpected bed conditions.

Numerous studies show the effects of SAV on water quality. SAV is often referred to as an "ecological engineer" since it alters the water conditions which can be beneficial or a hindrance to growth (De Boer 2007; Gruber and Kemp 2010; Van Der Heide et al. 2007). For example, SAV attenuates waves and currents, causing the deposition of sediment, which ultimately increases water quality (Gacia and Duarte 2001; Ward et al. 1984). Light is the overall limiting factor for growth when other factors are removed from the equation, and there is a light requirement necessary for these plants to prosper (Dennison et al. 1993; Kemp et al. 2004). The feedbacks combine in a series of events starting with sediment deposition and nutrient uptake, which lead to enhanced water clarity. From an increase in water quality, there is more light available for plants which allows for more vegetation growth. As the bed grows in size, more sediment is trapped continuing the feedback loop. It is important to look into the way these processes influence the abundance of SAV. During weather extremes, these processes may be altered in ways that change the conditions for SAV growth.

Heavy storm surges off the land bring extra sediment into the water and remove fine sediment that is easily picked up; this changes the composition of the sediment. Composition of the sediment influences the growth rate of macrophyte plants. Since different sediment sizes are able to hold various amounts of nutrients, plants grown in finer sized particles have been shown to grow taller and with more roots (Barko et al. 1986). The physical size of the sediment factors into the plants' abilities to withstand dislodgement (Handley and Davy 2002). Coarse sized sediment might predispose SAV to uprooting (Li et al. 2012). Maximum seed germination and growth in the bed occurs when the water temperature rises and spring winds decline in early June, since these winds cause too much disturbance of the bottom sediments for plants to establish themselves (Harlin et al. 1982). Along with adding extra sediment into the system, hurricanes and storms bring in high levels of allochthonous nutrients into the system (Castaneda-Moya et al. 2010). Elevated levels of nutrients cause a series of events leading to a decrease in water clarity, such as increased periphyton growth which can attenuate light and decrease light availability to SAV (Kemp et al. 2004). This summer, our observations and sampling was to figure out if the unexpected weather has had an influence on the water quality. Our goal was to quantify the composition and spatial distribution of suspended particles and bottom sediments in the upper Chesapeake Bay in order to better infer the cause of elevated turbidity at the Susquehanna Flats.

Methods

Study Site

Susquehanna Flats is a broad, shallow (mean water depth = 0.5 to 1.5 m) tidal fresh-water region of the upper mainstem Chesapeake Bay (Figure 4). The area covers about 75% of the open water in this region, with a relatively narrow channel (3-7 m deep) bordering three sides of the shallows. As of 2010, the SAV bed covered most of Susquehanna Flats (>5,000 ha) with dense stands of as many as 13 species, most notably *Vallisneria americana*, *Myriophyllum spicatum*, and *Heteranthera dubia*. Although plant cover and density have varied substantially during the last 100-150 years (Kemp et al. 2005), the dramatic resurgence during the last decade appears to be unprecedented (Kemp et al. 1983; Orth et al. 2010). The system is in direct line to receive the discharge of the Susquehanna River, with river and tidal water flowing around and over the bed depending on tidal stage. Eleven locations, divided into three groups in relation to the SAV bed, were chosen for this study (Figure 4). Two sites were up-bay of the bed (Flats 1 and 2), six sites were inside the bed itself (Flats 3-8), and three sites were down-bay of the bed (Flats 9-11).

Data Collection and Analysis

We sampled three times during the summer of 2012: June 11, June 28, and July 6. Water samples were collected in duplicates of 1-L Nalgene bottles at the sub-surface at each location. In the laboratory, water samples were homogenized by shaking and filtered into pre-weighed filters (25 µm GF/F). Filters were rinsed with deionized water to remove salt residue and dried at 60º C for 3 days. After drying, filters were re-weighed to determine total suspended solids (TSS). Filters were ashed at 450º C for 4 hours, cooled, and re-weighed to calculate particulate organic matter (POM). For chlorophyll-*a* (chl-a) analysis, a known volume of water (around 60 mL) was passed through filters, which were folded in aluminum foil and frozen. Within 2 months of sampling, chlorophyll-*a* filters were thawed, extracted in the dark with 90% acetone and 10%HCl, sonicated, filtered, and ran through a fluorometer (10-AU).

While at the study site, a data sonde (either Yellow Springs Instruments, Inc. YSI 6600 or YSI 85) was used to rapidly detect variables such as turbidity, salinity, chlorophyll, dissolved oxygen, conductivity, temperature, and pH. Data were collected at the surface and bottom when using YSI 85 and every 0.5 m for the YSI 6600. In addition, Secchi depth was taken at each site along with light measurements using a LICOR sensor. LICOR data were used to calculate the downwelling light attenuation coefficient (K_d).

Sediment samples were collected at each location, taking triplicate samples using push cores. Cores were cut into 1 cm sections, down to the bottom of the core. About 7 grams of sediment were sonicated and sieved through a 63 µm sieve using sodium metaphosphate to get mud and sand fractions, collected in pre-weighed beakers and aluminum boats. Sand fraction was further dried sieved using a Sieve Shaker to get weight of each grain size.

To get real-time data on the sediment concentrations and sediment size distribution, we used a Laser In Situ Scattering Transmissometer (LISST). This device emits a laser beam into the water column and strike particles, which cause light scattering at specific angles according to their size (Gray et al. 2004); this is then detected by the device and used to determine the distribution of sediment particle sizes at different locations in the water column (Figure 5). From this data we can find out what size particle dominates the water column at different locations along with the total concentration of sediments at each site (Figure 6).

Biomass samples were collected using push cores at two sites on July 6 at Flats 4 and 7. The core was pushed about 20 cm into the sediment. This was then removed, the sediment was sieved out using a mesh bag, and the biomass was collected and stored in Ziploc bags until processing. Samples were processed for both above (stem, shoots, and foliage) and below (roots, base, and runners) ground biomass within a week of sampling. These were dried in an oven (60ºC for 2 days) and weighed. Triplicate plant samples were collected at both sites and stored in plastic bags until processing for epiphytes. Epiphytes were scrapped off these samples into water, filtered onto pre-weighed filters (45 µm GF/F), dried (60ºC), and re-weighed. Epiphytes data were reported in weight of epiphyte per plant weight collected and averaged for all samples taken.

Using the software ArcGIS, parameters were plotted over a map of the Susquehanna Flats by GPS location. GPS locations recorded for each site during field days. A layer underneath the points shows the locations where SAV was present in 2010 (VIMS). To analyze the relationships between water quality parameters, the statistical software JMP was used to create a correlation matrix. Other graphs were generated using Microsoft Excel.

Results

Temporal and Spatial Variability of Water Quality

Particulates in the water were analyzed from the grab samples and data sonde during our second sampling date. Figure 7a-e shows the variable with respect to bed location: upriver is about 3-6.5 km north of the bed, and downriver is 2-5km south of the bed. Turbidity does not have a mean because this is not recorded at the CBIBS monitoring station. Total suspended solids (Figure 7a) and turbidity (Figure 7c) increased from up-bay to down-bay. Chlorophyll-a (Figure 7b) was highest inside the bed, followed by down-bay and then up-bay. Water clarity, indicated by secchi depth (Figure 7d) and K_d (Figure 7e), is greater at sites up-bay and at Flats 3 and 4 compared to the other sites. TSS (Figure 8a) and chlorophyll (Figure 8b) decreased as the summer progressed, while Secchi depth (Figure 8c) increased. It is interesting to see that Flats 3, which is “inside the bed” has higher water clarity (Figure 9c and d) and chlorophyll levels (Figure 9b) than other “bed” sites. The turbidity (Figure 9a) was lower at Flats 3 and 4.

Suspended sediment concentration (Figure 6) from up-bay to down-bay generally increases with some decreases (Flats 3, 4, 9, and 11). The highest concentrations of sediments are at Flats 8 and 10. Larger particles are more concentrated at the bed and down-bay locations than the up-bay.

Sediment Composition and Spatial Variability

Five shallow (<2 m) sites were sampled for bottom sediment characteristics. Sediment core samples were analyzed for grain size distribution. Flats 3 and 4 had more coarse grained sediment while Flats 5, 6, and 7 had finer grained sediment (Figure 10). Very fine sediment made up a small percent of the samples, except for Flats 5. Flats 6 had the highest percentage of Mud sized particles. The pie charts are based on the upper most centimeter of each core, but they are an accurate representation of the whole core.

SAV Biomass and Epiphytes

Collection of biomass and epiphytes samples came from two sites, Flats 3 and 7. There were different SAV species present at each site; *Vallisneria americana*, *Myriophyllum spicatum*,

and *Heteranthera dubia* found at Flats 7, and *Vallisneria americana*, *Hydrilla verticillata,* and *Naiad spp.* at Flats 3. Amount of epiphyte material on SAV leaves was higher at Flats 7, while above and below ground biomass were greater at Flats 3 (Figure 11).

Correlations and Regressions

There were many strong correlations among water quality variables, where stronger relations in the figure have red lines closer together and straighter (Figure 12). Table 1 shows the correlation coefficients for each respective relationship in Figure 12. Some key correlations are seen, for example, in that K_d positively correlates with all but secchi depth, and that TSS has a strong correlation with NTU and PIM, but a weaker correlation with chlorophyll-*a* and POM. There is a stronger regression between PIM and epiphyte weight as compared to POM (Figure 13).

Discussion

Temporal and Spatial Variability of Water Quality

Comparing our observed levels of water quality variables with long-term mean values for June, it seems that certain variables are above or below the average depending on location (Figure 7). All the chlorophyll values were below the June average, meaning the level of phytoplanktonic algae may be less than in a typical year. The TSS was higher in both the bed and down-bay from the bed, we would have expected it to be less at the bed sites and higher up-bay because sediments should settle out as the water slows and passes over the SAV bed. An explanation for this could be that the water picked up and resuspended sediment as it passed through the bed, as can happen when the bed is absent or sparse (Luhar et al. 2008). To add to this, the secchi depth (Figure 5d) was greater up-bay than average which shows that there is greater water clarity before the water gets to the more shallow waters at the bed. Values of K_d (Figure 5e) are expected to follow the opposite trend as secchi, which it does. The light does not reach as far down into the water column, or disappears quicker, in the more turbid water at the bed and down-bay sites.

The relatively short sampling period for this study limited our ability to detect temporal variations. The water has cleared up from when we first sampled in the beginning of June as compared to early July; shown by the turbidity and chlorophyll-*a* decreasing while secchi depth increases (Figure 6a-c). This may be a typical pattern of the bed, since the averages are for the whole month of June, they would not reflect this temporal change. During processing of chlorophyll-a, the samples did not respond as expected when acid was added; the values were anticipated to be reduced in half since the acid breaks apart phytoplanktonic cell bodies and destroys the chlorophyll. This could be a cause of the vast difference from the first sampling date and the latter two, since June 11 samples were processed separate from the others.

Sediment Composition and Spatial Variability

There appears to be more fine sediments found at Flats 5, 6, and 7 and coarser sediment found at Flats 3 and 4 (Figure 8). This is partially expected, since Flats 3 and 4 are at the mouth of the Susquehanna River, so the larger sediments would settle out there while the finer materials would continue on into the bed and eventually deposit out (Wright 1977). Although grain-size distribution for the bottom sediments follows according to expected trends, the

distribution for suspended solids does not; the same trend of larger sediment grain-size at the mouth of the river and smaller grains further down-bay would have been expected. The reasoning is the same: larger sediments should settle out first and then smaller particles settle out later on. However, Figure 9 shows this to not be true. Resuspension of bottom sediments is the likely cause for this pattern, along with the addition of large amounts of sediments from storms that have not had time to settle out (Figure 3). Abnormal weather conditions, such as wind driven waves can cause sediment to remain in suspension and this may be the case for the Susquehanna Flats (Anderson 1972).

Biomass

There seems to be a relationship between the amount of epiphyte and the amount of biomass, with more epiphytes there is less biomass at the site (Flats 7; Figure 11). At Station 7, there was a dense mat of blue-green algae, identified as *Lyngbya wollei,* covering the bottom of this site. Some of this algae was found tangled at the bottom of the plants, there is the possibility it affected the growth of the SAV at this spot. This algae was not included in the epiphyte weight at this site. There was greater biomass at Flats 3 (Figure 11), which had lower chlorophyll-a and turbidity levels than Flats 7 (Figure 9a and b). High levels of turbidity and chlorophyll-a cause a reduction in light available for the SAV plants to use (Kemp et al. 2004). In addition, positive feedback effects whereby the large and abundance SAV beds are expected to induce more sinking and trapping of suspended particles (Gruber and Kemp 2010, Gruber et al. 2011).

Correlations

From the multivariate correlation, we see that K_d is positively related to many other variables. This indicates that with increasing water clouding variables (suspended solids and photosynthesizing organisms) there is a greater amount of light attenuation. When more sediment and particulates are in the water, light will not penetrate as deep. Both TSS and NTU are more strongly correlated with PIM than POM, which suggests the suspended solids are composed of more inorganic materials as compared to organic. The weak correlations with TSS and NTU to both POM and chlorophyll-a reinforce this interpretation: if there is less organic matter, there should be less chlorophyll-a in the water column. Along with the suspended solids being more correlated to PIM (Figure 13b), there was a more direct relationship between PIM and epiphyte weight (Figure 13a). This could indicate that there is a higher level of inorganic matter that is attaching itself to the epiphytes than organic. This might also suggest that epiphytic material, which collects on plant leaves, is composed of the same particles that are suspended in the water column.

Conclusions

The current conditions of the bed do seem to be improving as the summer progresses. Plant abundance has increased from our first sampling to our third, but it is not as high as expected. Unexpected flooding associated with fall hurricanes, along with warmer winter weather, may have led to this unusual state of the Susquehanna Flats. Warmer water temperature may influence the germination timing and survival of young seedlings. Without knowing the rate of resuspension, it is difficult to say whether or not this is a factor influencing the water quality and sediment composition. The previous studies of how river sediment is deposited indicate this summer could be atypical for what we would expect for the water quality and sediment composition parameters quantified. Inorganic matter makes up a greater component of epiphyte and TSS weight than does organic matter. This is probably due to the

resuspension of the bottom sediments with some settling out on the plants. Since the site furthest up-bay has the very clear water and few sediments (Figures 5 and 6), it is unlikely to be sediment input from the river influencing the water clarity.

When comparing passed to present data, we are referring to the “bed’s” location as that found during 2010. This could very likely have changed since then, since the bed does not always grow in the same way or form from year to year. From overhead photographs taken mid-July (Figure 14a and b), we see that the bed is mostly concentrated to the eastern bank, leaving the majority of the 2010 bed missing. This complicates things when saying what is inside or outside the bed, and what type of trends we would expect. The sediment is shown in the photos suspended in areas without SAV. Flats 3 has the most clear water out of the bed sites, likely attributed to the SAV present there causing feedback processes to occur.

A future study, which provided information about sediment deposition inside and outside the bed (Gruber and Kemp 2010), would help define bed influence on water clarity. It would also give insight into the role SAV plays with regards to particle trapping and resuspension. This is a vital key to understanding how the resurgence of the Susquehanna Flats occur during the early 2000’s along with help understand the amount of growth expected in potential years. Understanding what causes the growth of SAV can help keep the beds prospering, and can help with prospective research in recreating natural beds elsewhere in the Chesapeake Bay.

References

Anderson, F. E. 1972. Resuspension of estuarine sediments by small amplitude waves. Journal of Sedimentary Petrology 42: 602.

Barbier, E. B., S. D. Hacker, C. Kennedy, E. W. Koch, A. C. Stier, and B. R. Silliman. 2011. The value of estuarine and coastal ecosystem services. Ecological Monographs 81: 169-193.

Barko, J. W., M. S. Adams, and N. L. Clesceri. 1986. Environmental-factors and their consideration in the management of Submersed Aquatic Vegetation-A Review. Journal of Aquatic Plant Management 24: 1-10.

Castaneda-Moya, E., R. R. Twilley, V. H. Rivera-Monroy, K. Q. Zhang, S. E. Davis, and M. Ross. 2010. Sediment and nutrient deposition associated with hurricane wilma in mangroves of the florida coastal everglades. Estuaries and Coasts 33: 45-58.

CBIBS. 2012. Chesapeake Bay Interpretive Buoy System. http://buoybay.noaa.gov/.

De Boer, W. F. 2007. Seagrass-sediment interactions, positive feedbacks and critical thresholds for occurrence: a review. Hydrobiologia 591: 5-24.

Dennison, W. C., R. J. Orth, K. A. Moore, J. C. Stevenson, V. Carter, S. Kollar, P. W. Bergstrom, and R. A. Batiuk. 1993. Assessing water-quality with submersed aquatic vegetation. Bioscience 43: 86-94.

Gacia, E., and C. M. Duarte. 2001. Sediment retention by a Mediterranean *Posidonia oceanica* meadow: The balance between deposition and resuspension. Estuarine Coastal and Shelf Science 52: 505-514.

Gray, J. R., Y. C. Agrawal and H. C. Pottsmith. 2004. The LISST-ST streamlined isokinetic suspended-sediment profiler. In: Proceedings, 9th International Symposium on River Sedimentation, C. Liu, ed., 549-2555. Yichang, 2China: Tsinghua University Press.

Gruber, R. K., and W. M. Kemp. 2010. Feedback effects in a coastal canopy-forming submersed plant bed. Limnology and Oceanography 55: 2285-2298.

Gruber, R. K., D. C. Hinkle, and W. M. Kemp. 2011. Spatial patterns in water quality associated with submersed plant beds. Estuaries and Coasts 34: 961-972.

Handley, R. J., and A. J. Davy. 2002. Seedling root establishment may limit *Najas marina* L. to sediments of low cohesive strength. Aquatic Botany 73: 129-136.

Harlin, M. M., B. Thornemiller, and J. C. Boothroyd. 1982. Seagrass sediment dynamics of a flood-tidal delta in Rhode Island (USA). Aquatic Botany 14: 127-138.

Heck, K. L., K. W. Able, C. T. Roman, and M. P. Fahay. 1995. Composition, abundance, biomass, and production of macrofauna in a New England estuary-comparisons amoung eelgrass meadows and other nursery habitats. Estuaries 18: 379-389.

Kemp, W. M., R. Batiuk, R. Bartleson, P. Bergstrom, V. Carter, C. L. Gallegos, W. Hunley, L. Karrh, E. W. Koch, J. M. Landwehr, K. A. Moore, L. Murray, M. Naylor, N. B. Rybicki, J.

C. Stevenson, and J. D. Wilcox. 2004. Habitat requirements for submerged aquatic vegetation in Chesapeake Bay: Water quality, light regime, and physical-chemical factors. Estuaries 27: 363-377.

Kemp, W. M. W. R. Boynton, J. E. Adolf, D. F. Boesch, W. C. Boicourt, G. Brush, J. C. Cornwell, T. R. Fisher, P. M. Glibert, J. D. Hagy, L. W. Harding, E. D. Houde, D. G. Kimmel, W. D. Miller, R. I. E. Newell, M. R. Roman, E. M. Smith, and J. C. Stevenson. Eutrophication of Chesapeake Bay: historical trends and ecological interactions. Marine Ecology-Progress Series 303: 1-29.

Kemp, W. M., R. R. Twilley, J. C. Stevenson, W. R. Boynton, and J. C. Means. 1983. The decline of submerged vascular plants in upper Chesapeake Bay - summary of results concerning possible causes. Marine Technology Society Journal 17: 78-89.

Li, Z. Q., L. Y. Kong, L. F. Yang, M. Zhang, T. Cao, J. Xu, Z. X. Wang, and Y. Lei. 2012. Effect of substrate grain size on the growth and morphology of the submersed macrophyte *Vallisneria natans* L. Limnologica 42: 81-85.

Luhar, M., J. Rominger, and H. Nepf. 2008. Interaction between flow, transport and vegetation spatial structure. Environmental Fluid Mechanics 8: 423-439.

NDBC. NOAA-national data buoy center. http://www.ndbc.noaa.gov/station_page.php?station=cbbv2.

Orth, R. J., M. R. Williams, S. R. Marion, D. J. Wilcox, T. J. B. Carruthers, K. A. Moore, W. M. Kemp, W. C. Dennison, N. Rybicki, P. Bergstrom, and R. A. Batiuk. 2010. Long-term trends in submersed aquatic vegetation (SAV) in Chesapeake Bay, USA, related to water quality. Estuaries and Coasts 33: 1144-1163.

USGS. 2011. United states geological survey. http://water.usgs.gov/.

Van Der Heide, T., E. H. Van Nes, G. W. Geerling, A. J. P. Smolders, T. J. Bouma, and M. M. Van Katwijk. 2007. Positive feedbacks in seagrass ecosystems: Implications for success in conservation and restoration. Ecosystems 10: 1311-1322.

VIMS. Virginia institute of marine science. http://web.vims.edu/bio/sav/.

Ward, L. G., W. M. Kemp, and W. R. Boynton. 1984. The influence of water depth and submerged vascular plants on suspended particulates in a shallow estuarine embayment. Marine Geology 59: 85-103.

Wright, L. D. 1977. Sediment transport and deposition at river mouths: A synthesis. Geological Society of America Bulletin 88: 857-868.

Figures and Tables

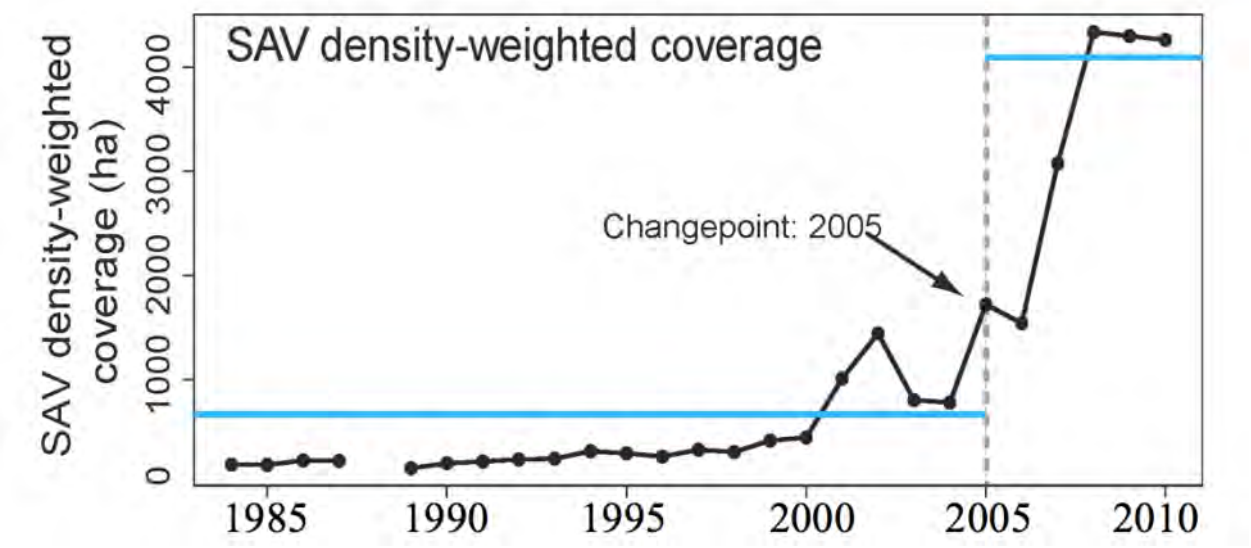

Figure 1. The abundance of the SAV at the Susquehanna Flats, taken from (Vims) aerial photos, has been plotted in relation to the year it was taken.

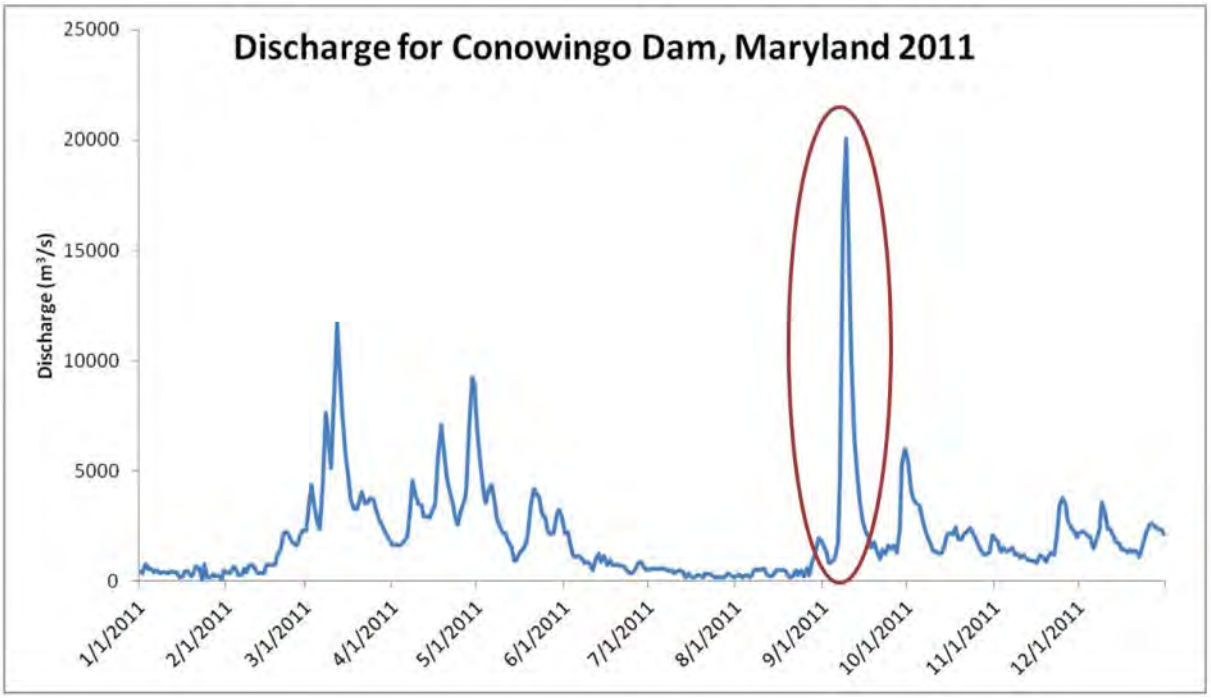

Figure 2. Discharge is plotted over time for the whole year of 2011. The red circle is pointing out the high peak water flow attributed to Tropical Storm Lee. This was after a time of drought in late June to early September (USGS 2011).

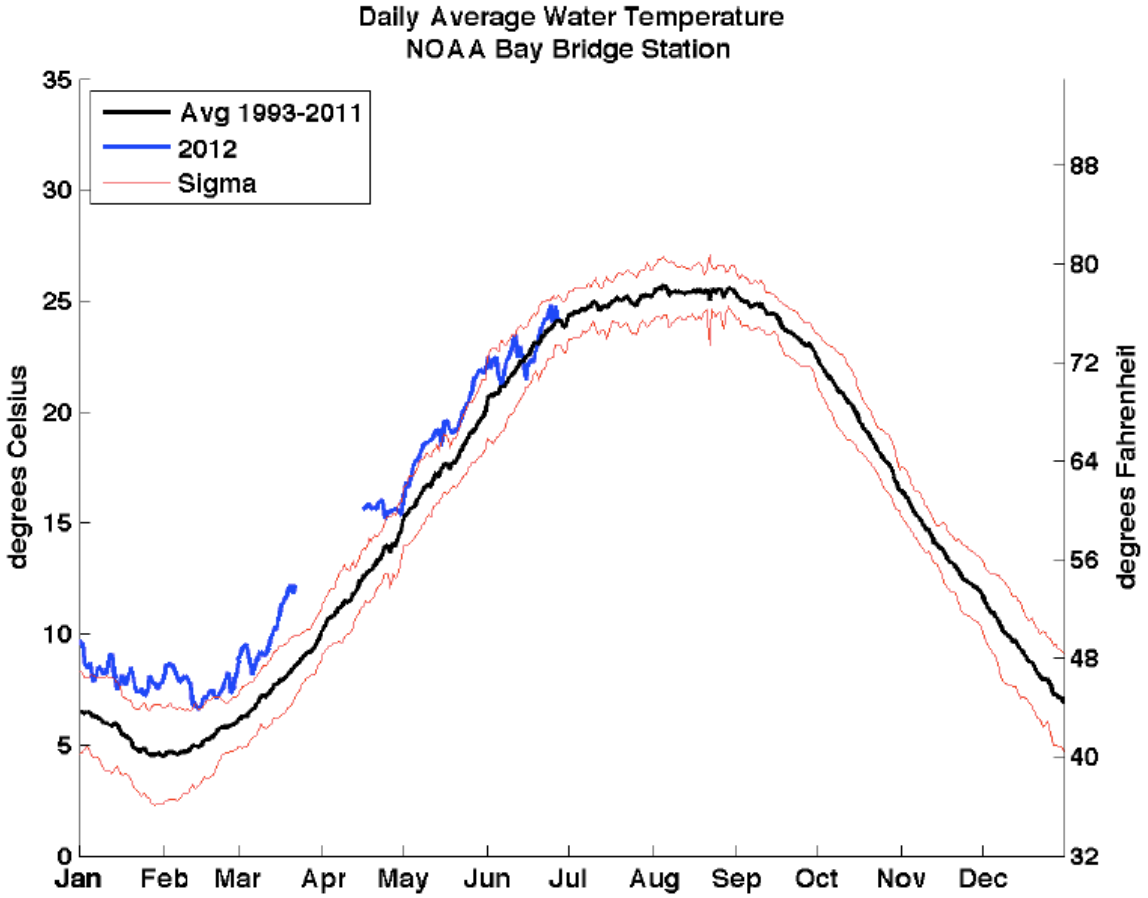

Figure 3. The average water temperature has been plotted from 1993-2011, with the red line representing standard deviation. The blue line represents the temperature for 2012 as of July 1st (NDBC).

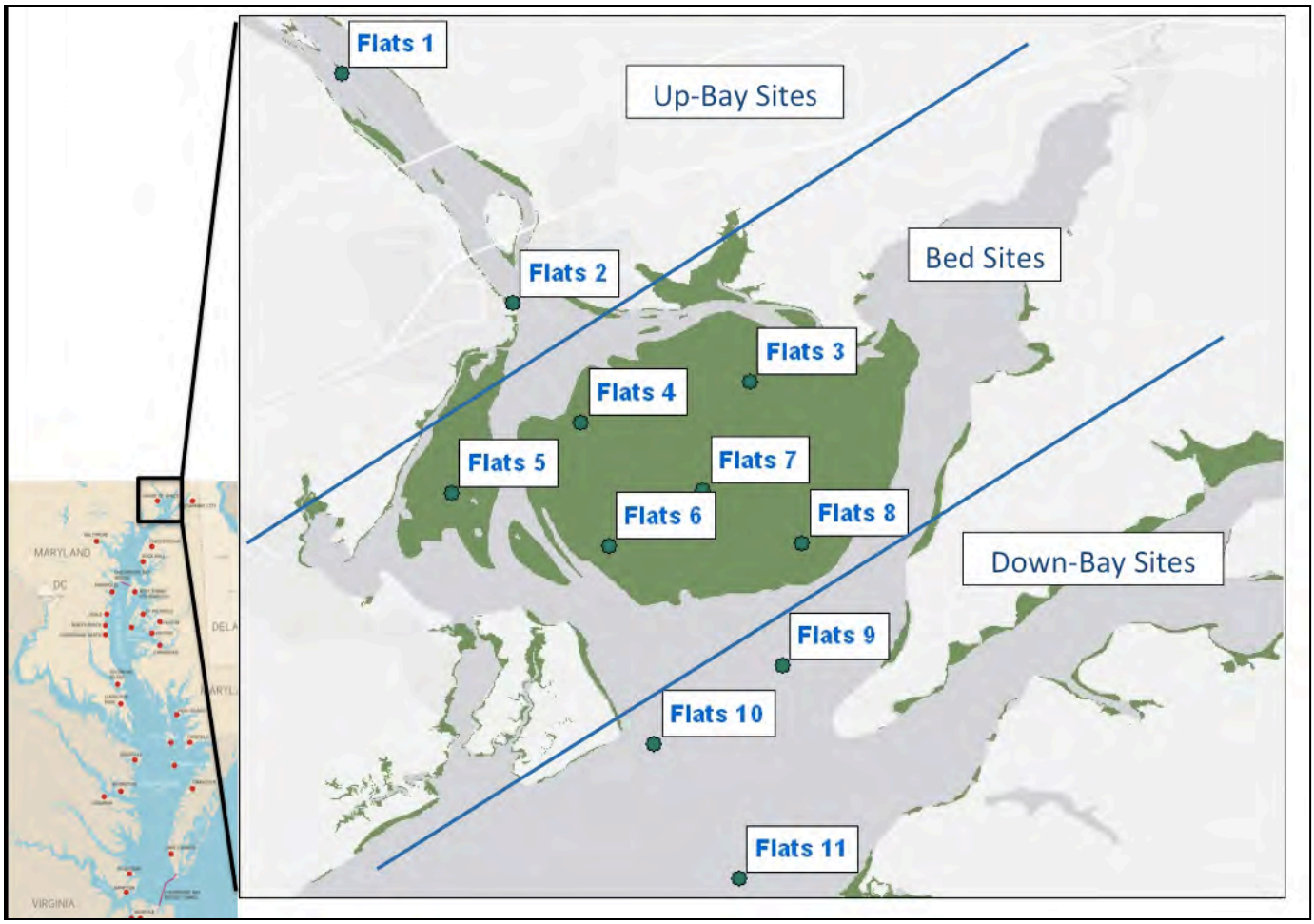

Figure 4. Spatial location of all eleven sites at the Susquehanna Flats. Smaller photo represents the Flats location in respect to the Chesapeake Bay. Upriver consisted of Flats 1 and 2, Bed consisted of Flats 3-8, and consisted of Flats 9-11.

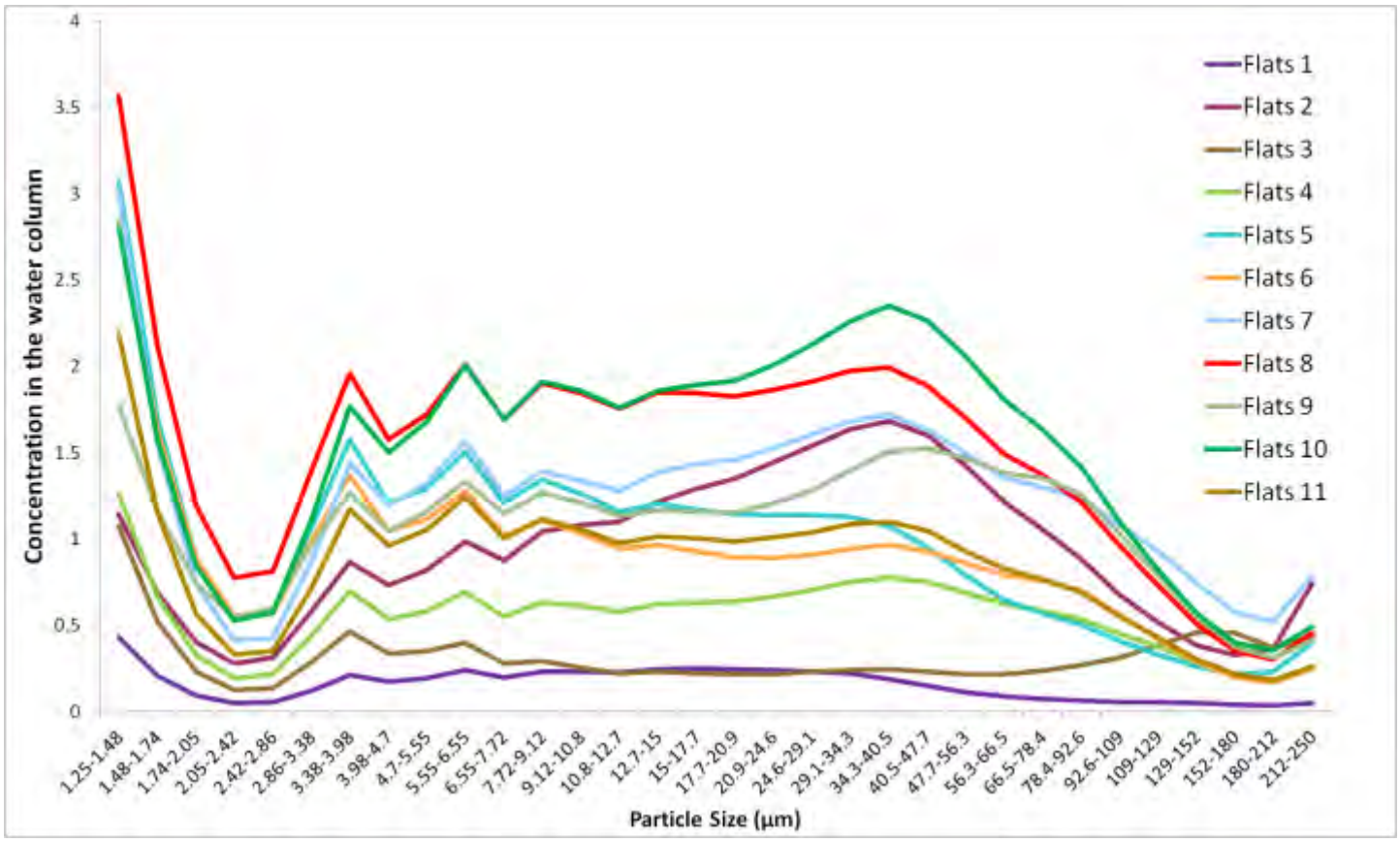

Figure 5. Data collected from the LISST sampler. This represents the concentration of each particle size at the 11 sites sampled.

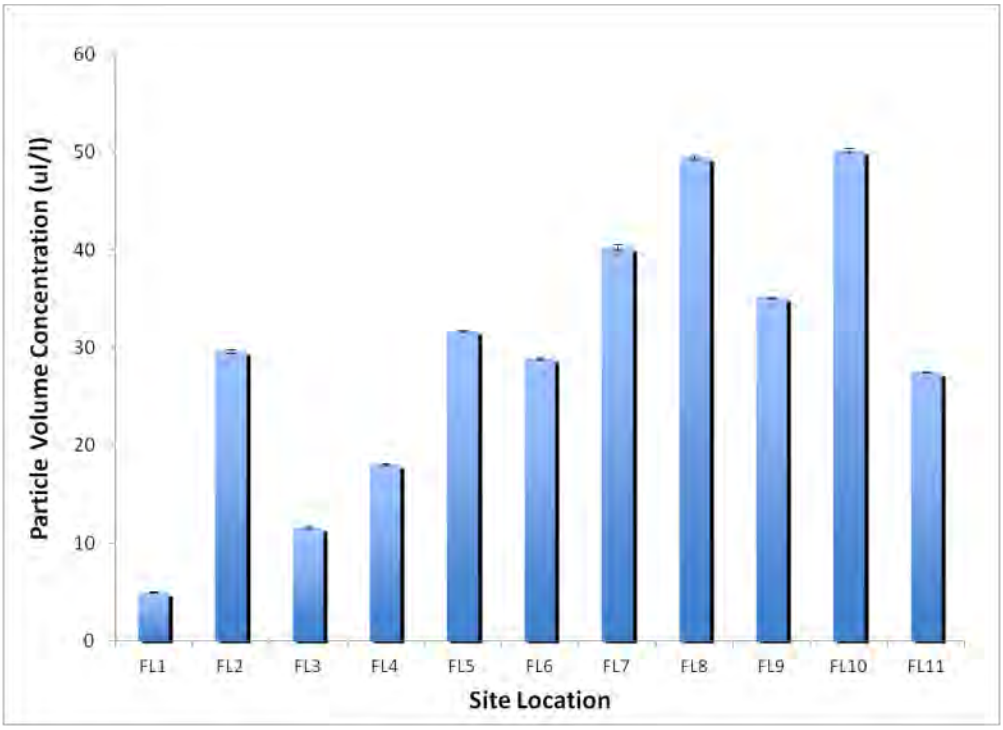

Figure 6. Sum of all concentrations of particles for each site, FL=Flats. Standard error bars are on top of each bar.

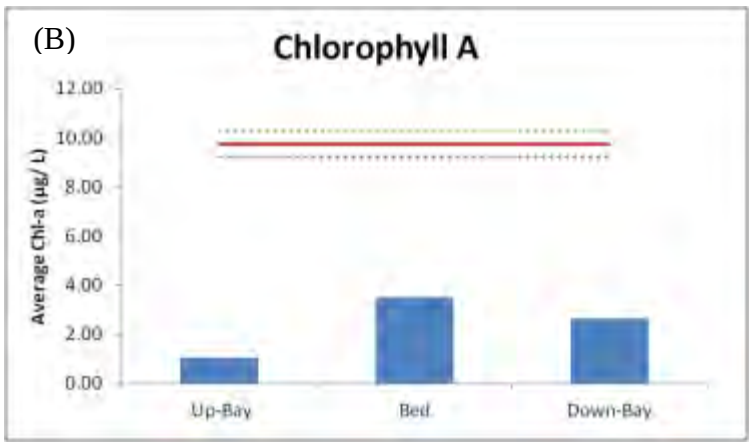

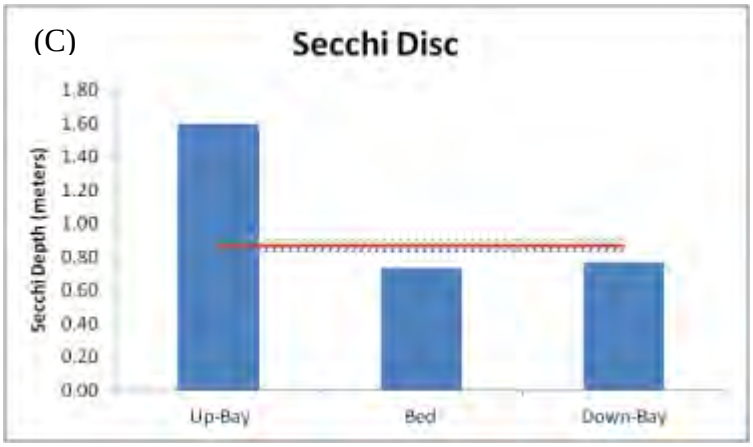

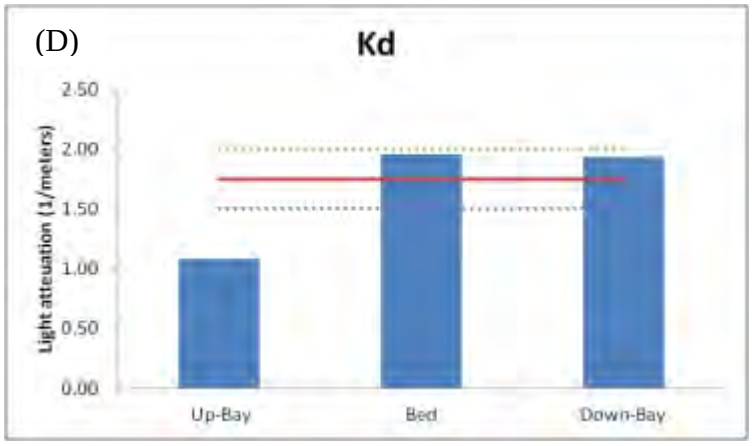

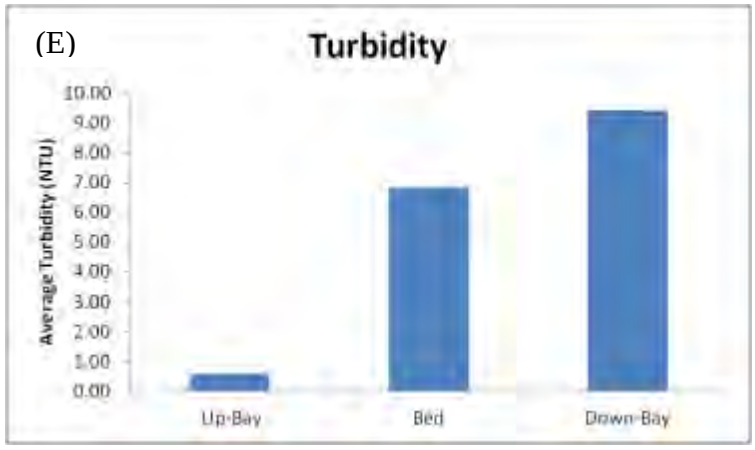

Figure 7(a-e). The five graphs above represent the average of their site for each parameter. The red bar in each graph represents the long-term mean value for the month of June, with error lines in green and purple, calculated using Chesapeake Bay Program data at the Harve de Grace monitoring system from 1984-2011 (CBIBS 2012). Turbidity is not measured at this monitoring station, so there is no month average to compare with.

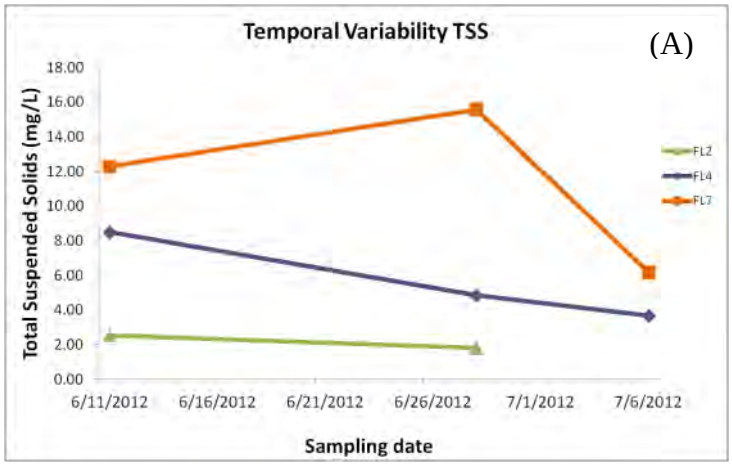

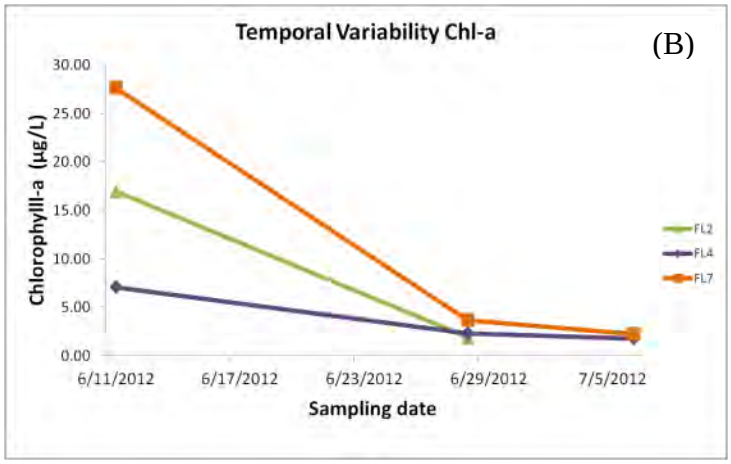

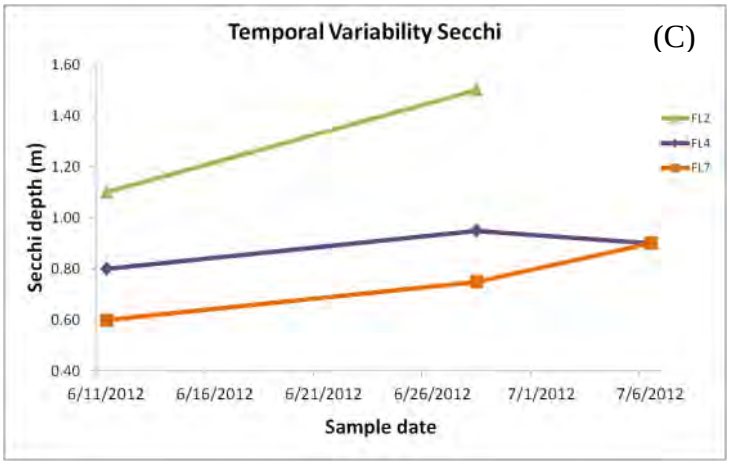

Figure 8(a-c). Above are the graphs using Flats 2, 4, and 7 to show the changes of TSS, Chlorophyll, and Secchi depth over the course of the summer.

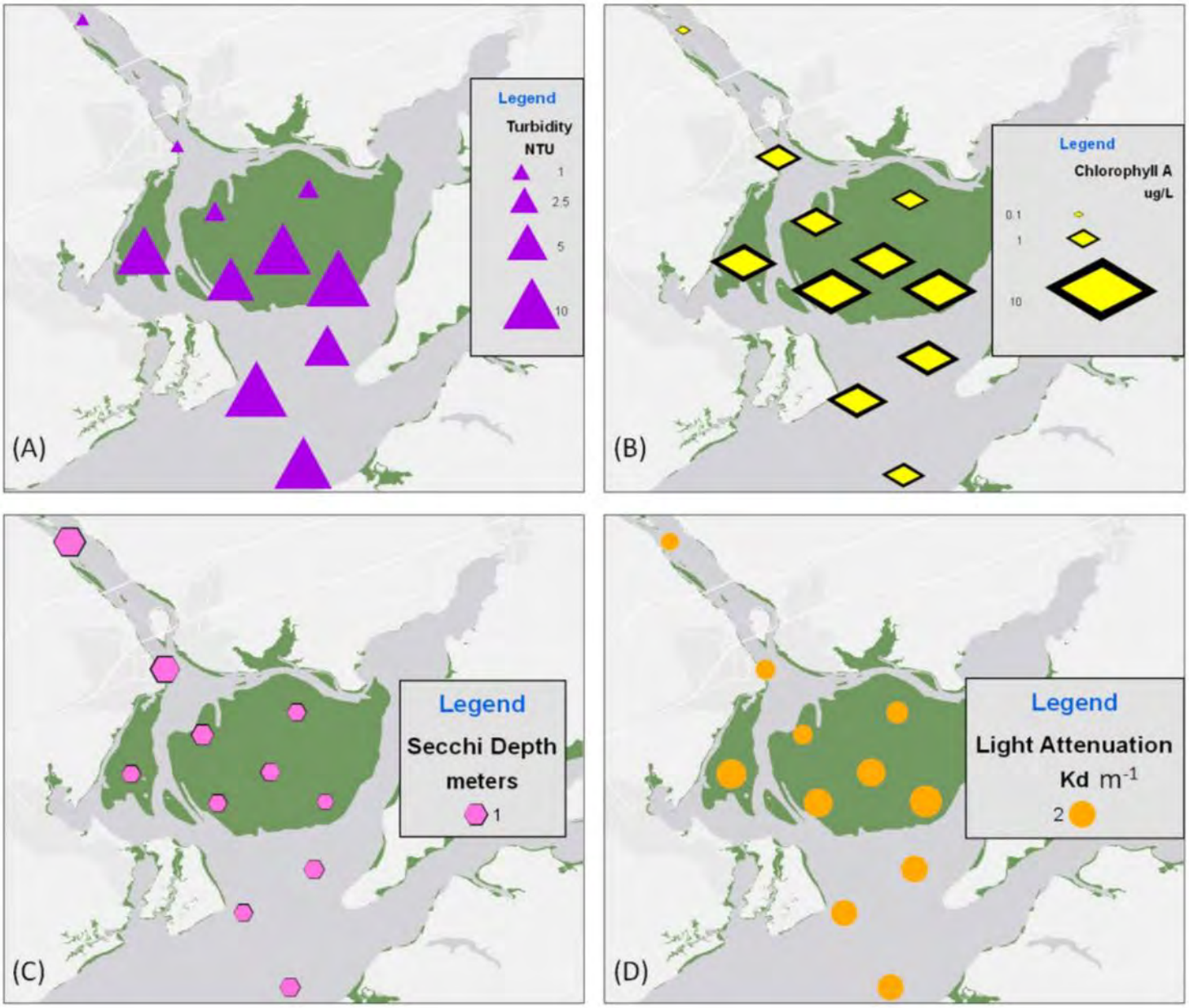

Figure 9(a-d). GPS location on top of VIMS biomass file (the green areas represent where SAV was present in 2010). The smaller the shape, the less of that parameter was present at this location, and the opposite for the larger. Turbidity(7a) was measured in NTU's, Chlorophyll-a (7b) in µg/L, Secchi (7c) in meters, and Kd(7d) in 1/meters. All 11 sites are shown for the data collected 6/28/2012.

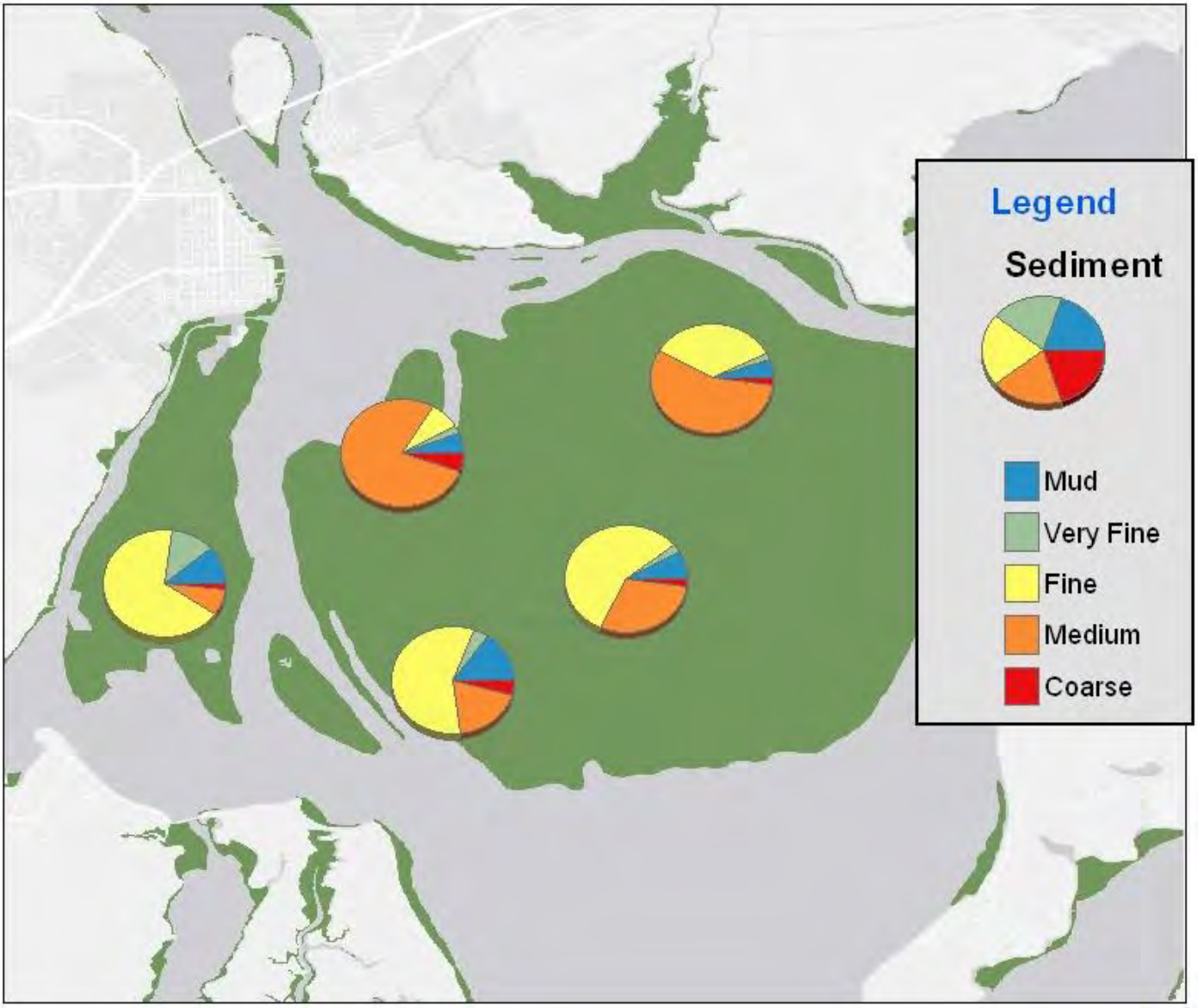

Figure 10. Percentage of each sediment size is shown by the pie charts above, with respect to their location of sampling. The sediment was fraction by the following factors sieve sizes; mud= <64µm, very fine sand= 64-120µm, fine sand= 120-250µm, medium= 250-500µm, and coarse= >500µm.

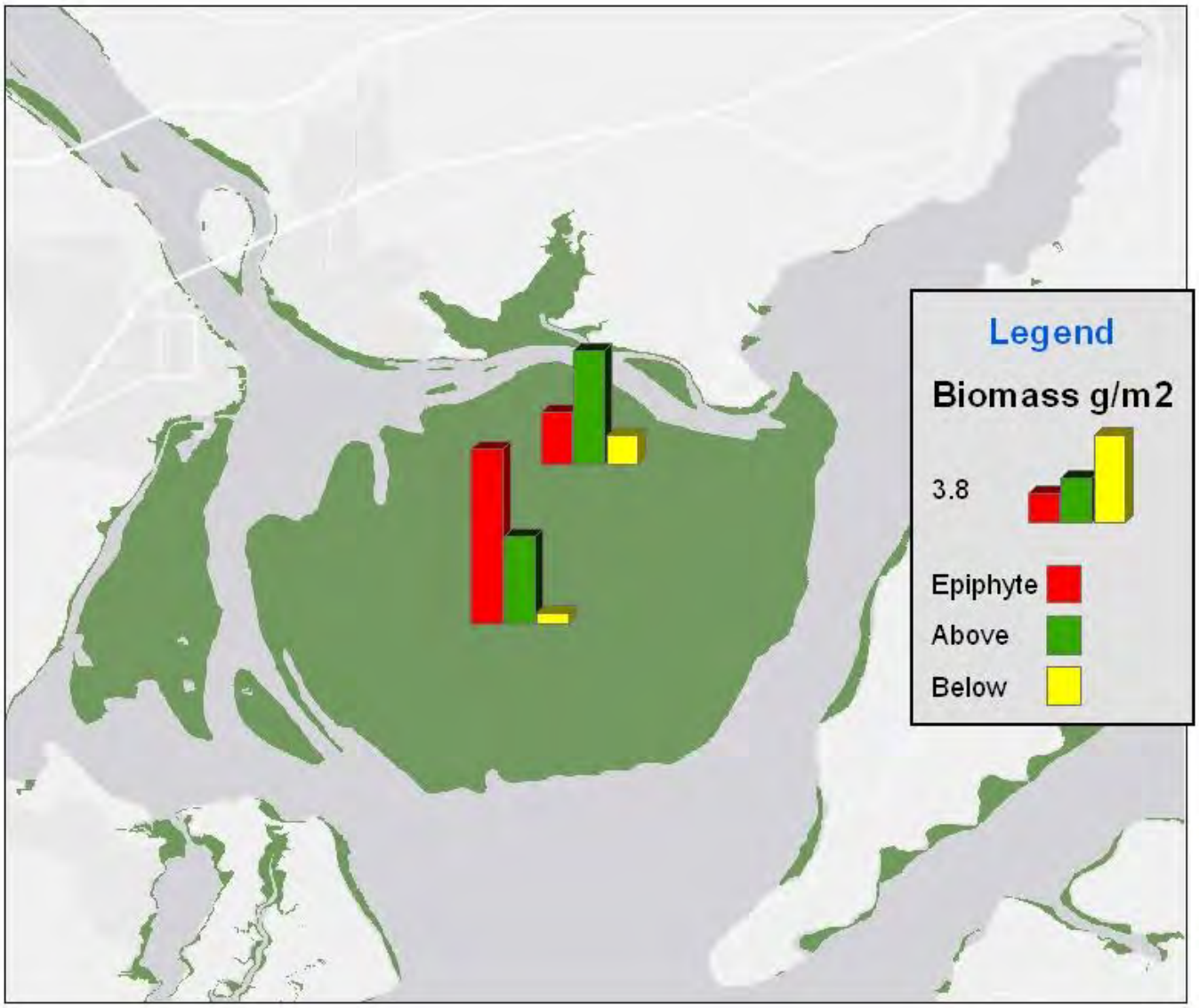

Figure 11. Biomass of above, below, and epiphyte values were plotted at the location they were sampled. The height represents the amount of biomass for each category. In the legend, 3.8 is the height of the tallest bar (yellow in the legend), and is for a comparison.

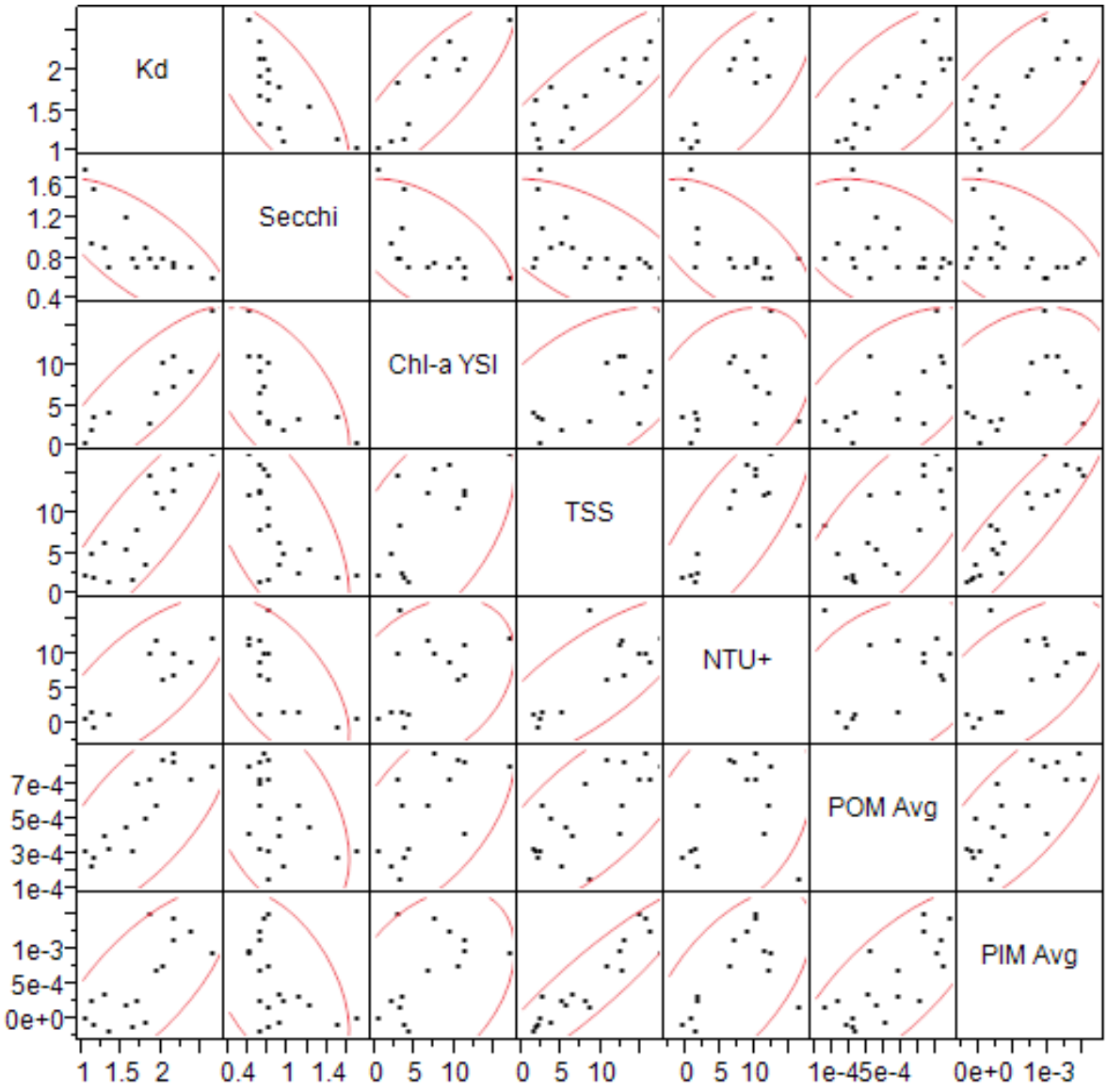

Figure 12. Correlation matrix from the JMP software. The table shows the coefficient of each correlation, with those closer to 1 more correlated. Red is negatively related, while blue is positively related. Chl-a=Chlorophyll-*a*, TSS=Total Suspended Solids, NTU+=Turbidity, POM=Particulate Organic Matter, and PIM=Particulate Inorganic Matter.

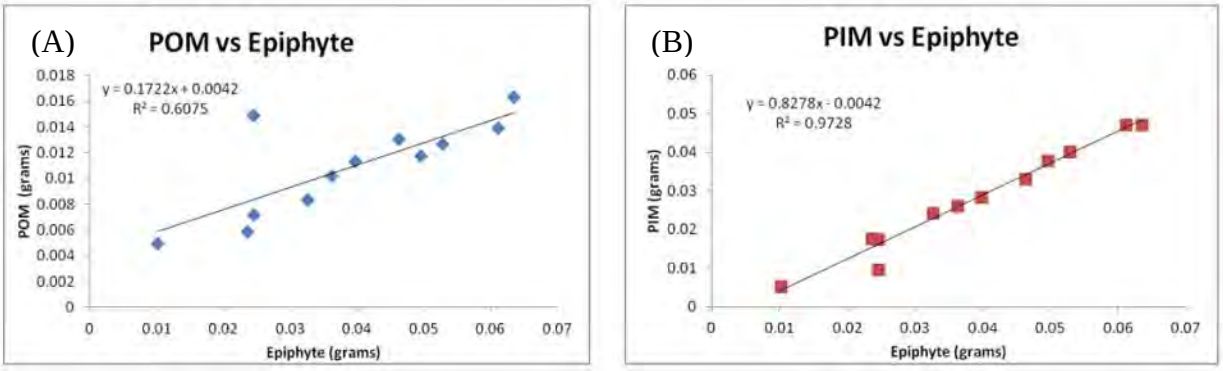

Figure 13(a-b). Regressions of the epiphyte weight verse the particulate matter, either Organic (POM) or Inorganic (PIM). R^2 value represents the strength of this relationship.

Figure 14(a-b). These photos were taken while flying over the Susquehanna Flats on July 17. 2011. The Susquehanna River is in the top left of both photos. The darker areas represent the SAV cover and the brown areas are likely bare areas.

Table 1. The correlation matrix run on jump gives the correlation coefficients in this table form. Closer to 1 is a closer positive correlation, -1 is negative correlation.

	Kd	Secchi	Chl-a YSI	TSS	NTU+	POM Avg	PIM Avg
Kd	1.0000	-0.7223	0.8390	0.8628	0.7103	0.6919	0.7345
Secchi	-0.7223	1.0000	-0.5773	-0.6166	-0.6226	-0.4444	-0.4974
Chl-a YSI	0.8390	-0.5773	1.0000	0.5292	0.3313	0.5676	0.3687
TSS	0.8628	-0.6166	0.5292	1.0000	0.7847	0.7287	0.9243
NTU+	0.7103	-0.6226	0.3313	0.7847	1.0000	0.3330	0.6141
POM Avg	0.6919	-0.4444	0.5676	0.7287	0.3330	1.0000	0.7648
PIM Avg	0.7345	-0.4974	0.3687	0.9243	0.6141	0.7648	1.0000

Presence of Ammonia-oxidizing Archaea and Bacteria Along Physiochemical Gradients in Coastal Beaches and Estuaries

Hannah Geiser, REU Fellow
Maryland Sea Grant

Dr. Alyson Santoro, Research Assistant Professor
Horn Point Laboratory, University of Maryland Center for Environmental Science

Abstract

Coastal intertidal estuaries in California and Maryland were analyzed for the presence of ammonia-oxidizing archaea and bacteria and correlation with dissolved inorganic nitrogen removal. DNA was extracted from sediment samples and real-time polymerase chain reaction was used to quantify the presence of the *amoA* gene subunit, a portion of the gene that encodes for the conversion of ammonia to hydroxylamine. Ammonia-oxidizing archaea and bacteria were found with relatively more archaea in the coastal sediments. The abundance of ammonia-oxidizing bacteria appeared to correlate with dissolved oxygen. Removal of dissolved inorganic nitrogen did not appear to be limited by the abundance of microbes found in the sediment.

Keywords: Ammonia, Nitrite, Archaea, Bacteria, Coastal estuary

Introduction

The nitrogen cycle is an essential part of biological life. Nitrogen gas (N_2) from the atmosphere is fixed into ammonia (NH_3) by synthetic and biological mechanisms. Once in the form of NH_3, nitrification converts the ammonia into nitrite (NO_2^-) and then nitrate (NO_3^-). The final step in the cycle is denitrification where the NO_3^- is converted back into N_2 and released into the atmosphere. Large quantities of nitrogen leak into the coastal water from a variety of sources. Over half of the dissolved inorganic nitrogen (DIN) that leaks into the estuaries and coastal water systems can be converted back into nitrogen gas (Rogers and Casciotti 2010), while other DIN is removed through anammox, anaerobic ammonia oxidation (Santoro et al. 2008).

Septic systems treating domestic waste often have large leach fields where the sewage leaks out nutrients. Fertilizers put onto agricultural fields also leak out nutrients, because once the soil is saturated with nitrates, the rest wash into the groundwater and then into the rivers and oceans. Nitrogen is usually present among the contaminants, including others such as phosphorous and pathogens (Swartz et al. 2006).

Recent research has shown that proteobacteria, which were once thought to be the only organisms to nitrify (Konneke 2005), share the role of nitrification with archaea. It used to be

thought that archaea only lived in harsh environments, but more recent studies have shown archaea to thrive in the marine system (Konneke 2005). These archaea have been shown to be an important step in nitrification. Ammonia-oxidizing archaea (AOA) and bacteria (AOB) oxidize ammonia into nitrite and also produce a side product of nitrous oxide (N_2O) (Ritchie and Nicholas 1972). Removing the excess ammonia is vital for the cycling of nitrogen which is why AOA and AOB are being investigated. The oxidation of ammonia to nitrite is the rate limiting step in nitrification and thus in removal of nitrogen from the water into the atmosphere (Rogers and Casciotti 2010).

AOA and AOB can be quantified by using quantitative polymerase chain reaction (qPCR) and the ammonia monooxygenase subunit A gene (*amoA*) to determine AOA and AOB abundances (Kowalchuk and Stephen 2001). *AmoA* is part of the gene found in ammonia-oxidizing organisms that is responsible for the first step in denitrification, the conversion of ammonia into hydroxylamine (Santoro et al. 2008). The number of *amoA* genes present also correlates on a relatively one to one basis with the abundance of ammonia-oxidizing organisms (AOO). The specificity of the AOB *amoA* gene primers shows few problems with amplification of other genes (Bernhard et al. 2005). Research has found that AOA are present both in fresh and saline bodies of water but that the AOB have a preference for freshwater in some situations. The ratio of AOA to AOB varies widely depending on the salinity and other unknown factors in the coastal waters (Bouskill 2012).

Preliminary testing and sampling have been done at three California beaches that are near residential areas on septic systems. The beaches—Los Osos, Carpinteria, and Stinson Beach—were transected and sediment samples were collected at the level of the groundwater with two samples on the beach and two in the ocean (Figure 2). Conductivity, salinity, dissolved oxygen (DO), pH, and DIN were measured at the sites. Stinson Beach and Carpinteria appear to show some removal of DIN across the salinity gradient while Los Osos appears to be adding DIN. The nitrification potentials increased on all three beaches moving from the land out to the sea, but the rates at Carpinteria were more than an order of magnitude larger than those at the other two beaches. Microbial analysis was performed this summer on the DNA extracted from the sediment samples.

A study on the shifting relative ratios of AOA and AOB was performed on Huntington Beach, California (Santoro et al. 2008). The net flow of groundwater played a significant role in the abundance of AOA and AOB. When fresh groundwater was flowing into the saline environment, more of the transect sample had higher ratios of AOB, but when the net flow of water was flowing in from the ocean, the opposite was true. Each transect covered a ~40 meter area that encompassed both the ocean and the coast that contained fresh water. The nitrite and nitrate concentrations were higher in the coastal sediments than in the ocean samples, but ammonia had the highest concentration at the boundary between coast and ocean (Santoro et al. 2008). The smaller tributaries in the Little Choptank River a smaller estuary within the Chesapeake Bay estuary in Maryland, and the differences between it and a larger estuary such as the Choptank River and Chesapeake Bay would be interesting to study.

The Little Choptank River in Maryland is a tidal river off of the Chesapeake Bay (Figure 1). It consists of many smaller creeks that branch out of the main bay area. Each creek that branches off has a different cardinal orientation that may cause changes in currents and biological activity. Most of the creeks are in residential areas where the inhabitants use septic systems. The influx of ammonia and nitrates from the septic systems may cause differences in the abundance of ammonia-oxidizing organisms. The beach at Horn Point Laboratory (HPL) that is along the Choptank River will be tested similarly to the Little Choptank sites. HPL is on a

sewer system that is connected with Cambridge, MD where it is processed, so the beach will function as a control for the other sites.

We hypothesized that the California beaches and Little Choptank branches would differ in amount of nitrifying organisms present because of different salinities, different sediment types, and different sewage treatment practices. Lower salinities in the Little Choptank might increase the ratio of AOA to AOB in comparison to the California samples. The higher dissolved oxygen levels might correspond to more proteobacterial *amoA* than in area of low oxygen.

Materials and Methods

Sediment samples at three California beaches (Los Osos, Carpinteria, and Stinson Beach) were collected in summer 2011 and frozen in a -80°C freezer. Sediment samples from the intertidal zones of Hudson Creek, Brooks Creek, and Fishing Creek as well as from the Horn Point Laboratory beach were collected using a plastic syringe to get a sediment core. The physical characteristics of the Little Choptank sites were measured with a CTD. The temperature, salinity, and dissolved oxygen at HPL were measured with a YSI 85 (Aquatic Ecosystems, Inc.). Two cores were taken side-by-side at two locations in each creek and at HPL. Plastic spatulas were used to take around 500 mg of sediment and placed in a pre-weighed vial with lysing Matrix E (MP Biomedicals). Both the cores and the smaller samples were flash frozen in liquid nitrogen.

Sediment samples from each core were weighed into aluminum weigh plates, dried in a drying oven for 51 hrs, and reweighed. The dry samples were then placed in a muffle furnace (Barnstead Thermolyne 30400 Furnace) for 4 hours at 500°C and the difference in mass was the organic carbon content by loss on ignition analysis (Hizon-Fradejas et al. 2010, 450°C). The sediment vials were thawed in ice and the DNA extracted using the FastDNA Spin kit for Soil (MP Biomedical) and following the manufacturer's instructions. The spinning of the beads and sediment samples was changed to use the Mini-Beadbeater 16 (Biospecs Products) for two 30 second cycles with the samples iced between and after the runs. After the binding matrix was added, the solution settled for 5 min and then 700 µL of solution was discarded. The penultimate step added 100 µL of DES before the sample were placed in a 55°C heat block for 5 minutes followed by centrifugation. Half of the DNA sample was kept for use as the working stock while the other 50 µL was preserved at -80°C.

DNA quantification for all California, Choptank, and HPL samples was analyzed using the Qubit 2.0 Fluorometer. A solution of 199 µL of Qubit buffer and 1 µL of Qubit reagent was mixed for each sample and for the two standards. The standards were made from 190 µL of the previous solution with 10 µL of the standard. Each sample was analyzed with 198 µL of solution and 2 µL of the sample. The sample solution was vortexed for 3 seconds and allowed to incubate at room temperature for 2 min before being placed in the Qubit monitor and the concentration of DNA recorded (Santoro et al. 2008). The DNA samples were first quantified with dsBR (double stranded broad range) Qubit reagents. Any sample that was undetected in the dsBR analysis was further analyzed with dsHS (high sensitivity) Qubit reagents.

Each working DNA solution was run in the qPCR on a BIO RAD CFX96 Real-Time System C1000 Touch thermal cycler to determine abundance of the *amoA* gene in AOA and AOB. 2 µL of DNA sample (1:100 dilution of the Choptank samples) was added to a mastermix of Bio-Rad SsoAdvance SYBR® Green Supermix E (10 µL), 10 µM forward primer (0.8 µL), 10 µM reverse primer (0.8 µL), and water (6.4 µL) for analysis. A series of 6 standard dilutions in duplicate was used for the standard curve. Each sample was run in triplicate (Choptank

samples in duplicate) on a low profile 96-well plate. The AOA was run in the qPCR at 98°C for 3 min, then the following sequence repeated 34 times,98°C for 15 sec, 58°C for 30 sec, 72°C for 30 sec, and finally a temperature ramp from 65°C for 5 sec to 95°C for the melt curve. The AOB was run in the qPCR at 98°C for 3 min, then the following sequence 36 times, 98°C for 10 sec, 58°C for 30 sec, 72°C for 10 sec, 80°C for 5 sec, and finally a temperature ramp from 65°C for 5 sec to 95°C for the melt curve (Santoro).

Dr. Nick de Sieyes and his colleagues measured the nitrification potential of the California beaches as well as all the physical characteristics.

Results

Carpinteria had an average AOA abundance spanning 2.3(1) - 9.0(2)·10^6 copies/g sediment (dry) across the salinity gradient of 1.19 to 32.76. The average AOB abundance spanned 8.7(1)·10^4 – 3.1(1)·10^6 copies. The AOB abundance increased with salinity with the exception of the most saline site (Figure 3). There was a significant correlation ($p < .05$) between AOB and temperature at Carpinteria. The highest AOA and AOB abundances were both at the second highest salinity which also had the highest DO. Ratios of AOB/AOA at the Carpinteria sites increase with salinity from 0.01 to 0.78 (Figure 4). Carpinteria had the highest nitrification potential of the California beaches with a range of 48.8 to 94.4 μmol day^{-1} kg^{-1} (Table 1) and a significant relationship ($p < 0.05$) with the AOB/AOA ratio and nitrification potential. Measuring salinity against DIN shows little nitrogen removal along the coastal sediments despite higher nitrification potentials than other locations.

Los Osos had an average AOA abundance spanning 3.5(3)·10^5 – 3.0(1)·10^7 copies across the horizontal transect with no AOA being detected at the lowest salinity site. The average AOB abundance spanned 3.9(2)·10^4 – 8.2(4)·10^5 copies and was not detected at the lowest salinity site (Figure 3). Lack of AOO detection at that site may have been caused by inhibition or possibly by no AOO being present. The salinity spanned 2.89 to 33.5 across the beach. The AOB abundance increased with salinity with the exception of the most saline site like at Carpinteria. There were large peaks of AOA at the 3rd and 4th most saline sites that were an order of magnitude higher than at the other Los Osos sites. The ratio of AOB to AOA increased from 0.01 to 1.23 across the four increasing salinity sites (Figure 4). The highest salinity site was the only site in the California sites tested that had more AOB than AOA. Lower salinity sites at Los Osos had less than 0.04 AOB to AOA ratio. The salinity spanned 2.89 to 33.5 across the beach. The only significant ($p < .001$) correlation was between the AOB to AOA ratio and the oxidation and reduction potential (ORP). Nitrification potentials at Los Osos ranged from 1.1 – 11.9 μmol day^{-1} kg^{-1} from least to most saline sites, however, the graph of DIN and salinity show addition of DIN across the sites (Table 1).

Stinson Beach had an average AOA abundance spanning 4.5(3)·10^5 – 9.9(8)·10^6 copies across the horizontal transect. The average AOB abundance spanned 3.42(4)·10^3 – 2.2(2)·10^6 copies and correlated with the moisture content of the sediment, temperature, and salinity ($p < 0.05$ for all) (Figure 3). The highest presence of both AOA and AOB was at the highest DO site which was the second highest salinity site. There was a similar pattern to Carpinteria in that the AOA abundance increased with salinity except for the most saline site. The two lowest salinities had lower AOB than the three highest salinities, but there were always more AOA present than AOB at each site. The ratio range of AOB to AOA spanned 0.01 to 0.46 correlating with temperature ($p < 0.05$) (Figure 4, Table 1).

A depth profile was collected at Stinson Beach with 5 samples taken at different depths above the water level. All AOA collected ranged between $3.6(2)\cdot10^5$ to $9.9(8)\cdot10^6$ copies/g sediment. The AOB was present in a greater range of $2(2)\cdot10^3$ to $6.0(5)\cdot10^6$ copies/g sediment (Figure 5). As a general trend, there was an increase in AOA as depth increased in the middle salinity sites. The AOB tended to increase then decrease with a peak at a middling depth except for the most saline site where the AOB abundance decreased at the middle depth. The ratio of AOB to AOA decreased with depth except at the most saline location (Figure 6). There was more AOB present than AOA around the sediment surface at the three most saline sites, but then the ratio decreased except at the most saline location (Figure 7). Other than the deepest and most saline site, the AOA fluctuated more than the AOB.

ANOVA tests of AOA, AOB, AOO, and AOB/AOA ratios showed no significant differences between the three beaches, but the lowest p-value was 0.058 for AOA (Figure 8) among the beaches. Taken as a whole, the AOB abundance at the beaches negatively correlated with temperature ($r=-0.62$, $p < 0.05$) and positively correlated with DO ($r = 0.72$, $p < 0.01$) (Figure 9). The range of AOB at Los Osos was smaller than the range and average at Stinson Beach and Carpinteria (Figure 10). Graphs of salinity versus DIN at each of the three beaches show increased removal of DIN from Stinson Beach and Carpinteria but the decreased removal of DIN at Los Osos.

Data from the Little Choptank River were collected in duplicate at two sites in each creek with the visual descriptions recorded (no grain size analysis or sedimentation rates performed, Table 2, Table 3). AOA ranged from $4(2)\cdot10^6$ to $7.7(3)\cdot10^6$ at the Little Choptank sites and $6.6(40)\cdot10^7$ to $5.0(4)\cdot10^8$ at the HPL sites. AOB ranged from $6.4(9)\cdot10^5$ to $2.9(7)\cdot10^6$ at the Choptank sites and $1.2(3)\cdot10^6$ to $6.3(9)\cdot10^6$ at the HPL sites. Both sites (silt and brown sand) in Brooks Creek (BC1, BC2), the sandy site in Fishing Creek (FC2), and the brown sand and clay sites at Hudson Creek (HC1, HC2) all had similar relative abundances of AOA and AOB (Figure 11). The peat site (FC1) at Fishing Creek had a higher ratio of AOB to AOA than any other site (Figure 12). The two sites at HPL (HP1, HP2) had significantly more AOA present than the other sites ($p < 0.05$). Because of the higher AOA at the HP sites, the ratio of AOB to AOA was much lower than at the Little Choptank sample sites.

When the Choptank and HPL data set was taken as a whole, there were several correlations of importance. The ratio of AOB to AOA positively correlated with organic content ($r = 0.93$, $p < 0.001$). Abundance of AOB negatively correlated with DO, salinity, and temperature ($r = -0.62, -0.59, -0.66$, $p < 0.05, 0.05, 0.01$). AOA abundance also negatively correlated with salinity ($r = -0.66$, $p < 0.01$).

Discussion

The microbiology of the California beaches was examined to better understand the cycling of DIN along the coastal sediments in relation to septic influx. Stinson Beach and Carpinteria are both located along the actual Pacific coast while Los Osos is in a relatively protected bay. Since Los Osos appeared to have more distinct characteristics than the other two beaches, it may be assumed that environment aspects account for the differences. The coastal estuary formed by the mixing of seeping groundwater with the saline ocean water should be removing DIN from the groundwater and preventing it from entering the ocean by releasing it back into the atmosphere. The amount of DIN present at Stinson Beach and Carpinteria were much higher than the DIN at Los Osos. Studies of the microbial communities of ammonia-oxidizing organisms were performed to analyze what might be causing the lack of removal of DIN at Los Osos. If the AOO were not present in Los Osos, it could be assumed that

a lack of nitrification was as the limiting step. However, there was a greater abundance of AOA at Los Osos than at either of the two other beaches. Despite this, the NO_3^- (the largest component of DIN in these samples) levels at Los Osos were an order of magnitude less than Stinson and Carpinteria. AOA play an important role in converting ammonia to nitrite, possibly even more so than AOB (Santoro et al. 2010) so the lack of DIN removal is unexpected. There are lower average AOB levels at Los Osos than the other two California beaches which may contribute to the higher DIN levels. A study performed in agricultural soil found that the conversion of ammonia to nitrite was correlated with AOB and not AOA (Jia and Conrad 2009), but agricultural soil and intertidal coastal sediment probably contain different environmental factors affecting AOO activity.

The high levels of nitrification potential in Carpinteria was interesting in that the other physical characteristics of the beach appear to be quite similar with the other beaches, especially Stinson beach. There is a possibility that the method of measuring nitrification potential is damaging to the microbial community because it disturbs the sediment, but the method of measurement across the beaches was the same. There did not appear to be any more AOO or increased DIN removal at Carpinteria in comparison with Stinson. Since no RNA was analyzed for actual activity of the AOO, there might be more activity at Carpinteria that is not shown by these data. The correlation between AOB/AOA and nitrogen potential is slightly at odds with the other results where nitrogen potential was found to correlate with AOA and not AOB in an estuary (Caffrey et al. 2007).

Previous studies have looked at abundance of AOA and AOB by depth in the water column, but little has been done in coastal sediments. The Stinson Beach depth profiles offer a good look at the ammonia-oxidizing community in a coastal estuary. The divergence of AOA and AOB abundance at the water table of the central three sites suggests that middle salinities may enhance archaeal communities. As the sites become more saline closer to the coast, the relative increase of AOB is readily evident. Other work suggests that AOB is more prevalent in saline water (Santoro et al. 2008). There was also a higher total abundance of AOO as the salinity increased until the final site 5 where the average abundance slightly decreased. Archaea tend to prefer a more freshwater environment (Santoro et al. 2008) even though they are present in the whole ocean as well as in numerous other soils.

The samples collected at HPL have significantly more AOA than at all other sample sites. Both locations are on either the Choptank River or a small inlet of the river. The organic matter floating in the water above samples HP2 might have contributed to the nutrients necessary for the AOO. There is an oyster hatchery located at HPL that pumps water through tanks of oyster spat and then is flushed into the river, possibly causing an increase in ammonia for the microbes. Ammonia, DIN, nitrification potentials and other data were not collected at the Maryland sites which might have helped to determine reasons why the sediment microbial community was significantly different that the Little Choptank and California sites. The Little Choptank samples appeared to vary more by sediment type than by any other defining characteristic. If the Little Choptank samples are grouped together, they have relatively similar AOA and AOB abundance across the board with the exception of FC1. AOA abundance at FC1 (Figure 11) appears lower than at the other Little Choptank sites and this may be caused by increased organic carbon content because previous studies have shown AOA abundance to be inhibited by organic carbon (Konneke et al. 2005). Future studies should be conducted with similar sediment type to better compare microbial communities.

The California, Choptank, and HPL sites all differ significantly in site location and type, but some similarities and differences may be extracted. The majority of the sample sites found

higher AOA concentrations than AOB in the sediment similar to another study of estuaries (Caffrey et al. 2007). The abundance of AOA at HPL is significantly higher than at all Choptank and California sites. The abundances of AOA and AOB between the Choptank and California sites were within the same order of magnitude despite differences in sediment. Though both the California and Choptank samples have correlations between AOB and percent dissolved oxygen, the slopes of those lines are drastically different (Figure 9). The CA samples appear to show increased DO has increased AOB while the opposite is true at the Choptank sites. However, the % DO is higher at all Choptank locations than at the CA sites. This suggests that there may be an ideal dissolved oxygen percentage for AOB. It could be that the %DO is caused by other particular environmental factors that all combine to form a successful niche for the AOB and that in this study the DO was just found to combine all of those factors to find a pattern.

Future analysis of the RNA extracts would be helpful in determining activity of the AOO present in the California beaches. Measurements of more physical characteristics in the Little Choptank River and HPL might decipher the causes of the spike in AOA in the sediment as well as how sediment type affects microbial communities. A preliminary analysis of possible inhibition in the samples was performed. Some samples appeared to be inhibited while others were enhanced by the addition of a known spike. A more in-depth analysis could lead to more accurate abundance values and knowledge about possible PCR inhibitors in the coastal sediments.

Conclusions

Upon analysis of the abundances of AOA and AOB in the coastal California sediments, it appears as though the microbial community is not the limiting reagent in the removal of DIN. There are correlations between AOB and dissolved oxygen as well as with the nitrification potential in the California beaches. The Choptank samples show more of a correlation by sediment type of AOO with the exception of the HPL samples with the extreme levels of AOA in comparison with other sites. However, there is still a correlation with dissolved oxygen despite the correlation being opposite of the California AOB and DO samples. The relative ratios of AOB to AOA varied with salinity and sediment type to support a healthy ecosystem.

Acknowledgements

Thank you to Dr. Alyson Santoro for providing both the expertise and equipment for this project. I would also like to thank Dr. Nick Nidzieko and Gabriel Ng for helping locating appropriate sample sites and for help in collection of the sediments. Thank you to Horn Point Laboratory and Maryland Sea Grant for providing the funding that made this possible.

References

Bernhard, A.E., T. Donn, A.E. Giblin, and D.A. Stahl. 2005. Loss of diversity of ammonia-oxidizing bacteria correlates with increasing salinity in an estuary system. Environmental Microbiology 7:1289-1297. doi:10.1111/j.1462-2920.2005.00808.x

Bouskill, N.J., D. Eveillard, D. Chien, A. Jayakumar, and B. Ward. 2012. Environmental factors determining ammonia-oxidizing organism distribution and diversity in marine environments. Environmental Microbiology 14:714-729.

Caffrey, J.M., N. Bano, K. Kalanetra, and J.T. Hollibaugh. 2007. Ammonia oxidation and ammonia-oxidizing bacteria and archaea from estuaries with differing histories of hypoxia. Multidisciplinary Journal of Microbial Ecology 1:660-662.

de Sieyes, N.R., K. Yamahara, B. Layton, E. Joyce, and A. Boehm. 2008. Submarine discharge of nutrient-enriched fresh groundwater at Stinson Beach, California is enhanced during neap tides. Limnology and Oceanography 53:1434-1445.

Hizon-Fradejas, A.B., Y. Nakano, S. Nakai, W. Nishijima, and M. Okada. 2010. Utilizing dredged sediment for enhancing growth of eelgrass in artificially prepared substrates. International Journal of Environmental and Earth Sciences 1:57-62.

Jia, Z., and Conrad, R. 2009. Bacteria rather than archaea dominate microbial ammonia oxidation in an agricultural soil. Environmental Microbiology. 11:1648-1671.

Konneke, M., A. Bernhard, J. de la Torre, C. Walker, J. Waterbury, and D. Stahl. 2005. Isolation of an autotrophic ammonia-oxidizing marine archaeon. Nature 437:543-546.

Kowalchuk, G.A., and J.R. Stephen. 2001. Ammonia-oxidizing bacteria: a model for molecular microbial ecology. Annual Review of Microbiology 55:485-529.

Ritchie, G.A, and D.J. Nicholas. 1972. Identification of the sources of nitrous oxide produced by oxidative and reductive processes in *Nitrosomonas europaea*. Biochemical Journal 126:1181-91.

Rogers, D.R., and Casciotti, K.L. 2010. Abundance and diversity of archaeal ammonia oxidizers in a coastal groundwater system. Applied and Environmental Microbiology 76:7938-7948.

Santoro, A.E., A. Boehm, and C. Francis. 2006. Denitrifier community composition along a nitrate and salinity gradient in a coastal aquifer. Applied and Environmental Microbiology 72:2102-2109.

Santoro, A.E., C. Francis, N. de Sieyes, and A. Boehm. 2008. Shifts in the relative abundance of ammonia-oxidizing bacteria and archaea across physiochemical gradients in a subterranean estuary. Environmental Microbiology 10:1068-1079.

Santoro, A.E., K. Cassciotti, and C. Francis. 2010. Activity, abundance and diversity of nitrifying archaea and bacteria in the central California Current. Environmental Microbiology 12:1989-2006.

Swartz, C.H., S. Reddy, M.J. Benotti, H. Yin, L.B. Barber, B.J. Brownawell, and R.A. Rudel. 2006. Steroid estrogens, nonylphenol ethoxylate metabolites, and other wastewater contaminants in groundwater affected by a residential septic system on Cape Cod, MA. Environmental Science and Technology 40:4894-4902.

Tourna, M., M. Stieglmeier, A. Spang, M. Konneke, A. Schintlmeister, T. Urich, M. Engel, M. Schloter, M. Wagner, A. Richter, and C. Schleper. 2011. *Nitrososphaera viennensis*, an ammonia oxidizing archaeon from soil. Proceedings of the National Academy of Science 108:8420-8425.

Figures and Tables

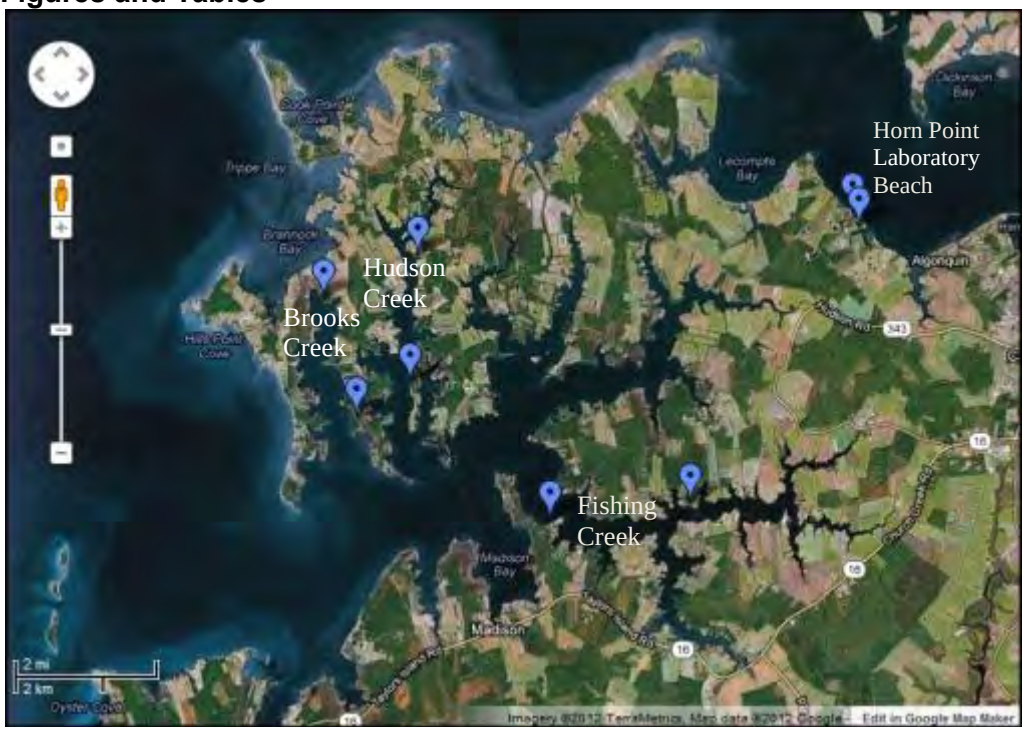

Figure 1. Sampling sites at the Little Choptank River, Maryland.

Figure 2. Sampling location in California.

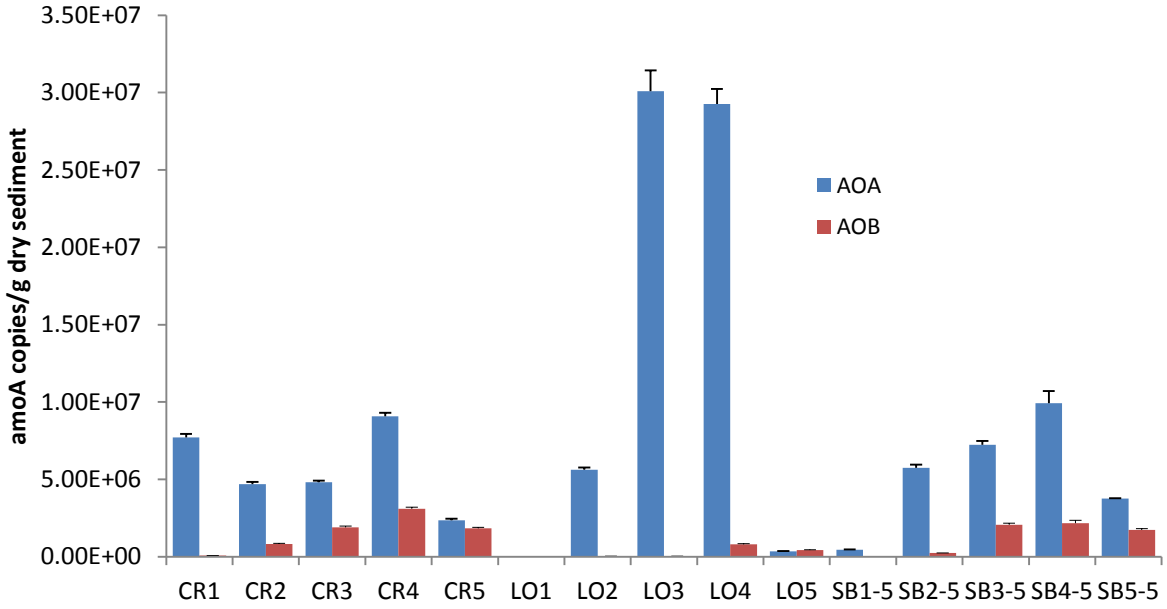

Figure 3. Abundances of AOA (blue) and AOB (red) per gram dry sediment at the California beaches – Carpinteria (CR), Los Osos (LO), Stinson Beach (SB) – with standard deviation.

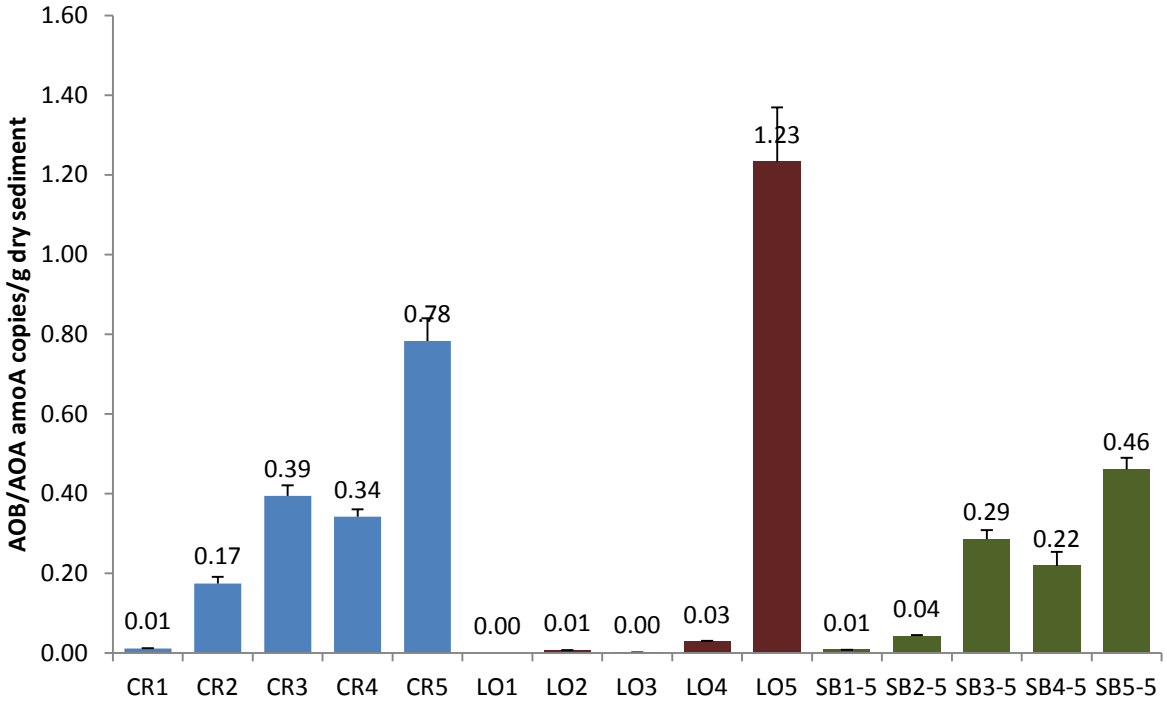

Figure 4. Ratio of AOB to AOA per gram dry sediment at the California beaches – Carpinteria (CR - blue), Los Osos (LO - red), Stinson Beach (SB - green) – with standard deviation.

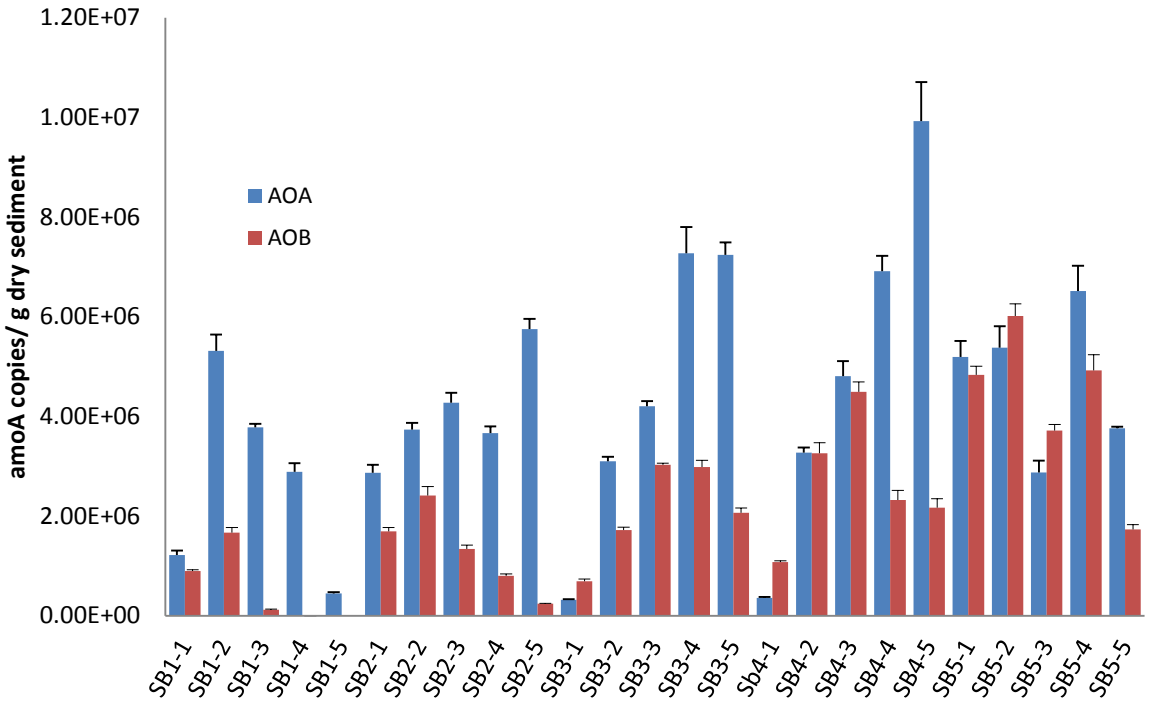

Figure 5. Abundances of AOA (blue) and AOB (red) per gram sediment are shown by depth in Stinson Beach (SB) with standard deviation. The salinity gradient increases from SB1 to SB5 and the depth increases from 1-1 to 1-5.

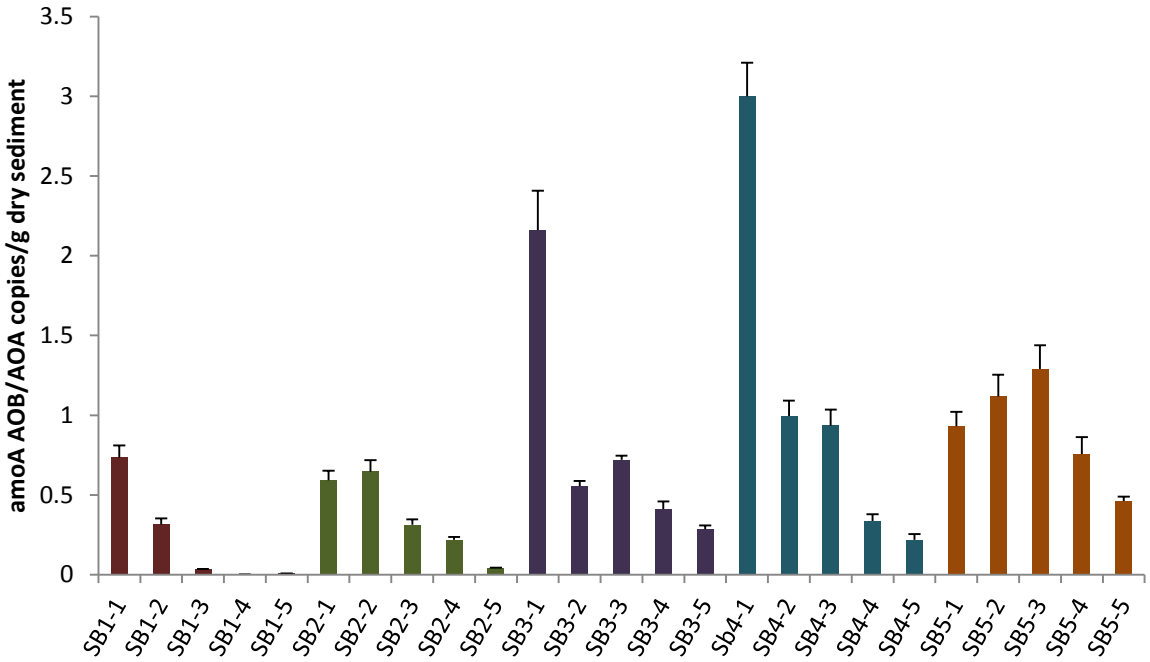

Figure 6. The ratio of AOB to AOA per gram dry sediment at Stinson Beach with standard deviation is shown by depth (1-1 to 1-5) and also by salinity increasing from SB1 to SB5.

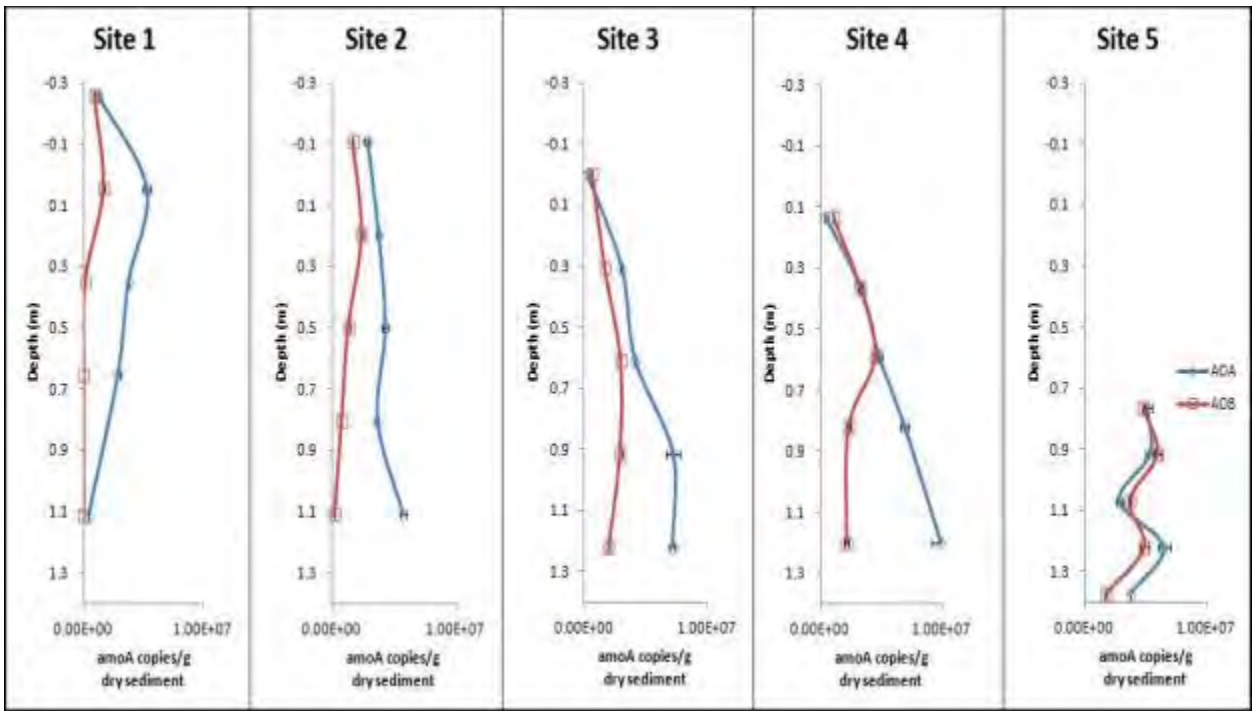

Figure 7. The Stinson Beach depth profiles by increasing salinity (site 1 to site 5) are shown with abundances of AOA (blue) and AOB (red) and standard deviation.

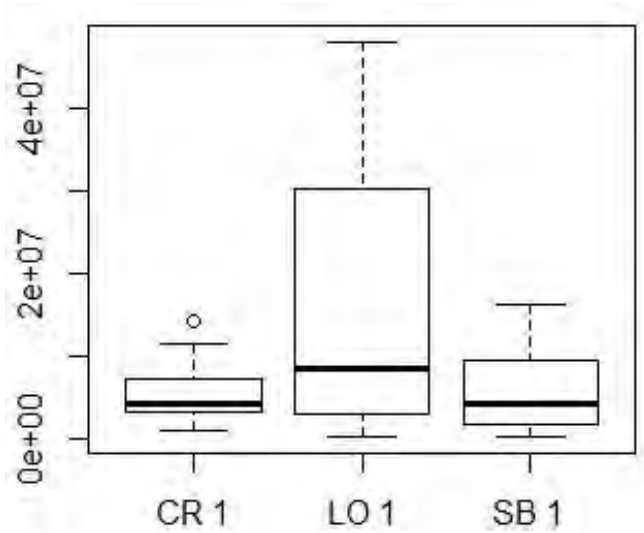

Figure 8. Each beach – Carpinteria (CR), Los Osos (LO), and Stinson Beach (SB) – is graphed against the copies of AOA per g dry sediment ($p = 0.058$).

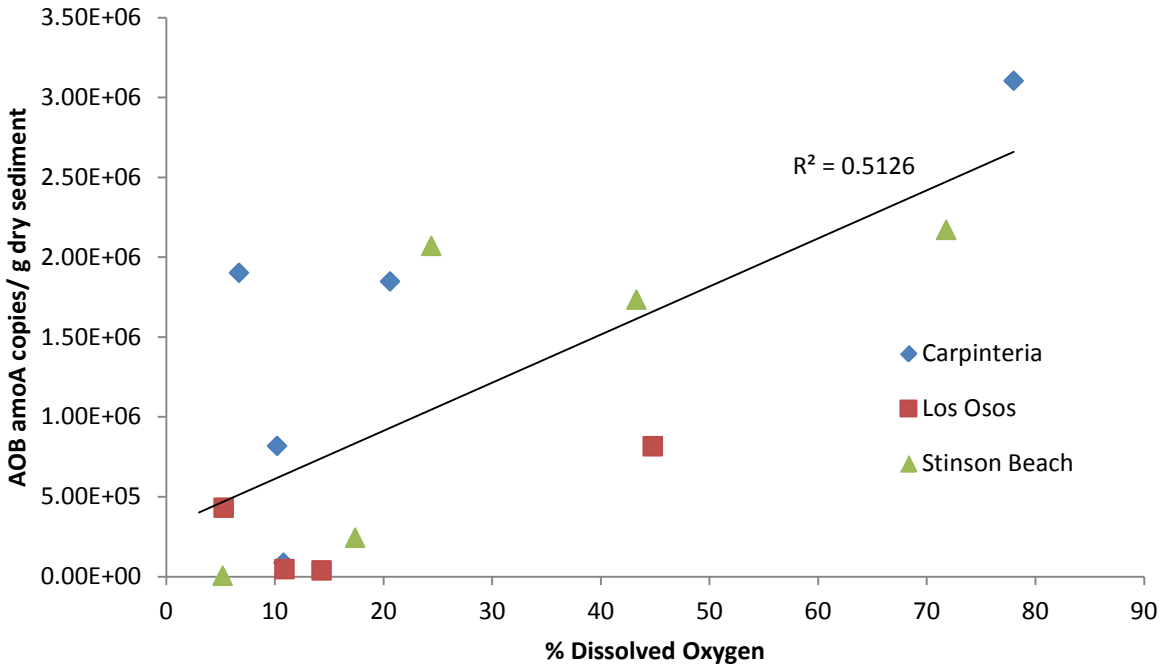

Figure 9. The AOB abundance of each California beach – Carpinteria (CR - blue), Los Osos (LO - red), Stinson Beach (SB - green) – against the dissolved oxygen gradient ($p < 0.01$).

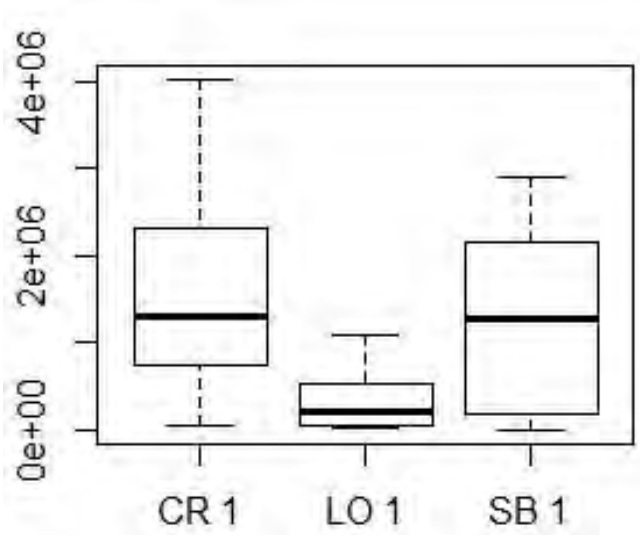

Figure 10. Each California beach – Carpinteria (CR), Los Osos (LO), Stinson Beach (SB) – is measured against AOB per gram dry sediment.

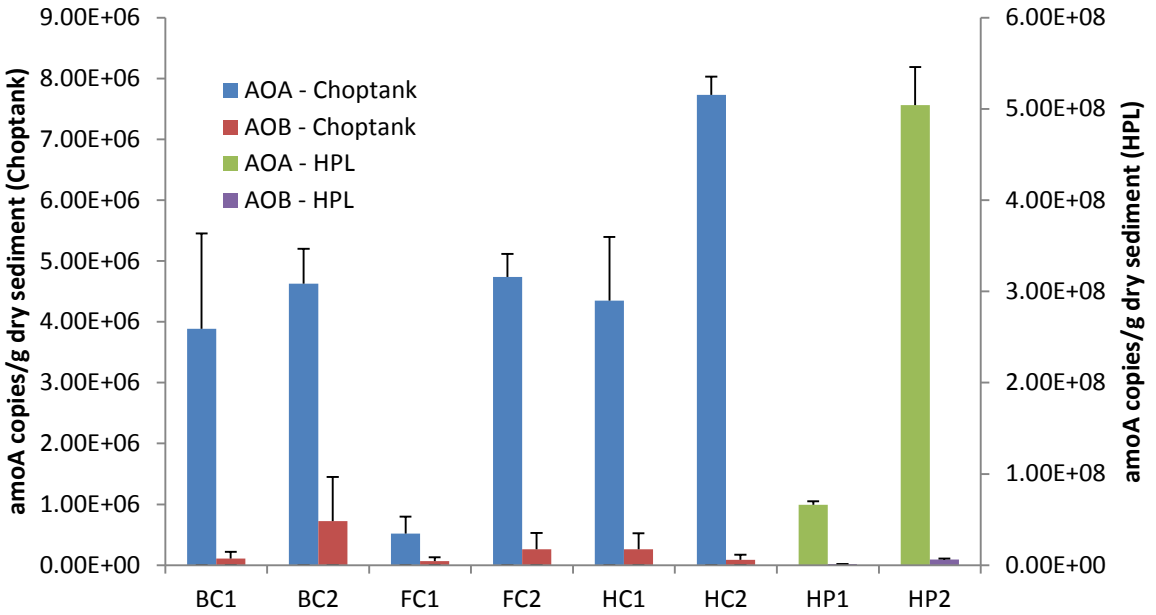

Figure 11. The AOA and AOB abundances of the Little Choptank River (CH) and Horn Point Laboratory (HPL) are shown with a second axis for the HPL samples.

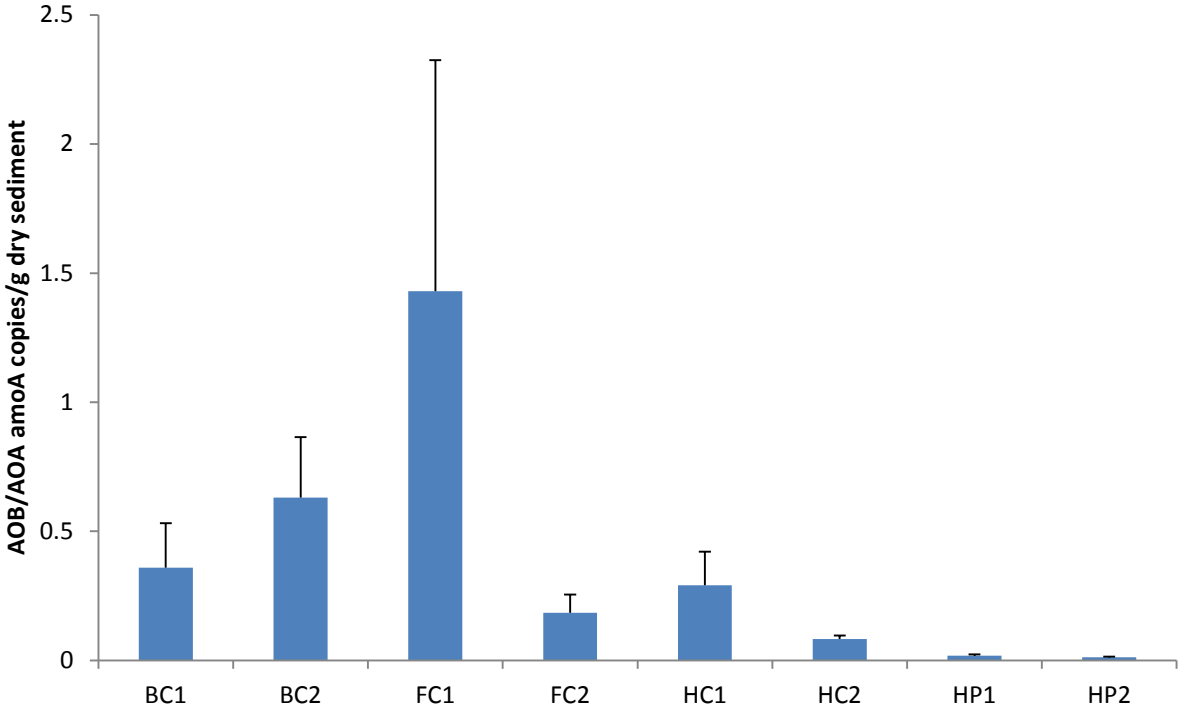

Figure 12. Ratio of AOB to AOA in the Little Choptank River samples – Brooks Creek (BC), Fishing Creek (FC), Hudson Creek (HC), and Horn Point (HP) – with standard deviation.

Table 1. Physical characteristics of the CA beaches – Carpinteria (CR), Los Osos (LO), Stinson Beach (SB).

Station	Moisture (%)	Depth (m)	Salinity (ppt)	Dissolved Oxygen (%)	Nitrification Potential (μmol day^{-1} kg^{-1})
CR1	39.6	1.3716	1.19	10.8	52
CR2	36.6	1.3716	1.39	10.2	48.8
CR3	43.3	0	16.15	6.7	74.3
CR4	46.5	0.9144	32.66	78	71.4
CR5	46.2	0.4572	32.76	20.6	94.4
LO1	39.1	0.762	2.89	3	1.1
LO2	45.4	0.762	23.9	14.3	3.3
LO3	47.3	0.6096	32.52	10.9	6.3
LO4	46.6	0.4572	33.5	44.8	5.4
LO5	47.4	0.3048	31.7	5.3	11.9
SB1-5	36.6	1.3716	0.46	5.2	1.1
SB2-5	31.3	1.2192	1.7	17.4	0
SB3-5	41.5	1.2192	18.12	24.4	1.3
SB4-5	43.1	1.0668	32.08	71.8	4.6
SB5-5	42.1	0.6096	32.2	43.3	6.5

Table 2. Physical characteristics of the Little Choptank samples - Brooks Creek (BC), Fishing Creek (FC), Hudson Creek (HC), Horn Point (HP).

Site	DO (%)	Salinity (ppt)	Temperature (°C)	Moisture (%)	Organic Carbon (%)
BC1	79.2454	12.295	23.782	0.419408539	0.034365782
BC2	85.69193	11.9146	23.4499	0.219338313	0.019084963
FC1	89.52	11.97	24.9	0.809375	0.247747748
FC2	104.7146	11.9805	23.9167	0.177794337	0.004115226
HC1	93.186	12.2513	24.838	0.553810578	0.052577014
HC2	98.83528	12.2077	25.0259	0.268308081	0.038425978
HP1	101	9.8	24.5	0.194498519	0.002951933
HP2	79.5	9.9	23.5	0.297859621	0.021719806

Table 3. Visual description of the Little Choptank samples - Brooks Creek (BC), Fishing Creek (FC), Hudson Creek (HC), and Horn Point (HP).

Site	Description
BC1	silt on the top
BC2	brown sand
FC1	peat
FC2	sandy
HC1	silt, dark sand, then peat
HC2	brown/tan clay
HP1	sandy
HP2	sandy with silt and organic debris on top

Sedimentation Trends and Their Effect on Nitrogen Burial in the Lower Potomac River

Benjamin Green, REU Fellow
Maryland Sea Grant

Dr. Cindy Palinkas, Assistant Professor
Horn Point Laboratory, University of Maryland Center for Environmental Sciences

Abstract

Nitrogen burial through sediment accumulation is a major sink within the proposed nitrogen cycle for the Potomac River. This study explored the relationship between nitrogen concentration and deposition patterns. ^{210}Pb geochronology was used to calculate sedimentation rates for sediment cores collected in the Potomac River. There were examples of both steady-state accumulation and event-layer deposition at different points along the river. Upon further analysis, it was found that sediment deposition patterns have a direct relationship to the rates of nitrogen burial. It is postulated that either channel location or river position affects dominant deposition patterns, with differences also noted in profiles of median grain size profiles and nitrogen concentration profiles.

Keywords: Lead-210 geochronology, Sediment accumulation, Nitrogen, Potomac River

Introduction

The Nitrogen Cycle and Coastal Nutrient Budgets

The nitrogen cycle is composed of biochemical pathways through which oxidation and reduction (redox) reactions cause nitrogen to change from various forms: Ammonium [NH_4^+] (reduced), Nitrate [NO_3^-] (oxidized), and atmospheric nitrogen [N_2]. Through these reactions, organisms are able to manipulate nitrogen so that it can be used effectively in respiration and other various biochemical syntheses (Canfield et al., 2010). All of these reactions occur on a broader spatial scale through a system of nitrogen sources and sinks in estuaries, where nitrogen cycling occurs in both the water column and bottom sediments. In sediments, the nitrogen cycle is characterized by the initial burial of organic matter, which is then transformed into NH_4^+, NO^-_3, and N_2, depending on subsurface conditions (Cornwell et al., 1999). A current study being undertaken by members of the University of Maryland Center for Environmental Science (UMCES) has proposed a model of the nitrogen budget for the Potomac River (Harris et al., 2012). A simplified version of this budget can be seen in Figure 1.

It is of great importance to monitor nutrient cycling as it can negatively affect regional water quality. An example of this is an algal bloom, which is commonly found along coastal regions. These events can have disastrous impacts on a marine ecosystem - threatening the aesthetically pleasing aspects of an ecosystem as well as organisms that aquaculture industries

depend on, such as submerged aquatic vegetation and oysters. Because of these harmful implications, those in charge of land management within a region may want to limit the total nitrogen load (implementing agricultural limitations (esp. fertilizer), enforcing stricter wastewater effluent regulations, etc.). In order for regional management practices to be effective, it is important to consider a truly comprehensive nutrient budget. However, it is difficult to account for every aspect of a nutrient budget within a system.

There has been considerable study on the overall rate of sedimentation within the Potomac River (Brush et al., 1982; Knebel et al., 1981) as well as its nutrient cycling processes (Boynton et al., 1995). However, there has not been significant work done exploring the connection between the two processes (more specifically, nitrogen burial). The aim of this study is to determine the dominant sedimentation trends in the Potomac River, and how they impact the nutrient composition of sediments found throughout the channel. This study will give a clearer idea as to where the nitrogen from the Potomac River is ultimately going, as well as what it means for the overall nutrient budget of the system.

Using the ^{210}Pb radiometry and total nitrogen concentration analysis, both the nature of sediment accumulation in the Potomac River, as well as what it means for the nitrogen accumulation through sediment burial, will be determined.

Measurement of ^{210}Pb Activity and Determination of Accumulation Rates

Radiometric dating of a certain radioisotope can be used to measure geologic activity (in this case, sediment accumulation) within a period four or five times greater than its half-life. Since ^{210}Pb has a half-life of 22.3 years, it can be used to measure relatively recent depositional patterns – that is, having occurred within the last century (Nittrouer et al., 1979). When found in excess in an environment, ^{210}Pb will accumulate in the water column and then, through sorption and depositional processes, accumulate in the sediment column (Mullenbach and Nittrouer, 2000).

There are three common features found within a ^{210}Pb activity profile: 1) the intensely mixed surface layer (SML), 2) the layer exhibiting decreasing ^{210}Pb activity in an exponential fashion, and 3) the background layer, exhibiting uniform activity that would be expected from the decay of ^{226}Ra (of which ^{210}Pb is the daughter isotope) already in residence (Jaeger et al., 1998).

Radionuclide decay, a first-order process, can be described using the equation (Harris et al., 2012):

$$A = A_0 e^{-\lambda t} \tag{1}$$

where A = the activity at time t, A_0 = the initial activity, and λ= the decay coefficient (which is 0.03114 yr^{-1} for ^{210}Pb). Activity within sediments can be described using the equation:

$$A = A_0 e^{\left(\frac{-\lambda x}{w}\right)} \tag{2}$$

where A = the activity (dpm g^{-1}) at depth *x* within the sediment (cm) and w = the sediment accretion rate (cm yr^{-1}). This equation is known as the constant initial concentration (CIC) model

of ^{210}Pb sedimentation, and depends on three major factors: 1) constant input fluxes of both sediment and excess ^{210}Pb within the pre-sampled environment, 2) little post-depositional mobility of ^{210}Pb within the sediment column, and 3) little sediment mixing due to biological (bioturbation) or physical processes. To model the excess ^{210}Pb that can be seen in the zone of decay in a typical activity profile, equation (2) is log transformed:

$$\ln A = \ln A_0\left(\frac{-\lambda x}{w}\right) \tag{3}$$

where *x/w*, similar to *m* in equation (5) is the slope of the linear regression of *x* and $\ln A$, with A_0 being the intercept of the regression.

An alternative to the CIC model is the constant rate of supply (CRS), which is summarized in Appleby and Oldfield (1978). When using the CRS model, one assumes that fluxes of ^{210}Pb into the sediment occur at a constant rate, but sediment particle flux may occur at a variable rate. The age of sediment can be calculated at a given depth by first calculating the total excess ^{210}Pb within a sediment core (Robbins, 1978):

$$t = \frac{\left[\ln\left(1 - \frac{\sum M}{\sum \infty}\right)\right]}{\lambda} \tag{4}$$

where $\sum M$ = the excess ^{210}Pb inventory above a given section of the core (dpm cm^{-2}), $\sum \infty$ = the total amount of excess ^{210}Pb inventory within the core (dpm cm^{-2}), and t = the time in years. By verifying a period of time elapsed for given core intervals, sedimentation rates (cm yr^{-1}) may be calculated for selected regions throughout the core. This technique has been used before in the Chesapeake Bay area, as in Mason et al. (2004) where it was used to quantify sedimentation rates in Baltimore Harbor.

Similar equations were utilized in Jaeger et al. (1998) in studying sedimentation rates along the coast of Alaska. Assuming steady-state sedimentation and that bioturbation is negligible below the SML:

$$S = \frac{-\lambda}{m} \tag{5}$$

where S = the rate of accumulation of sediment, and m = the slope of the linear regression fit to the natural log of the excess ^{210}Pb activity.

Different depositional patterns will result in varying profiles for cores collected over an area. These different profiles can be seen in Figure 2 from Jaeger et al. (1998). Figure 2(A) is a model of how a ^{210}Pb activity profile would appear if the core being examined were collected from a depositional setting prone to steady-state accumulation.

Severe meteorological events occurring over short periods of time (e.g. storms or floods) may have a noticeable effect on ^{210}Pb activity profiles due to increased runoff from the surrounding watershed (Cronin et al., 2003). This runoff can entrain a greater amount of

sediment, leading to a layer of decreased ^{210}Pb activity in the profile (and therefore, a temporary increase in sedimentation rate) because ^{210}Pb cannot be adsorbed by other particles as effectively when the particles are found in high concentration (Mullenbach and Nittrouer, 2000). An example of this can be found in Figure 2(B), with the event layer clearly identified.

Another pattern that may be observed within an activity profile is that of a change in rate of accumulation, which can be seen in Figure 2(C). From this two regressions can be calculated using equation (5).

Also, there may be instances where no clear pattern may be observed (i.e. exhibiting many different patterns). As can be seen in Figure 2(D), the specific rate of sediment accumulation cannot be calculated, but the minimum rate of accumulation (S_{min}) can in fact be calculated by dividing the maximum depth of excess activity (x_{max}) by the number of years:

$$S_{\min} = \frac{x_{\max}}{100y} \tag{6}$$

Verification of the validity of this method of measurement has been provided in various other studies (Brush et al., 1982; Nittrouer et al., 1984).

The relationship between nitrogen burial and sediment accumulation has not been extensively studied in the Potomac River. The focus of this project was to use ^{210}Pb geochronology to analyze core samples in order to close this gap in understanding. We proposed to do this by calculating the rates of sediment accumulation within the lower Potomac River (area delineated in Figure 3) and determining the influence they had on nitrogen concentrations within those sediments. Two distinct depositional patterns were of interest: steady-state accumulation and event-layer deposition. The hypotheses for this project were formed from consideration of the SML. As is discussed by Wheatcroft and Drake (2003), sediment passing through the SML is subject to various processes leading to its disturbance, and potential re-suspension within the water column. Due to this increased potential for re-suspension, steady-state accumulation would lead to less burial of nitrogen than event-layer deposition, in which case sedimentation events would accelerate the rate at which sediment passed through the SML. It was hypothesized that samples collected from areas of steady-state accumulation would yield lower nitrogen concentrations than those from areas of prevalent event-layer deposition.

Methods

Study Area

The Potomac River can be divided up into different portions (Figure 3). First, there is the upper reach of the river extending into Maryland, Virginia, and West Virginia, ending near the Washington, D.C. and Montgomery county line (Knebel et al., 1981). The lower (a.k.a. “tidal”) region is generally characterized as beginning around the Little Falls region of the river near the fall line, and then transitioning into the estuarine Potomac near the mouth at Point Lookout, MD.

Studies of sedimentation rates in the Chesapeake Bay have been made using various methods, including ^{210}Pb dating (Knebel et al., 1981; Officer and Lynch, 1984) and pollen geochronology (Brush et al., 1982). A summary of estimates can be found in Officer and Lynch (1984) as well as in Cronin et al. (2003), with rates ranging from ~0.16 cm yr^{-1} at the mouth to

~1.5 to 1.8 cm yr^{-1} towards the beginning of the tidal region and the upper estuaries. A study of the tidal Potomac by Smith et al. (2003) estimated that nearly 67% of sediment influx comes from the upper reaches of the river, 25% from erosion processes along the shore, with the remaining sediment being delivered by tributaries below the fall line near Little Falls.

Field Methods

Eight core samples were collected during a research cruise aboard the R/V Rachel Carson from May 9 – 10, 2012, using a shallow-water piston corer. Cores were typically ~90 cm in length. The core locations are indicated in Figure 4. Following collection the samples were immediately sectioned into 1- and 2-cm increments, and then were stored and refrigerated at Horn Point Laboratory (HPL) in Cambridge, MD until further analysis was performed.

Laboratory Methods

Sedimentation rates within the core samples were analyzed using ^{210}Pb activity analysis, following the same procedure as utilized in Palinkas and Nittrouer (2007) using alpha spectroscopy. We performed an acid digestion of the collected sediment using HCl and HNO_3, then soaked silver planchets in the digestion solution for ~24 hours, allowing for the ^{210}Pb to bind to the silver. These planchets were then placed within the alpha spectrometer and counted for ~24 hours. After the counting was completed, the activities were compiled to create profiles over depth within each core, which were then analyzed to calculate the sediment accumulation rates corresponding to each core.

A SediGraph III machine was used to analyze the grain-size distribution of 32 of the 72 samples (technique summarized in Coakley and Syvitski (1991)) to help interpret data collected from activity counts. The samples were first wet-sieved at 64 μm in order to remove potential biota or detritus, as well as separate muddy and sandy sediment. The mud sediment was then dispersed in sodium metaphosphate and sat in an ultrasonic bath before it was analyzed using the SediGraph III. Midway through the analyses, the SediGraph machine began to malfunction. The remaining samples were then analyzed using standard pipette procedures (Folk, 1974). The pipette method required the collection of subsamples, via pipette, that represent a proportion of the sample representative of certain Φ values. Each subsample was collected in a pan, dried, and massed. The median grain size can be determined by fitting a linear regression line to data points above and below 50% of the masses of the collected subsamples.

Subsamples were sent to Analytical Services at HPL where nitrogen concentrations were measured using a CHN analyzer following a procedure described in Cornwell et al. (1996). For all analyses, choosing samples <10 cm deep in cores minimizes potential error due to physical mixing or bioturbation, as well as seasonal variability of nitrogen concentrations in the near-surface water column (Mullenbach and Nittrouer, 2000).

Results

The results from the analyses for each core can be seen in Figures 5A-H (cores have been listed in order of decreasing proximity to the mouth of the Potomac River). It is important to note that although an effort was made to avoid the SML when choosing samples for analysis (by beginning collection at a depth of 10 cm), there are still some cases where mixing may have occurred at depths >10 cm. It should also be noted that there was not sufficient time to complete counting ^{210}Pb activity within all of the cores, and because of this cores POTN6, POTN12, and POTN22 were not analyzed for ^{210}Pb activity levels or accumulation rate.

^{210}Pb activity

The objective of analyzing the amount of ^{210}Pb in the sediments was to determine the patterns of accumulation in various locations along the Potomac River. Some of the cores, specifically POTN2 and POTN19, exhibited clear patterns of steady-state deposition. It is evident that the layer of decay has begun at ≤10 cm down into these cores. There is some slight variation further down within POTN2, but these 'jumps' are centered around what can be identified as the background layer. The background layer was not reached for POTN19, as the ^{210}Pb activity is still decreasing up to the greatest depth that was collected, however there is considerable consistency to the rate of decay, further suggesting steady-state sediment accumulation. There were other cores, however that did not exhibit a distinct pattern. An example is core POTN4 (Figure 5B), where ^{210}Pb activities appear to 'jump' from higher to lower levels, but doing so with some consistent levels in between. This could be due to different event layers being deposited over time, but further comparison with its' respective median grain-size profile would be necessary. There is one clear example of event-layer deposition that is found by examining the activity profile of POTN30 (Figure 5H). The rate of accumulation was calculated for cores that were analyzed for ^{210}Pb activity. The results of these calculations can be seen in full in Table 1. It was strange to see that these values were lower than what has been measured in previous studies included ranges of >10mm yr^{-1} - >47mm yr^{-1} to 21mm->114mm as well as 7.5 mm yr $^{-1}$ – 50.83 mm yr^{-1} in the most recent study (Brush et al., 1982; Cronin et al., 2003; Knebel et al., 1981). Though the actual values may differ, there is still a similar trend in decreasing accumulation rates towards the mouth of the river (Cronin et al., 2003).

Median Grain Size

Plotting the median grain size of a core at different depths allows not only for comparison with ^{210}Pb activity profiles, but it also can provide an idea of the physical forces within an area. For example, a larger median grain size indicates that stronger forces were at work, of which only the larger particles were able to settle out and become deposited since smaller particles are much more easily entrained. A smaller median grain size, conversely, indicates that those same stronger forces were not present, which allowed for smaller sediment to settle out in much greater proportion to the larger sediment. Perhaps more important than the actual values of the median grain size of the cores, though were the ranges of values over a depth profile, due to the indication of depositional patterns. One could infer that a consistent median grain size over the depth of a core (such as POTN2 in Figure 5A) would indicate that forces leading to the accumulation of sediment were unchanging, thus indicating a steady-state depositional pattern, while varying median grain sizes (as can be seen for POTN30 in Figure 5H) would indicate the occurrence of event-layer deposition. As was mentioned, the technique employed for analyzing the median grain size of each sample changed when ~50% of the samples had been analyzed due to technical malfunctions experienced by the SediGraph. It was found that in some cases, although consistent median grain size values were calculated for a core, they would vary between SediGraph and standard pipette results. An example of this can be seen in Figure 5D, in which the lower values, though within a small range of each other, differ considerably from values obtained using the SediGraph. These variations were taken into account when analyzing the median grain size data, considering that even though values were different, consistencies still remained.

Nitrogen Concentration

The nitrogen concentrations at different depths within each sample were a relatively unknown factor during the beginning stages of this project. Levels were measured, and then trends were analyzed based on data obtained from the ^{210}Pb activity and median grain size analyses. It seemed that there were equal numbers of cores that exhibited either consistent or varying concentrations at different depths (Figures 5A-H). Although the changes in concentration were small (>0.01% at times), considering that the total nitrogen concentration levels within each sample were small, these changes can have significant implications as to the effect of sediment accumulation on nutrient burial.

Discussion

There are two clear patterns of sediment accumulation: steady-state and non-steady-state. The latter could be further divided into event-layer deposition and transitional deposition.

Steady-state

There were three cores that exhibited data trends characteristic of steady-state accumulation: POTN2, POTN12, and POTN19 (Figures 5A, 5E, and 5F, respectively). In POTN2, both a layer of decreasing activity as well as a background layer are easily identifiable, with the background layer beginning at a depth of ~40 cm. There are no easily identifiable event-layers within the core, as the rapid changes in activity at greater depth are not substantial enough to be attributed to sedimentation events. The grain size distribution varies somewhat moving down the core, but there is a fairly consistent presence of data (disregarding any seemingly spurious points) at ~35 ɥm. It appears that the depositional pattern influenced the nitrogen burial within the core, as the total N concentrations remain consistent at greater depth. It is possible that the change in concentration near the surface was due to surface mixing. Similar patterns were exhibited by the data from POTN19. The activity profile displayed a smooth zone of decay that may extend deeper, as it was not evident that the background layer was reached with the analyzed samples. The nitrogen concentration decreases slightly moving down the core, but not significantly enough to cause serious speculation of any other depositional patterns. Although there was not sufficient time to calculate the activity rate of POTN12, it could be inferred from both the median grain size and nitrogen concentration profiles that this area also experienced patterns of steady-state accumulation, with a well-contained range of median grain sizes and nitrogen concentrations. These steady depositional patterns could be attributed to each core's proximity to the mouth of the Potomac River. Assuming there is greater water depth found near the mouth of the Potomac River, this would allow for less variable conditions than would be found in shallower waters (due to isolation from wave and tidal forces found near the surface). It could be argued that POTN19 could not be considered of close proximity to the mouth of the Potomac River, but it is located in the center of the channel in a considerably wide segment. Further bathymetric studies would be needed to verify the accuracy of this statement, but it is certainly reasonable to believe that POTN19 was deep enough to be isolated from significant forces affecting rates of deposition on a short-term temporal scale.

Non-steady-state

There were another three cores that exhibited clear signs of non-steady-state accumulation: POTN4, POTN22, and POTN30 (Figures 5B, 5G, and 5H, respectively). This is

not to say, though, that significant event-layer deposition was present, simply that it does not exhibit characteristics of steady-state accumulation. The data obtained from POTN30 may be the best example of these differing patterns, as it exhibits a 210Pb activity profile that “spikes” in certain parts of the core. Two of these ‘spikes’ in activity are an area of decreasing activity at ~25 cm and an increase in activity at ~40 cm. It is reasonable to assume that these are event layers because of the return to a consistent trend line of activity found at other points in the core. These points seem to exhibit significant influence on the nitrogen concentration within the cores, where nitrogen had decreased with a decrease in activity (and therefore, accumulation) and then had increased with an increase in deposition. There is also a wide range of median grain sizes, as well as an intriguing nitrogen concentration profile (as was mentioned). When examined as a single set of data, the activity profile of POTN4 does not exhibit any signs that it is of non-steady-state in nature. However, examination of the corresponding nitrogen and grain size profiles implies that there was variation in depositional patterns over time. POTN22 was another core that could not be analyzed for ^{210}Pb activity due to time constraints, however one could infer (similar to what was done for POTN12) from both the median grain size and nitrogen concentration profiles, that a great deal of variation was occurring within the area. Proximity to the mouth of the river could also be considered for all of these cores, as both POTN30 and POTN22 were collected the furthest upriver. Although POTN4 is the second closest point to the river mouth, it is located considerably closer to the shoreline than POTN2 or POTN19, both of which exhibited steady-state accumulation. It would be interesting to observe what changes occurred in ^{210}Pb activity and nitrogen concentration if this sample had been collected further out in the channel. Another factor that could explain the variability in depositional patterns between samples collected either downriver or upriver is the Estuarine Turbidity Max (ETM). Studies of the Potomac River and Chesapeake Bay estuaries (Knebel et al., 1981; Cronin et al., 2003, respectively) have defined the ETM as a feature of large tributaries subject to tidal influence, where finer sediments become contained and subject to varying rates of re-suspension or re-deposition (Cronin et al., 2003). The location of the ETM could vary within a system due to a complex relationship between tidal forces, influx of freshwater, as well as gravitational forces within the water column (Cronin et al., 2003). This seasonal variation could be a major cause of sedimentation rates along the Potomac River.

Transitional

Two cores that were processed, POTN6 (Figure 5C) and POTN11 (Figure 5D), did not exhibit data patterns that were indicative of one definite trend. In POTN6, although the ^{210}Pb was not analyzed, the grain size profile and the nitrogen concentration profile differed in that one was extremely steady, while the other seemed to show a gradual decline. The activity profile would help portray a more complete picture of what the local depositional pattern. Data gathered from POTN 11 are inconclusive as well, as the activity profile seems to portray steady-state accumulation, yet there is a potential event-layer “spike” in what would appear to be the background layer. In addition to this, there is a relatively stable nitrogen concentration profile (perhaps even increasing with depth), as well as an unchanging grain size distribution. One could argue that this trend supports what was originally hypothesized, that is, steady-state leads to decreased nitrogen burial. Due to the minority of this trend from the collected data, however, it appears that this may be an anomaly of sorts. Furthermore, this anomaly does not correctly model the relationship between depositional pattern and nitrogen burial.

Future Implications

The initial hypotheses are not supported due to the apparent connection between steady-state accumulation and consistent nitrogen concentrations within those steadily

accumulating sediments. However, although it was clear that varying activity rates over time lead to varying concentrations at depths within the cores, it could not be determined at this point as to what extent nitrogen burial was affected. This could be a point of interest in future studies on this topic. One can infer, then, that although mixing may occur in the surface layer, the nitrogen stays tightly bound to the sediment particles and thus is buried as the sediment is (Jaeger et al., 1998; Wheatcroft and Drake, 2003). This means that the depositional patterns do not have as great an influence on the amount of nitrogen buried through sedimentation as was predicted, however the results are still inconclusive. On a broader scale, it was found that depositional patterns varied regionally within the Potomac River, along with accumulation rates. Patterns closer to the head of the river exhibited non-steady state accumulation, with a steady transition to more steady-state patterns near the mouth of the river. This was supported by the trends observed from the depth profiles compiled for ^{210}Pb activity, median grain size, and nitrogen concentration. This is due, most likely, to the complex interaction of many biochemical processes such, as the Potomac River ETM, as well as the varying core locations within the river channel. To further test these claims, additional cores will need to be collected from sites close to the coring locations used for this project. Also, it would be beneficial to analyze samples from transects of cores taken across the channel of the Potomac River to determine the effect water depth (and proximity to shore) has on depositional patterns within the river.

Conclusions

Although there is indeed a relationship between the patterns of sediment accumulation and the rate of nitrogen burial, they did not follow the patterns proposed at the beginning of this project. In most samples, steady-state accumulation of sediment over time did not lead to decreased nitrogen burial, as was originally hypothesized. On a more regional scale, there seems to be an influence on the rate of sedimentation patterns (and therefore, nitrogen burial) in certain areas due to proximity to both the shoreline and the mouth of the river. Variation in accumulation rates along the river could explain the areas of non-steady-state depositional patterns. When there is more sediment being deposited, there is a greater opportunity for variations to be recorded within the depositional record, exhibiting depth profiles indicative of non-steady-state deposition. Ultimately, the relationship between sediment accumulation and nitrogen burial will be examined further. It would be ideal if more sediment cores were to be collected from different locations within the channel to determine if shoreline proximity (and therefore, water depth) had any significant impact on the processes that were studied in this project. To be sure, this project is only the beginning, but it was an important first step in what will hopefully lead to a more comprehensive understanding of marine processes within the Potomac River.

Acknowledgements

I would like to thank Dr. Cindy Palinkas, whose thoughtful help and guidance were greatly appreciated through this entire process. I would also like to thank the District of Columbia Water and Sewer Authority, who provided the funding for the all-encompassing project that I worked within the guidelines of. Finally, I want to thank Drs. Mike Allen and Fredrika Moser, as well as Maryland Sea Grant. Without making an investment in me through their generous grant, I would have missed out one of the best experiences of my life.

References

Appleby, P. G., and F. Oldfield. 1978. The calculation of lead-210 dates assuming a constant rate of supply of unsupported 210Pb to the sediment. CATENA 5:1-8.

Boynton, W., J. Garber, R. Summers, and W. Kemp. 1995. Inputs, transformations, and transport of nitrogen and phosphorus in Chesapeake Bay and selected tributaries: Estuaries and Coasts 18:285-314.

Brush, G.S., E.A. Martin, R.S. DeFries, and C.A. Rice. 1982. Comparisons of 210Pb and pollen methods for determining rates of estuarine sediment accumulation: Quaternary Research 18:196-217.

Canfield, D.E., A.N. Glazer, and P.G. Falkowski. 2010. The evolution and future of earth's nitrogen cycle. Science 330:192-196.

Coakley, J., and J. Syvitski. 1991. SediGraph technique: Principles, methods, and application of particle size analysis 129-142.

Cornwell, J.C., D.J. Conley, M. Owens, and J.C. Stevenson. 1996. A sediment chronology of the eutrophication of Chesapeake Bay: Estuaries 19:488-499.

Cornwell, J. C., W.M. Kemp, and T.M. Kana. 1999., Denitrification in coastal ecosystems: methods, environmental controls, and ecosystem level controls, a review. Aquatic Ecology 33:41-54.

Cronin, T., L. Sanford, M. Langland, D. Willard, and C. Saenger. 2003. Chapter 6. Estuarine sediment transport, deposition, and sedimentation. 03-4123.

Folk, R.L. 1974. The petrology of sedimentary rocks. Austin, TX: Hemphill Publishing Company.

Harris, L.A., W.R. Boynton, J. Cornwell, and C. Palinkas. 2012. Measurement of Sedimentation Rates and Nutrient Burial in the Potomac Estuary and Continued Support of Monthly Monitoring: Potomac River, Maryland, USA. District of Columbia Water and Sewer Authority.

Jaeger, J. M., C.A. Nittrouer, N.D. Scott, and J.D. Milliman. 1998. Sediment accumulation along a glacially impacted mountainous coastline: North-east Gulf of Alaska. Basin Research 10:155-173.

Knebel, H.J., E.A. Martin, J.L. Glenn, and S.W. Needell. 1981. Sedimentary framework of the Potomac River estuary, Maryland. Geological Society of America Bulletin 92:578-589.

Mason, R.P., E.H. Kim, and J. Cornwell. 2004. Metal accumulation in Baltimore Harbor: current and past inputs. Applied Geochemistry 19:1801-1825.

Mullenbach, B.L., and C.A. Nittrouer. 2000. Rapid deposition of fluvial sediment in the Eel Canyon, northern California. Continental Shelf Research 20:2191-2212.

Nittrouer, C.A., D.J. Demaster, B.A. McKee, N.H. Cutshall, and I.L. Larsen. 1984. The effect of sediment mixing on Pb-210 accumulation rates for the Washington continental shelf. Marine Geology 54:201-221.

Nittrouer, C.A., R.W. Sternberg, R. Carpenter, and J.T. Bennett. 1979. Use of Pb-210 geochronology as a sedimentological tool: application to the Washington continental shelf. Marine Geology 31: 297-316.

Officer, C.B., and D.R. Lynch. 1984. Nonlinear parameter estimation for sediment cores. Chemical Geology 44: 203-225.

Palinkas, C.M., and C.A. Nittrouer. 2007. Modern sediment accumulation on the Po shelf, Adriatic Sea. Continental Shelf Research 27:489-505.

Robbins, J.A. 1978. Geochemical and geophysical applications of radioactive lead isotopes, *in* Nriagu, J. O., ed., Biogeochemistry of Lead. Amsterdam: Elsevier.

Saxby, T., and K. Boicourt. 2010. USA MD: Potomac River. University of Maryland Center for Environmental Sciences - Integration and Application Network.

Smith, S., J. Herman, T. Cronin, G. Schwarz, M. Langland, K. Patison, and L. Linker. 2003. Integrated approaches to sediment studies 03-4123.

Wheatcroft, R.A., and D.E. Drake. 2003. Post-depositional alteration and preservation of sedimentary event layers on continental margins, I. The role of episodic sedimentation. Marine Geology 199:123-137.

Figures and Tables

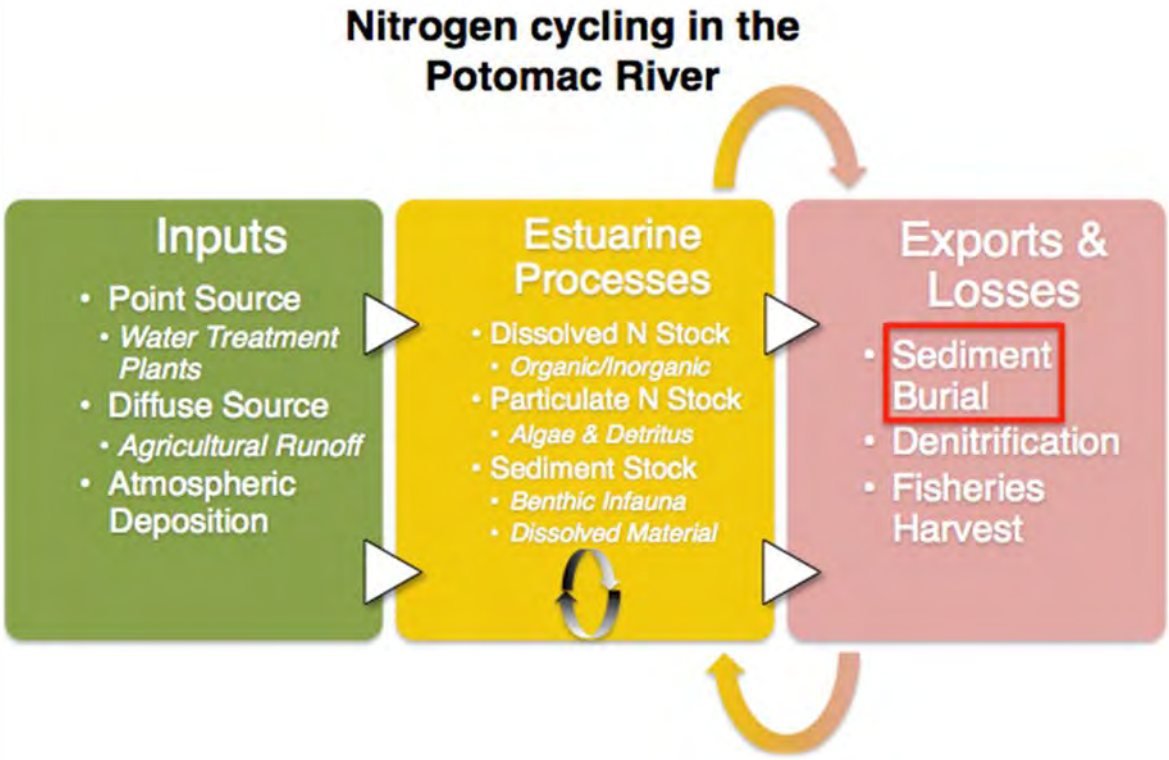

Figure 1: A diagram characterizing the nitrogen budget of the Potomac River. The focus of this study, sediment burial, has been indicated with a red box. Adapted from Harris et al. (2012).

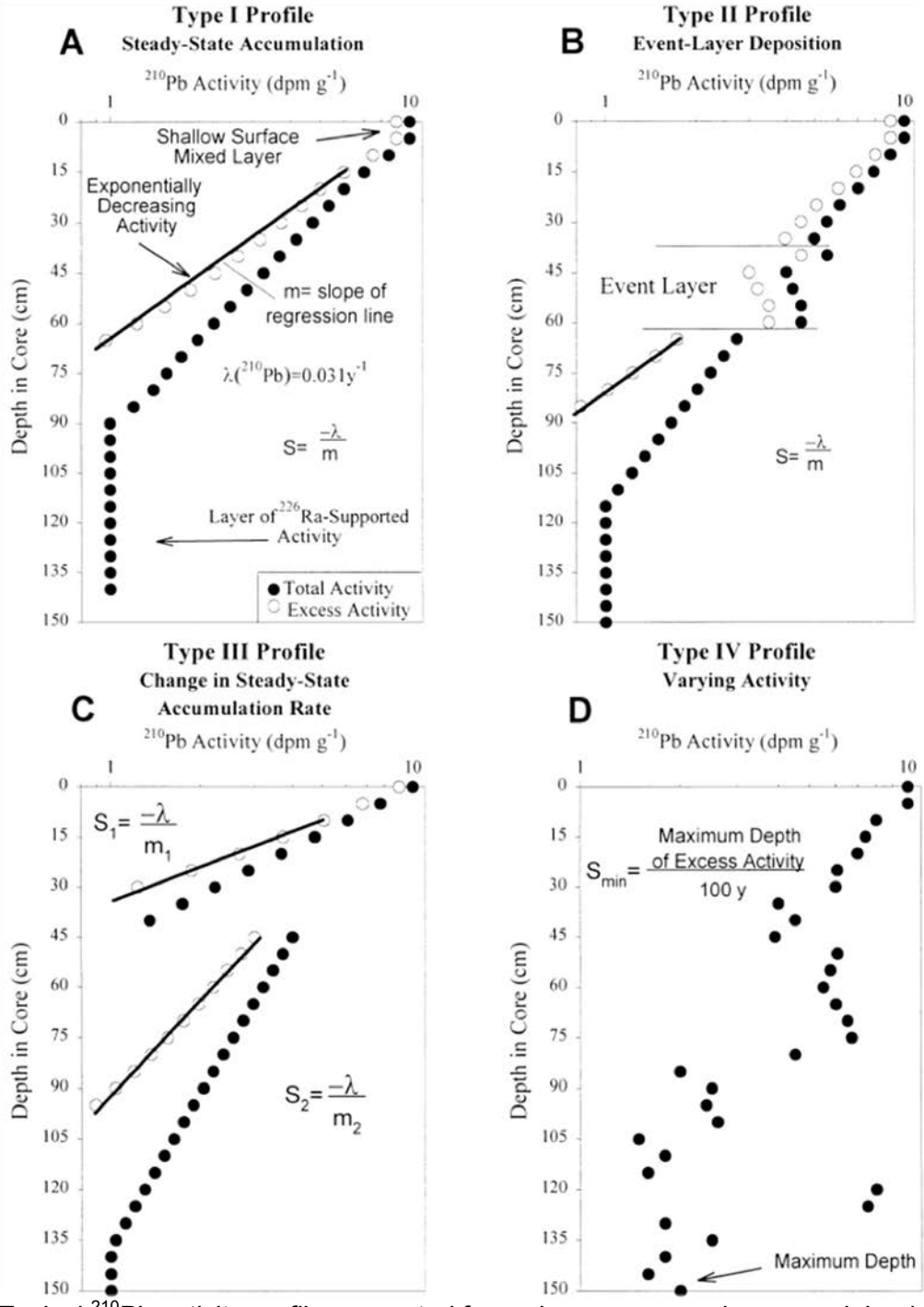

Figure 2: Typical ^{210}Pb activity profiles expected for various core samples as explained in Jaeger et al. (1998). (A) Steady-State: Note the steady slope of the regression line plotted from excess points in the layer of decreasing activity. (B) Even-Layer Deposition: The event layer can be seen as the activity increased due to an increased rate of accumulation. (C) Change in steady-state rate: one can clearly identify where the rate of accumulation within the core environment changed. Both rates can still be calculated using (5). (D) Varying ^{210}Pb Activity: Note the indicated maximum depth of activity ($x_{\max}$).

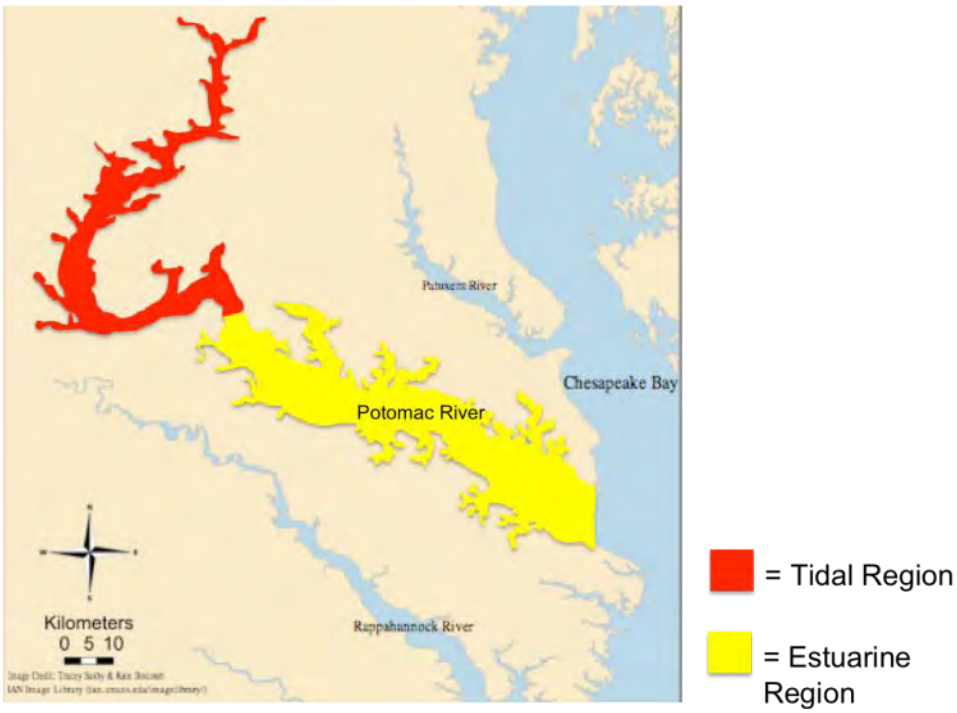

Figure 3: A map of the Potomac River, indicating both its tidal and estuarine regions. For this study, samples from both regions will be analyzed (Saxby and Boicourt, 2010).

Figure 4: Map of the samples collected aboard the R/V Rachel Carson on May 9th and 10th, 2012.

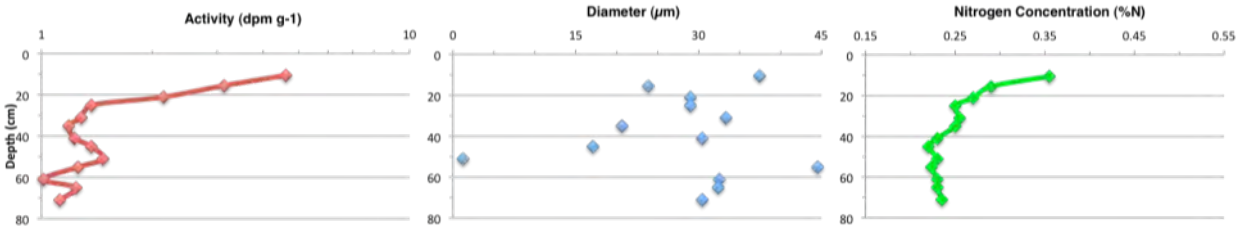

Figure 5A: POTN2 ^{210}Pb activity, median grain size, and nitrogen concentration at depth.

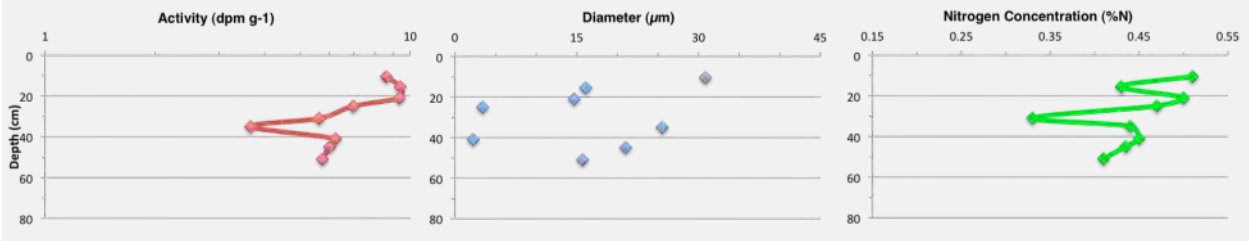

Figure 5B: POTN4 ^{210}Pb activity, median grain size, and nitrogen concentration at depth.

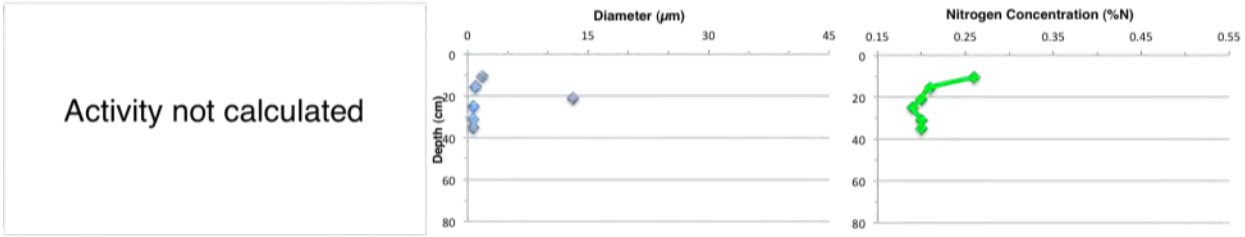

Figure 5C: POTN6 median grain size, and nitrogen concentration at depth.

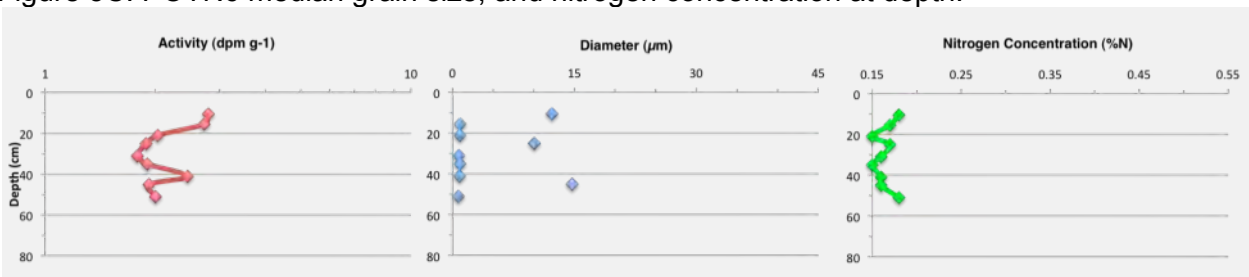

Figure 5: ^{210}Pb activity, median grain size, and nitrogen concentration at depth.

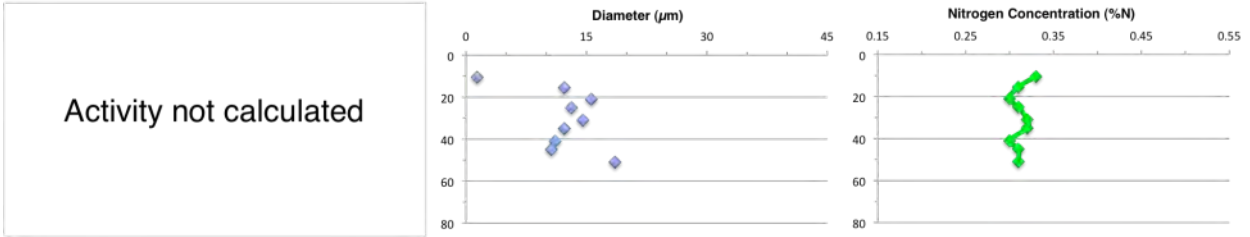

Figure 5E: POTN12 median grain size and nitrogen concentration at depth.

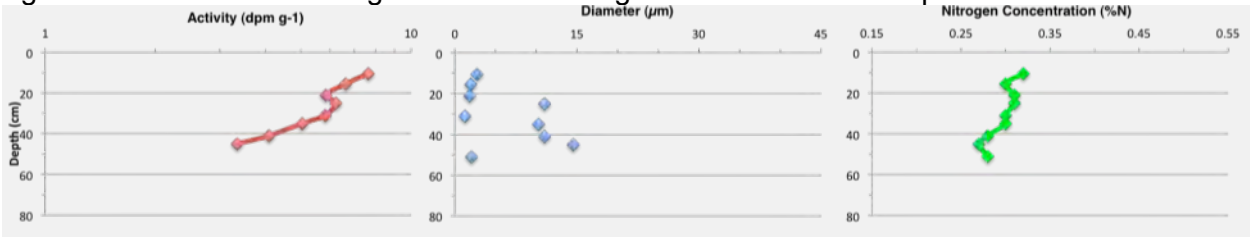

Figure 5F: POTN19 ^{210}Pb activity, median grain size, and nitrogen concentration at depth.

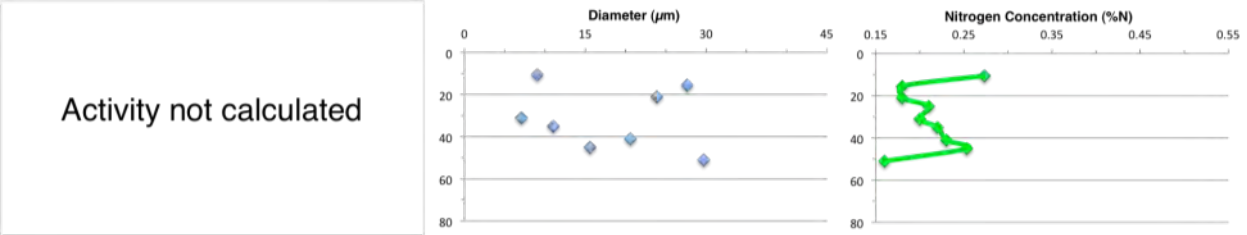

Figure 5G: POTN22 ^{210}Activity, median grain size, and nitrogen concentration at depth.

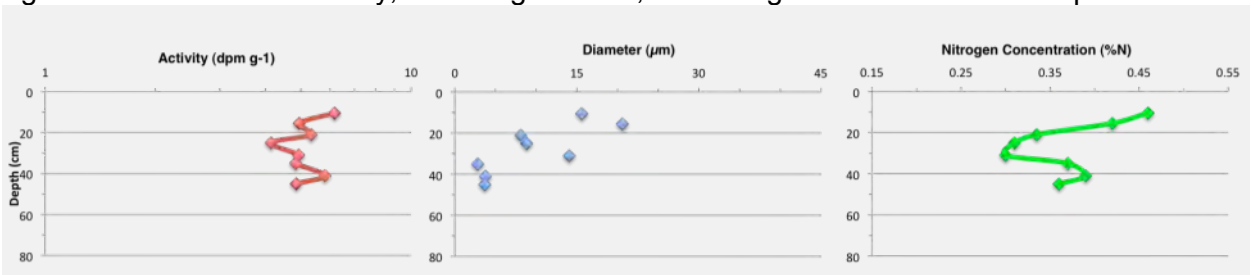

Figure 5H: POTN30 ^{210}Pb activity, median grain size, and nitrogen concentration at depth.

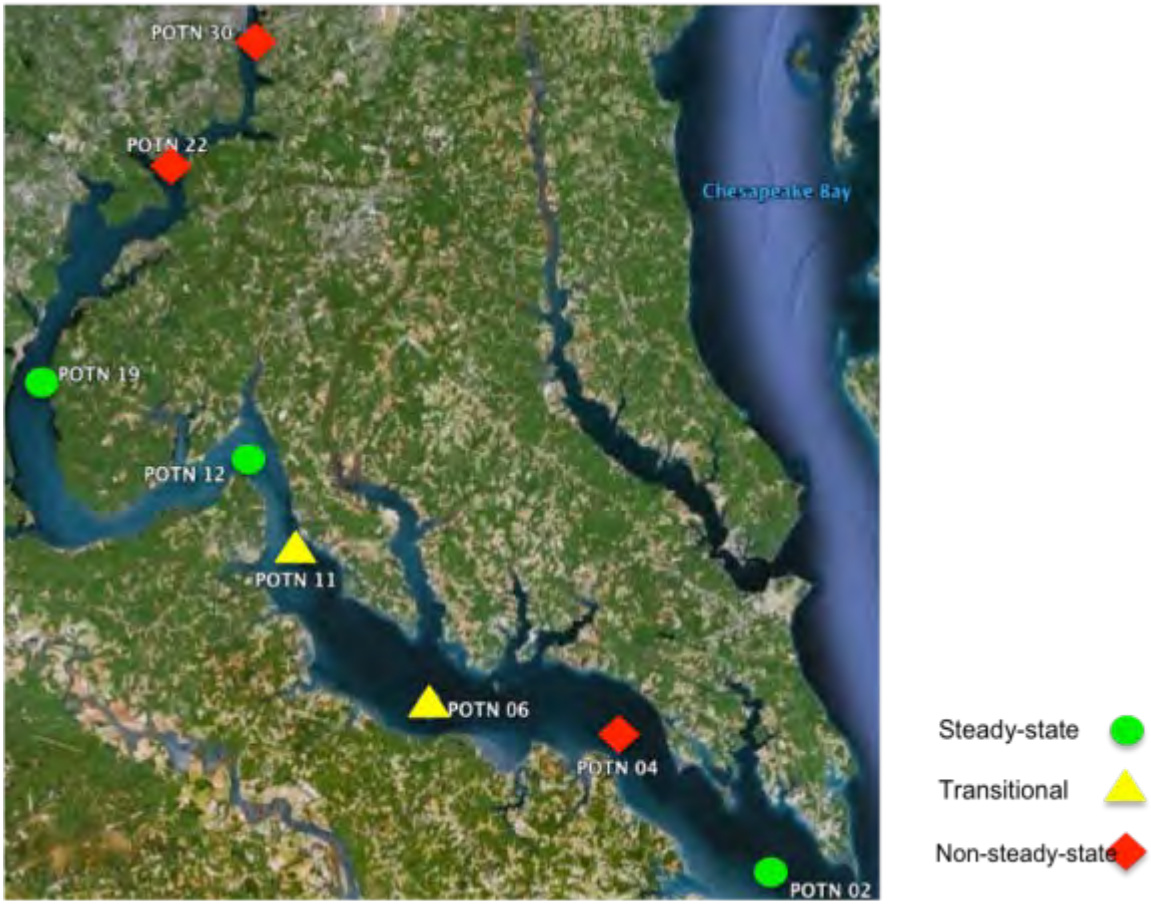

Figure 6: Depositional patterns determined for core sites.

Table 1: Calculated rates of accumulation, "S", from cores. Refer to introduction for technique.

Sample	S (mm yr^{-1})
POTN2	1.8
POTN4	1.6
POTN6	-
POTN11	3.3
POTN12	-
POTN19	8.8
POTN22	-
POTN30	≥ 5.0

(Blank)

Modeling Effects of Community History on Phytoplankton Diversity under Micro-Scale Physicochemical Variations

Michael Macon, REU Fellow
Maryland Sea Grant

Dr. Mike Stukel, Assistant Research Scientist
Horn Point Laboratory, University of Maryland Center for Environmental Science

Dr. Victoria Coles, Research Associate Professor
Horn Point Laboratory, University of Maryland Center for Environmental Science

Abstract

The paradox of plankton has remained an open question in oceanography since it was proposed by Hutchinson in 1961. This project explored the effects of two theories, contemporaneous disequilibrium and mixing of patchy plankton communities. A fully functioning, 3-dimensional physical model was paired with an 80 state model including 77 taxa of phytoplankton. Lagrangian particles, paired with a phytoplankton community, were run through the model under various levels of biological mixing to represent different levels of micro-scale patchiness. Surface plots and vertical profiles indicated that the model was effectively depicting real world conditions. Results showed that decreased levels of biological mixing restricted and reduced the biodiversity of a phytoplankton community. A phytoplankton community which was completely isolated and prevented from mixing yielded the lowest biodiversity among communities. This low biodiversity observed at reduced mixing rates indicates that greater biodiversity is not supported by community history during micro variations in physical and chemical properties. The increased biodiversity at moderate to high mixing indicates that mixing between patchy or semi-isolated communities increases the biodiversity of each community.

Keywords: Plankton, Diversity, Patchiness, Model

Introduction

The diversity-stability hypothesis states that the more diverse a community is then the more stable and resistant to change it will be. As this theory is still debated among scientists, there have been numerous studies that support the claim (Lehman and Tilman, 2000; Tilman, 1996) and refute it (Goodman, 1975). In particular, Worm et al. (2006) described the impacts of loss in biodiversity on a marine ecosystem. A decrease in biodiversity resulted in poor water quality, stability and recovery potential for the community. However, by restoring biodiversity to the system, production increased extensively while reducing the variability by 21% on average. Worm et al. (2006) concluded that a loss in marine biodiversity would ultimately lead to loss in overall food production, water quality and recovery rates for the system.

The biodiversity of a system, whether terrestrial or marine, depends on both the species richness of the system and the evenness in which the individuals are distributed between the existing species. The species richness is defined simply as the number of species present in the system where evenness is a measure of how evenly dispersed the individuals are among the present species. The greater the species richness and the more evenly the individuals are spread between them, the greater the biodiversity of the region. However, it is not a simple task to accurately measure the biodiversity of a specific region. Not only is it difficult to sample all of the existing species (Smith et al., 2005), but there are several methods for calculating biodiversity. The effectiveness of each method depends on the size of the populations and the ability to account for every individual of the system (Pielou, 1966). For the purpose of this study, the Shannon index will be used. The Shannon index accounts for both the abundance and evenness of species present and is calculated as

$$H' = -\sum_{i=1}^{R} p_i \ln p_i, \quad (1)$$

where H' is the Shannon Index, R is the species richness and p_i is the proportion of the total biomass represented by species i.

The high diversity of phytoplankton found in the open ocean under the presence of finite limiting nutrients has come to be known as the "Plankton Paradox" (Hutchinson, 1961). This paradox arose after Hardin (1960) introduced the exclusion principle, which was later concluded that species richness is limited by the number of limiting resources of the system (Armstrong and McGehee, 1980). Given limiting resources such as nitrogen and phosphorous, as well as light and a variety of other trace elements, one would expect to see a relatively low number of species according to the exclusion principle. However, we continue to observe exceedingly high species richness, as high as 85 species within some communities (Jeppesen et al., 2000). Many theories have been proposed for the existence of such a large number of species, such as selective grazing via zooplankton (Cyr and Curtis, 1999), nutrient pulses (Sommer, 1984), patchiness of plankton due to relatively slow mixing (Richerson et al., 1970) and the frequency of physical disturbances (Abele, 1976).

The goal of this study is to test 2 theories. The first theory is of contemporaneous disequilibrium, which states that a plankton community which experiences relatively low mixing will support its diversity via variations in its water properties. Simply, the conditions are changing so frequently that a dominant phytoplankton can't arise. The second theory is micro-scale patchiness, which states that plankton exists in isolated communities and mixing between these communities promotes greater biodiversity. A range of water parcel turnover rates with respect to mixing (time taken for the entire plankton community to mix with its surrounding) will be investigated within an 80 state model including 77 taxa of phytoplankton. A fully functioning, 3-dimensional physical model with a domain in the tropical North Atlantic Ocean will be used in the investigation. We will attempt to investigate two hypotheses. The first hypothesis is that decreased mixing will allow an isolated community to undergo micro variations in physicochemical properties within the water column and allow the community history to drive the biodiversity, resulting in a greater biodiversity. Our second is that moderate levels of mixing of patchy phytoplankton communities will yield a greater biodiversity within the community.

Materials and Methods

The physical model is a fully functioning, 3-dimensional model. The model was run at a resolution of 2^o of latitude by 2^o of longitude. Each grid region contained 28 distinct vertical layers within it. The forcing functions (wind, temp, etc.) of the model were based upon a 20 year data collection of climate data. These forcing functions changed every 6 hours in the model.

The biological model was based on the concept of a simple NPZ model. Our model was composed of 4 general compartments; nitrate (N), dissolved organic nitrogen (DON), detritus, and 77 phytoplankton taxa (Figure 1). Each phytoplankton was randomly assigned a light growth parameter (I_o) and nitrate half saturation constant (K_s) on a log scale. Due to the exponential decay of light through the water column, a log scale is necessary to insure plankton will be present at low light regions. There was a light inhibition factor (I_{in}) which was calculated by

$$I_{in} = {I_o}^2. \tag{2}$$

This prevents low light adapted plankton from thriving in high light, surface waters. The maximum growth rate (μ_{max}) of phytoplankton was found by

$$\mu_{max} = 0.5 + 3 \times \tanh K_s. \tag{3}$$

All phytoplankton experienced an identical grazing pressure, implying there is no selective grazing performed via zooplankton. By including the light present (I) and the concentration of nitrate (N), along with universal grazing pressure (G_{max}), the realized growth rate for each phytoplankton species (dp/dt) is calculated by :

$$\frac{dP}{dt} = \mu_{max}\left(\frac{N}{N+K_s}\right)\left(1 - e^{-I/I_o}\right)\left(e^{-I/I_{in}}\right) - G_{max} \times P_i\left(\frac{P_{tot}}{K_z+P_{tot}}\right) \tag{4}$$

where P_i is the biomass of phytoplankton species i, P_{tot} is the total biomass of phytoplankton and K_z is a grazing coefficient. There was a total of 10 uniquely random initialized plankton communities.

The species richness of a community is described as the number of species that are present at a given time. The biological model is designed on the idea that everything is everywhere, meaning that the concentration for any species will never reach zero, but stay at very low levels. Therefore, to measure species richness, a species was noted as present if its biomass was greater than a threshold. If

$$P_i \geq {P_{tot}}/{1000}, \tag{5}$$

then species i was included in the species richness count. If the biomass was not above this thresh hold, the species was ignored for the purpose of species richness as well as biodiversity.

This biological model was run within the Eulerian 3-dimensional physical model. Thus, in every compartment of our physical model, there is a biological component as well. Biological variables were advected and diffused from grid cell to grid cell with water and physical state variables (salinity and temperature).

To test the effects of micro scale patchiness and community history on plankton communities, Lagrangian particles were used. These particles acted as tracers within the model, following the path of water and recording its location and water quality over a 180 day period. Particles were initialized within the model at randomized location, depth and time. This prevented two particles from being replicates of each other. Initially, these particles simply float through the model, sampling the water for water quality and the composition of the plankton community present. This approach sampled the biology, chemistry, and physics within the Eulerian framework of the model. To test various levels of mixing, a unique plankton community was maintained within the Lagrangian particle. Initially, this community was set equal to the community sampled by the Lagrangian particle at the time that the Lagrangian particle was

released. The biological model was then run on these sequestered communities with various levels of mixing with the Eulerian model. The community maintained within the Lagrangian particle is mixed with the Eulerian model prior to the running of the biological model. The rate at which these communities were mixed will be referred to as the Biological Mixing Rate (BMR) and include 100%, 50%, 25%, 10%, 5%, 1% and 0% (or complete isolation). To model the completely isolated community, there will be no mixing of the community (BMR = 0%). Each of the 10 uniquely random initialized plankton communities will be tested under the various biological mixing rates.

At the end of the 180 day run period, the biodiversity index for each float was calculated with the Shannon Index. The biodiversity indices from each BMR were grouped and the BMRs were compared via ANOVA tests to determine any significant change in biodiversity from different levels of biological mixing.

Results

Surface plots of average biodiversity from the Eulerian model (Figure 2) and nitrate (Figure 3) indicate that the lowest biodiversity regions occur in areas of high nitrate. These regions are located along the equator and around 15^{o}N along the west coast of Africa. Likewise, surface plots for species richness (Figure 4) indicate that the lowest species richness was approximately 10 and also in regions of high nitrate. The surface waters ranged in biodiversity from 1.4 to 2.7 on the Shannon index. Species richness reached a maximum of 40 species with a minimum of 10 species.

A vertical profile along a transect at 20^{o}W (Figure 5) reveals that maximum biodiversity is found at depth, reaching up to an index of greater than 2.6 at depth around 25^{o}N. There is a relatively low biodiversity observed through the entire water column between 10^{o}N and 20^{o}N. At the equator, there is a local maximum in biodiversity observed from the surface down to approximately 100m. At the bottom of the vertical profile, biodiversity drops to less than 0.6.

The mean biodiversity index ranged from 2.314 experienced at a BMR of 100% to 1.104 experienced at a BMR of 0% (Table 1). The biodiversity visibly increases with the biological mixing rate in a logarithmic relationship (Figure 6). There was no significant evidence ($P > 0.7$, $\alpha = 0.05$) to support that the biodiversities under the mixing rates of 5%, 10%, 25%, 50% and 100% were statistically different (Table 2). However, there was significant evidence ($P < 0.05$, $\alpha = 0.05$) to support that the biodiversity experienced under a BMR of 0% and 1% were significant different from each other and all other BMR values, with 0% BMR yielding the lowest biodiversity and 1% BMR being in between the 0% and the remaining BMR values. Reduced biodiversity at low mixing rates of 1% and 0% indicate that an isolated community, experiencing micro variations in physicochemical properties, yields a reduced biodiversity than a community that is not isolated. The increase in biodiversity with increased mixing indicates that mixing of phytoplankton communities yields an increased biodiversity.

Discussion

Biodiversity in both surface waters and throughout the water column was found North West of Africa, around 25^{o}N to 30^{o}N and 20^{o}W. Within the model, the phytoplankton communities are relaxed in this region as water flows into the region from the North Atlantic. This means that the phytoplankton enter the region at relatively equal concentrations, yielding close to the maximum biodiversity possible.

A biodiversity of 1.104 to 2.314 out of a potential 4.344 for 77 species would indicate that the plankton community was dominated by a select few species. This is not surprising if we look at how our model was set up. Given any depth range and levels of nitrate, we would expect to see a limited number of phytoplankton that are best adapted for those conditions.

In regions of high upwelling, such as the Guinea Dome of the west coast of Africa, there is reduced biodiversity throughout the water column. Upwelling brings high levels of nitrate to surface waters, where high light is present. With the development of phytoplankton species, there should be a limited number of plankton that will thrive and out compete the other phytoplankton. A plankton community which is dominated by limited species will yield a low diversity. These patterns have been observed in the open ocean (Suzuki et al., 2001) and confirm that our model is acting relatively realistically.

With the isolated community and 1% BMR yielding the lowest biodiversity, there is significant evidence to reject our first hypothesis that an isolated community will sustain a greater biodiversity via the contemporaneous disequilibrium theorem. We assume that this relationship may be due to lack of vertical motion and exposure to significant variations in physical and chemical properties. Further studies are needed to confirm the effects of contemporaneous disequilibrium. Conversely, the greater diversity with increased rates of mixing supports the theory of micro-scale patchiness. An isolated community exposed to mixing with its surroundings yielded a significantly greater biodiversity than with reduced or no mixing.

Conclusions

The spatial pattern of biodiversity and regions of upwelling indicate that the biological model is working and depicts the open ocean at a substantial level. There was significant evidence to reject our first hypothesis that isolated communities of phytoplankton retain high biodiversity through variations in physical and chemical properties. However, our second hypothesis was supported. The biodiversity of semi-isolated plankton communities exposed to moderate to high levels of mixing yielded a greater biodiversity than low mixing. Therefore, there is significant evidence to say that mixing of patchy plankton communities increases the biodiversity. It is possible to better represent biodiversity in numerical models by better representing the mixing that occurs between phytoplankton patches.

References

Armstrong, R.A., and R.McGehee. 1980. Competitive exclusion. The American Naturalist 115:151-170.

Franks, P.J.S. 2002. NPZ models of plankton dynamics: Their construction, coupling to physics, and application. Journal of Oceanography 58:379-387.

Franks, P.J.S., and C. Chen. 1996. Plankton production in tidal fronts: A model of Georges Bank in summer. Journal of Marine Research 54:631-651.

Goodman, D. 1975. The theory of diversity-stability relationships in ecology. The Quarterly Review of Biology 50:237-266.

Hardin, G. 1960. The competitive exclusion principle. Science 131:1292-1297.

Hutchinson, G.E. The paradox of the plankton. The American Naturalist 95:137-145.

Jeppesen, E., J.P. Jensen, M. Sondergaard, T. Lauridsen and F. Landkildehus. 2000. Trophic structure, species richness and biodiversity in Danish lakes: changes along a phosphorus gradient. Freshwater Biology 45:201-218.

Lehman, C.L., and D. Tilman. 2000. Biodiversity, stability, and productivity in competitive communities. The American Naturalist 156:534-552.

Richerson, P., R. Armstrong, and C.R. Goldman. 1970. Contemporaneous disequilibrium, a new hypothesis to explain the paradox of the plankton. Proceedings of the National Academy of Sciences 67:1710-1714.

Smith, V., B.L. Foster, J.P. Grover, R.D. Holt, M.A. Leibold, and F. deNoyelles Jr. 2005. Phytoplankton species richness scales consistently from laboratory microcosms to the world's oceans. Proceedings of the National Academy of Sciences 102:4394-4396.

Sommer, U. 1984. The paradox of the plankton: Fluctuations of phosphorous availability maintain diversity of phytoplankton in flow-through cultures. Limnology and Oceanography 29:633-636.

Suzuki, M.T., C.M. Preston, F.P. Chavez, and E.F. DeLong. 2001. Quantitative mapping of bacterioplankton populations in seawater: field tests across an upwelling plume in Monterey Bay. Aquatic Microbial Ecology 24:117-127.

Tilman, D.. 1996. Biodiversity: Population versus ecosystem stability. Ecology 77: 350-363.

Worm, B., E. B. Barbier, N. Beaumont, J.E. Duffy, B.S. Halpern, J.B.C. Jackson, H.K. Lotze, F. Micheli, S.R. Palumbi, E. Sala, K.A. Selkoe, J.J. Stachowicz, and R. Watson. 2006. Impacts of biodiversity loss on ocean ecosystem services. Science 314:787-790.

Figures and Tables

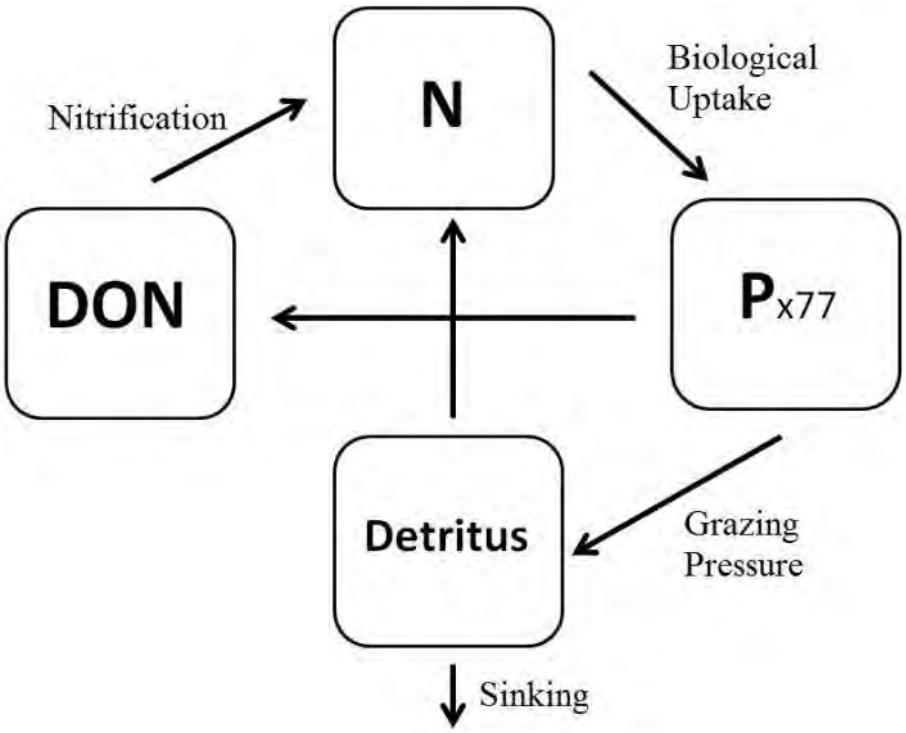

Figure 1. Diagram representing the compartments for the biological model. Arrows indicate direction that nutrients flow and some processes are identified alongside.

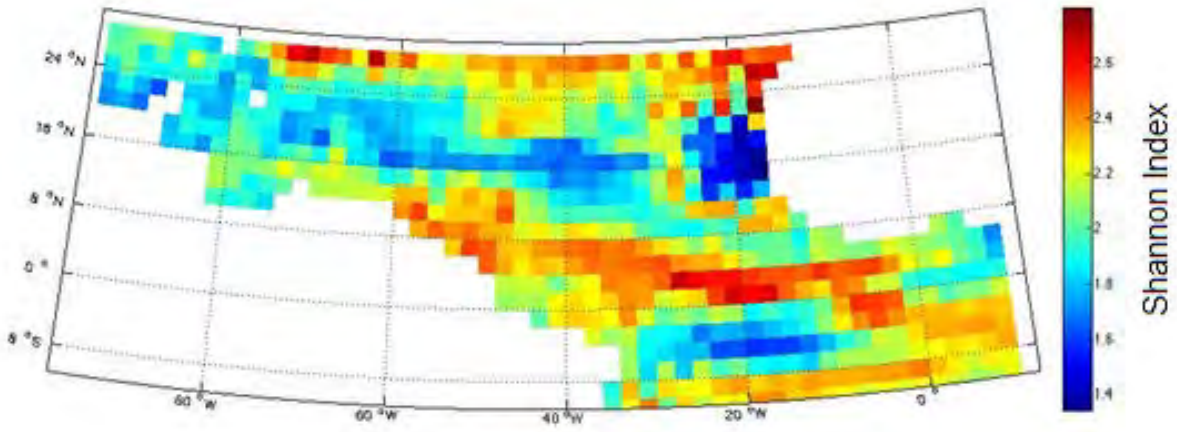

Figure 2. Surface plot of the average biodiversity using all 10 unique phytoplankton communities during the month of May, 1980. Lowest diversity is observed off the coast of Africa just west of the Sahara. White spaces are land masses.

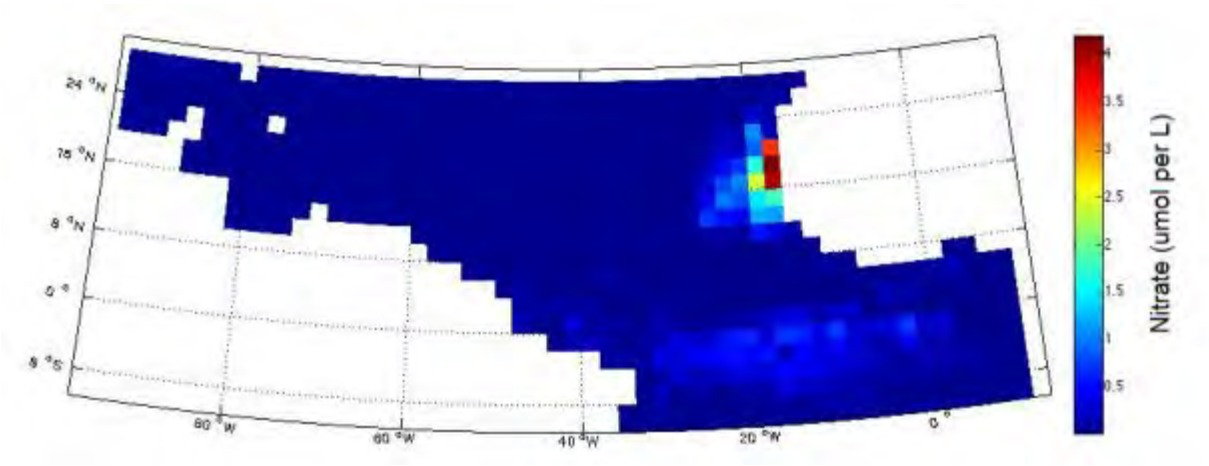

Figure 3. Surface plot of nitrate levels during the month of May, 1980. Large areas of upwelling along equatorial region and off the west coast of Africa.

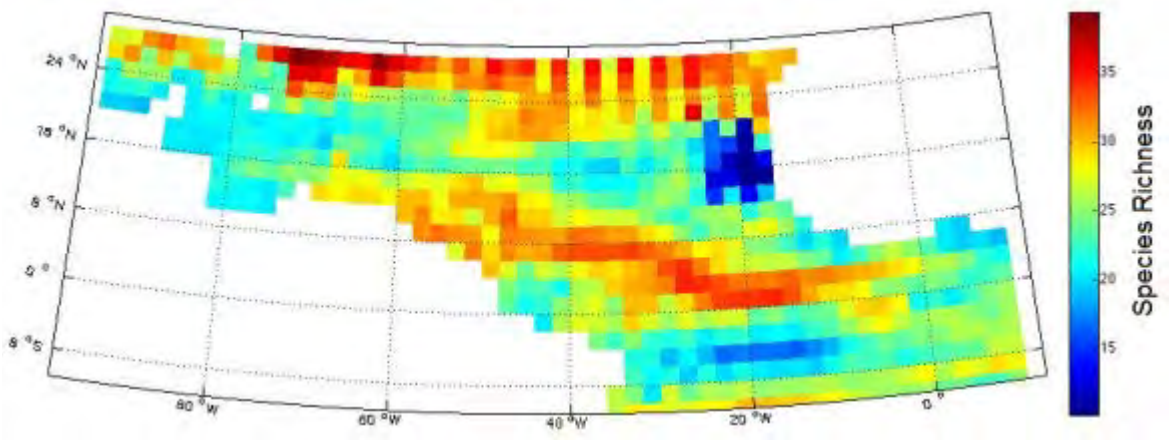

Figure 4. Surface plot of the average species richness during the month of May. Low species richness observed off the west coast of Africa and between 0° and 5°S latitude.

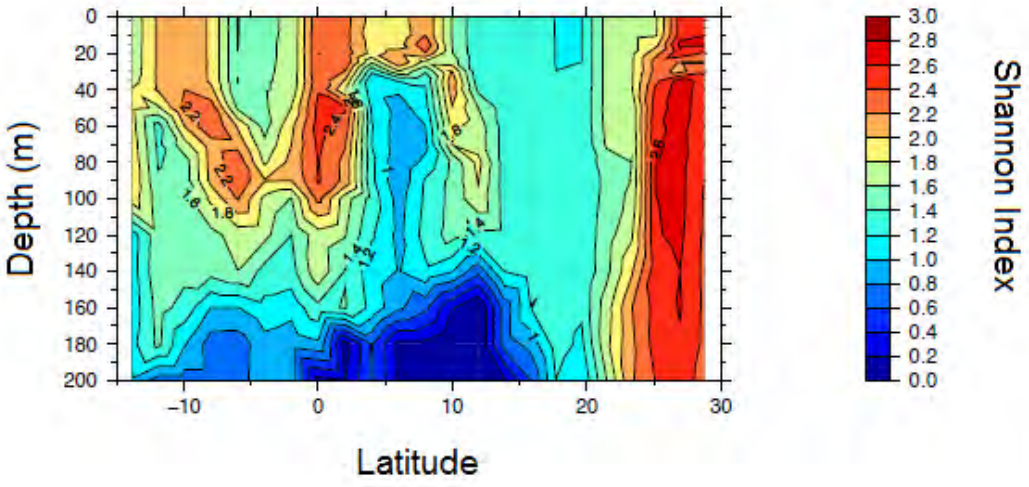

Figure 5. Vertical profile of the average biodiversity along a transect at 20°W.

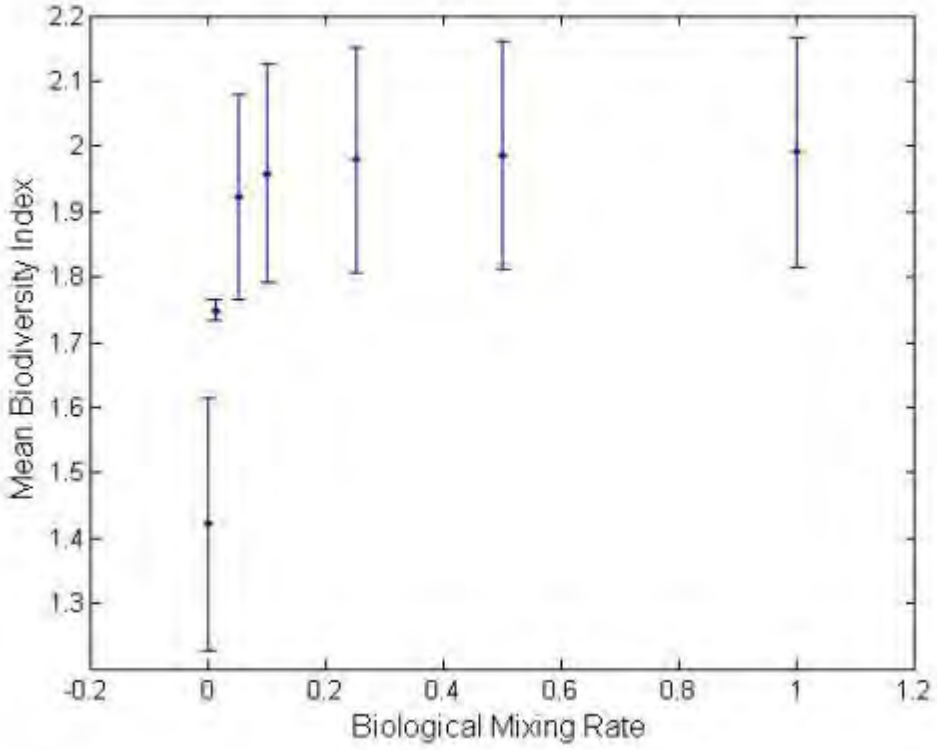

Figure 6. The mean Shannon Weaver Biodiversity Index obtained from 10 unique model runs and under assorted biological mixing rates (BMR). Standard deviations were constructed using the variance between the mean biodiversity experienced during each of the 10 runs.

Table 1. The mean Shannon Index for biodiversity of floats after 180 day run period under specific biological mixing rates. Each run has unique phytoplankton growth parameters and float initialization conditions, contributing to variations in biodiversity index between runs.

Run Number	1.00 BMR	0.50 BMR	0.25 BMR	0.10 BMR	0.05 BMR	0.01 BMR	0.00 BMR
60	1.737435514	1.734000238	1.724837067	1.696923	1.652889	1.440837	1.103999
61	1.940465706	1.929127179	1.918503063	1.885213	1.843463	1.716445	1.474107
62	2.313822576	2.301932888	2.289858701	2.241758	2.156402	1.863732	1.482977
63	1.990730526	1.990518826	1.988885312	1.981501	1.962409	1.837314	1.457771
64	2.108121023	2.10661814	2.102202421	2.089756	2.064615	1.910187	1.71721
65	1.985556984	1.982124689	1.982095082	1.973647	1.944481	1.778687	1.402479
66	1.977805157	1.974290497	1.962355406	1.932179	1.899224	1.752391	1.393556
67	2.126866044	2.123590822	2.116204322	2.100715	2.08259	1.969565	1.675539
68	2.010536077	2.001044077	1.991314708	1.958633	1.905668	1.647975	1.351395
69	1.716480511	1.716430172	1.717251694	1.721867	1.719827	1.576789	1.156029

Table 2. P-Values from ANOVA (α = 0.05) tests run between the Biological Mixing Rates (BMR) using the mean biodiversities found under 10 unique model runs. See Table 1 for exact biodiversity means.

	Isolated (0%)	1% BMR	5% BMR	10% BMR	25% BMR	50% BMR
100% BMR	1.04006E-07	0.00494299	0.37746677	0.77139337	0.8850678	0.95167276
50% BMR	2.05445E-06	0.00545667	0.40886329	0.71984595	0.93293117	
25% BMR	2.27025E-06	0.00480328	0.53628	0.78354456		
10% BMR	3.05632E-06	0.00886226	0.80341477			
5% BMR	5.18384E-08	0.00045785				
1% BMR	1.31152E-06					

Effects of Hypoxia on Copepod Predation by the Ctenophore, *Mnemiopsis leidyi*, in Chesapeake Bay

Carolina Méndez, REU Fellow
Maryland Sea Grant

Katherine W. Liu, PhD Student
Horn Point Laboratory, University of Maryland Center for Environmental Science

Dr. Jamie J. Pierson, Assistant Research Scientist
Horn Point Laboratory, University of Maryland Center for Environmental Science

Abstract

The seasonal occurrence of low dissolved oxygen (DO) in Chesapeake Bay, caused by excess of nutrients and vertical stratification, affects most of the main deep channel of the estuary. Gelatinous zooplankton, such as the ctenophore *Mnemiopsis leidyi*, can switch the energy transfer in the food web from fish to jellies because some species are more tolerant to low dissolved oxygen concentrations than their prey and competitors. However, few studies have observed predation rates under different dissolved oxygen concentrations. We examined the gut content of the lobate ctenophores, *M. leidyi* and *Beroe ovata*, collected at two sites in the Chesapeake Bay with distinct DO concentrations. In addition, we performed a clearance rate experiment on *M. leidyi* feeding on biane shrimp *Artemia salina*, under saturated oxygen concentration. Our results indicate that at moderate low DO levels ctenophores are preying more on copepods than higher and anoxic DO levels. Early feeding experiments with *A. salina* suggest high ingestion and clearance rates of ctenophores. Understanding how gelatinous zooplankton change the energy transfer under low dissolved oxygen levels will enhance management tools could allow for better management of fisheries in the bay.

Keywords: Clearance rate, Gut content, Low dissolved oxygen, Zooplankton, *Beroe ovata*

Introduction

Low dissolved oxygen (DO) directly affects organism performance and indirectly can change the distribution, abundance and trophic interactions of organisms (Breitburg et al. 2009). The Chesapeake Bay is the largest estuary in the USA and suffers from low DO concentrations (hypoxia, oxygen <2 mg l^{-1}), especially during the summer months (Hagy et al. 2004; Kemp et al. 2005) (Figure 1). Hypoxia occurs in the deeper middle portion of the bay with as much as 80% of water column affected (Hagy et al. 2004) and is caused by inputs of anthropogenic nutrients, or eutrophication, mainly from fertilizers. This causes enhanced productivity and subsequent respiration, which depletes oxygen in the estuary (Breitburg et al. 2009). In the middle of the bay, lower zooplankton biomass has been observed when hypoxic water is present (Figure 2). These hypoxic conditions not only decreased zooplankton densities but also

can decrease the vertical habitat available for copepods (Roman et al. 1993; Roman et al. 2005; Zhang et al. 2006).

Copepods are important in transferring primary production of phytoplankton to higher trophic levels (Kimmel and Roman 2004). In the Chesapeake Bay, *Acartia tonsa* is one of the most abundant copepod species (Figure 3b). *Acartia tonsa* is important in the estuary as both a dominant grazer of phytoplankton and a primary food resource for planktivourous fishes and gelatinous zooplankton (Jung and House 2004; Purcell and Decker 2005). Under laboratory observations, hypoxic water directly reduced the survival rate (Roman et al.1993, Stalder and Marcus 1997; Marcus et al. 2004; Richmond et al. 2006) and hatching success of copepod eggs (Roman et al. 1993; Marcus et al. 1994; Marcus et al. 1997; Richmond et al. 2006). Indirectly, hypoxic bottom water reduces vertical migration distance and diel shifts in vertical distribution of copepods (Roman et al. 1993; Keister et al. 2000; North and Houde 2004; Kimmel et al. 2009, 2010) affecting trophic levels interactions.

The distribution of copepods can affect the dynamics of coastal food web interactions (Richmond et al. 2006). For instance, gelatinous zooplankton may prey more on copepods than fish larvae under hypoxic water. The predatory ctenophore, *Mnemiopsis leidyi*, and scyphomedusan, *Chrysaora quinquecirrha*, are more tolerant of hypoxic water than fish (Breitburg et al. 1994: Purcell et al. 2001) and are found in greater abundance under low DO concentrations than fish (North and Houde 2004) (Figure 3a). Higher abundance of predators could rapidly deplete copepod densities under hypoxic conditions. This could alter the abundance of the bay anchovy, an important food resource for many economically and ecologically important fishes, because its primary food resource is copepods (Adamack 2007), especially during the summer months when hypoxia is more pronounced and abundance of gelatinous zooplankton increases.

The lobate ctenophore, *M. leidyi*, is native to the Atlantic estuaries in North and South America and the population can drastically increase in the spring and summer (Puercell et al. 2001). In general, ctenophores are voracious feeders preying on meso- and micro-zooplankton, fish eggs and fish larvae (Puercell et al. 2001). However, ctenophore abundance can be affected by the presence of the Atlantic sea nettle, *C. quinquecirrha*, because both gelatinous zooplankton prey on the same food sources (Grove and Breitburg 2005). In addition, the Atlantic sea nettle preys and damages ctenophores. However, ctenophores have higher clearance rates than the Atlantic sea nettle for many common prey taxa including copepods and fish eggs (Grove and Breitburg 2005). Studies on the feeding behavior of ctenophores in laboratory experiments are scarce, mainly because of their fragile body. Specialized tools have been developed to collect intact species because it is important to minimized handling and stress but also to avoid air bubbles entering their body cavity, which could damage the organism. Expensive kreisel tanks could provide a rearing habitat for culturing ctenophores but modified inexpensive tanks are necessary to reduce cost and expand studies for gelatinous zooplankton.

The objective of this study was to understand the effect that low DO had on predation of ctenophores on copepods in Chesapeake Bay. I hypothesized that under hypoxic conditions, ctenophores would prey more on copepods than under normoxic conditions, because decreasing DO concentrations would increase the stress of copepods and decrease their jumping frequency, making copepods an easier prey for ctenophores (Decker et al. 2004). Gut content of field-collected ctenophores was used to calculate clearance rates and laboratory, feeding experiments were performed to calculated ingestion and clearance rates. The comparison will provide understanding of predation by ctenophores on copepods under laboratory and field settings and normoxic and hypoxic water conditions.

Materials and Methods

Gut Content of Ctenophores

Ctenophores were collected from two sites, north (37° 43.68' N, 076°12.0' W) and south (38° 31.32' N, 076° 24.48' W), in Chesapeake Bay during the Dead Zone Zooplankton research cruise in 2011 (NSF Project 091942) (Figure 4). Although cruises occurred in May, July and September, ctenophores were not present in May; therefore, ctenophores were collected from July 19-25 and September 22-28. *Beroe ovata* and *M. leidyi* ctenophore species were collected from the cruises (Figure 3b,c). CTD casts were conducted to determine the depths on the pycnocline and vertical tows were performed in the surface, pycnocline and bottom layers using a Jel-net (1m diameter, 2500μm mesh) attached to a 15 L bucket. The Jel-net was gently raised and individual ctenophores were preserved in 5% buffered formalin jars. In addition, control jars were collected from the same Jel-nets but with no ctenophores to determine the zooplankton concentration in the ambient water. Gut content was counted and identified using a dissecting microscope and the ctenophore tentacle bulb length was measured (mm). Clearance rate (*F*, L ind $^{-1}$ h^{-1}) of *A. tonsa* by *M. leidyi* was calculated as follow:

$$F = \frac{G}{(D * C)} \quad (1)$$

where *G* is the prey content in gut (prey ind^{-1}), *D* is prey digestion time (h) and *C* is the prey concentration (prey L^{-1}) (Granhag et al. 2011). Digestion time of 1 h was used based on Reeve 1980 and Granhag et al. (2011) experiments under different temperatures of *M. leidyi* feeding on adult *A. tonsa*. In addition, wet weight (g) was calculated as follows:

$$W = 0.81x^{1.913} \quad (2)$$

where x is the bulb length (mm) (Purcell 1988).

Feeding Experiment

Ctenophores and copepods were collected in Chesapeake Bay in June and July 2012. In separate buckets/tanks ctenophores and zooplankton were cultured. Copepods were fed daily with algae (*Thalasiossira pseudonana* and *Rhodomonas spp*), and ctenophores were fed copepods or brine shrimp (*Artemia salina)*. A modified kreisel tank was constructed for ctenophore cultures because they need slow moving water (Figure 5). The tank contained a protection shield made from a plastic cylinder and many 3 cm diameter holes covered with 2000 μm mesh. Inside the shield, a stir bar and air stone were placed to protect the ctenophores while providing moving water and oxygen. The grazing experiment consisted of placing copepods and ctenophore at natural concentrations (ml^{-1}) in jars and counting the copepods eaten every 15 minutes under the following DO concentrations: saturated (7 mg l^{-1}), 4 mg l^{-1} and 1 mg l^{-1}. After food was depleted, we observed the time it takes for ctenophores to empty their stomachs.

As a result of time and difficulty of culturing *M. leidyi*, I was only able to conduct a trial experiment to determine the adequate jar size that will be used for the feeding experiments with ctenophores grazing on copepods. I gently transferred 1 ctenophore to 1L and 4L jars with approximately 30 and 120 *A. salina*, respectively. *Artemia salina* is a good supplementary food source and easy to hatch at adequate laboratory settings (K. Liu pers. comm.). I placed the jars in a rotating plankton wheel and roughly estimated the number of *A. salina* left in the jar every

30 minutes. The experiment lasted 90 minutes and ctenophores were returned to the tank and uneaten *Artemia* was counted. Ingestion rates (*I*, ind h^{-1}) were calculated as follow:

$$I = \frac{p}{t} \quad (3)$$

where *p* is the number of prey ingested and *t* is the time (h) it takes to ingest prey (Madsen and Riisgård 2010). Clearance rate (*F*, L ind $^{-1}$ h^{-1}) was also calculated as follow:

$$F = \frac{I}{c} \quad (4)$$

where *I* (ind h^{-1}) is the ingestion rate and *c* (ind L^{-1}) is the prey concentration (Madsen and Riisgård 2010).

Results

Dissolved oxygen was always lower at the north site than the south site. In July, DO in the bottom layer of the north site was anoxic (0 mg l^{-1}) while the bottom layer in the south site was at hypoxic (<2 mg l^{-1}) conditions, whereas the surface layer at both sites were normoxic conditions (>2 mg l^{-1}, Figure 6). In September, the surface dissolved oxygen concentration at both stations was saturated (7 mg l^{-1}). However, the bottom water at the north site was hypoxic while the south site was at normoxyic (Figure 7). The ctenophore *M. leidyi* was not found in September at the south site. However, the ctenophore species *B. ovata* was found in the bottom layer of both the north and south sites in September (Table 1).

Gut Content of Ctenophores

The field collected *M. leidyi* wet weight ranged in the north site from 2.7 – 21.0 g with an average (± s.d.) of 8.2 ± 4.9 g and for the south site 1.22 – 24.9 g with an average (± s.d.) of 8.8 ± 5.7 g. In the north and south sites 28 and 39 ctenophores were collected, respectively. Of the 67 ctenophores collected 86% have identifiable prey in the guts and 13% contained empty guts. In total, 9 prey taxa were identified in the guts. Most of the prey taxa found in the gut were also found in the ambient water. The majority of identified prey in the guts were *A. tonsa* copepodites and unidentified copepod nauplii. The total number of prey found in the gut was not correlated to the ctenophore bulb length for either site (Table 2). At the north site in the bottom and surface samples for July and September, the most common prey taxa found in the guts was copepod nauplii and *A. tonsa* copepodites, corresponding to what was found in the ambient environment (Figure 8). In the south site, only *M.lediyi* samples were found in July. At the surface, the composition of prey taxa in the guts did not correspond to the ambient water (Figure 8). Approximately 9% of *Tintinnid ciliates* were found in the gut and 0% found in the ambient water at the surface. At the bottom, composition of prey was similar between the guts and the ambient water with distribution between copepod nauplii and *A. tonsa*.

Comparing the number of *A. tonsa* found in the gut of the ctenophores with the ambient water reveals whether the ctenophore is preying on the copepod. Predation occurred in July and September of the north site in the surface for *M. leidyi* (Figure 9). In the south, predation occurred at the surface, pycnocline and bottom for *M. leidyi* in July (Figure 9). The ctenophore *B. ovata*, only found at the bottom layer during September, appeared to have higher predation in the north and no predation in the south (Figure 9).

The field calculated clearance rates contained digestion times from other studies based on the prey copepod, *A. tonsa*. Reeve (1980) and Granhag et al. (2011) derived digestion time of 1 h for *A. tonsa*. Clearance rate for *M. leidyi* feeding on *A. tonsa* was only calculated because *A. tonsa* was the most abundant prey found in the gut. The clearance rates ranged between 0.18 – 1.23 L ind $^{-1}$ h^{-1} and the bulb length was not correlated to clearance rates (Table 3).

Feeding Experiment

The lobate ctenophore *M. leidyi* is a delicate gelatinous zooplankton and as a consequence it is difficult to study live organisms outside their natural environment. In order to conduct the feeding experiments, we needed the ctenophores to be alive at least a week. However, the early-elevated temperatures this summer led to increased sea nettle populations and it became difficult to collect *M. leidyi* as the summer progressed. In addition, the animals that were successfully brought to the laboratory died within days, perhaps from a paucity of food during culture conditions. However, from the trial feeding experiment of *M. leidyi* feeding on *A. saline*, ingestion rate (I, ind h^{-1}) was calculated. For the 1 L and 4 L jars ingestion rate was 50 and 66 ind h^{-1}, respectively. While clearance rate was 1.67 and 2.2 L ind $^{-1}$ h^{-1} for the 1 L and 4L jars, respectively.

Discussion

Results of this study indicated that ctenophores are preying more heavily on copepods under moderate low dissolved oxygen concentrations, based on the analysis of gut contents from the field samples. In addition, predation by *B. ovata* on *A. tonsa* at the bottom is much higher under hypoxic water in the north site than under normoxic conditions in the south site. The vertical location in the water column at which prey and predator interact is also important in determining the effects of hypoxia on trophic interactions (Keister et al. 2000). Because jumping frequency is lower for *A. tonsa* under low DO concentration (Decker et al. 2004), we anticipated that gelatinous zooplankton and copepods would overlap more and predation would be higher under these conditions. However, Decker et al. (2004) found that a relative low dissolve oxygen levels (anoxic) the jumping frequency and encounter rates decreased, explaining the less predation at the anoxic bottom north site.

Digestion times are essential for calculating clearance rates from gut content samples. Although the literature has reported a wide range of digestion time for ctenophores feeding on copepods (0.7 – 5.4 h), Purcell (2009) suggested that digestion times are inversely correlated with temperature. However, digestion time depends on the size of the ctenophore and prey, the prey concentration in the guts, and the water physical characteristics such as, temperature and salinity. For this reason, further studies should be conducted in the laboratory to understand how these factors affect the digestion times, which are crucial for measuring clearance rates for field-collected samples.

The field calculated clearance rates were much lower than previously reported by other studies. Although Decker et al. (2004) found that different DO treatments did not affect digestion times, calculated clearance rates were different for field-collected ctenophores and laboratory experiments. Laboratory measurements of clearance rates could be lower based on the confinement effects from small containers and suggests why laboratory experiments are lower than analyses of gut content from field samples (Purcell 2009). However, the results showed higher clearance rates for the laboratory experiments using *A. saline* than the calculated field-collected samples using *A. tonsa*. Our field measurements might be underestimated because of

the used of other laboratory experiments digestion time and also because clearance rate is a response to the prey found in the guts. It is crucial to combine laboratory and field data to better understand these changes of predation caused by hypoxia.

Prey selectivity suggests that a prey taxon is ingested in higher fractions than the concentration in the ambient water (Granhag et al. 2011). Our results indicated that ctenophores are not prey selective because they will feed more on the highest prey concentration in the water. In addition, clearance rates could be used to measure prey selectivity because it measures ingestion time per prey concentration in the ambient water. Although our calculated clearance rates were underestimated, the highest clearance rates corresponded to the higher fraction of prey (*A. tonsa*) in the ambient water, further supporting that ctenophores will feed on the food available rather than being selective. Clearances rates should be calculated for copepod nauplii because it was another prey found at high concentrations in the ambient water and ctenophore guts.

Although we were not able to conduct the feeding experiments at the laboratory, we learned helpful lessons about keeping ctenophore culture.

1. In order for ctenophores to feed, they need slow moving water if not they will seat at the bottom.
2. Because ctenophores are voracious grazers, they could eat up 1000% of their wet body weight per day.
3. Gradual change of water should be done daily, changing less than 10% of water.

The fragile bodies of ctenophores and high maintenance to keep them alive have made it difficult to study these organisms at the laboratory. It is crucial that different methods should be tried and shared among scientists to illuminate the research on these species.

Conclusions (Anticipated Benefits)

In the last 50 years, hypoxia has expanded and is more pronounced in the estuary affecting trophic interactions between organisms (Hagy et al. 2004). It is crucial to first, understand how food-web alterations occurred under hypoxic water and second, to favor management plans that will reduce changes in food-web interactions. This study will enhance our knowledge about how copepods, which are essential to transfer energy to higher trophic levels, such as fish, distribution and abundance are affected by hypoxia. This project is part of a dissertation looking at part of the food web to understand how predation changes caused by hypoxia on ctenophores feeding on copepods and oyster larvae, and copepods and ctenophores feeding on microzooplankton. This study provides understanding of how hypoxia could favor predation by *M. leidyi*, ultimately decreasing copepod abundance. Understanding this problem will provide knowledge that can be implemented into models for ecosystem-based management of the Chesapeake Bay.

Acknowledgements

I am deeply thankful to my mentor, Dr. Jamie Pierson, who supported me through the entire process, treated me as a scientist and shared his enthusiasm and passion for a field that I knew little about. As Katherine W. Liu and I struggled together to move the project forward, I learned that doing science takes patience and many trials. Thank you Katherine for the charisma, dedication and willingness to share your knowledge with me. Moreover, I want to thank the peeps at Mike Roman and Jamie Pierson's lab for allowing me to use the equipment. I found support in the HPL community and was able to learn more from Chesapeake Bay though them. I would also want to thank Mike Allen, Fredrika Moser and the Maryland Sea Grant staff

for trusting in my abilities as a scientist and for providing an unforgettable experience. Maryland Sea Grant and the National Science Foundation supported the project described, and I am deeply grateful for such a generous contribution to my education.

References

Adamack, A.T. 2007. Predicting water quality effects on bay anchovy (*Anchoa mitchilli*) growth and production in Chesapeake Bay: linking water quality and individual-based fish models. PhD Dissertation, Louisiana State University, Baton Rouge, LA

Breitburg, D.L., N. Steinberg, S. DuBeau, C. Cooksey, and E.D. Houde.1994. Effects of low dissolved oxygen on predation on estuarine fish larvae. Marine Ecology Progress Series 104:235-246.

Breitburg, D.L, D.W. Hondrop, L.A. Davias, and R.J. Diaz. 2009. Hypoxia, nitrogen, and fisheries: Integrating effects across local and global landscapes. Annual Review of Marine Science 1:329-349.

Decker M.B., D.L. Breitburg, and J. E. Purcell. 2004. Effects of low dissolved oxygen on zooplankton predation by the ctenophore *Mnemiopsis leidyi*. Marine Ecology Progress Series 280:163-172.

Granhag, L., L.F. Moller, and L.J. Hansson. 2011. Size-specific clearance rates of the ctenophore *Mnemiopsis leidyi* based on *in situ* gut content analyses. Journal of Plankton Research 33:1043-1052.

Grove, M., and D.L. Breitburg. 2005. Growth and reproduction of gelatinous zooplankton exposed to low dissolved oxygen. Marine Ecology Progress Series 301:185-198.

Hagy, J.D., W.R. Boynton, C.W. Keefe, and K.V. Wood. 2004. Hypoxia in Chesapeake Bay, 1950-2001: long term change in relation to nutrient loading and river flow. Estuaries 27:634-658.

Jung, S., and E.D. Houde. 2004. Production of bay anchovy *Anchoa mitchilli* in Chesapeake Bay: application of size-based theory. Marine Ecology Progress Series 281:217-232.

Keister J.E., E.D. Houde, and D.L. Breitburg. 2000. Effects of bottom-layer hypoxia on abundances and depth distributions of organisms in Patuxent River, Chesapeake Bay. Marine Ecology Progress Series 205:43-59.

Kemp, W.M., W.R. Boynton, J.E. Adolf , D.F. Boesch, W.C. Boicourt, G. Brush, J.C. Cornwell, T.R. Fisher, P.M. Glibert, J.D. Hagy, L.W. Harding, E.D. Houde, D.G. Kimme, W.D. Miller, R.I.E. Newell, M.R. Roman, E.M. Smith, and J.C. Stevenson. 2005. Eutrophication of the Chesapeake Bay: Historical trends and ecological interactions. Marine Ecology Progress Series 303:1-29.

Kimmel, D.G., and M.R. Roman. 2004. Long term trends in mesozooplankton abundance in Chesapeake Bay, USA: influence of freshwater input. Marine Ecology Progress Series 267:71-83.

Kimmel, D.G, W.D. Miller, L.W. Harding, E.D. Houde, and M.R. Roman. 2009. Estuarine ecosystem response captured using a synoptic climatology. Estuaries and Coasts 32:403-409.

Kimmel, D.G, W.C. Boicourt, J.J. Pierson, M.R. Roman, and X. Zhang. 2010. The vertical

distribution and diel variability of mesozooplankton biomass, abundance and size in response to hypoxia in the northern Gulf of Mexico USA. Journal of Plankton Research 32:1185-1202.

Madsen, C.V., and H.U. Riisgård. 2010. Ingestion-rate methods for measurements of clearance rates of the ctenophores *Mnemiopsis leidyi*. Aquatic Invasion 5: 357-361.

Marcus, N.H., R. Lutz, W. Burnett, and P. Cable. 1994. Age, viability, and vertical distribution of zooplankton resting eggs from an anoxic basin: evidence of an egg bank. Limnology and Oceanography 39:154-158.

Marcus, N.H., R.V. Lutz, and J.P. Chanton. 1997. Impact of anoxia and sulfide on the viability of eggs of three planktonic copepods. Marine Ecology Progress Series 146:291-295.

Marcus, N.H., C. Richmond, C. Sedlacek, G. A. Miller, and C. Oppert. 2004. Impact of hypoxia on the survival, egg production and population dynamics of *Acartia tonsa*. Journal of Experimental Marine Biology and Ecology 301:111-128.

North, E.W., and E.D. Houde. 2004. Distribution and transport of bay anchovy (*Anchoa mitchilli*) eggs and larvae in Chesapeake Bay. Estuarine, Coastal and Shelf Science 60: 409-429.

Purcell, J.E. 1997. Pelagic cnidarians and ctenophores as predators: selective predation, feeding rates, and effects on prey populations. Annales de l'Institut Oceanographique 73: 125-137.

Purcell, J.E. 2009. Extension of methods for jellyfish and ctenophores trophic ecology to large-scale research. Hydrobiologia 616:23-50.

Purcell, J.E., T.A. Shiganova, M.B. Decker, and E.D. Houde. 2001. The ctenophore *Mnemiopsis* in native and exotic habitats: US estuaries versus the Black Sea basin. Hydrobiologia 451:145-176.

Purcell, J.E., and M.B. Decker. 2005. Effects of climate on relative predation by scyphomedusa and ctenophores on copepods in Chesapeake Bay during 1987-2000. Limnology and Oceanography 50:376-387.

Reeve, M.R. 1980. Comparative experimental studies on the feeding of chaetognaths and ctenophores. Journal of Plankton Research 2:381-393.

Richmond, C.R., N.H. Marcus, C. Sedlacek, G.A. Miller, C. Oppert. 2006. Hypoxia and seasonal temperature: Short-term effects and long-term implications for *Acartia tonsa dona*. Journal of Experimental Marine Biology and Ecology 328: 177-196.

Roman, M.R., A.L. Gauzens, W.K. Rhinehart, and J.R. White. 1993. Effects of low oxygen waters on Chesapeake Bay zooplankton. Limnology and Oceanography 38: 1603-1614.

Roman, M.R., X. Zhang , C. McGilliard, and W. Boicourt. 2005. Seasonal and annual variability in the spatial patterns of plankton abundance in Chesapeake Bay. Limnology and Oceanography 50: 394-406.

Stalder, L.C., and N.H. Marcus.1997. Zooplankton responses to hypoxia: behavioral patterns

and survival of three species of calanoid copepods. Marine Biology 127:599-607.

Zhang, X., M. Roman, C. McGilliard, D. Kimmel and W. Boicourt. 2006. Spatial variability in plankton biomass and hydrographic variables along an axial transect in the Chesapeake Bay. Journal of Geophysical Research 111 (C05S11).

Figures and Tables

Figure 1. Water surface in Chesapeake Bay showing hypoxic and anoxic regions (map from the Chesapeake Bay Foundation).

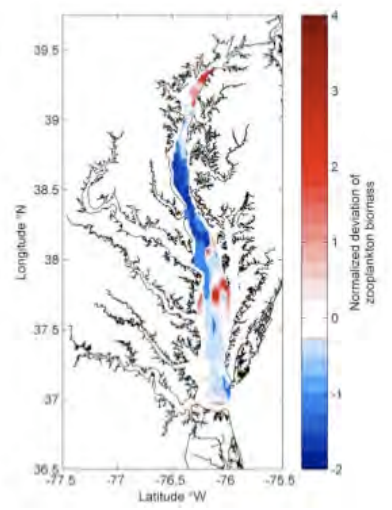

Figure 2. Zooplankton biomass at the surface and DO concentration based on depth at Chesapeake Bay (Roman et al. 2005).

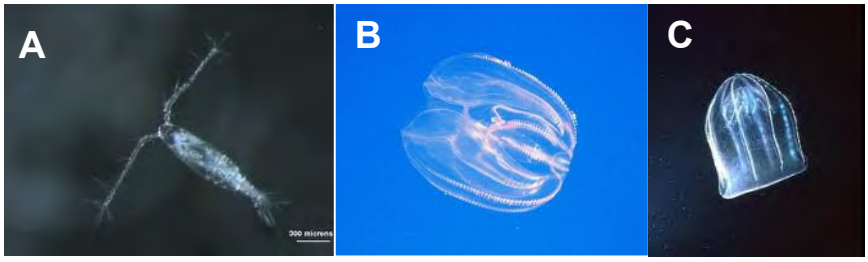

Figure 3. Abundant zooplankton found in the Chesapeake Bay: a) *Acartia tonsa* (1 mm), b) *Mnemiopsis leidyi* (20 mm), c) *Beroe ovata* (20 mm).

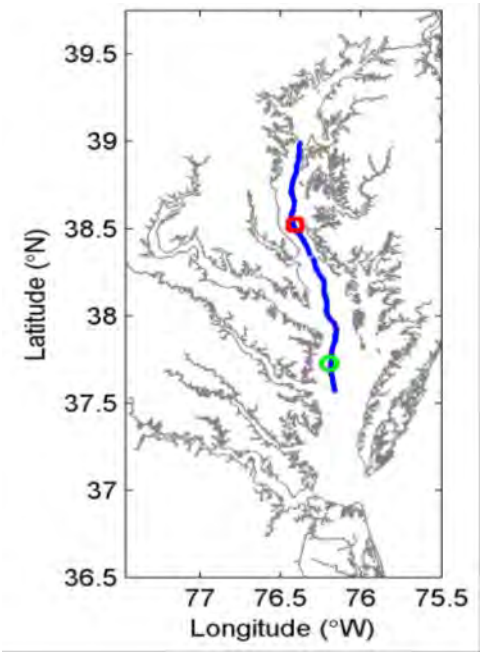

Figure 4. North site (red) circle and South site (green) circle sampled in the Dead Zone Zooplankton research cruise in July and September 2011 (Katherine W. Liu).

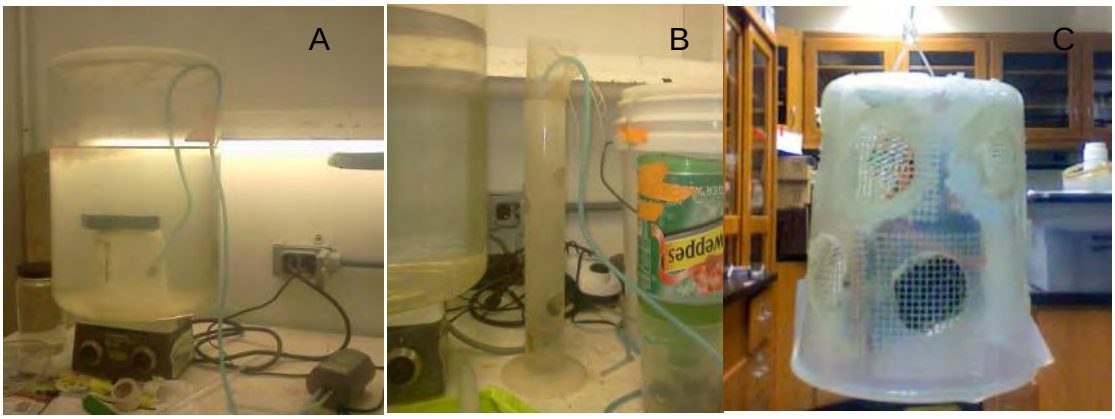

Figure 5. Modified kreisel tank (a) and tested protection shields (b and c) used to cultured *M. leidyi*.

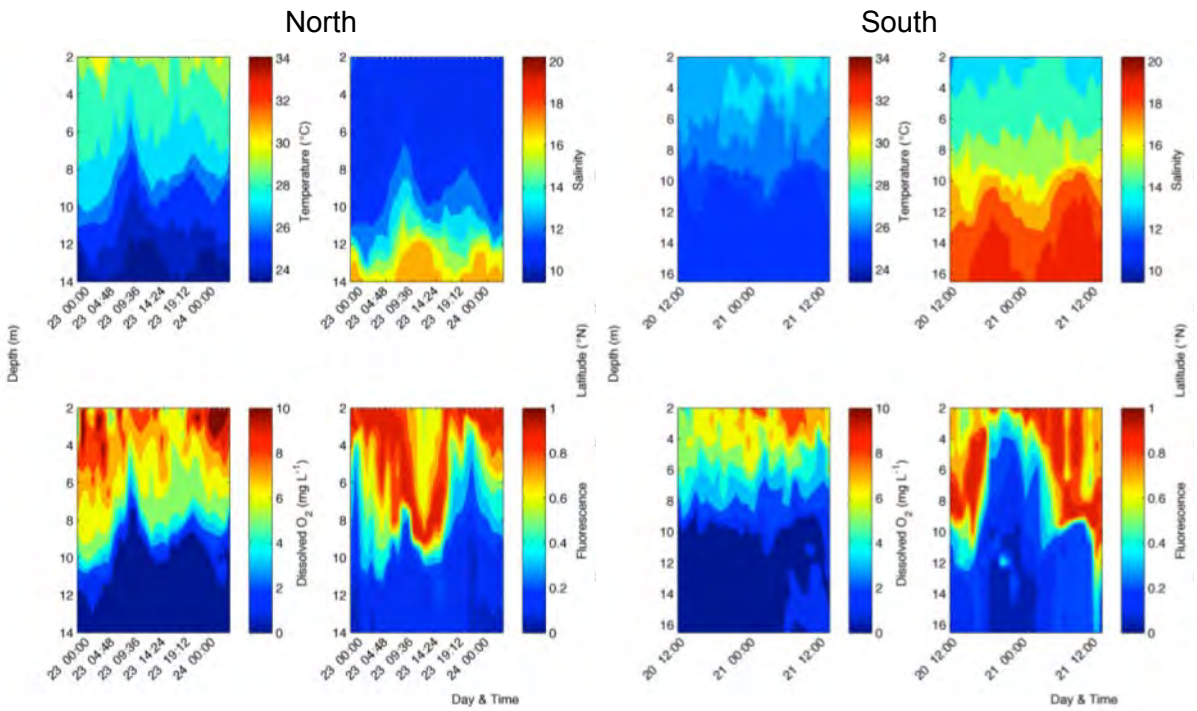

Figure 6. Vertical profile of dissolved oxygen (mg L^{-1}), temperature (ºC), salinity, and relative fluorescence from the north and south sites in Chesapeake Bay, July 2011 (Jamie Pierson).

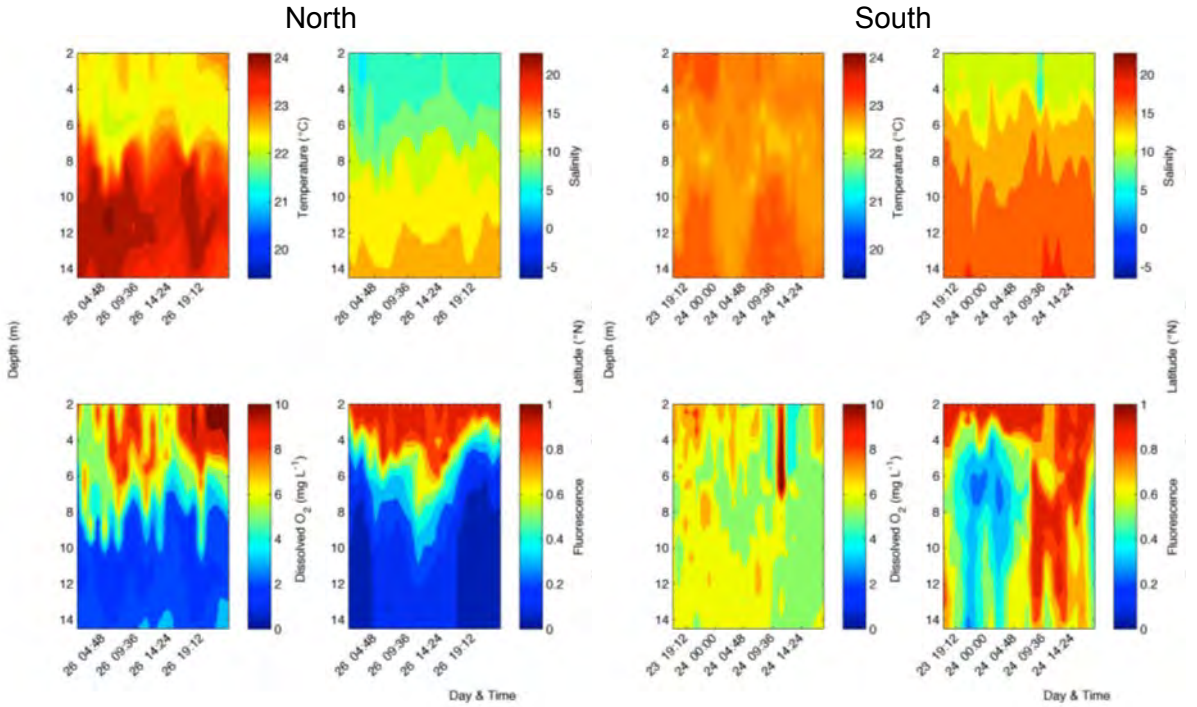

Figure 7. Vertical profile of dissolved oxygen (mg L^{-1}), temperature (ºC), salinity, and relative fluorescence from the north and south sites in Chesapeake Bay, September 2011 (Jamie Pierson).

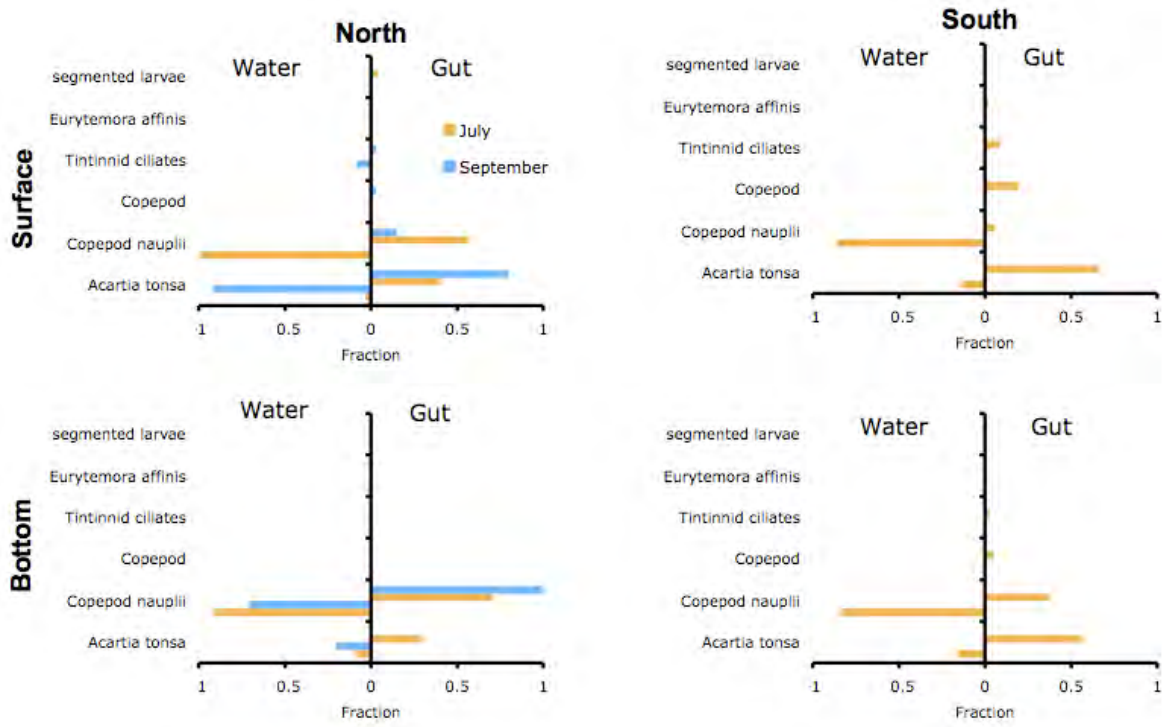

Figure 8. Composition of zooplankton in the control water and guts of *M. leidyi* from samples collected vertically at the bottom and surface in the north and south sites in Chesapeake Bay, July (orange) and September (blue) 2011. Right side of graph corresponds to the prey fraction of the total zooplankton in the guts of *M. leidyi.* Left side of graph corresponds to the prey fraction of the total zooplankton in the water.

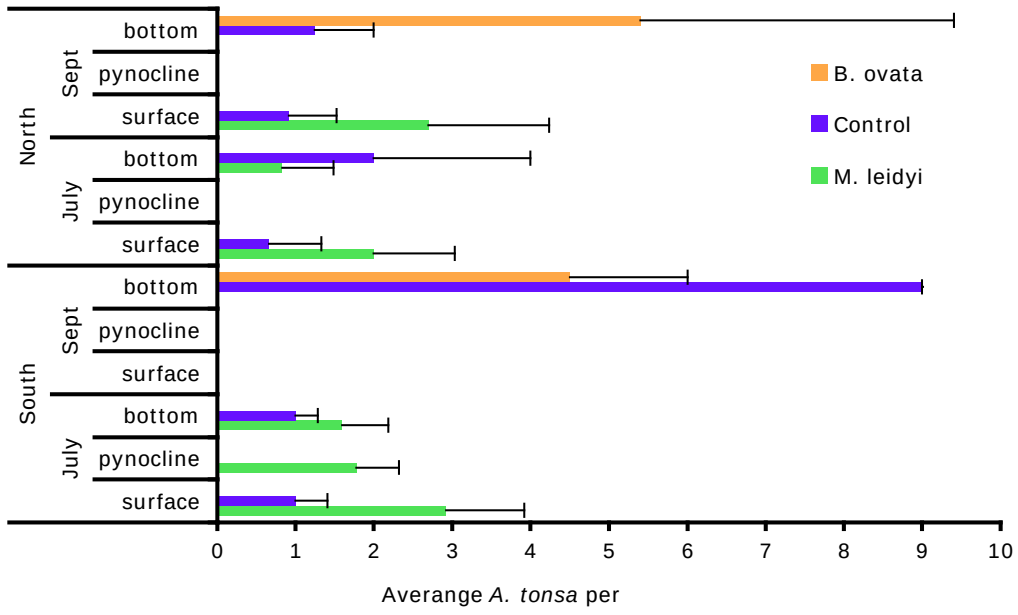

Figure 9. Average number of *A. tonsa* found in the gut of *M. leidyi* and *B. ovata* compared to the ambient water from samples collected in the north and south sites at three depths in Chesapeake Bay, July and September 2011.

Table 1. Number of samples for the south and north sites during the Dead Zone Zooplankton Cruise, July and September 2011.

			Water	*M. leidyi*	*B. ovata*
South	July	surface	3	6	0
		pycnocline	0	0	0
		bottom	2	6	0
	Sept	surface	12	10*	0
		pycnocline	0	0	0
		bottom	4	0	5
North	July	surface	4	13	0
		pycnocline	1	10	0
		bottom	6	15**	0
	Sept	surface	0	0	0
		pycnocline	0	0	0
		bottom	2	0	2

* 1 bulb missing ** 2 bulb missing

Table 2. Linear regression of the total number of prey (plankton) present in *M. leidyi* guts against the bulb length (mm).

		n	slope equation	R^2	p-value
North	Surface	15	1.45 + 0.95x	0.05	0.45
	Bottom	7	4.12 - 0.23x	0.01	0.85
South	Surface	13	1.40 + 0.92x	0.04	0.54
	Pycnocline	9	2.88 - 0.21x	0.02	0.75
	Bottom	13	2.93 - 0.01x	0	0.99

Table 3. Linear regression of *M. leidyi* bulb length against clearance rate for the north and south sites.

			n	clearance rate (L ind $^{-1}$ h^{-1}) mean $\pm$ SD	r^2	p-value
North	July	surface	6	0.21 $\pm$ 0.27	0.05	0.66
		bottom	6	0.18 $\pm$ 0.35	0.16	0.43
	Sept	surface	10	1.23 $\pm$ 2.22	0.24	0.18
South	July	surface	13	0.45 $\pm$ 1.26	0.05	0.46
		bottom	15	0.89 $\pm$ 0.55	0	0.87

(Blank)

The Effects of Differential Water Mixing on the Zooplankton Community

Gabriel Ng, REU Fellow
Maryland Sea Grant

Dr. Nicholas Nidzieko, Assistant Professor
Horn Point Laboratory. University of Maryland Center for Environmental Science

Abstract

River ecosystems are influenced not only through environmental parameters but also through the mixing of different water currents. Mixing of water can alter zooplankton population dynamics through the change in environmental parameters; alternatively, movement of water can alter zooplankton populations through the removal or addition of new individuals. In addition to measuring the impact mixing has on zooplankton population, the study is also examining how different tributaries might have different mixing coefficients. Within the Little Choptank River, there are numerous tributaries that run in several axes. One hypothesis is that tributaries that run north to south will mix differently than tributaries that run from east to west. The different hypotheses were tested using thermistors and weather stations to calculate the heat budget; a zooplankton net was used to survey the zooplankton community. Results showed that while mixing did occur, they did not differ at various tributaries; furthermore, mixing is positively correlated with zooplankton, but zooplankton did not correlate with any other environmental parameters except for suspended solids. This would indicate that mixing is moving zooplankton instead of altering their environment.

Keywords: Zooplankton, Chesapeake Bay, Water mixing, Population dynamics

Introduction

Though minute in size, zooplankton are important organisms in marine ecosystems. Zooplankton are animals that have limited mobility whose movements are mostly dictated by currents. They cover a wider range of taxa and ecological niches. Arthropods, mollusks, fish, and cnidarians are just some example of the diversity of zooplankton; some of them are filter feeders and graze upon phytoplankton, while others are predatory. Not only are they unique organisms, zooplankton are also abundant organisms, comprising a substantial amount of the biomass within an aquatic ecosystem (Humes 1994). Average zooplankton biomass is around 5.52 mg of C/m^3 (Stromber et al. 2009).

Because of their high abundance, zooplankton play a large role in the marine food web. Since a wide array of animals feed upon zooplankton, and zooplankton are the dominant grazers of phytoplankton, zooplankton are the main pathway in which energy from producers is transferred to higher trophic levels (Vargas et al. 2009; White et al. 1992). In addition to playing a large role in the marine food web, zooplankton are also important within the context of

anthropogenic eutrophication. Eutrophication occurs when excess nutrients are added to a body of water stimulating phytoplankton growth; as the phytoplankton die, bacteria use oxygen in the water to decompose the organic matter. If phytoplankton biomass is significantly increased, the drop in dissolved oxygen can lead to hypoxic conditions, causing fish and other organisms to either leave or die. Because zooplankton are the dominant grazers, they are known to control algal population (Vadstein et al. 2004). It is possible then for zooplankton to limit the magnitude of hypoxia by controlling the amount of phytoplankton that will decompose in the water (White et al. 1992). From an anthropogenic standpoint, zooplankton are crucial for several reasons: they are food for the juveniles of game fish, and they affect water clarity through consumption of phytoplankton. Investigating what affects zooplankton density and composition will be important both for ecological and anthropogenic reasons.

Ecological factors that affect zooplankton population can range from predation to environmental parameters. Studies have shown that the amount and type of phytoplankton in the water column may impact how fast copepods grow (Vargas et al. 2009). Additionally, predators of zooplankton may play a role in controlling their population size. Studies done on the comb jelly, *Mnemiopsis leidyi,* indicated that while ctenophores may not be limiting copepod population growth, other predators such as zooplanktivorous fish can exert some influence on copepod population levels (Purcell et al. 1994). This is further supported by a survey done by Uye et al. (1998) where a combination of high levels of phytoplankton and an absence of engraulids, a family of zooplanktivorous fish, led to dense population levels of copepods (Uye et al. 1998). Additionally, changes in abiotic factors, such as salinity and dissolved oxygen levels can alter zooplankton composition over the course of the year (White et al. 1992).

Study Location

The Little Choptank River is an estuarine complex along the Eastern Shore of Chesapeake Bay, near Cambridge, MD (Figure 1). Several tributaries enter into the Little Choptank River; these creeks are entirely subtidal with freshwater inputs limited almost exclusively to groundwater discharge. Consequently, these systems can be considered a closed basin, with exchange primarily controlled by tidal and wind forcing. Some of the creeks are oriented primarily north-south while others are oriented east-west. Because the creeks lie in various axes, the hypothesis is that they will mix in different amounts with the main part of the Little Choptank River. Depending on the direction the wind moves, certain tributaries might flow more into the main stem of the river than other tributaries. If differential mixing does occur, we hypothesize that zooplankton community composition will differ between these otherwise similar creeks owing to variable wind-driven mixing.

The purpose of this project is to determine if tributaries within the Little Choptank River do mix differently from each other and how variable environmental parameters affect zooplankton community composition. Our hypothesis is that spatially variable mixing between the tributaries of the Little Choptank River will produce gradients in zooplankton abundance and community composition. Specifically, based on initial observations, we hypothesize that there will be a “sweet spot” for zooplankton growth that is governed by flushing time and favorable salinity/temperature conditions. This hypothesis is supported by studies that show how microzooplankton are affected differently in a salinity gradient (Carpenter et al. 2006), and we will examine this at comparatively high resolution at a specific site.

Materials and Methods

Following the approach of Hearn, mixing can be quantified with a dispersal coefficient (Hearn 1998). This coefficient can be calculated by using a tracer in the water, such as temperature or salinity. In this study we will use temperature as a tracer; we will measure the surface heat flux and horizontal temperature distribution and use this information to estimate the amount of mixing between the Little Choptank River and Chesapeake Bay. These physical measurements will be used to infer spatial and temporal changes in zooplankton community composition.

In a contained body of water, the net surface heat flux is due to the net amount of short wave and long wave radiation added via solar radiation plus the change in temperature due to evaporation of water, and the change in temperature due to a difference in temperature between air and water (Hearn 1998). If the body of water is subjected to mixing, change in heat can also be influenced by input and output of the original water along with the surface heat flux. This can be represented by the equation

$$\frac{dT}{dt} = \frac{Q}{\rho h C_p} - K_x \frac{\Delta T}{\Delta L^2}$$ (Hearn 1998). (1)

In this equation, the first term, $\frac{dT}{dt}$, represents the change in heat storage; Q is the net surface heat flux input into the body of water, C_p is the specific heat of the water, ρ is density, and h represents the average depth of the Little Choptank River (Hearn, 1998). Lastly, the third term, which is the dispersive flux, is represented by $\frac{\Delta T}{\Delta L^2}$, the change in temperature over distance, and K_x, the mixing coefficient. (Hearn 1998). The equation can be rearranged to

$$\frac{L^2 Q}{p h C_p \Delta T} - \frac{L^2}{2}\left(\frac{dT}{dt}\right) = K_x$$ (2)

If all of the variables on the left-hand side can be measured, it is then possible to calculate the dispersion coefficient for various parts of the Little Choptank.

The goal of this project is to determine how dispersion can affect zooplankton communities. Because zooplankton are affected by different parameters, and dispersion rates affect both biotic and abiotic environmental factors, it is possible that areas within the Little Choptank with differential dispersion coefficients can have dissimilar zooplankton communities. The dispersion coefficient can be calculated by measuring the variables given in the equation using thermistors and weather data. Additionally, other factors that might be influenced by mixing, such as nutrients or salinity, are also measured. Zooplankton will be sampled using a plankton net to determine if there is a correlation between extent of mixing and zooplankton community; if such a correlation exists, more specific parameters, such as nutrients, temperature, or salinity, can then be used to determine how they affect zooplankton.

Thermistors are deployed around various sites in Little Choptank to record continuous temperature data. The thermistors are attached to docks or posts with a buoy and enough nylon rope for the buoy to sink and float with the tide. If the sites are determined to be deep enough to have different temperatures at different depths, a second thermistor is also deployed at a lower depth than the first one. In addition, several depth loggers, which record water level data, are also added to several of the buoys with thermistors. Two weather stations are also placed at

various points around the bay in order to collect data on precipitation, and wind speed. One of the weather station has a sensor to measure the amount of shortwave and longwave radiation coming from the sky and how much is reflected from the water.

In addition to the thermistors, physical data are collected with a conductivity, temperature, and depth sensor (CTD) around the Little Choptank once every two weeks. CTD sites are denoted with a pin in Figure 1. The sampling sites center around three parts of the Little Choptank River, three sites in the middle of the main branch of the river, three sites in a tributary that runs north to south, and four sites in an east to west tributary. In addition to the CTD, water samples are also collected at the surface using a syringe to measure nutrients. Additional water samples are filtered on site to collect particulates for chlorophyll and total suspended solids measurements.

To sample zooplankton, zooplankton tows are performed at several sites in the Little Choptank. These sites are denoted with a star in Figure 1, which are also CTD sites. The sampling sites are chosen such that there is a north south transect and an east west transect. Zooplankton are collected with a 200 micron net while being towed behind the boat at around a speed of 1 knot for 2 minutes. A flowmeter is attached to the net to record the distance the net is towed, and since the radius of the net is known, the volume of water sampled can be determined. The sample is then immediately filtered with a colander to remove macroscopic cnidarians and ctenophores, and the zooplankton is then fixed in 5% formalin. After fixing the zooplankton, a graduated cylinder is used to measure the biovolume of gelatinous animals.

Within the lab, the zooplankton samples are diluted with water into a known volume. Using a Stempel pipette, a subsample of a known volume is taken from the zooplankton sample. The subsample is then examined under a dissecting scope and zooplankton are identified and counted to lowest taxonomic level feasible. Knowing the size of the sample and the volume of the subsample, total zooplankton of each taxon can be calculated for the sample; furthermore, since the volume of water sampled in the field is known from the diameter of the net and the flowmeter, the density of zooplankton can then be calculated. Zooplankton hauls are performed once every two weeks in order to gather a time series of zooplankton density and composition over the various sites.

Results

To calculate the equation given by Hearn (1998), several variables must first be calculated. In the equation, Q represents the total heat flux of the river, which is composed of incoming solar radiation, evaporative loss, and sensible heating from the air. These parameters are standardized by dividing them with the density of the water, the heat capacity of the water, and the depth of the water, which is provided with depth sensors set out in the Little Choptank River. The three parameters are shown in Figure 2. Solar radiation, both longwave and shortwave, is measured with sensors on the weather station. It is the combined watts per meter squared of both longwave and shortwave radiation minus the amount of radiation being reflected by the water as shortwave radiation or irradiated by the water as longwave radiation. This is seen in the first panel where the red line represents net shortwave radiation, the blue line represents net longwave radiation, and the black line is the sum total of both long wave and shortwave radiation. Standardizing solar radiation results in change in degrees per second in the water.

In addition to solar radiation, the heat flux is composed of evaporative cooling, which is seen in the second panel. Evaporation is calculated using the equation:

Evaporation = (wind eddy coefficient)*(wind speed)*(water vapor pressure-relative humidity*air temperature) (3)

The weather stations provide the numbers for the equation, and evaporation can be calculated as degrees changed per second. Lastly, as seen in the third panel, sensible heat can be calculated using the equation

Sensible heat = (density of water)*(heat capacity of water)*(wind eddy coefficient)*(water temperature – air temperature) (4)

This calculation is seen in the third panel of Figure 2, which represents the heat flux of the river based on meteorological data. The last panel of Figure 2 is a summation of the three variables to represent total heat flux; the blue line depicts the measured change in temperature from the thermistors' data.

To calculate the actual change in temperature over time, all of the temperature values from the thermistors at various sites were averaged into one time series. The difference in temperatures between each time point is taken and divided by the length of time, which results in the change in temperature over time. The first panel in Figure 3 superimposes the change in temperature over time, the red line, and the calculated heat budget, the blue line. If no mixing occurs, the two plots should be identical. However, since mixing does occur, there are discrepancies between what the change in temperature should be based on the heat budget and what the actual change in temperature is. The green line in the first panel of Figure 3 illustrates the differences between measured changes in temperatures and calculated changes. This difference is the last term in the equation: Kx(dT/dx) (1). dT/dx can be calculated by taking the difference in temperatures among various sites and dividing it by the distances between those sites. We have calculated dT/dx for the north-south transect and one for the east-west transect. Once dT/dx has been calculated, Kx can then be solved; the last panel on Figure 2 shows the different mixing coefficients for the two transects.

Figure 4 presents an overview of the zooplankton abundance over time. The x-axis denotes time, and the y-axis represents the four sampling sites; density of zooplankton is indicated with a color gradient. However, an ANOVA test shows that the zooplankton abundance over time does not differ significantly from each other at various sites with a p-value of 0.8437. In addition to zooplankton density, the third panel in Figure 4 also shows the average percent composition of the various zooplankton at each site. An ANOVA test indicates that *Acartia tonsa*, calanoid copepod, is the dominant taxon within the zooplankton community followed by barnacle nauplii.

Table 1 summarizes the correlation tests of various environmental parameters versus zooplankton abundance. Most parameters do not significantly correlate except for ammonium, mixing coefficient, and total suspended solids; however with an R^2 value of 0.21, it does not account for the variation in zooplankton abundance as much as the mixing coefficient, which has an R^2 value of 0.956. There is also a significant positive correlation between zooplankton and total suspended solids.

Figure 5 shows the correlation between mixing coefficients and zooplankton abundance; there appears to be a strong positive correlation between mixing and zooplankton abundance. The second panel shows a boxplot of the mixing coefficients between the east-west transect

and the north south transect. An unpaired t-test calculated that there is no significant differences between the mixing coefficients of the two different transects.

Discussion

Based on the thermistor and weather station data, we were able to successfully calculate the mixing coefficients for several tributaries of the Little Choptank River. The thermistor data showed that temperatures fluctuate on a diel cycle but also respond to general warming trend as the summer progresses. Additionally, the thermistors, which represent the measured heat change, are not equal to the surface heat flux, which is the sum of solar radiation, evaporative heat loss, and sensible heat transfer. This difference is the dispersive flux term, which can then be used to find the mixing coefficients by dividing the dispersive flux by the change in temperature over the change in distance. The calculated mixing coefficients support the hypothesis that the tributaries do mix with the main part of the Little Choptank River. As a result, the expected temperature changes, based on solar radiation, evaporation, and sensible heat, will not match the measured temperature changes within the tributaries. Mixing coefficients appears to have a certain range from -3000 m^2/sec to 2000 m^2/sec with several outliers. This would indicate that mixing in the Little Choptank River fluctuates weekly from removing heat to bringing heat into the water. However, the negative mixing coefficients imply that water mass is mixing against a temperature gradient where heat is being brought into warmer areas. Though this might appear counterintuitive, the mixing could be caused by salinity gradients instead. Figure 5 shows that though mixing is apparent, the mixing coefficients between the north-south transect and the east-west transect do not differ significantly. It is possible that despite flowing in different directions, the small size of the transects coupled with the proximity to each other would result in both creeks experiencing the same water circulation when a mixing event occurs.

When examining the zooplankton data, an ANOVA test shows that the four sites do not differ in abundance significantly over the course of the field study. This is to be expected since the mixing coefficients are similar along the two transects. Additionally, the zooplankton community compositions of the four sites are similar with *Acartia tonsa* composing the major part of the community. Though the hypothesis that the creeks have different mixing coefficients was not supported, there is a significant positive correlation between density of zooplankton and strength of mixing coefficients. Mixing itself can alter zooplankton populations in two ways: through exchange of other environmental parameters that influence zooplankton growth or to carry zooplankton into a new location. From the CTD casts and chemical analyses of the water, there is a plethora of data on the environmental parameters of the Little Choptank River. Running correlation tests between these parameters and zooplankton abundance shows that there is no strong correlation between numerous environmental factors and zooplankton growth, which can be seen in Table 1. This might indicate that fluctuations in zooplankton populations from sampling date to sampling date is influenced by how moving waters are concentrating or dispersing zooplankton. This alternate hypothesis that the zooplankton are acting more as particles than living entities is supported by the fact that there is a significant correlation between total suspended solids and zooplankton growth. It would appear that when mixing accumulates suspended particulates in the water column at a specific location, it also carries zooplankton along with it.

The result that environmental parameters do not affect zooplankton is surprising as it contradicts other studies that have shown that zooplankton have preferences for certain environmental parameters (White et al. 1992; Halsband-Lenk et al. 2002). Additionally, studies have shown that bottom up and top down effects do exist for zooplankton communities, which is

also not seen in this experiment (Vadstein et al. 2004; Purcell et al. 1994; Lampert et al. 1986). One possible explanation for this is that zooplankton are being treated as particles. From the mixing coefficients, it is possible to calculate the turnover rate within the reaches of the tributaries. Table 2 shows this calculation, where the length of the transects squared divided by the mixing coefficients show the turnover rate for that tributary. This is exemplified in the following equation:

$$\frac{L^2}{K_x} = \text{turnover rate} \qquad (5)$$

The average turnover rates for the transects is 4.67 days and 3.94 days for the north-south transect and the east-west transect, respectively. Studies done on copepods have shown their generation times to vary from around 20 to 60 days depending on the temperature (Halsband-Lenk et al. 2002). Since the turnover rate of the water within the tributaries is faster than the generation times of zooplankton, the zooplankton's population dynamics at a given location will be dictated more by water currents than biological controls. Consequently, even if a certain site is more conducive for zooplankton growth, the population will emigrate due to water currents before it can be significantly affected by the current environmental conditions.

Conclusions

From the surveys of temperature and zooplankton, it would appear that mixing is a significant force within the Little Choptank River's tributaries in terms of zooplankton dynamics. However, it is the physical movement of the zooplankton community rather than differential ecological factors that are controlling zooplankton population at a given site. Therefore, ecological factors might not produce the expected response in the zooplankton population. If there is an influx of nutrients resulting in a phytoplankton bloom, zooplankton might not have time to take advantage of that before being carried away. Coming from a management standpoint, this might indicate that zooplankton might not be able to exert an effect on phytoplankton blooms in an eutrophication event if the mixing coefficients are large. Population dynamics is influenced by numerous factors, ranging from food availability to habitat compatibility. With zooplankton, one has to also account water currents depending on the habitat.

References

Carpenter, K., J. Johnson, and C. Buchanan. 2006. An index of biotic integrity based on the summer polyhaline zooplankton community of the Chesapeake Bay. Marine Environmental Research 62:165-180.

Halsband-Lenk, C., H.J. Hirche, and F. Carlotti. 2002. Temperature impact on reproduction and development of congener copepod populations. Journal of Experimental Marine Biology and Ecology 271:121-153.

Hearn, C. 1998. Application of the Stommel model to shallow Mediterranean estuaries and their characterization. Journal of Geophysical Research 103:10391-10404.

Humes, G. 1994. How many copepods? Ecology and Morphology of Copepods 292/293:1-7.

Purcell, J., J. White, and M. Roman. 1994. Predation by gelatinous zooplankton and resource limitation as potential controls of *Acartia tonsa* copepod populations in Chesapeake Bay. Limnology and Oceanography 39: 263-278.

Stromberg, K. H., T. Smyth, J. Allen, S. Pitois, and T. O'Brien. 2009. Estimation of global zooplankton biomass from satellite ocean colour. Journal of Marine Systems 78:18-27.

Uye, S., N. Nagano, and T. Shimazu. 1998. Biomass, production and trophic roles of micro- and net-zooplankton in Dokai Inlet, a heavily eutrophic inlet, in summer. Plankton Biology and Ecology 45:171-182.

Vargas, C., R. Martinez, R. Escribano, and N. Lagos. 2010. Seasonal relative influence of food quantity, quality, and feeding behaviour on zooplankton growth regulation in coastal food webs. Journal of the Marine Biological Association of the United Kingdom 90: 1189-1201.

Vadstein O., H. Stibor, B. Lippert, K. Loseth, W. Roederer, L. Sundt-Hansen, and Y. Olsen. 2004. Moderate increase in the biomass of omnivorous copepods may ease grazing control of planktonic. Marine Ecology Progress Series 270:199-207.

White, J., and M. Roman. 1992. Seasonal study of grazing by metazoan zooplankton in the mesohaline Chesapeake Bay. Marine Ecology Progress Series 86:251-261.

Figures and Tables

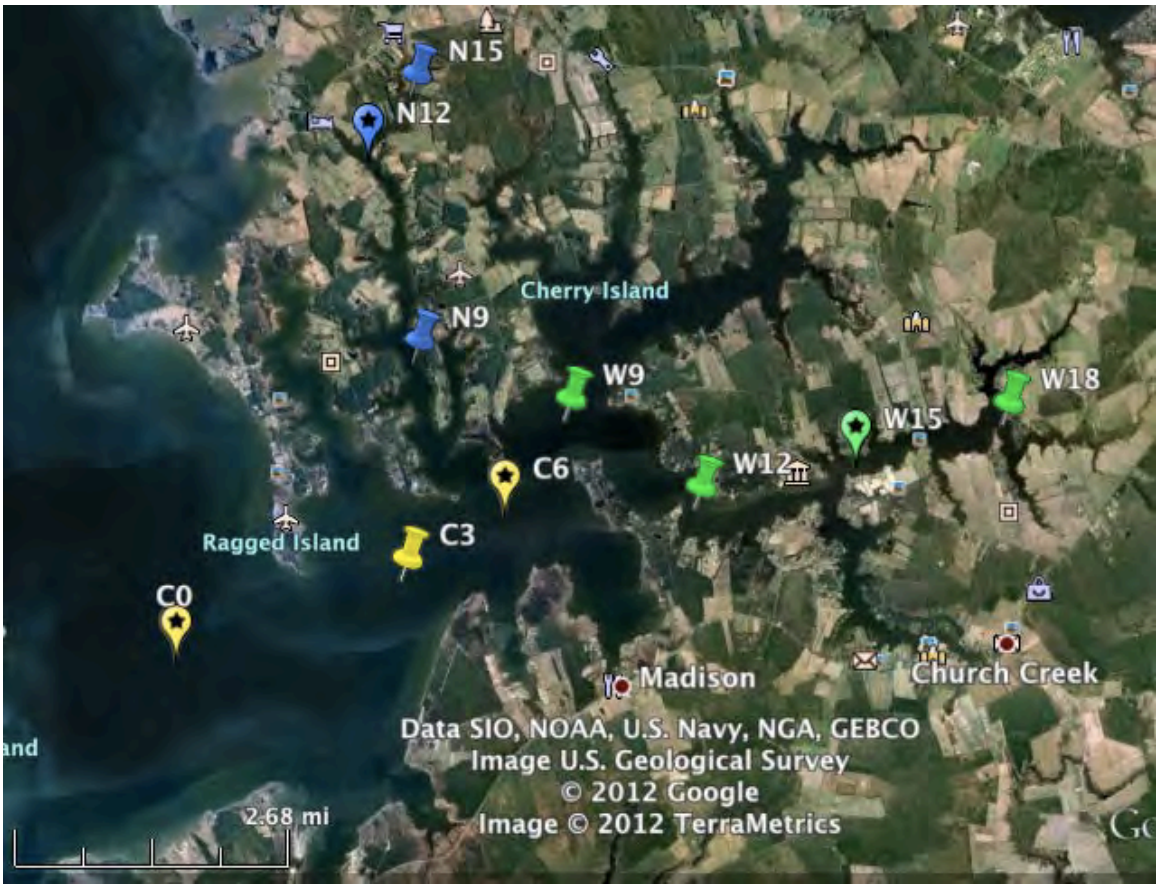

Figure 1. Map of the study sites. The pins represent sites where the CTD is launched. Yellow pins indicate the central axis of the Little Choptank River. Blue pins are sites used for the north-south transect, and green pins are sites used for the east west transect.

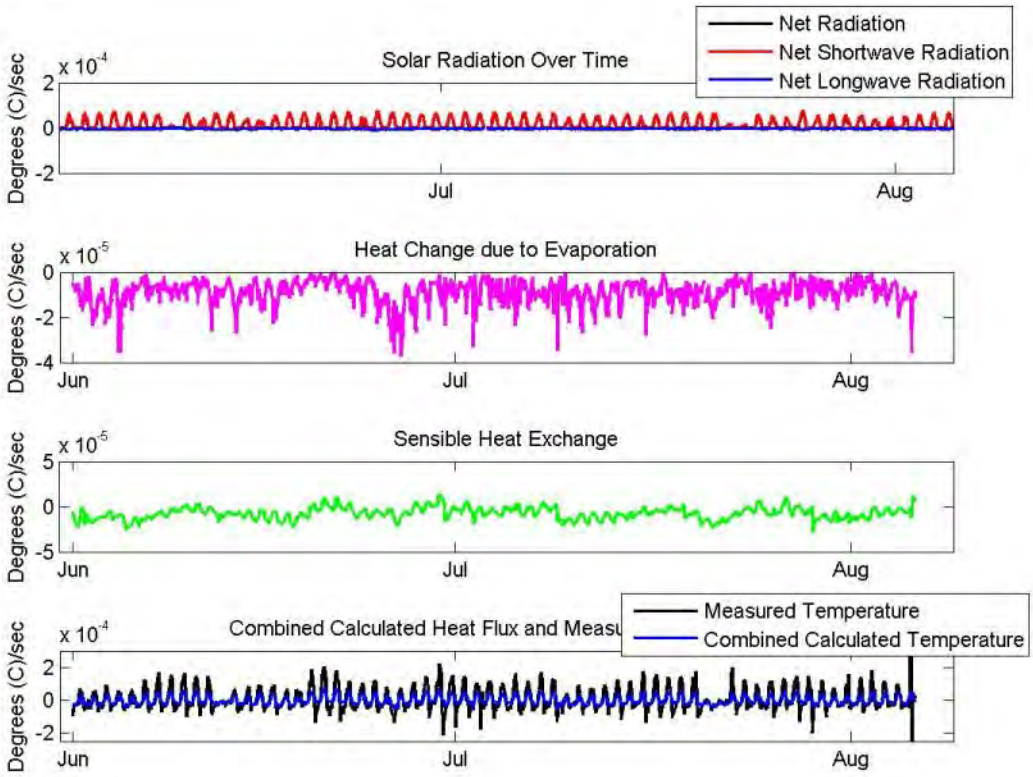

Figure 2. Heat flux data for the Little Choptank River. Graphs represent solar radiation, evaporative heat change, and sensible heat flow for the Little Choptank River. The last graph sums up the three variables and represents the calculated surface heat flux in the black line. The blue line represents the actual change in temperature from the thermistor data.

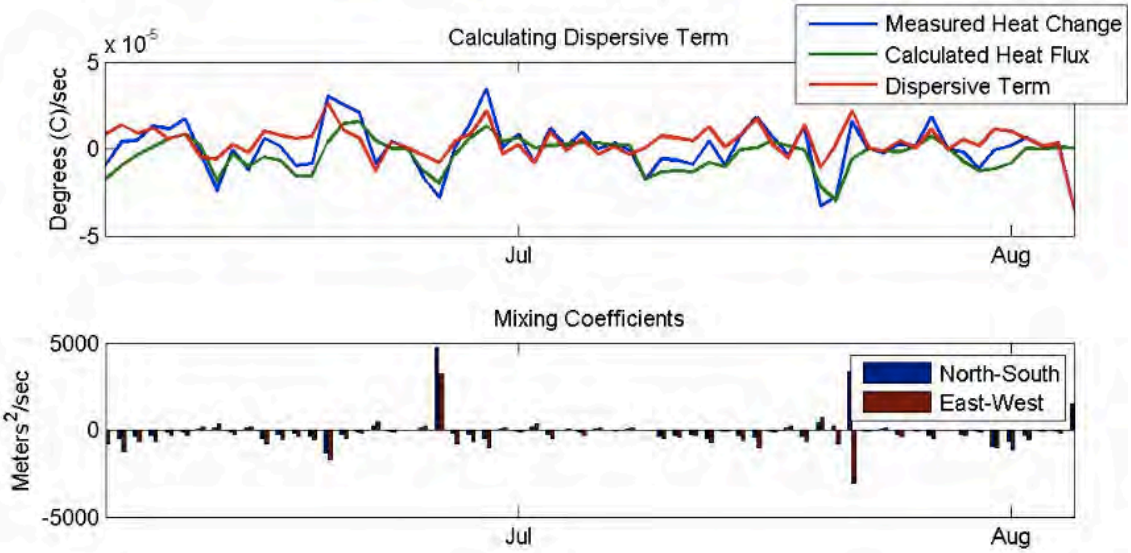

Figure 3. The first panel shows the disparity between calculated heat budget versus measured heat changes. The bar graph shows the calculated mixing coefficients for both north and west transects.

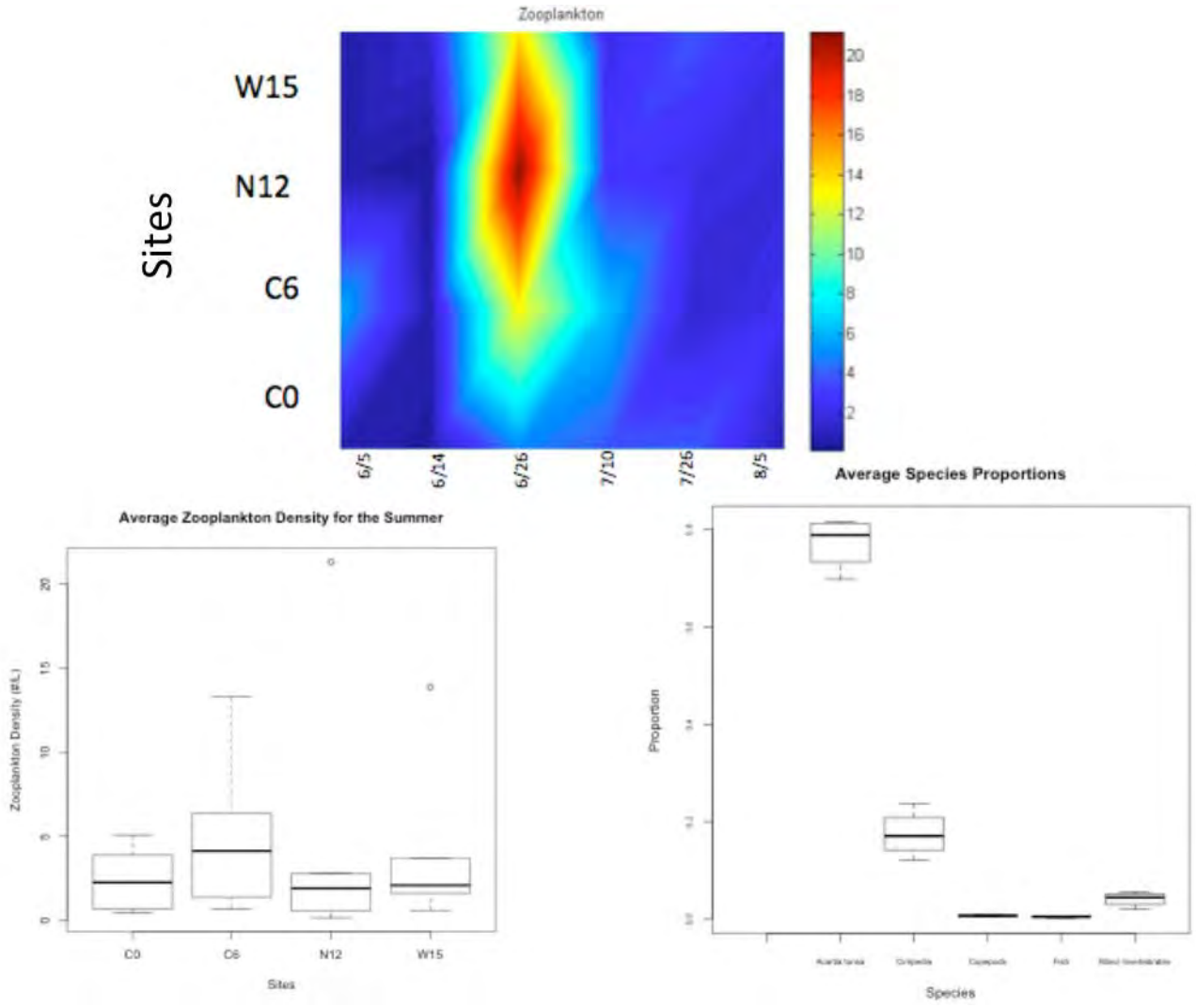

p = 0.8437

p = 5.86E-15

Figure 4. The first panel shows the change in zooplankton density over time and space, and the second panel is a boxplot of the average zooplankton density across various sites. The third panel illustrates a boxplot showing the composition of the zooplankton community over time.

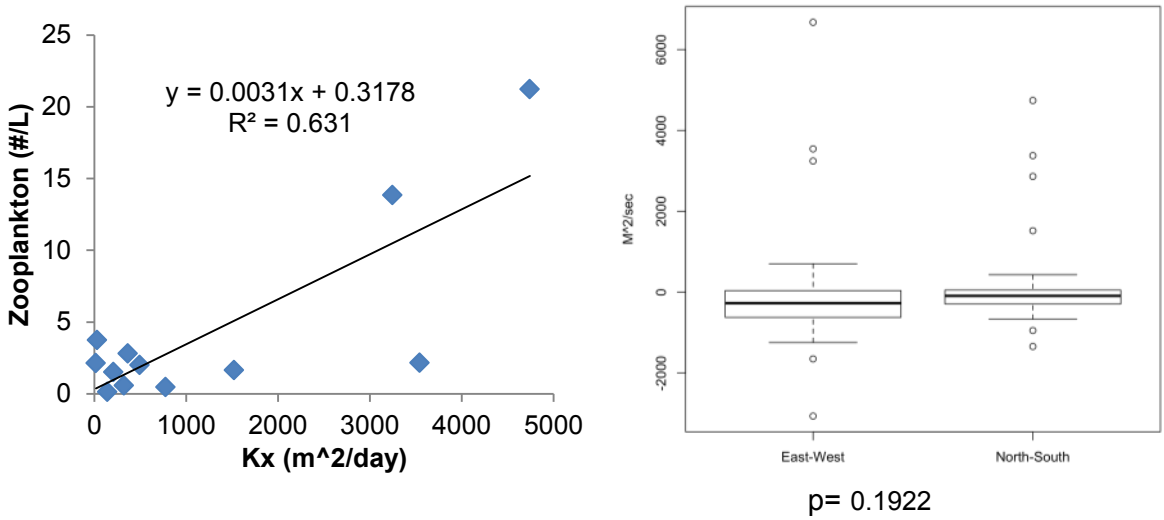

p= 0.1922

Figure 5. A graph of the correlation between mixing coefficients and zooplankton abundance. The second panel represents a boxplot of the mixing coefficients between the East-West transect and North-South transect.

Table 1. The p-values of the correlation among various environmental factors and zooplankton abundance.

Environmental Parameters	P value	R^2
Temperature	0.8086	0.00354
Salinity	0.8206	0.00983
Nitrite + Nitrate	0.4046	0.0389
ORP	0.4977	0.02592
NH4	0.04139	0.21138
Chl a	0.6776	0.01271
Perid	0.9489	0.0003
Radiata	0.7848	0.00425
DO	0.942	0.00876
Kx	0.002027	0.631
TSS	0.0352	0.22336

Table 2. Calculations to find the turnover rate in the two transects.

	average Kx	km	m	m^2	m^2/k=T (seconds)	days
North	415.8372041	12.95	12950	167702500	403288.8312	4.667694805
West	658.7408681	14.97	14970	224100900	340195.8355	3.9374518

(Blank)

Identifying Nitrogen and Microbial Contaminant Hotspots in Tributaries of Johnson Bay, Maryland Coastal Bays

Caroline Rodriguez, REU Fellow
Maryland Sea Grant

Dr. Judith O'Neil, Research Assistant Professor
Horn Point Laboratory, University of Maryland Center for Environmental Science

Abstract

Water quality in Maryland's Coastal Bays has been declining dramatically due to land runoff. In Johnson Bay, nutrient levels are quite high considering low-density land usage. We hypothesize that nutrients and microbial contaminants may be from runoff of poultry manure from feeding operations and agricultural fields. We also hypothesize that microbes from these sources will exhibit resistance to common antibiotics used in nearby feeding operations. This study seeks to measure water quality parameters to identify nitrogen sources and assess antibiotic resistance and abundance of isolated indicator species of bacteria (e.g. *Escherichia coli* and *Enterococcus* spp.). Surface water samples were collected at three sites along three creeks that flow into Johnson Bay in order to measure water quality parameters and determine bacterial abundance. Specific agar plates were used to assess bacterial contaminant abundance and a modified chromogenic agar impregnated with four different antibiotics (tetracycline, ciprofloxacin, gentamicin, and oxacillin) were used to assess *E. coli* antibiotic resistance. Nutrient levels were very high, particularly nitrogen at the head of Powell, which was in excess of 600 µM and fecal bacterial abundances were extremely high at the majority of sites. High nutrient levels and contaminant bacterial abundances measured in Powell Creek indicate it is the main source of pollutants. Finally, bacteria demonstrated the highest resistance to oxacillin, but overall the data was inconclusive because it did not decisively identify the sources of nutrient pollutants. These findings will help to better understand how land use patterns affect water quality and sources of contamination from runoff.

Keywords: Antibiotic resistance, Bacterial abundance, Eutrophication, Fecal bacteria, Johnson Bay, Maryland Coastal Bays

Introduction

Coastal Bays

The Coastal Bays of Maryland are a system of shallow, interconnected estuaries between the Delmarva Peninsula and the outer barrier islands (Figure 1). Although the Chesapeake Bay has undergone many restoration efforts, few have been successful. The Chesapeake Bay has also been the site of many research studies, but there is very little

research focused on the Maryland Coastal Bays, even though they suffer from some of the same problems (Beckert 2008).

The predominant land cover surrounding the Maryland Coastal Bays is wetlands and forest, but a significant portion is dedicated to agricultural farming (Beckert 2008). The Delmarva Peninsula is dominated by poultry farming with 570 million chickens raised in Maryland alone (Urbina 2008). The $700 million industry (Urbina 2008) includes raising chickens and using their manure to fertilize crops that are grown as feed for the chickens. Forests, wetlands, grasslands, and aquatic habitats are in danger and are decreasing in size due to increasing farmland. Reducing riparian zones allows terrestrial runoff, both organic and inorganic, to enter the Coastal Bays due to decreased natural retention of nutrients (Beckert 2008; Mallin et al. 2001).

Increasing farmland not only leads to the reduction of the extent of riparian zones, but also increases the direct nutrient input into the Coastal Bays. Even though there was a period of time in the 1990s where water quality was improving from extensive restoration efforts, the trend has reversed and now the Coastal Bays face extensive degradation (Dennison et al. 2009). Although the main problem in the Coastal Bays is anthropogenic nutrients leading to eutrophication, the Coastal Bays are also experiencing a plethora of other problems. Turbidity in the Coastal Bays is high and blocks seagrass growth. Combining the high turbidity with the lack of circulation in bays contributes to the common occurrence of macroalgae. While macroalgae occur naturally in Maryland's Coastal Bays, Chincoteague Bay, in particular, has high amounts of macroalgae that are nutrient-responsive. Elevated levels of macroalgae reduce dissolved oxygen (DO) and consequently, over 78% of sites studied in the Chesapeake Bay have lower DO levels than necessary for most living resources (Dennison et al. 2009).

The other problems the Coastal Bays are facing stem from physical features including their size and the lack of tidal exchange that make them particularly sensitive to eutrophication. The Coastal Bays are shallow and relatively small in size which permits the concentration of nutrient loads. In addition, tidal exchange is limited and there are long residence times. For example, the Chincoteague Bay has an average residence time of 63 days and this permits nutrient accumulation (Beckert 2008).

Although studies of the Coastal Bays have found that they are degraded with high levels of nutrients, there is an uneven distribution of degradation. Water quality follows a general pattern of degraded water quality in the north to fair water quality in the south. The grading of degradation generally follows land use patterns. The north is characterized by large urban populations and small enclosed bays with longer flushing times, whereas the south is dominated by wetlands, forests, agriculture and better flushing and tidal exchange (Wazniak et al. 2007). The water quality index, which measures and scores levels of nitrogen, phosphorus, chlorophyll *a*, and dissolved oxygen, was low in upstream tributaries due to degraded water quality, while open waters in the southern regions of the Chesapeake Bay ranged from degraded to good water quality. The upper tributaries are highly enriched with nitrogen while southern regions, like Chincoteague Bay, are only moderately enriched (Dennison et al. 2009). However, in the southern bays, trends in nitrogen and phosphorus that were improving have switched and are now degrading (Dennison et al. 2009). Since the southern bays used to be healthier, the current reverse in water quality in the southern Coastal Bays is alarming.

Johnson Bay

Johnson Bay is a 50 square kilometer sub-embayment of the Maryland Coastal Bays located on the western side of Chincoteague Bay (Figure 2). Boxiron Creek drains into the

northern lagoon, Scarboro and Pikes Creeks drain through marshes into the lower part of the bay, and Powell Creek drains to the most southern part of the bay. The E.A. Vaughn Wildlife Management Area occupies the western boundary of the bay and there is only one developed town, Girdletree, which is between Boxiron and Scarboro Creek. Girdletree has a population just above 100 and the dominant human waste disposal method in the town and the surrounding scattered settlements is septic systems (Beckert 2008). Farming and poultry feeding operations are also present in the Johnson Bay watershed with poultry houses near Scarboro Creek. The dominant forms of land use are row crops and poultry farming, which are found near Powell Creek (Beckert 2008).

The Johnson Bay watershed is 9,935 hectares and is 37.4% forest, 29.1% wetland, 31.1% crop agriculture, 2.2% urban, and 0.1% feeding operations. The watershed is characterized by land that is mostly flat and sandy where water can travel through the watershed easily (Beckert 2008). The declining water quality is concerning considering the lack of development, better flushing, and absence of large numbers of feeding operations combined with the high percentage of wetland and forest coverage (Dennison et al. 2009).

Water Quality

The biggest threat to coastal lagoons is anthropogenic nutrients (Dennison et al. 2009). The overload of nutrients (nitrogen and phosphorus) can change primary production from seagrasses to epiphytes, which cover the seagrasses. Macroalgae continue to increase until phytoplankton dominate and cause a shift from benthic to pelagic production. The abundance of phytoplankton reduces the amount of light that can reach the bottom and robs the water of oxygen when they decompose. This can lead to hypoxia or anoxia and is termed eutrophication (Beckert 2008; Dennison et al. 2009). Eutrophication is often the result of anthropogenic activity including enlarged impermeable surfaces, increased septic runoff and poor wastewater treatment, increased agricultural runoff, excessive wetland and forest clearing, and changes in land use (Beckert 2008).

Johnson Bay has extremely high stable nitrogen isotope ratios ($\delta^{15}N$), which can be used to identify human and animal wastes (Beckert et al. 2008; Fertig et al. 2009). High $\delta^{15}N$, which represents a ratio of ^{15}N: ^{14}N, signifies human and animal sources of nitrogen because volatilization of ammonia and denitrification remove ^{14}N, while low $\delta^{15}N$ indicates chemically synthesized nitrogen fertilizer because nitrogen fixation favors the lighter ^{15}N. Knowledge about areas with high $\delta^{15}N$ is helpful for studying eutrophication because it can help to identify the source of a nutrient and whether it is point source or nonpoint source (Beckert 2008).

Both Chincoteague Bay and its sub-embayment, Johnson Bay, suffer from elevated nutrient levels from anthropogenic inputs. Fertig et al. (2006) found that Chincoteague Bay had low total nitrogen (TN), but high $\delta^{15}N$ values, which suggested human nitrogen sources. According to Dennison et al. (2009), nutrient levels have increased, phytoplankton have increased, and dissolved organic nitrogen (DON) has increased in Chincoteague Bay. Johnson Bay also suffers from nutrient loading. Johnson Bay had high total phosphorus (TP) (Beckert et al. 2008), high turbidity, and low DO with no obvious source (Fertig et al. 2006). Total nitrogen was above the threshold of 46μM for seagrasses, fisheries, and other aquatic life and peaked at 77μM. Of all of the nitrogen species, organic nitrogen is the dominant form. The Bay also suffers from extremely high $\delta^{15}N$ values and had a value of 14.54 in previous studies (Beckert et al. 2008). Therefore, both Chincoteague and Johnson Bays suffer from high levels of nutrients. This project will use contaminant bacteria as an indicator to potentially identify the sources of nutrient pollution.

Contaminant Bacteria and Antibiotic Resistance

Coliforms and fecal streptococci are commonly found in human and animal feces and thus, are indicators of human or animal sewage contamination. Enterococci are a subgroup for fecal streptococci that are found in the digestive systems of warm-blooded animals and can survive in salt water. They closely mimic other pathogens and are more human specific than fecal coliforms; therefore they are the most effective indicators (US-EPA 1997). Fecal bacteria are commonly found in human and animal feces and their presence in aquatic environments indicates the possibility for the presence of pathogenic bacteria. *E. coli* is a gram negative bacterium that is also commonly found in the digestive systems of animals. Both *E. coli* and enterococci can only survive outside of the body for a limited period of time; therefore both bacteria are useful indicator organisms. Consequently, in this study we will assess enterococci abundances to discover the sources of possible contamination.

Prior research (O'Neil et al. 2011) indicated high concentrations of bacteria including elevated levels of enterococci (Figure 3 and Figure 4). Powell Creek consistently showed the greatest abundances of enterococci (with a mean of 852 and 930 colonies/mL at the mid and mouth, respectively) whereas Scarboro Creek showed the fewest enterococci (with a mean of 17 colonies/mL). In contrast, total bacteria abundance was low at the mid and mouth of Powell while there was high bacterial abundance (2.83×10^7 mL^{-1}) in Scarboro (O'Neil et al. 2011).

Mallin et al. (2001) found a correlation between mean estuarine bacterial counts and land use. Watershed population, percent developed area, and percent of impermeable coverage were positively correlated to bacterial count. Bacterial populations showed a positive response to fertilizers applications, drainage basin size, and manure production (Dennison et al. 2009). However, considering the lack of development in Johnson Bay, the source of the high concentrations of enterococci is not clear. This study will work to identify the cryptic sources of enterococci.

In order to counter potential disease causing bacteria like *Salmonella*, *Campylobacter*, and *Escherichia coli*, poultry farmers feed chickens low-levels of antibiotics at therapeutic doses, but antibiotics are also administered at sub-therapeutic doses for growth promotion (Food Marketing Institute; Singer and Hofacre 2006). The Food and Drug Administration (FDA) approved the use of antibiotics in feed at sub-therapeutic doses 50 years ago, but further research has discovered evidence of a link between low-level use in animals and antibiotic resistance in humans (Food Marketing Institute). Resistance occurs because antibiotics exert a selection pressure and potentially select for bacterial strains that are resistant to the antibiotic. Over time, bacteria emerge that are resistant to the same antibiotics that are given to humans, rendering the drug inept in treating bacterial infections (Food Marketing Institute; Singer and Hofacre 2006). In addition, bacteria have the ability to transfer resistance genes. Bacteria can perform horizontal gene transfer where one microbe acquires genetic material from a much different microbe and then incorporates the genetic material into its own genome. This makes the microbe develop resistance to an entirely different antibiotic (Keiger 2009; Sayah et al. 2005).

Due to public pressure, the FDA, European Union (EU), and World Health Organization (WHO) have been selectively banning drugs that are used in both humans and animals in order to reduce resistance of drugs used to treat infections in humans (Food Marketing Institute). Despite the fact that these major organizations are enforcing strict regulations on antibiotic use, there is controversy over the veracity of antibiotic resistance resulting from sub-therapeutic use in animal feed. In general, the scientific community is opposed to the use of antibiotics for

growth promotion and WHO, specifically, is strongly opposed. There are a plethora of scientific studies that have found increased resistance to different antibiotics after increased use of antibiotics including Sojka et al. in 1961 who documented an increase in resistance of tetracycline of 3.5% in 1957 to 63.2% in 1960 and Smith in 1966 who found that twenty-nine percent of avian isolates portrayed resistance to antibiotics (Singer and Hofacre 2006). However, the 2003 Conference on Antimicrobial Agents and Chemotherapy found that risk of humans acquiring resistant bacteria from eating meat was less than one in ten million per year for *Campylobacter* (Food Marketing Institute). Most animal health experts state that humans, and not animals, consume the majority of antibiotics. The American Health Institute (AHI) claims that each ton of animal feed contains four to 25 grams of antibiotics and the European Federation of Animal Health states that humans consume 65 percent of all antibiotics versus the 35 percent consumed by animals (Food Marketing Institute). Although agricultural antibiotic use invokes passionate debate, antibiotic usage data are difficult to obtain, and because of this, different organizations have created estimations that vary widely (Singer and Hofacre 2006).

This study will assess antibiotic resistance of four specific antibiotics: tetracycline, ciprofloxacin, gentamicin, and oxacillin based on previous data shown in Figure 5. Tetracyclines are a group of broad-spectrum antibiotics that are being reduced in usage due to high resistance rates (Joseph et al. 2001; Sayah et al. 2005). Sayah et al. (2005) found that out of 12 tested antibiotics, tetracycline was the agent that demonstrated resistance most frequently. Additionally, tetracycline exhibited the highest resistance in all of the studied animals and for poultry, in particular, 35.05 percent of fecal isolates portrayed resistance. Despite this high resistance, in the Maryland Coastal Bays, tetracycline exhibited no resistance in Boxiron, Scarboro, or Powell Creek in previous studies (Leight unpublished data). Ciprofloxacin is a quinolone antibiotic used to treat bacterial infections. According to Dr. Randy Regal (2002), ciprofloxacin is the only effective antibiotic used to treat *Pseudomonas aeruginosa* and one of the antibiotics used to treat anthrax. Resistance of *Campylobacter* to ciprofloxacin increased from zero percent in 1988 to 34.1 percent in 2007. Ciprofloxacin resistance is high and in a study by Hein et al. (2003), 50 percent of all poultry isolates and 39 percent of all human isolates were resistant to ciprofloxacin. Furthermore, ciprofloxacin was used in the anthrax scare of 2001 and about 10,000 postal employees were prescribed the antibiotic. Therefore, resistance is likely to be higher than in 2001 (Regal 2002). Gentamicin had a higher percentage of microbial resistance in Johnson Bay than both tetracycline and ciprofloxacin (Leight unpublished data). Gentamicin is a type of ionophore called an aminoglycoside antibiotic that is not used to treat human infections. *E. coli* had shown some resistance, but the drug is shown to have little absorption into edible tissues or muscles (MacNeil and Cuerpo 1995). Finally, oxacillin portrayed the highest percentage of antimicrobial resistance in 2010 and 2011 in Johnson Bay (Leight unpublished data). It is a beta-lactam antibiotic used to treat penicillin-resistant *Staphylococcus aureus*, but resistance to Methicillin-resistant *Staphylococcus aureus* (MRSA) is highly prevalent and *E. faecium* has shown resistance (Joseph et al. 2001).

Understanding rates of antibiotic resistance as well as the quality of surface waters is important in order to protect human health and help inform water quality management. Accordingly, we measured water quality parameters in Johnson Bay and its tributaries and identified the type of nitrogen and microbial contaminants entering the bay. We also assessed whether the nitrogen and bacterial contaminants were from a common source and assessed the antibiotic resistance in isolated bacteria. We hypothesized that nutrient levels would be highest and enterococci would be the most abundant in Powell Creek, due to both residential and agricultural land uses. In regards to antibiotic resistance, we hypothesized that resistance would be highest for oxacillin followed by gentamicin and ciprofloxacin whereas resistance to tetracycline would be the lowest, but would have increased from 2010 and 2011.

Materials and Methods

Study Locations

Surface water samples were taken on June 26th and on July 25th from the head, middle, and mouth of three tributaries of Johnson Bay: Boxiron Creek, Scarboro Creek, and Powell Creek (Figure 2), although sampling was not possible at the head of Scarboro in July because it was dry due to drought conditions in the region. Boxiron Creek is located to the north of Johnson Bay and is predominately surrounded by forestland although there is a farmstead located at the head. Scarboro Creek is located at the middle of the Johnson Bay watershed and is almost entirely bounded by wetlands, but extensive cropland and pasture are also present. Additionally, there is a poultry house in the watershed. The Powell watershed is dominated by residential drainage and agricultural cropland where poultry fertilizer is used (Studholme 2011). Three water samples were collected from each site by kayak at the middle and mouth of each creek as well as in Johnson Bay; sampling at the head was completed via car due to the shallow water depths. Water samples were collected in carboys and kept away from sunlight until they could be filtered or frozen for analysis.

Water Quality

Samples were taken for water quality and total suspended solids (TSS) measurements at the head, mid and mouth of creeks that flow into Johnson Bay: Boxiron Creek, Scarboro Creek, and Powell Creek. Additionally, sampling was conducted in Johnson Bay in order to compare measured parameters along the water quality gradient. After sampling, carboys were kept cool and away from light until they were filtered and/or frozen for microbial or nutrient analyses by Analytical Services at the University of Maryland Center for Environmental Science Horn Point Laboratory. Samples were analyzed for TN, TP, NH_4, PO_4, and NO_x. A multi-probe YSI was used to measure DO, pH, salinity, and temperature in the field. Samples were also taken for δN and chlorophyll *a* analyses; however the results of these analyses are not presented in this report.

In addition, water samples were collected to analyze TSS. We filtered 170-250 mL of the water samples onto pre-weighed Whatman GF/F filters, dried them overnight at 60˚C, and then re-weighed the filters to get TSS values. Subsequently the filters were combusted at 450˚C for five hours in a Fisher Scientific isotemp muffle furnace in order to burn off the organic material, which left the inorganic material.

Bacterial Abundance and Antibiotic Resistance

In order to enumerate the amount of enterococci in the water, a modified version of the membrane filter (MF) method 1106.1 using a membrane-Enterococcus (mE) agar (US-EPA 2002) was implemented. After collecting the water sample, it was filtered through a sterile membrane filter. The membrane with the bacteria was placed on labeled mE agar plates and incubated for 48 hours at 35˚C. The enterococci colonies develop a black or reddish-brown precipitate and these colonies were counted using a dissecting microscope. In order to calculate the number of enterococci per 100 mL, we used the following equation:

Abundance = (Number of colonies/volume of filtered sample) x 100 (1)

E. coli resistance was assessed using a Difco MI agar impregnated with tetracycline, ciprofloxacin, gentamicin, and oxacillin. The modified agar uses a fluorogenic component and a

chromogenic component that detects *E. coli* in a variety of water types, including brackish water. First all reagents were autoclaved and all of the antibiotics were dissolved separately in dilutions previously determined to maximize the suitable colony counts per plate that meet statistical growth requirements. Next 36.5 g of Difco MI powder was dissolved in 1 L of sterile water. After heating and boiling each solution, a set of plates was prepared for each one of the antibiotics as well as a set of control plates with no antibiotics. Finally, each antibiotic was added separately to the plates and incubated for 24 hours at 35˚C until the blue *E. coli* colonies were counted with a dissecting microscope (Watkinson et al. 2007).

Results

Physical Parameters

Water temperature ranged from 18˚C at the head and mid of Powell Creek to 26.7˚C in the mid of Scarboro Creek in June. In July, the head of Powell exhibited a temperature of 19.2˚C while there was a temperature of 28˚C at the middle of Boxiron Creek.

During June sampling, salinities varied between 0.1 at the head of Scarboro and the head and mid of Powell to 29.5 in Johnson Bay. Following a long period of time without rain, salinities were higher in July and ranged from 0 at the mid of Powell to 35.8 in Johnson Bay.

Surface waters at the head of Scarboro were the most acidic with pH values of 5.0 while pH was highest (7.0) in both Johnson Bay and the mouth of Powell in June. In July, pH values were higher and ranged from 6.9 to 8.3 at head of Boxiron and the mouth of Powell, respectively.

Dissolved oxygen was the lowest at the head of Boxiron (3.5-3.3 mg L^{-1}) and the highest at the mouth of Powell (15.8-16.2 mg L^{-1}) following a rain event in June. Dissolved oxygen was even lower in July at the head of Boxiron (0.52-0.41 mg L^{-1}) in comparison to June sampling. The highest DO in July (11.66 mg L^{-1}) was at the mouth of Powell (Table 1).

Chemical Parameters

Mean total nitrogen (TN) concentrations were highest in June by far in Powell creek with the mid site having the highest TN of 742 µM while the head and mouth had concentrations of 680 µM and 311 µM, respectively. In contrast, the lowest TN concentrations were at the head of Scarboro (58.1 µM) and in Johnson Bay (59.8 µM) (Figure 6). In July, the highest TN was in Powell at both the head (795 µM) and mid (761.5 µM) while the lowest TN was in Johnson Bay (52.53 µM) (Figure 7). NH_4 concentrations ranged from 0.51 µM at both the mid and mouth of Scarboro to 2.76 µM at the head of Scarboro in June. In July, Johnson Bay displayed the lowest NH_4 concentration (0.50 µM) while the highest NH_4 concentration was 1.30 µM at the mouth of Powell (Figure 8). In both June and July, Powell consistently exhibited the highest NO_x values, by far, with concentrations ranging from 184.33 µM to 658.67 µM in June and concentrations of 184.67 to 752.33 µM in July. In contrast, the lowest NO_x values in both months were 0.32 µM in June and 0.61 µM in July at the mid of Scarboro and the mouth of Scarboro, respectively (Figure 9).

Total phosphorus (TP) was highest at the mouth of Boxiron (7.38 µM) and the mouth of Powell (7.31 µM) and lowest in Johnson Bay (2.41 µM) in June (Figure 10). In July, the mouth of Boxiron exhibited the highest TP (9.0 µM) while the lowest TP was at the mid of Powell (1.7 µM) (Figure11). The head of Powell consistently showed high concentrations of PO_4 (Figure 12) in

June (1.55 µM) and July (1.71 µM) whereas the mouth of Scarboro and Johnson Bay consistently had lower concentrations of PO_4 from June to July (0.19 to 0.42 µM at the mouth of Scarboro and 0.19 to 0.26 µM in Johnson Bay) (Table 2).

The amount of TSS increased substantially from June to July. In June, TSS were lowest at the head of Scarboro (9.33) and highest at the mouth and mid of Scarboro (164.39 and 158.12, respectively) and in Johnson Bay (158.69). In July, Johnson Bay still exhibited the highest TSS values (325.40) while the mid of Powell (22.22) had the lowest values (Figure 13). The percentage of organic volatile suspended sediments (VSS) also increased in July. In June, percent organic ranged from 22.66% (Boxiron mouth) to 92.22% (Scarboro head) while percent organic ranged from 62.75% (Scarboro mouth) to 100% (Powell mid) in July (Figure 14).

Bacterial Abundance

Enterococci were extremely abundant at all sites and the vast majority exceeded the EPA primary contact standard of 35 colonies 100 mL^{-1}. Enterococci were more abundant in June with the head of Scarboro having an abundance that was overwhelmingly the highest (6320 colonies 100 mL^{-1}) while the lowest abundance was at the mouth of Scarboro (41.1 colonies 100 mL^{-1}) (Figure 15). Although enterococci abundance was lower in July, there were 3251.1 colonies 100 mL^{-1} at the head of Powell and 1491.1 colonies 100 mL^{-1} at the middle of Powell. Johnson Bay had the lowest enterococci both months with 3 colonies 100 mL^{-1} in June and 4.4 colonies 100 mL^{-1} in July (Figure 16).

E. coli colonies were also very abundant at all sites except the mouth of Powell and well above the EPA primary contact standard of 126 colonies 100 mL^{-1}. In June *E. coli* colonies ranged from 600 colonies 100 mL^{-1} at the mid of Powell to 4013.3 colonies 100 mL^{-1} at the mid of Boxiron, although Boxiron mouth, Scarboro mid, Scarboro mouth, Powell mouth, and Johnson Bay were not enumerated due to lack of agar (Figure 17). *E. coli* abundance increased markedly in July at the head and mid of Powell to 4443.3 colonies 100 mL^{-1} and 2870 colonies 100 mL^{-1} while there were no *E. coli* colonies at the mouth of Powell (Figure 18).

Antibiotic Resistance

For both months, bacteria demonstrated the highest antibiotic resistance to oxacillin. In June (Figure 19), resistance to oxacillin ranged from 98.97% at the head of Scarboro to 100% at the mouth of Boxiron. Resistance to oxacillin was still extremely high in July (Figure 20) and the highest resistance (100%) occurred at the head of Powell. In June, the next highest resistance was to tetracycline. The only tested sites, Boxiron head, Boxiron mid, and Powell middle, demonstrated tetracycline resistance of 3.71%, 5.95%, and 11.46%, respectively. However, in July all sites exhibited 0% resistance except for Powell. There was 25% resistance to tetracycline at the mouth of Powell and only 0.5% and 0.1% resistance at the head and mid of Powell, respectively. In July, the next highest resistance was to gentamicin, although over half of the sites had 0% resistance. During this month, there was the highest resistance (25%) at the mouth of Powell. Out of all four antibiotics, bacteria exhibited the lowest resistance to ciprofloxacin during both months. In June, resistance to ciprofloxacin ranged from 0% at the mid of Boxiron, the head of Scarboro and the mid of Powell to 0.51% resistance at the head of Boxiron and 0.61% resistance at the head of Powell, although the remaining sites were not tested due to an insufficient quantity of agar. Resistance to ciprofloxacin decreased from June to July and all sites exhibited 0% resistance.

Correlations: Enterococci Abundance and Physical/Chemical Parameters

The statistical software program SAS 9.2 (SAS Institute Inc., Cary, NC) was used for comparison of the enterococci abundance and nutrient parameters For both June and July there was a negative correlation between enterococci abundance and temperature (R^2= 0.187 in June and R^2=0.491 in July) (Figure 21) as well as salinity (R^2=0.357 in June and R^2=0.651 in July) (Figure 22). There was no correlation between enterococci abundance and DO in June (R^2=.033) or July (R^2=0.014), but there was a strong positive correlation between bacterial abundance and NH_4 (Figure 23) in June (R^2=0.803) and a lower correlation in July (R^2=0.212). No correlations were observed in June between enterococci abundance and NO_x (R^2=0.001), but in July there was a slight positive correlation (R^2=0.168) (Figure 24). Finally, at the June sampling, there was no correlation between PO_4 and enterococci abundance (R^2=0.045), but there was a strong positive correlation in July (R^2=0.708) (Figure 25).

Discussion

In general, there were several differences observed between June and July samplings. Both pH and salinity increased at all sites (except for the salinity at the head and mid of Powell) in July, which is expected considering the lack of rain in July. Temperatures at all of the sites were also higher in July, reflecting the warmer temperatures as the summer progressed. TSS were also much higher in July despite the lack of rainfall which generally increases nutrient runoff and indicates uptake of nutrients into particulate matter. Most of the nutrient levels decreased in July, although Powell still demonstrated excessive NO_x values independent of rainfall. Enterococci abundances were also lower in July, except in Powell and at the mouth of Scarboro where abundances increased. Finally antibiotic resistance was lower at the majority of sites in July. Lower bacterial abundance and antibiotic resistance as well as decreased nutrient levels could be related to fertilizer application. Poultry fertilizer is applied early in the crop-growing season and consequently, lower nutrient levels and bacteria abundances could be a result of both the lack of rainfall and decreased poultry manure fertilizer concentrations.

TSS data indicates that other than the mid and mouth of Scarboro and Johnson Bay (all of which had high TSS values), suspended solids are not the primary pollutants in the tributaries. Although TSS values were much higher in July, dissolved nutrients are the likely cause of degraded water quality in the region. This indicates that high nutrient input is converted to particulate and is a possible indicator of the source of nutrients. Additionally, this also explains why the dissolved nutrients decrease at the mouth at both Boxiron and Scarboro. Therefore, dissolved nutrients from the tributaries being deposited into the bay are the primary concern.

Although most of the Coastal Bays have high levels of organic nutrients, the head and mid of Powell creek seem to have exceptionally large concentrations of inorganic nitrogen. Both the head and mid of Powell had extremely high NO_x values in excess of 600 µM for both months and the lowest organic nitrogen concentrations in June (19.44 µM head and 22.2 µM mid). These areas also had high PO_4 concentrations in both June and July, which also signify inorganic nutrient input, and high DO levels, which indicate an environment that is not organic rich. Additionally, the temperature in both the head and mid of Powell creek (a range of 18-19.6˚C for both months) was the lowest out of all of the sampling locations, which exhibited a range of 21.3-28.8˚C for both months. There was also no variation in the salinity between June and July. Considering that there was no variation following a dry or wet event, the cold temperature and stable salinity indicate a constant point-source input like groundwater. Since groundwater has long residence times, it is possible that legacy chemical fertilizer is being directly discharged into the head and mid of Powell creek and causing the lower temperatures and high inorganic concentrations as in the past δN values from this site have also been low

(O'Neil et al. 2011). In addition, the head and mid sites of Powell also exhibited high bacterial abundances and high TN. Enterococci and *E. coli* are both contaminant microbes that originate in the digestive tracts of warm-blooded animals and are not bacteria that naturally occur in these creeks, indicating a combination of pollutant sources. Therefore, the nutrients and bacteria most likely stem from animal manure fertilizer or human septic waste running off into the creek. A map on Google Earth reveals several large pools of water near the head of Powell that are being aerated and are open to the atmosphere (Figure 26). The adjacent residential area, Captain's Cove was constructed in the 1970s and included an old sewage plant, which was used to irrigate the golf course. The community was scheduled to switch from a septic system to a sewer system, but the change has never happened since the development has gone bankrupt and instead, the old pools of sewage remain inactive. Therefore, the Captain's Cove sewage facility may best explain the high nutrients and bacterial abundance while groundwater input best explains the unchanged temperature and salinity.

The mouth of Powell contrasts entirely from both the head and mid of Powell in that it is not dominated by NO_x and PO_4. The mouth of Powell exhibited low PO4 concentrations and significantly lower NOx concentrations in comparison to the head and mid of Powell. The mouth is generally well flushed and tidally influenced which could account for the significantly lower NO_x and PO_4 concentrations. There was also an extremely high organic nitrogen concentration in June and thus, shows a very high organic load to the system. The mouth also exhibited high TN and TP, which indicate a nutrient rich environment. In addition, the temperature in this site was higher than the head and mid and, combined with the organic nutrient loading, indicates potential organic input from fertilizer runoff from agricultural farms. The mouth of Powell exhibited the highest DO of all of the sites and demonstrated some of the lowest contaminant bacterial abundance, both enterococci and *E. coli*. Low concentrations of ambient bacteria could explain the high DO while it is possible that the increased flushing at the mouth (in comparison to both the head and mid) could be the reason that fecal bacteria abundance is lower than the other two sites at Powell Creek. Another possibility is that fecal contaminants are unable to survive the transit down the creek and therefore, concentrations of fecal bacteria are lower at the mouth.

Scarboro Creek is also divided into different nutrient hotspots. The head of Scarboro is fueled by direct runoff and is largely affected by rainfall because in July, after a prolonged dry period, the head was completely dry. This site had high NH_4 values that imply nitrogenous waste input and it is likely that rain caused animal waste from a farm directly adjacent to this site to directly flow into the head of Scarboro. Microbial contaminants were also extremely prevalent with high abundances of both enterococci and *E. coli*. These bacteria also suggest waste input from animal manure and support the conclusion that the head is fueled by animal waste. Conversely, there were low TN and TP values in comparison to the other sites, but values are still higher than standard. Hence, although this site did not have the highest TN or TP values, nutrient levels are still high and those present likely emanate from animal sources.

The mid and mouth of Scarboro are both very rich in organic nutrients. Both sites had high organic nitrogen as well as very low NH_4, NO_x, and PO_4 values, which indicate a lack of inorganic nutrients. Thus, the mid and mouth sites of Scarboro are high organic environments. However, there were low abundances of both types of fecal bacteria at both study sites. Consequently the mid and mouth of Scarboro have an abundance of organic nutrients, but they do not necessarily stem from animal manure runoff. If animal runoff were the primary cause, both enterococci and *E. coli* abundances would be higher. Total suspended solids were also very high in both June and July in comparison to the other sites. High TSS combined with low

NH_4, NO_x, and PO_4 values suggests that there is more sediment than dissolved solids at the mid and mouth of Scaboro.

The head of Boxiron had an extremely low DO combined with high organic nitrogen, TP, and PO_4. Low DO can be a result of high organic nutrient loading and high bacterial respiration, but considering the comparatively lower nutrient levels, it is likely that there are high levels of ambient microbes in the system. The high TP and PO_4 levels also support this conclusion because phosphorus promotes bacterial growth and the large amounts of respiration by ambient bacteria could also be the cause of the low DO. The head of Boxiron also had extremely high contaminant bacterial abundance, particularly for enterococci abundance. These contaminant bacteria likely come from organic inputs from fertilizers considering the high organic nitrogen and inorganic PO_4, which are indicators of human or animal waste.

The mid and mouth of Boxiron are characterized by high PO_4 and high TP. These sites also had lower enterococci abundances in comparison to the head of Boxiron, but still had abundances well over the EPA primary contact standard. In comparison to the head of Boxiron, the mid and mouth had a significantly larger *E. coli* abundance. High levels of phosphorus support microbial growth; therefore, the phosphorus rich water supports a suitable environment for these contaminant bacteria. Sewage, either human or animal, could be causing the high PO_4 values.

In contrast to the three tributaries, low nutrient levels and low bacterial abundance characterized Johnson Bay. Johnson Bay is well mixed as a result of tidal exchange and lacks the direct nutrient input found in the tributaries. Although Johnson Bay had lower nutrient levels and a lower microbial contaminant concentration, declining water quality is still problematic considering the extremely high TSS values and high *E. coli* abundance as well as the relatively high NO_x and TN values. The declining water quality is likely the result of the tributaries depositing nutrient laden water and particulate matter into the bay. Furthermore, the shallow water and wind-drive resuspension of sediment could cause a decrease in water quality in Johnson Bay.

An overall comparison of the creeks indicates that nutrient sources are focused in Powell and Scarboro and Boxiron do not have as large an impact on Johnson Bay in comparison to Powell. Nutrient levels and bacterial abundances decreased at the mouth in both Scarboro and Powell while both of these parameters were much higher at the mouth of Powell. Considering Powell has higher nutrient and bacteria concentrations, it seems to deposit more contaminants into Johnson Bay.

Finally, one of the objectives of the study was to assess antibiotic resistance using a chromogenic agar. Although the method proved successful and it was possible to calculate resistance, the data proved to be inconclusive. Bacterial resistance was used as an indicator to potentially identify the sources of nutrient pollution based on the idea that certain antibiotics are used in poultry farming for growth promotion while others are used on humans to treat bacterial infections. The four antibiotics based on their physical properties as well as their usage on either poultry or humans. However, the chosen antibiotics are not specific to either humans or poultry and it is plausible that these antibiotics are used in both poultry farming and treating human infections with the exception of gentamicin, which is solely used on animals. Therefore, assessing resistance was inconclusive because it did not clarify the difference between human and animal microbial contaminants. Despite this, it is possible to draw several conclusions. Oxacillin exhibited the highest resistance in all sites and demonstrated 100 percent resistance in several sites. In comparison to 2010 and 2011 (Figure 5), oxacillin resistance was comparable

while ciprofloxacin and gentamicin decreased markedly. Ciprofloxacin exhibited 0 percent resistance in both months and even though gentamicin resistance was 25 percent in July at the mouth of Powell, the highest resistance was over 60 percent in 2010 and 2011. Resistance to tetracycline increased the most, as was hypothesized, from 0 percent in 2010 and 2011 to 11.46 percent in June and 25 percent in Powell in July. Resistance was not site specific although the head of Boxiron and the mid of Powell had the highest oxacillin while the mid of Powell also exhibited the highest tetracycline resistance. Finally, the mouth of Powell showed the highest resistance to gentamicin. Although this data does not decisively identify the difference between human and animal contaminants, the information is still useful for awareness about human health hazards for both recreational purposes and the safety of food sources. In addition, these results demonstrate broad spectrum antibiotic resistance to commonly used antibiotics, like oxacillin.

Conclusions

In conclusion, nutrient levels and bacterial abundances differed at spatial and temporal scales, but all physical and biological measurements were high and most were above EPA standards. Despite this, nutrient sources are mostly focused in Powell Creek while comparatively; Boxiron and Scarboro are not depositing as many pollutants into Johnson Bay. The physical, chemical, and biological parameters show that Powell Creek has high nutrients and contaminant bacteria and spatial mapping indicates Captain's Cove sewage facility as the source. Additionally, a modified chromogenic agar is efficacious for assessing antibiotic resistance. Although the antibiotic resistance data did not identify the source of contaminants, it did indicate high resistance to ordinary antibiotics.

Further research should be conducted focusing on groundwater and stable isotope analysis in order to determine whether nutrients and contaminant bacteria originate from the Captain's Cove sewage facility as hypothesized or from poultry manure runoff. In addition, future studies using antibiotic resistance as an indicator should use an array of antibiotics that are more specific to either humans or animals in order to better determine the source of nutrients.

Acknowledgments

I would like to thank Maryland Sea Grant, The National Science Foundation, and the Maryland Coastal Bays Program for providing funding for this project. I would like to thank my mentor, Dr. Judy O'Neil for her invaluable support, dedication, and enthusiasm for my project. I would also like to thank Horn Point Laboratory for providing me with the necessary facilities. I want to acknowledge both Dr. Fredrika Moser and Dr. Mike Allen from Maryland Sea Grant for making this incredible REU experience possible. Finally, I would like to thank Simon Costanzo for his help with sampling in the field and guidance through the presentation of my project.

References

Arar, E.J., and G.B. Collins. 1997. Method 445.0: *In Vitro* Determination of Chlorophyll *a* and Pheophytin *a* in Marine and Freshwater Algae by Fluorescence. Washington, D.C.: US-EPA.

Azam, F., T. Fenchel, J.G. Field, J.S. Gray, L.A. Meyer-Reil, and F. Thingstad. 1983. The Ecological Role of Water-Column Microbes in the Sea. Marine Ecology Progress Series 10:257-263.

Beckert, K., B. Fertig, J. O'Neil, T. Carruthers, C. Wazniak, B. Sturgis, M. Hall, A. Jones, and W. Dennison. 2008. Fine scale patterns of water quality in three regions of Maryland's Coastal Bays: assessing nitrogen source in relation to land use. Cambridge, MD: IAN Press.

Beckert, K.A. 2008. Watershed land use and nutrient dynamics in Maryland Coastal Bays, U.S.A. University of Maryland, College Park.

Correll, D.L. 1998. The role of phosphorus in the eutrophication of receiving waters: A review. Journal of Environmental Quality 27:261-261.

Dennison, W.C., J.E. Thomas, C.J. Cain, T.J.B. Carruthers, M.R. Hall, and R.V. Jesien, 2009. Shifting Sands: Environmental and cultural changes in Maryland's coastal bays. Cambridge, MD: IAN Press.

Fertig, B., T.J. Carruthers, C. Wazniak, B. Sturgess, M. Hall, A.B. Jones, and W.C. Dennison. 2006. Water quality in four regions of the Maryland Coastal Bays: Assessing nitrogen source in relation to rainfall and brown tide. Cambridge, MD: IAN Press.

Fertig, B., T.J. Carruthers, W.C. Dennison, A.B. Jones, F. Pantus, and B. Longstaff. 2009. Oyster and Macroalgae Bioindicators Detect Elevated δ15N in Maryland's Coastal Bays. Estuaries and Coasts 32:773-786.

Food Marketing Institute. Low-Level Use of Antibiotics in Livestock and Poultry. Washington, D.C.:Food Marketing Institute.

Hein, I., C. Schneck, M. Knogler, G. Feierl, P. Pless, J. Kofe, R. Achmann, and M. Wagner. 2003. *Campylobacter jejuni* isolated from poultry and humans in Styria, Austria: epidemiology and ciprofloxacin resistance. Epidemiology and Infection 130:377-386.

Joseph, S.W., J.R. Hayes, L.L. English, L.E. Carr, and D.D. Wagner. 2001. Implications of multiple antimicrobial-resistant enterococci associated with the poultry environment. Food Additives and Contaminants 18:1118-1123.

Keiger, D. 2009. Farmacology. Johns Hopkins Magazine. Baltimore, MD.

MacNeil, J.D. and L. Cuerpo. 1995. Gentamicin. In: Residues of some veternary drugs in aminals and foods FAO food and nutrition paper 41/7, 45-55. Food and Agriculture Organization.

Mallin, M.A., S.H. Ensign, M.R. McIver, C. Shank, and P.K. Fowler. 2001. Demographic, landscape, and meteorological factors controlling the microbial pollution of coastal waters. Hydrobiologia 460:185-193.

O'Neil, J.M., B. Fertig, K. Studholme, A.K. Leigh. 2011. Cryptic nitrogen sources in Johnson Bay. Report to Maryland Coastal Bays, Berlin, MD.

Regal, R. 2002. Resistant Microbes, Antibiotic Abuse, and the Threat to Public Health. Speech presented at the University of Michigan, Ann Arbor, MI.

Sayah, R.S., J.B. Kaneene, Y. Johnson, and R. Miller. 2005. Patterns of antimicrobial resistance observed in escherichia coli isolates obtained from domestic- and wild-animal samples, human septage, and surface water. Applied and Environmental Microbiology 71:1394-1404.

Singer, R.S. and C.L. Hofacre. 2006. Potential impacts of antibiotic use in poultry production. Avian Diseases 50:161-172.

Urbina, I. 2008. In Maryland, focus on poultry industry pollution. The New York Times.

US-EPA. 1997. Volunteer Stream Monitoring: A Methods Manual. Washington, D.C.: US-EPA.

US-EPA. 2002. Method 1106.1: Enterococci in water by membrane filtration using membrane-enterococcus-esculin iron agar (mE-EIA). Washington, D.C.: US-EPA.

Watkinson, A.J., G.R. Micalizzi, J.R. Bates, and S.D. Costanzo. 2007. Novel method for rapid assessment of antibiotic resistance in *Escherichia coli* Isolates from environmental waters by use of a modified chromogenic agar. Applied and Environmental Microbiology 73:2224-2229.

Wazniak, C.E., M.R. Hall, T.J.B. Carruthers, B. Sturgis, W.C. Dennison, and R.J. Orth. 2007. Linking water quality to living resources in a Mid-Atlantic lagoon system, USA. Ecological Applications 17:S64-S78.

Figures and Tables

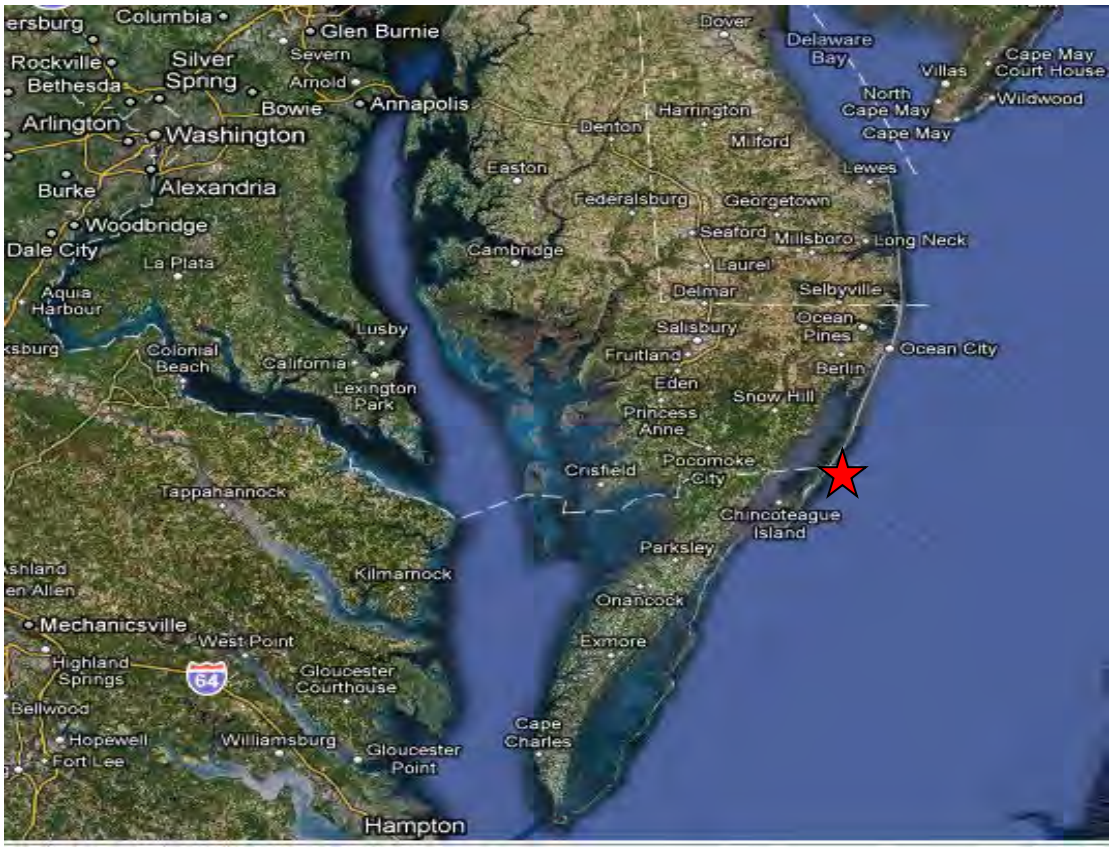

Figure 1. Maryland coastal bays in relation to the Chesapeake Bay region. The star denotes Johnson Bay. Image credit: Google Maps.

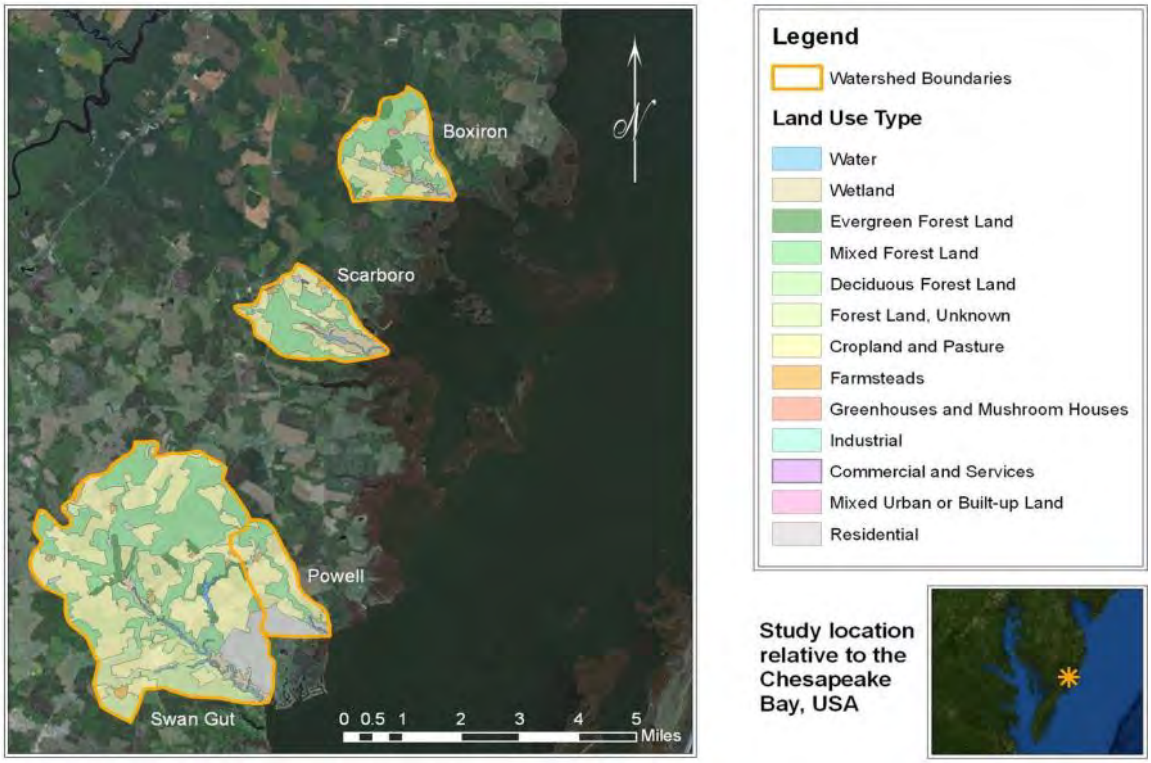

Figure 2. Boxiron, Scarboro, and Powell Creeks study locations in the Johnson Bay area (Studholme 2011).

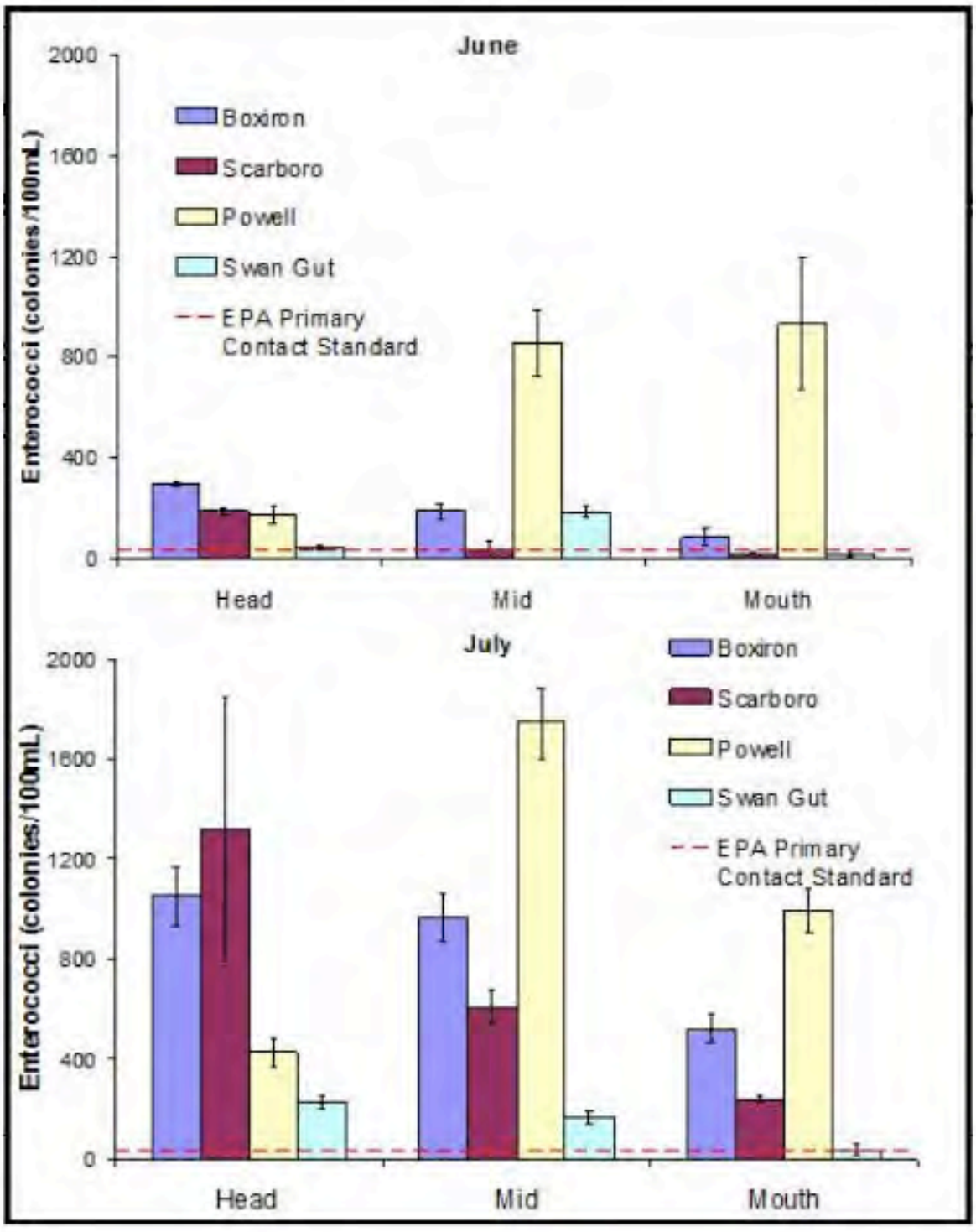

Figure 3. Total enterococci for June and July 2010 at the head, mid, and mouth of creeks emptying into Johnson Bay. Sampling in June followed a dry period while sampling in July followed a rain event. Powell exhibits highest enterococci counts (Studholme 2010).

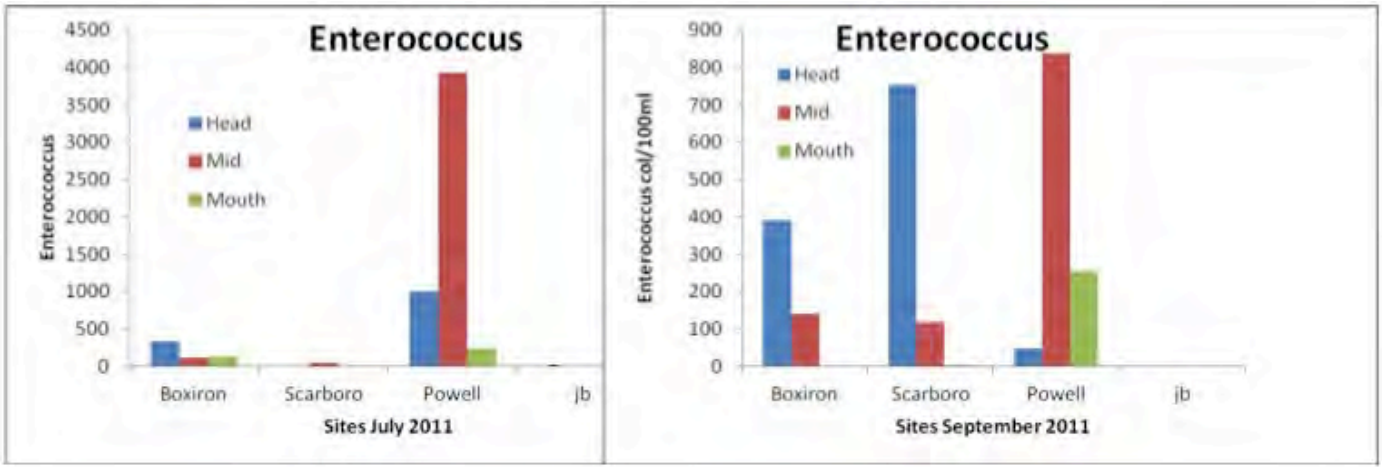

Figure 4. Total enterococci for July and September 2011 at the head, mid, and mouth of creeks emptying into Johnson Bay. September sampling followed Hurricane Irene. Similar to summer 2010, Powell exhibits the highest enterococci counts (O'Neil et al., 2012).

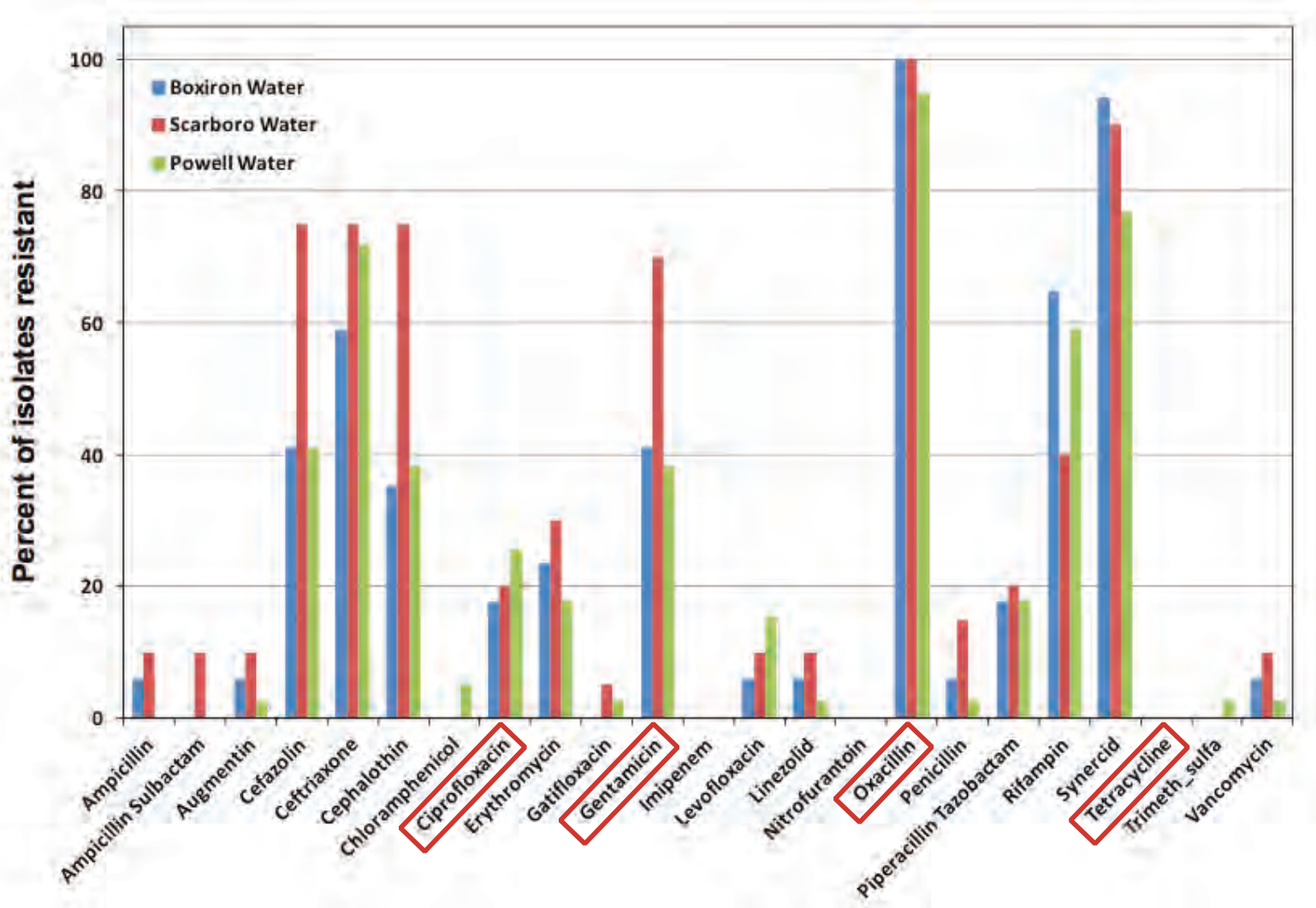

Figure 5. Results from Antimicrobial Resistance Patterns of Enterococcus in Johnson Bay for 2010 and 2011 shows a high percentage of antimicrobial resistance for several antibiotcs. Antibiotics circled in red indicate tested antibiotics (A.K. Leight unpublished data).

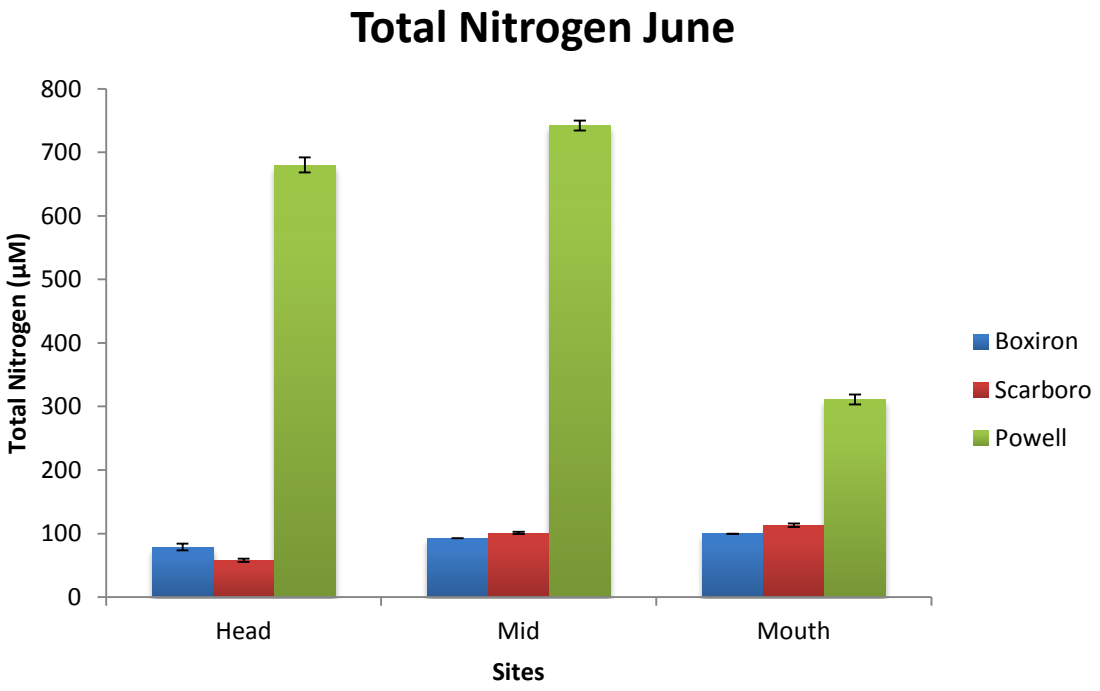

Figure 6. Total nitrogen in June at sampling locations along the three tributaries.

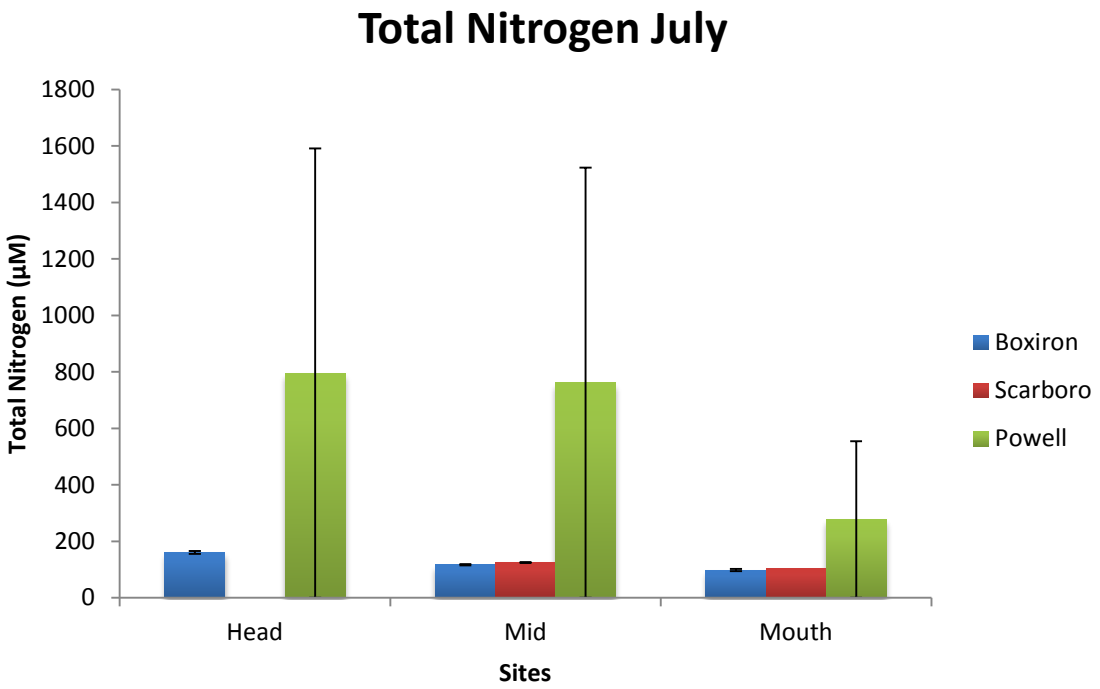

Figure 7. Total nitrogen in July at sampling locations along the three tributaries.

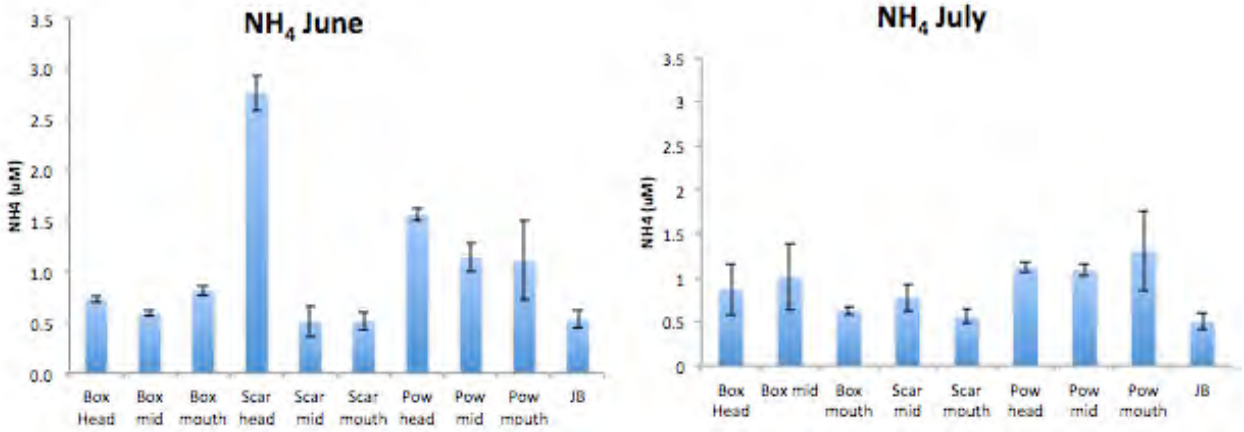

Figure 8. NH_4 concentrations in June and July at sampling locations along the three tributaries.

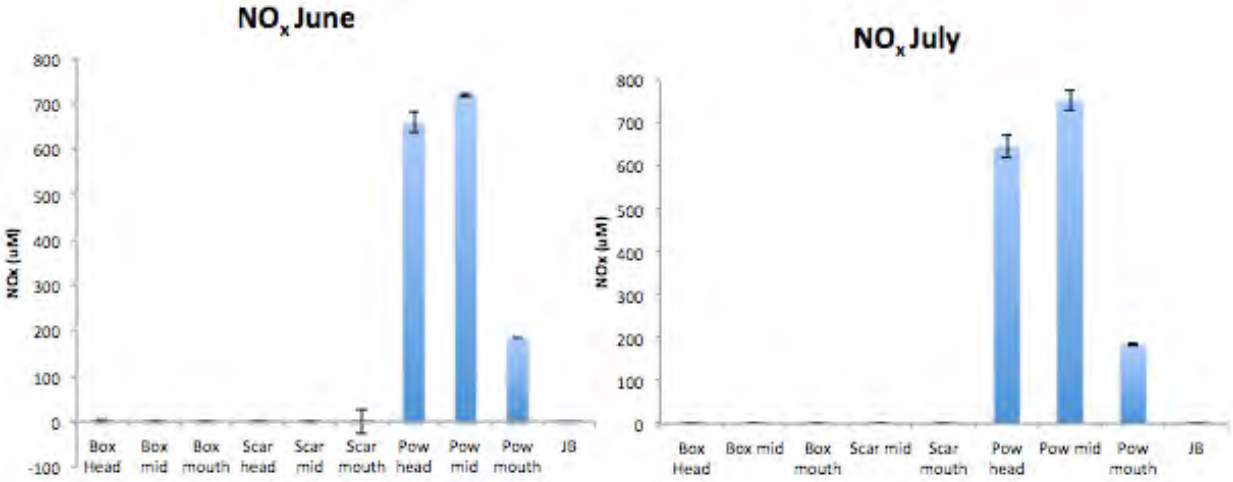

Figure 9. NO_x concentrations in June and July at sampling locations along the three tributaries.

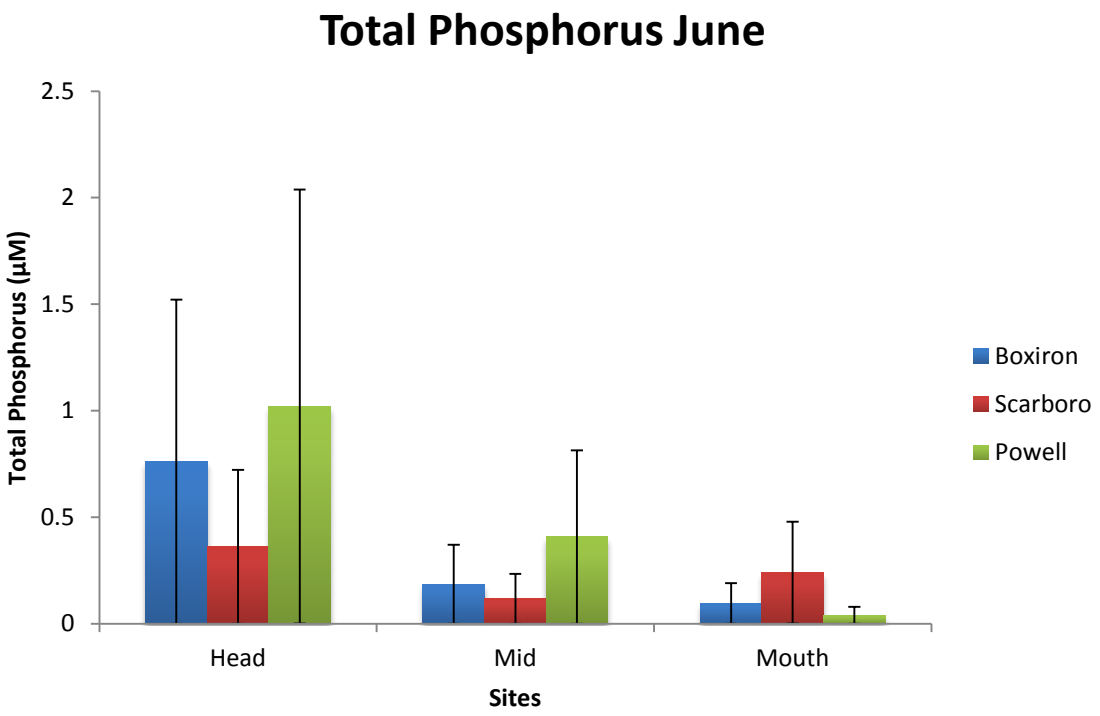

Figure 10. Total phosphorus in June at sampling locations along the three tributaries.

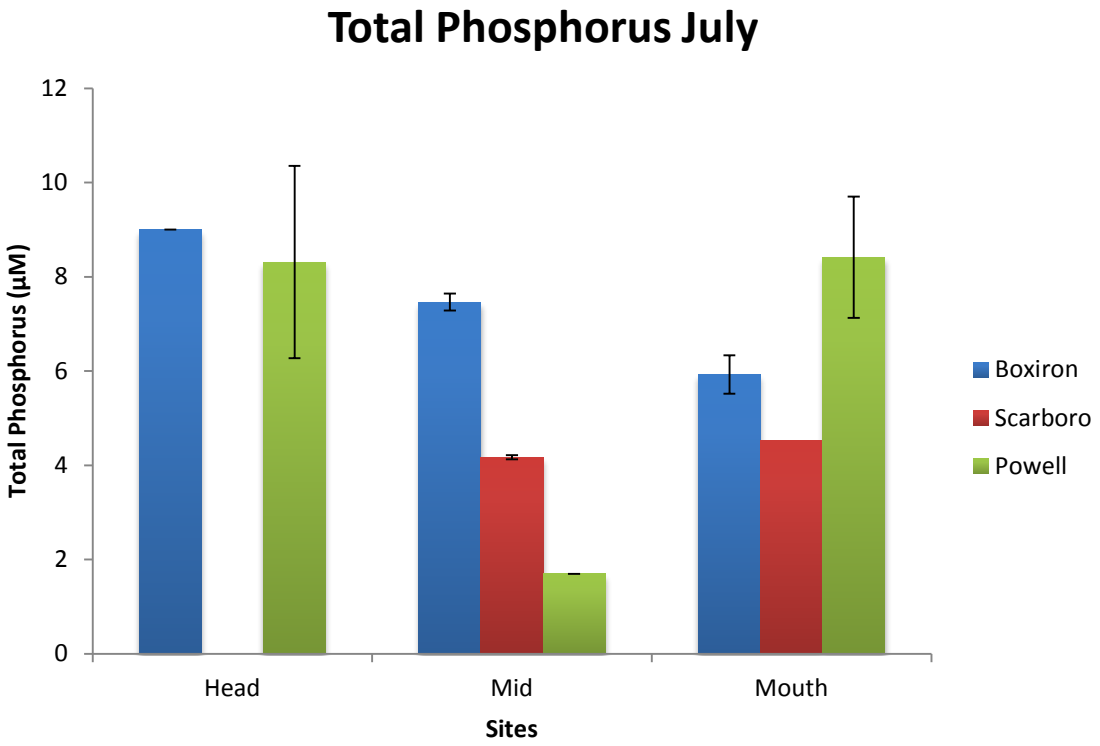

Figure 11. Total phosphorus in July at sampling locations along the three tributaries.

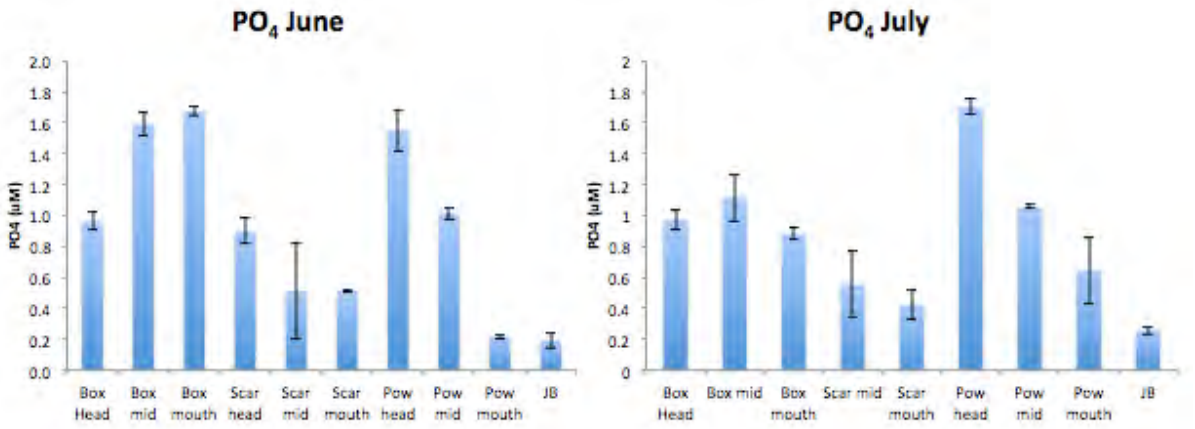

Figure 12. PO_4 concentrations in June and July at sampling locations along the three tributaries.

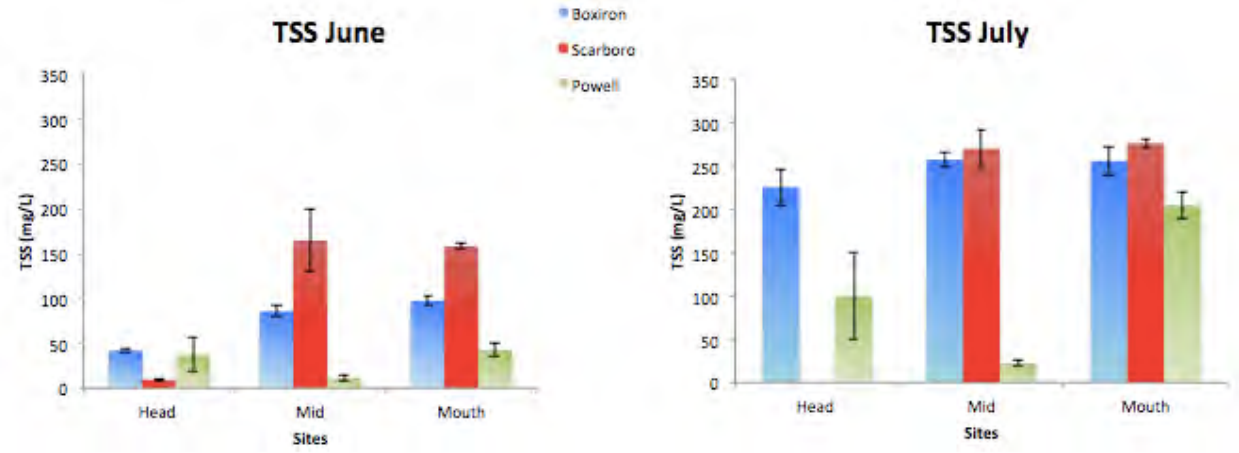

Figure 13. Total suspended solids (TSS) in June and July at sampling locations along the three tributaries.

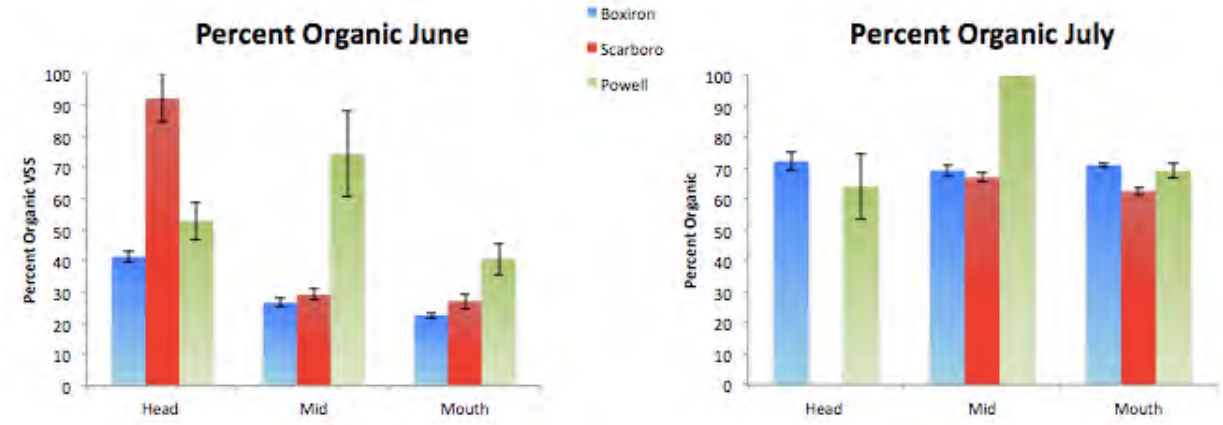

Figure 14. Percent organic volatile suspended sediments (VSS) in June and July at sampling locations along the three tributaries.

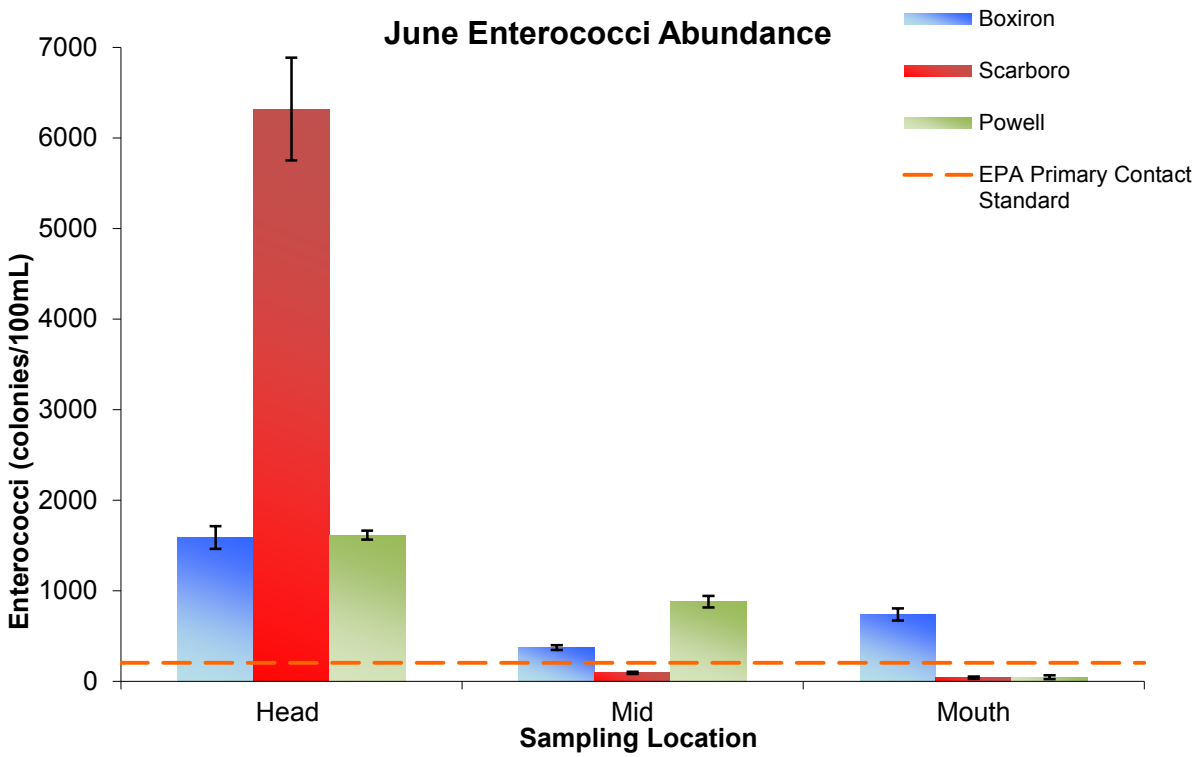

Figure 15. Enterococci abundance in June at sampling locations along the three tributaries.

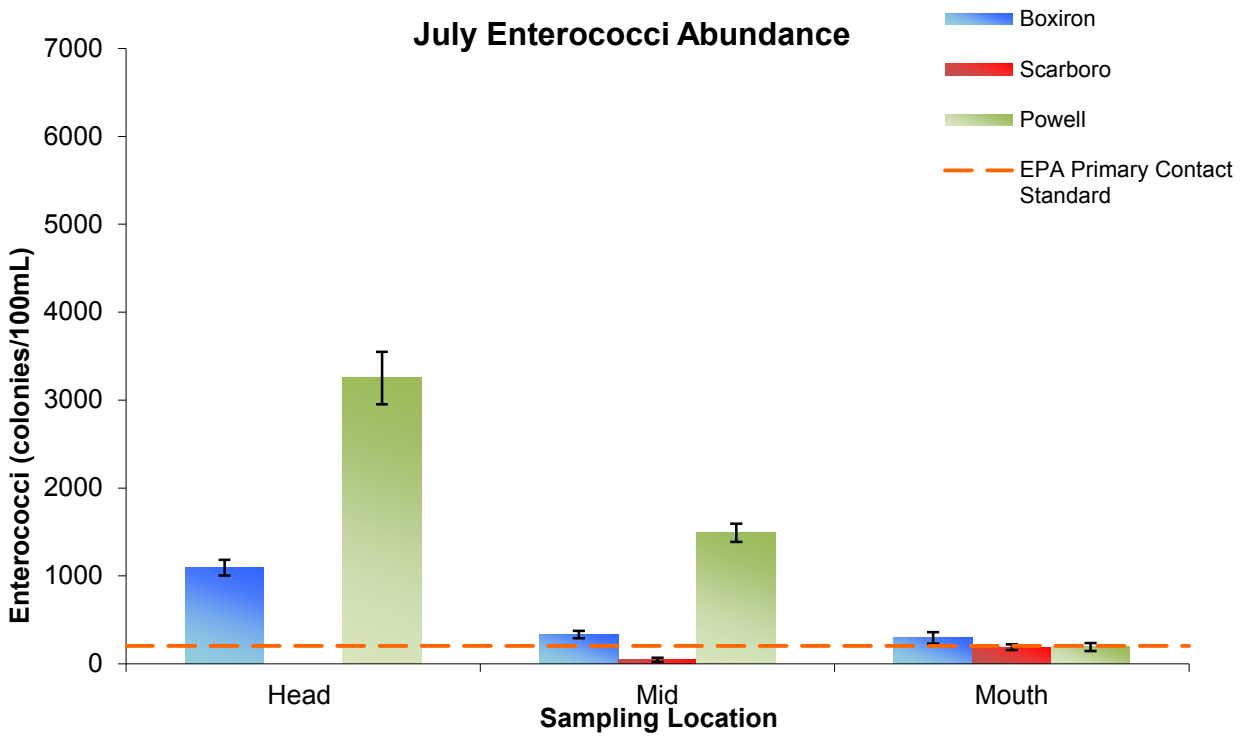

Figure 16. Enterococci abundance in July at sampling locations along the three tributaries.

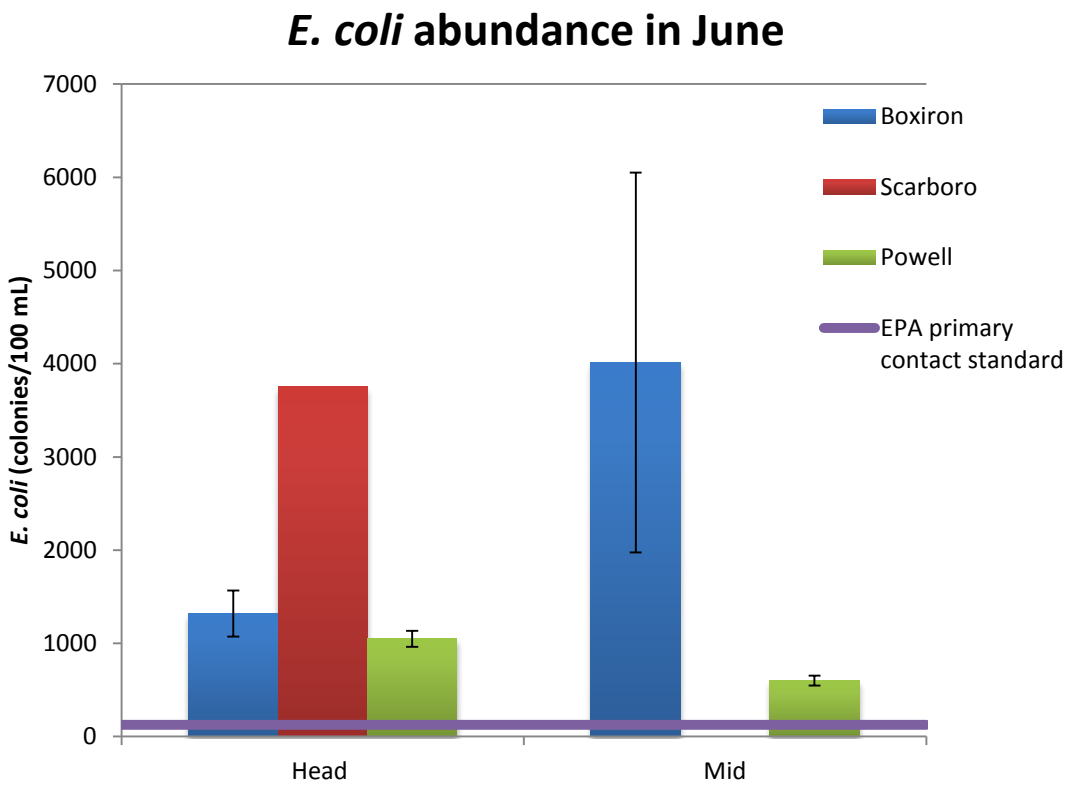

Figure 17. *E. coli* abundance in June at sampling locations along the three tributaries.

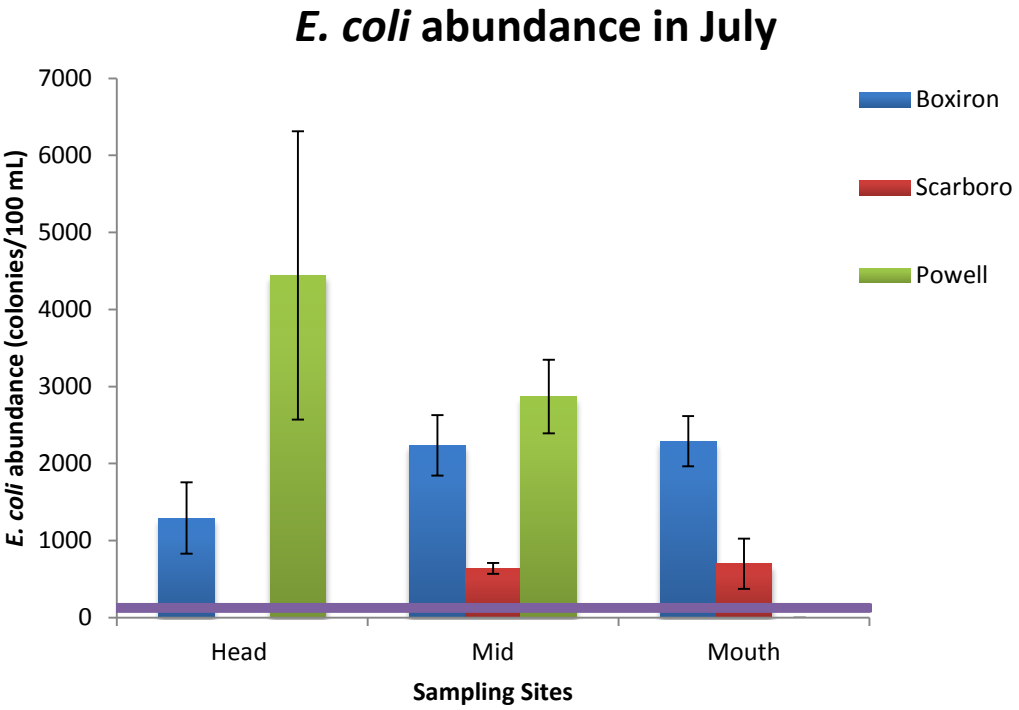

Figure 18. *E. coli* abundance in July at sampling locations along the three tributaries.

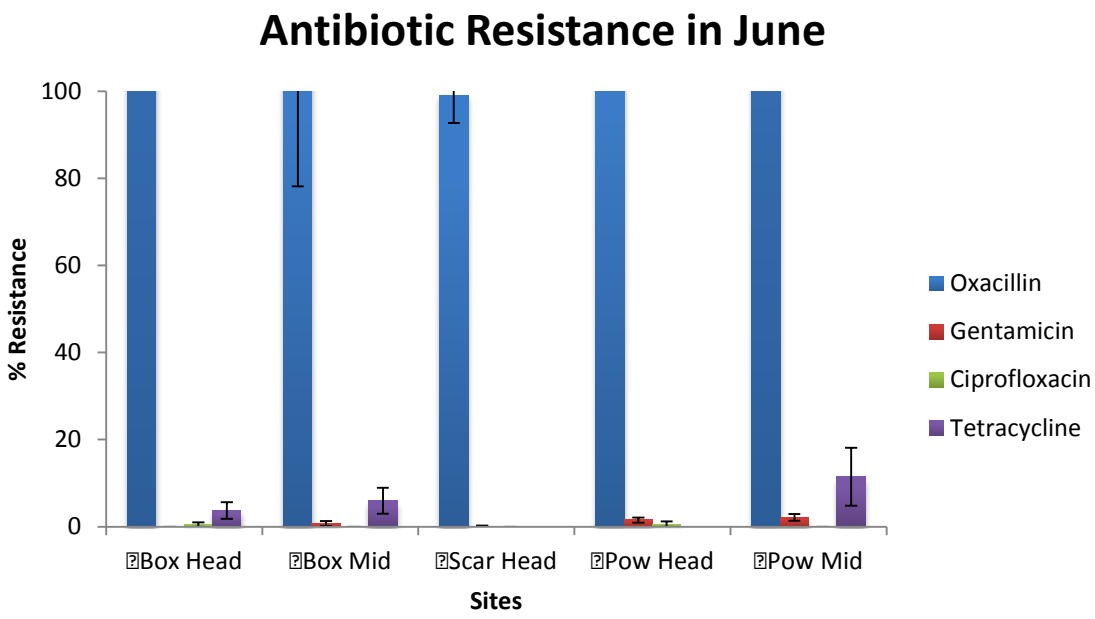

Figure 19. Antibiotic resistance of four antibiotics at sampling locations along the three tributaries in June.

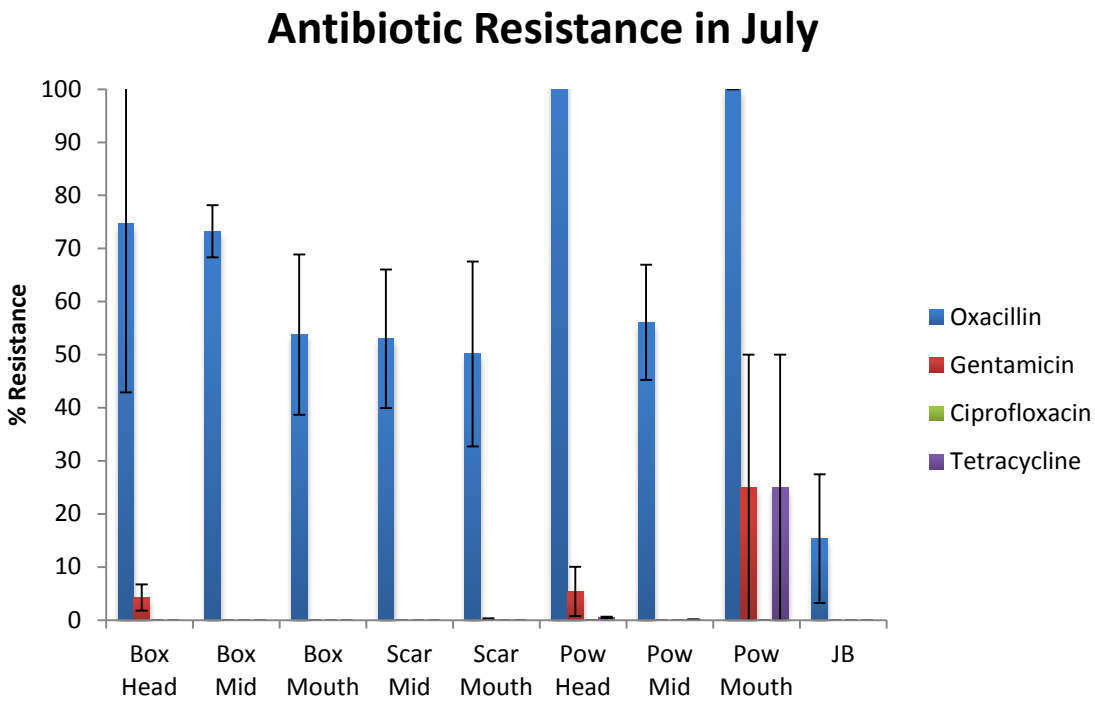

Figure 20. Antibiotic resistance of four antibiotics at sampling locations along the three tributaries in July.

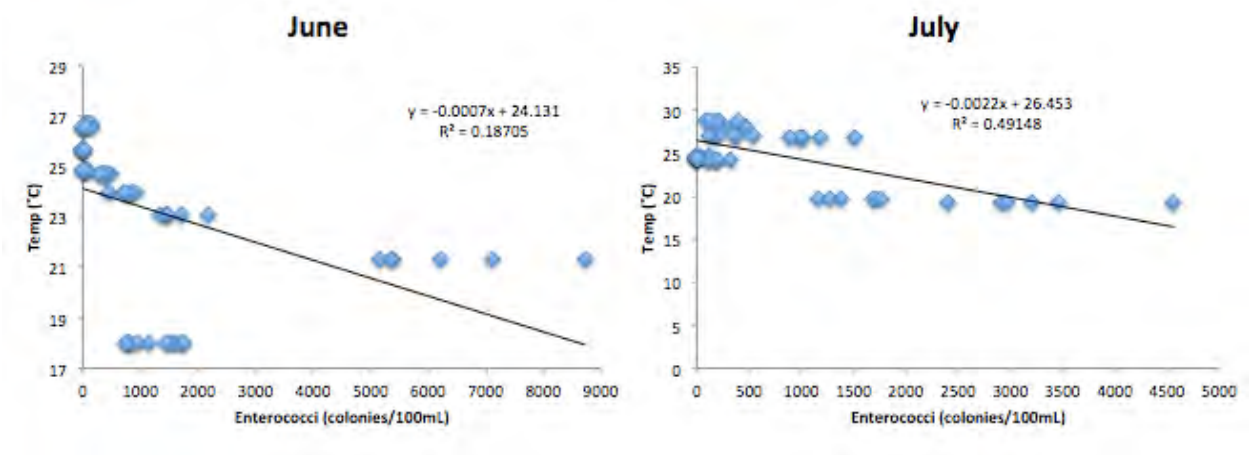

Figure 11. Negative correlation between enterococci abundance and temperature in June (p=.00056) and no correlation in July (p=3.57e -09).

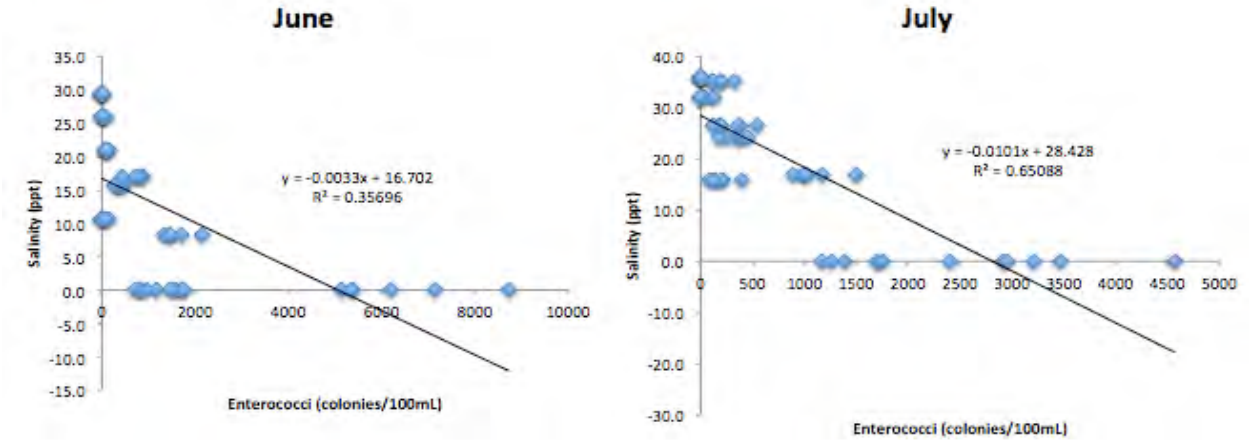

Figure 22. Negative correlation between enterococci abundance and salinity observed in June (p=4.66e -07) and July (p=1.71e -13).

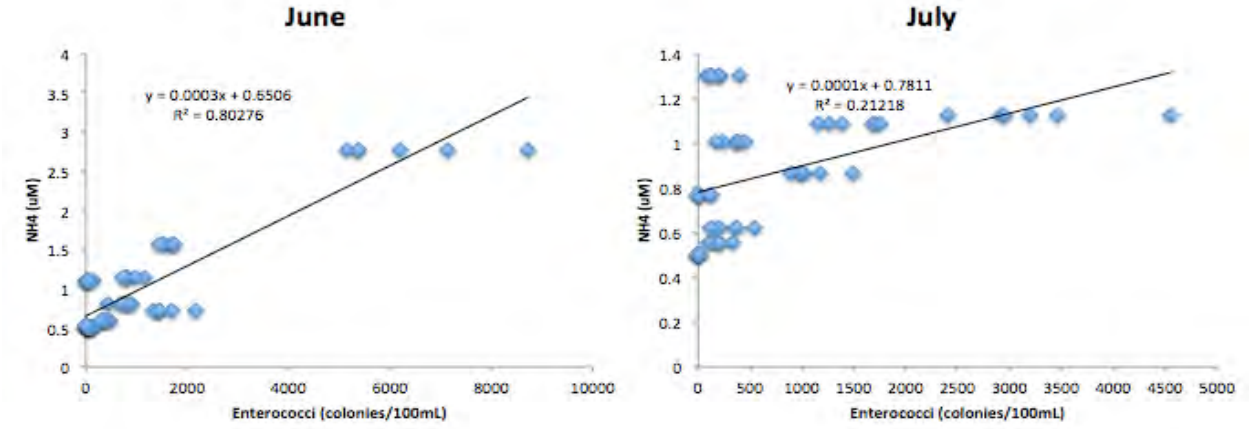

Figure 23. Positive correlation between enterococci abundance and NH4 in June (p<.001) but not in July (p=0.0003).

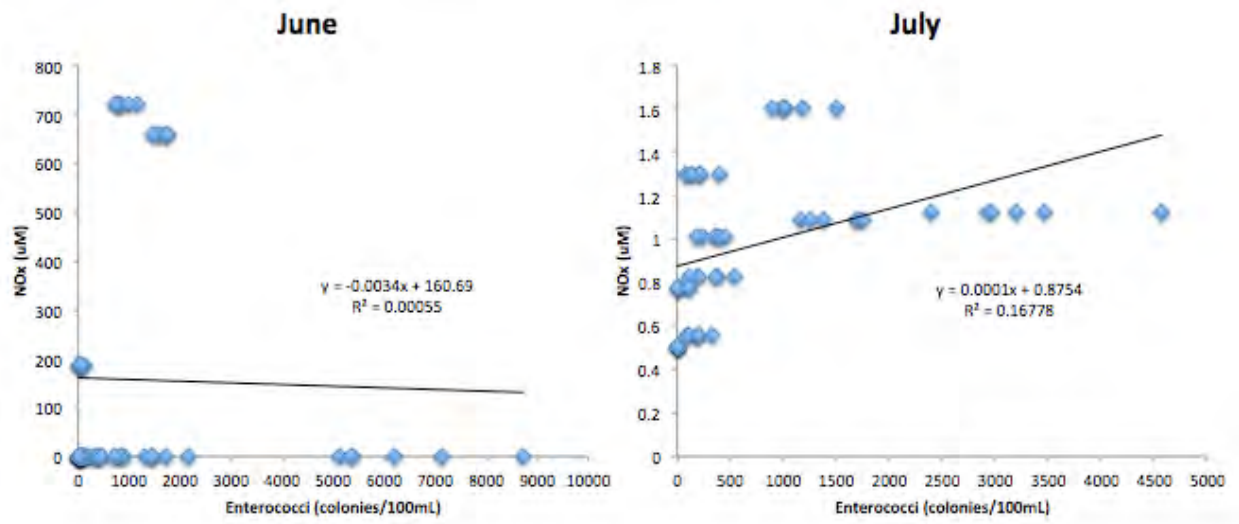

Figure 24. Enterococci abundance and NOx were not correlated in June ($p>0.05$), while there was a positive correlation in July ($p<0.001$).

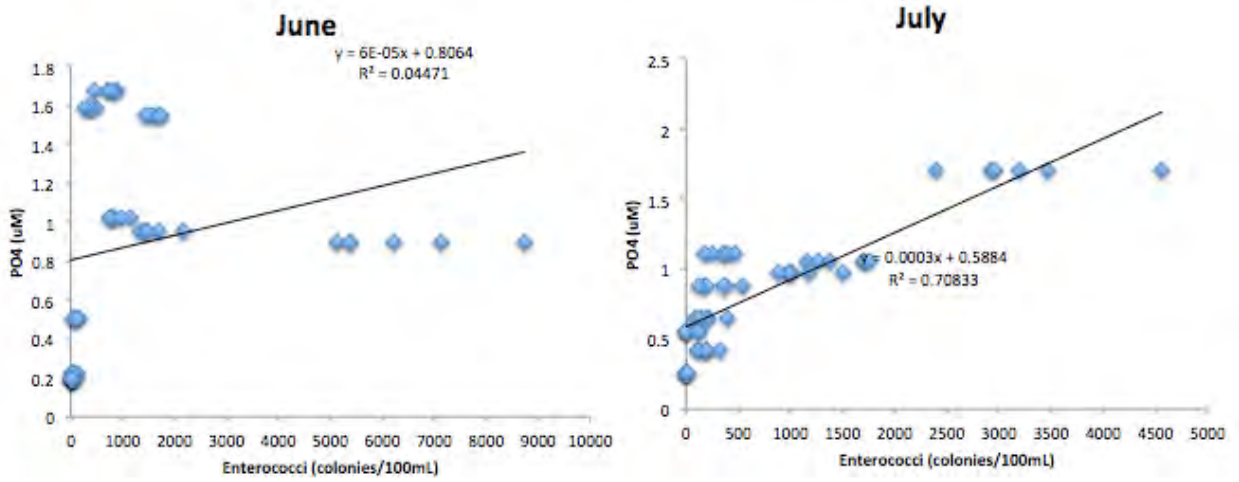

Figure 25. There was a positive correlation between enterococci abundance and PO4 in June ($p<0.0001$) and July ($p<0.0001$).

Figure 26. Google Earth image of the land surrounding Powell Creeks reveals several large pits of water that appear similar to a sewage facility (circled in red).

Table 1. Physical data from surface water samples at different locations in June and July.

Date	Creek	Site	Temperature (˚C)	Salinity	pH	DO (mg/L)	DO%
June 26	Boxiron	Head	23.1	8.3	6.0	3.5-3.3	43-41
		Mid	24.7	15.6	6.5	5.10	66
		Mouth	24.0	16.9	6.5	4.37	56.5
	Scarboro	Head	21.3	0.1	5.0	5.10	54.8
		Mid	26.7	21.0	6.5	4.50	67.5
		Mouth	24.9	26.1	6.5	5.27	73.5
	Powell	Head	18.0	0.1	--	9.46	96.3
		Mid	18.0	0.1	6.0	10.49	97.6
		Mouth	26.6	10.7	7.0	15.8-16.2	200.0
	Johnson Bay		25.7	29.5	7.0	5.65	82.5
July 25	Boxiron	Head	26.9	16.8	6.9	0.52-0.41	6.0
		Mid	28.0	24.0	7.4	5.50	75.4
		Mouth	27.0	26.4	7.2	2.33	33.3
	Scarboro	Head	--	--	--	--	--
		Mid	24.6	32.2	7.5	5.50	66.7
		Mouth	24.3	35.1	7.6	5.60	65.1
	Powell	Head	19.2	0.1	7.8	7.68	84
		Mid	19.6	0.0	7.6	7.39	80.9-40.4
		Mouth	28.8	15.7	8.3	11.66	163.8
	Johnson Bay		24.5	35.8	8.1	5.10	58.4

Table 2. Chemical data from surface water samples at different locations in June and July.

Date	Creek	Site	NH4 (µM)	NOx (µM)	PO4 (µM)	TN (µM)	TP (µM)	Organic N (µM)
June 26	Boxiron	Head	0.73	0.98	0.96	79	6.44	77.29
		Mid	0.59	1.12	1.59	92.6	7.19	90.9
		Mouth	0.81	0.42	1.68	99.6	7.38	98.33
	Scarboro	Head	2.76	1.19	0.90	58.1	3.42	54.1
		Mid	0.51	0.32	0.51	101	4.17	100.10
		Mouth	0.51	0.46	0.19	113	4.01	112.4
	Powell	Head	1.56	658.67	1.55	680	5.51	19.44
		Mid	1.14	719.00	1.02	742	2.46	22.2
		Mouth	1.11	184.33	0.22	311	7.31	125.89
	Johnson Bay		0.53	0.35	0.19	59.8	2.41	58.9
July 25	Boxiron	Head	0.87	1.60	0.97			
		Mid	1.01	1.01	1.12			
		Mouth	0.62	0.83	0.88			
	Scarboro	Head	--	--	--	--	--	--
		Mid	0.77	0.67	0.55			
		Mouth	0.56	0.61	0.42			
	Powell	Head	1.12	645.00	1.71			
		Mid	1.09	752.33	1.06			
		Mouth	1.30	184.67	0.65			
	Johnson Bay		0.50	0.62	0.26			

Diurnal Variations in N_2O Fluxes from Agricultural Fields

Mohamed Sackor, REU Fellow
Maryland Sea Grant

Dr. Thomas Fisher, Professor
Horn Point Laboratory, University of Maryland Center for Environmental Science

Dr. Rebecca Fox, Assistant Research Scientist
Horn Point Laboratory, University of Maryland Center for Environmental Science

Abstract

Nitrous oxide (N_2O) is a greenhouse gas and a stratospheric ozone depletor produced by denitrification and nitrification. Agriculture is an important source of N_2O. For my project, I looked at changes in N_2O fluxes over the course of the day to evaluate whether time of day matters to sampling. Static soil chambers were used to measure the fluxes. Low positive and negative fluxes were measured during a 10 hour sampling in a corn field, but fluxes were only significantly above or below zero for 50 percent of the measured fluxes. In a longer 24 hour sampling N_2O fluxes were below detection for the entire 24 hour period. I was unable to determine if a diurnal flux cycle existed because fluxes were typically undetectable. The low to non-existent fluxes are likely due to extremely low soil moisture and high soil temperatures.

Keywords: Denitrification, Nitrification, Nitrous oxide (N_2O), Moisture

Introduction

Nitrous oxide (N_2O) is a greenhouse gas that is soluble in water. It is a colorless, non-toxic gas, and a stratospheric ozone depletor (Galloway et al. 2003). N_2O is approximately 320 times more powerful than carbon dioxide as a greenhouse gas and can last for up to 120 years in the atmosphere (IPCC 2007). N_2O is produced in the soil through the processes of nitrification and denitrification and diffuses out to the atmosphere.

N_2O has two main effects in the atmosphere. The first effect of nitrous oxide is to react with ozone, a gas in the stratosphere which protects the planet from ultra-violet light. The reaction between N_2O and ozone destroys the ozone layers and allows the flow of ultra-violet light to the earth's surface which is dangerous for human beings and plants (Sey et al. 2008). The second effect of N_2O is to accumulate in the lower atmosphere which tends to increase absorption of infra-red emissions from the earth, contributing to global warming (Sey et al. 2008).

N_2O is a product of the earth's nitrogen cycle (Figure 1). Nitrogen gas (N_2) comprises 78% of the gas in the atmosphere (Canfield et al. 2010), but only dissolved inorganic forms can

be utilized by plants and animals. Nitrogen compounds are found in proteins, amino acids, and nucleic acids, and nitrogen is extremely important to both animals and plants. The nitrogen cycle has three main steps: fixation, nitrification, and denitrification.

Fixation is the process in which N_2 is converted to ammonia (NH_3, Figure 1). Fixation requires considerable energy to break the triple bonds between the two nitrogen atoms (Canfield et al. 2010); and fixation can be atmospheric, biological, or industrial (Figure 1). Atmospheric fixation occurs by lightning, and biological fixation occurs through a symbiotic relationship between plants and microbes in the soil. Industrial fixation is the Haber-Bosch chemical process which is used to manufacture fertilizers under great pressure and temperature.

Nitrification is the biological oxidation of ammonia (NH_3) in the presence of oxygen to nitrate (Figure 2, Wrage et al.2001). Nitrification can be broken into two steps: ammonia oxidation and nitrite oxidation. Ammonia oxidation is the process that oxidizes ammonia to hydroxylamine in the presence of mono-oxogenase; hydroxylamine is then oxidized to nitrite in the presence of oxido-reductase. Nitrite oxidation is the process that oxidizes nitrite to nitrate in the presence of oxido-reductase (Figure 2). The microbes involved are *Nitrosomonas* and *Nitrobacter*. *Nitrosomonas* oxidizes ammonium to nitrite (NO_2^-), and *Nitrobacter* oxidizes nitrite to nitrate (NO_3^-, Galloway et al. 2003). During ammonia and nitrite oxidation, N_2O is produced and can later diffuses into the atmosphere (Figure 2).

Denitrification is the reduction of nitrate to N_2 through the intermediates of nitrite, nitric oxide (NO), and N_2O (Keith et al. 2001). This process occurs in soil aggregate micro-pores in the absence of oxygen (Wrage et al. 2001). N_2O is an intermediate of denitrification, which can be produced in high quantities in low-oxygen environments with sufficient nitrate and metabolizable organic carbon (Wrage et al. 2001). Denitrification reduces nitrate to nitrite in the presence of the enzyme nitrate reductase. Nitrite is reduced to nitric oxide by the enzyme nitrite reductase, and nitric oxide can then be reduced to N_2O by nitric oxide reductase (Figure 3, Wrage et al. 2001). The final step in the denitrification process is the reduction of N_2O to N_2 by N_2O reductase. N_2O can accumulate to high concentrations and not be further reduced to N_2 in environments with low pH (Rivett et al. 2008), high nitrate (Blackmer et al. 1978), and low organic carbon (Mathieu et al. 2006).

Soils are the major contributor to the global N_2O budget (IPCC 2007). N_2O emitted by soils can be produced during denitrification, which is anaerobic respiration, and during nitrification which is aerobic respiration (Figures 1, 2, 3). N_2O is increasing in the atmosphere and agriculture is the primary contributor (IPCC 2007). It is estimated that agriculture contributes 36.5% of the yearly anthropogenic nitrous oxide emissions (Isermann 1994). Nitrification and denitrification are associated with the application of fertilizer (ammonia or urea) on crop plants and lawns (Khalil et al. 2004).

Our research group quantified N_2O fluxes from corn fields treated with sludge (Figure 4). We sampled only once a day for an hour, and our field measurements indicate significant fluxes of N_2O from the soil to the atmosphere (Figure 5). My summer project investigated diurnal variations in N_2O fluxes from agricultural fields using the static chamber method to put once per day measurements into a daily perspective. The goal of this research was to help us understand the variations in N_2O flux out of the soil to the atmosphere.

I hypothesized that there are diurnal variations in N_2O fluxes from agricultural fields due to diurnal variations in soil temperature and soil moisture. Therefore, I expect to see variations

in the fluxes of N_2O from the soil over the course of the day and into the night. I expect that these variations will be caused by changes in soil temperature and soil water content influencing the processes of nitrification and denitrification. To test this hypothesis I will determine the variation in N_2O fluxes in an agricultural field over a 10 to 24 hour period.

Materials and Methods

Gas samples for analysis of N_2O were taken using replicate soil surface chambers (Figure 4). Chambers consist of a standard five gallon bucket cut to 28 cm high, a gamma seal lid, a vent port, and a Swagelok connector sealed with an Exetainer septa. The inside of the bottoms of the bucket are marked at 1 cm increments to determine the depth to which the chambers have been inserted into the ground.

I deployed two chambers on a fertilized corn field. I inserted the chambers 5 -7 cm into the soil using a hammer, and then I closed each chamber with its lid. At time zero, I took a gas sample, and additional samples were taken after 20, 40, and 60 minutes. I plotted the N_2O concentrations over time (Figure 5) and I used the slope of the line to calculate N_2O flux as described below.

To take gas samples from the chamber, I inserted a 30 mL syringe with the needle through the chamber lid septum. Prior to taking the sample, I mixed the chamber by pulling out and pushing back in 10 mL of chamber headspace three times. For the actual gas sample, I took 17 mL of air from the chamber. I removed the syringe from the chamber lid septum and ejected 2 mL of air into the atmosphere. I then injected the remaining 15 mL into the evacuated 12 mL Exetainer, over pressurizing the sample, which I analyzed in the laboratory on a gas chromatograph for N_2O content. While taking the samples, I recorded the air temperature and the time at which the sample was collected.

N_2O samples were analyzed using a gas chromatograph. Evacuated 12 mL Exetainer® tubes were used to store chamber headspace samples as described above. The concentration of N_2O within the Exetainer was determined on a Shimadzu GC-14B equipped with an electron capture detector (ECD) and a Porapak Q column. Matheson Tri-Gas standards and prepared gas mixtures were used along with a blank and an atmospheric air injection to create a standard curve.

N_2O fluxes from soil to the atmosphere were computed from changes in N_2O concentrations within each chamber, and the chamber volume and area. In the absence of N_2O fluxes from the soil, we anticipated no change in N_2O concentrations (C, μmol N_2O-N/L) within a chamber during the ~1 hour incubation (dC/dt = 0). We have observed several zero flux incubations prior to fertilization of the fields at Lewis Farm. However, in most cases following fertilization, we expected to obtain linear increases in N_2O concentrations during the 1 hour incubation (dC/dt > 0, μmol N_2O-N L^{-1} h^{-1}). Fluxes of N_2O from soil to the atmosphere (F, μmoles m^{-2} h^{-1}), were computed as:

$$F = \frac{dC}{dt} * \frac{V}{A} \quad (1)$$

where V = chamber volume (m^3) and A is chamber area (m^2). A and V were determined empirically for each chamber and are a function of insertion depth into the soil.
I used linear regression to find the slope of the line which is the rate of change in N_2O concentration inside the chamber over time.

Statistical Analysis

Diurnal flux differences were tested using SigmaPlot 11 to find the slope of the line, which is the rate of change in N_2O concentration inside the chamber. If the slope was not significant ($p>0.05$), I reported $dC/dt = 0$.

Results

N_2O fluxes were low to detectable in a fertilized corn field on July 5th, 2012 (Figure 7). Sampling took place over a 10 hour period starting at 10:22 am and ending at 7:47 pm. Replicate chambers were deployed less than 1 m apart, yet one chamber had both positive and negative fluxes while the other chamber did not have any flux. This shows the spatial variability in soil. The air temperature during sampling was high (35 to 45ºC), as was soil temp (30 to 32 ºC, Figure 8). Soil moisture was extremely low, approximately 8 %. No diurnal flux cycle was observed. In comparison with measurements made on May 3, 2012 after sludge application when the soil was cooler and moister, my flux measurements were much lower to flux measurements (Figure 7).

N_2O fluxes were not significant in a soybean field on July 24th, 2012 (Figure 9). Sampling took place over a 24 hour period starting at 6:47 am and ending at 3:47 am. Replicate chambers were deployed to measure the flux of N_2O from the soil into the atmosphere. The chambers were less than a 1 m apart, and I saw no N_2O fluxes in either chamber. The air temperature was high, approximately (27.2 to 27.9ºC), and the soil temperature was 23.2 to 24.2 ºC (Figure 10). In this field, the soil moisture was extremely dry and barely reached 8%. In comparison to the Fisher research group's April 3, 2012 result from the same soybean field during the spring with lower temperature and greater soil moisture, there were significant and larger N_2O fluxes.

Discussion

The N_2O fluxes from soil to the atmosphere in two agricultural fields in this study were not significant. There were minor N_2O fluxes from a corn field and no detectable fluxes from the soybean field. This differs from the Fisher research group's sampling results from a corn field on May 3, 2012, which had significant N_2O fluxes (Figure 5). The results obtained from this summer research were affected by many factors. One of the factors was ability of the soybean field to fix nitrogen. Another factor was the extremely dry summer, which led to the low soil moisture and high temperature. Decreases in soil moisture reduce N_2O production. It is suggested that the presence of oxygen in the soil repressed denitrifying bacteria production of N_2O (Knowles et al. 1982). Even in the presence of oxygen, denitrifying bacteria will be repressed from 40 min to 3 hour (Knowles et al. 1982). The presence of oxygen in the soil is important for nitrifying bacteria. These are bacteria that work best in the presence of oxygen to produce N_2O fluxes. However, by looking at the Fisher research group's results and other studies that have been done, it is likely that the reason why I could not find significant N_2O fluxes from these bacteria was because they were stressed by the low soil moisture content and high soil temperature. As for denitrifying bacteria, they work best in soil micro-pores where oxygen is absolutely absent; in this case, they were unable to produce any flux.

Temperature and percent water-filled space pore (WFPS) plays a critical role in the production of N_2O fluxes from an agricultural field. Microbial processes initiate in the soil between temperatures of 5 -12 ^oC with an increase in WFPS, but significant N_2O is produced from 0 - 5^oC at 88% WFPS after a rain fall which leads to denitrification (Dobbie et al. 2001).

Based on this, I assumed that the little N_2O flux I obtained from the corn field came from nitrification which does not require sufficient amount of rainfall, but requires oxygen. Significant increases in soil WFPS increase soil volume and soil respiration which could probably lead to denitrification (Dobbie et al. 2001).This help explains that in order to measure significant N_2O fluxes from an agricultural field, it is important for both temperature and WFPS to increase simultaneously for nitrification and denitrification to occur and produce significant N_2O fluxes. During my research, the WPFS was low, the soil temperature was between 23.2 to 32ºC, and soil moisture rarely reached 8 % with no rain fall. These conditions led to the lack of N_2O produced (Figure 9). In conclusion, it was difficult to find out the best time of the day where significant N_2O is released from the soil into the atmosphere because low significant fluxes were observed. Weather can interfere with best laid plans, which in this case low soil moistures, high soil temperature and high air temperature made me powerless to find the best time of the day during which significant amount of N_2O can diffuse out into the atmosphere.The scientific anticipated benefits of my project was to find if there is a best time of day at which to measure N_2O and to find that time of day that best represents the average daily flux. The social anticipated benefit was to understand the controls on N_2O fluxes from agricultural soils and to help farmers reduce N_2O inputs into the atmosphere. Unfortunately, due to dry, hot conditions, I was unable to obtain those benefits.

References

Blackmer, A.M., J.M. Bremner. 1978. Inhibitory effect of nitrate on reduction of N2O to N2 by soil microorganisms. Soil Biology and Biochemistry. 10:187-191.

Canfield E. D., A.N. Glazer, and P.G. Falkowski. 2010. The evolution of future of Earth's nitrogen cycle. Science. 330:192-196.

Isermann, K. 1994. Agriculture's share in the emission of trace gases affecting the climate and some cause-oriented proposals for sufficiently reducing this share. Environmental Pollution:95-111.

Smith, K., and K.E. Dobbie. The impact of sampling frequency and sampling times on chamber-based measurements of nitrous oxide emissions from fertilized soils. Global Change Biology 7:933-945.

Galloway, J.N., J.D. Aber, J.W. Erisman, S.P. Seitzinger, R.W. Howarth, E.B. Cowling, and B.J. Cosby. 2003. The nitrogen cascade. BioScience:341-356.

Intergovernmental Panel on Climate Change. 2007. Climate Change: The physical science basis.

Khalil, K., B. Mary, and P. Renault. 2004. Nitrous oxide production by nitrification and denitrification in soil aggregates as affected by oxygen concentration. Soil Biology and Biochemistry 36:687-699.

Mathieu, O., J. Lévêque, C. Hénault, M.-J.Milloux, F. Bizouard, and F. Andreux. 2006. Emissions and spatial variability of N2O, N2 and nitrous oxide mole fraction at the field scale, revealed with 15N isotopic techniques. Soil Biology and Biogeochemistry 38:941-951.

Rivett M.O., S.R. Buss, P. Morgan, J.W. Smith, and C.D. Bemment. 2008. Nitrate attenuation in groundwater: A review of biogeochemical controlling processes. Water Resources 42:4216-4232.

Sey, B.K., A.M. Manceur, J.K. Whalen, E.G. Gregorich, and P. Rochetter. 2008. Small-scale heterogeneity in carbon dioxide, nitrous oxide and methane production from aggregates of a cultivated sand-loam soil. Soil Biology and Biochemistry 40:2468-2473.

Wrage N., G.L. Velhof, M.L. van Beusichem, O. Oenema. 2001. Role of nitrifier denitrification in the production of nitrous oxide. Soil Biology and Biochemistry 33:1723-1732.

Figures and Tables

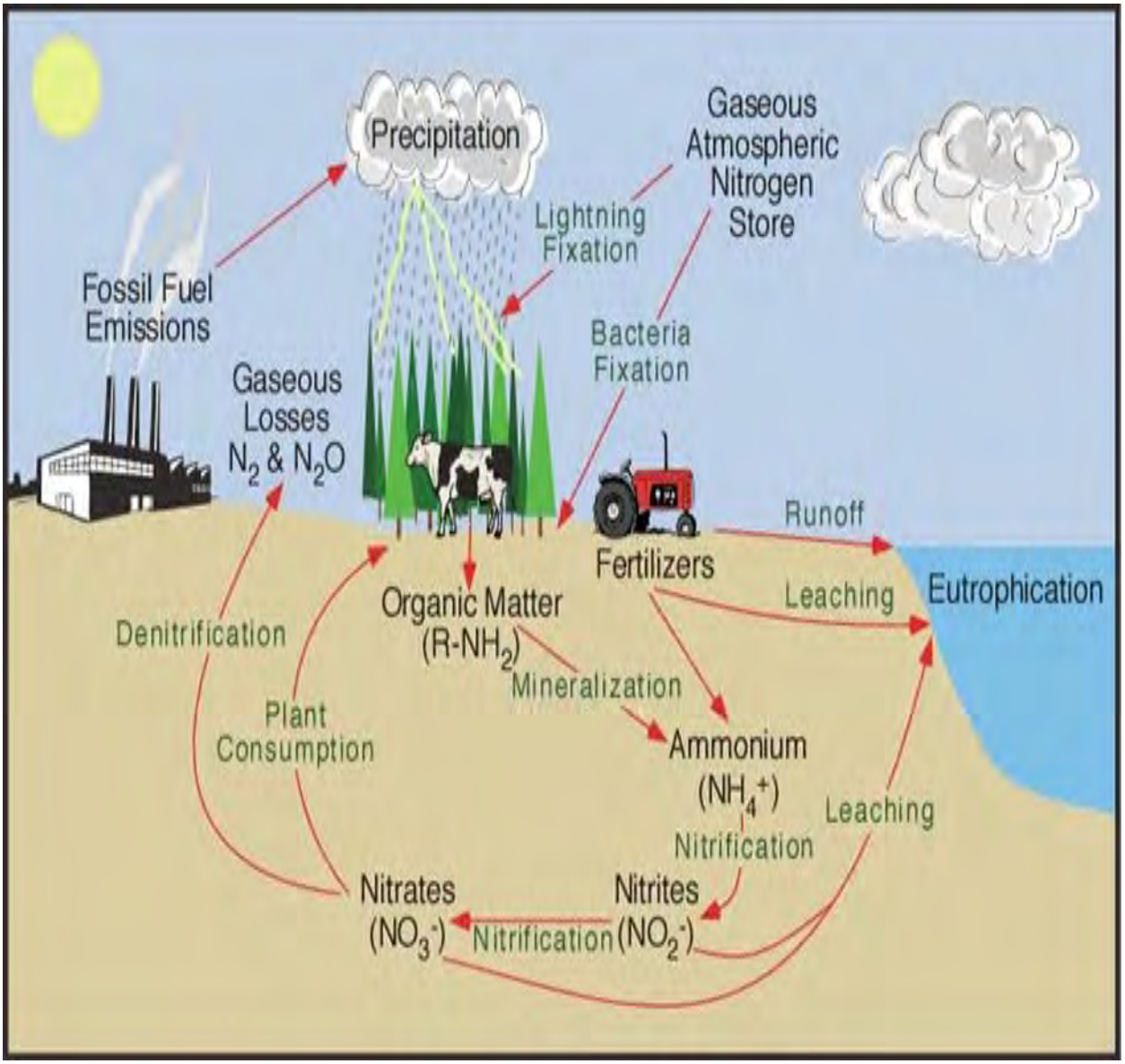

Figure 1. The nitrogen cycle (http://www.physicalgeography.net/fundamentals/9s.htm).

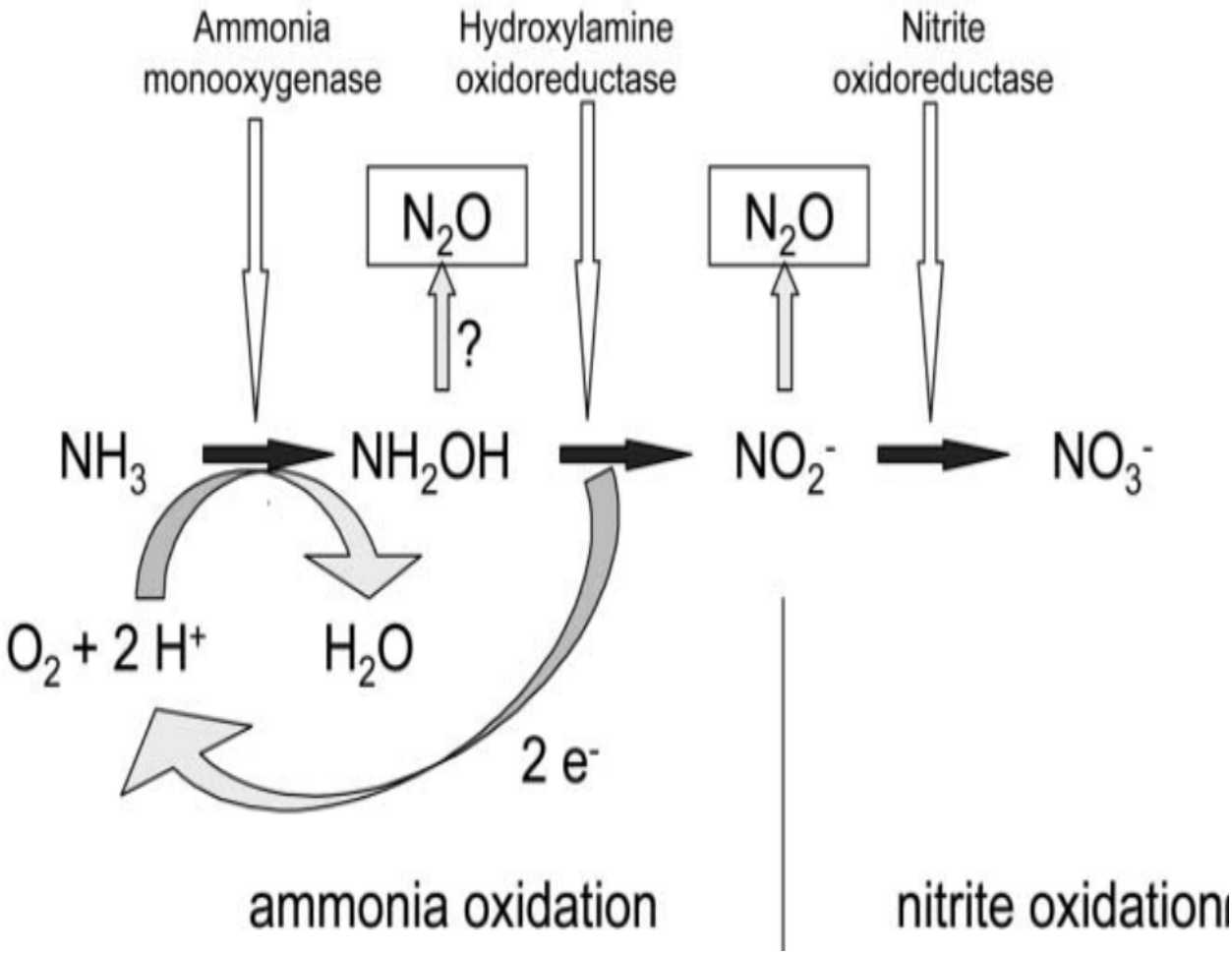

Figure 2. Nitrification - biological oxidation of ammonia to nitrate through the intermediates of hydroxylamine and nitrite (Wrage et al 2001).

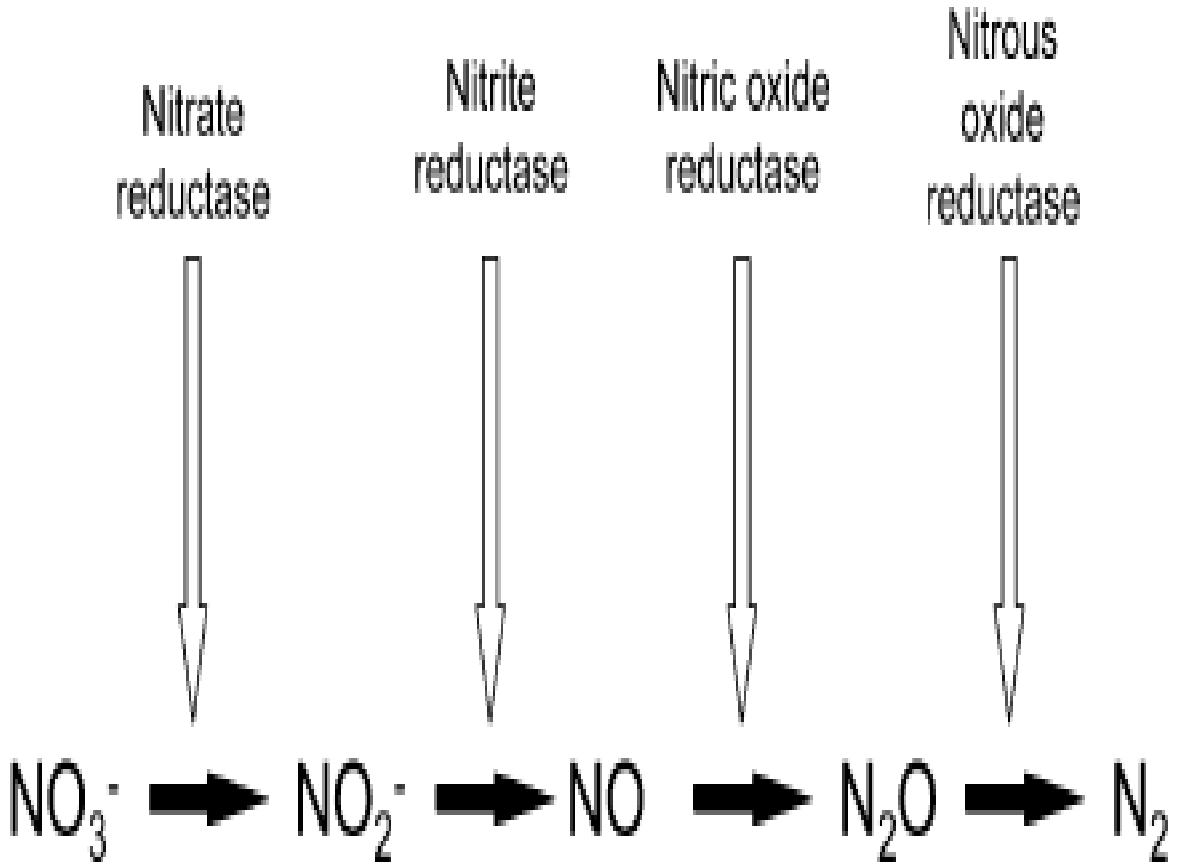

Figure 3. Denitrification- the reduction of nitrate to nitrogen gas through the intermediates of nitrite, nitric oxide, and nitrous oxide (Wrage et al. 2001).

Figure 4A. Deploying a soil surface chamber.

Figure 4B. Taking an atmospheric air sample.

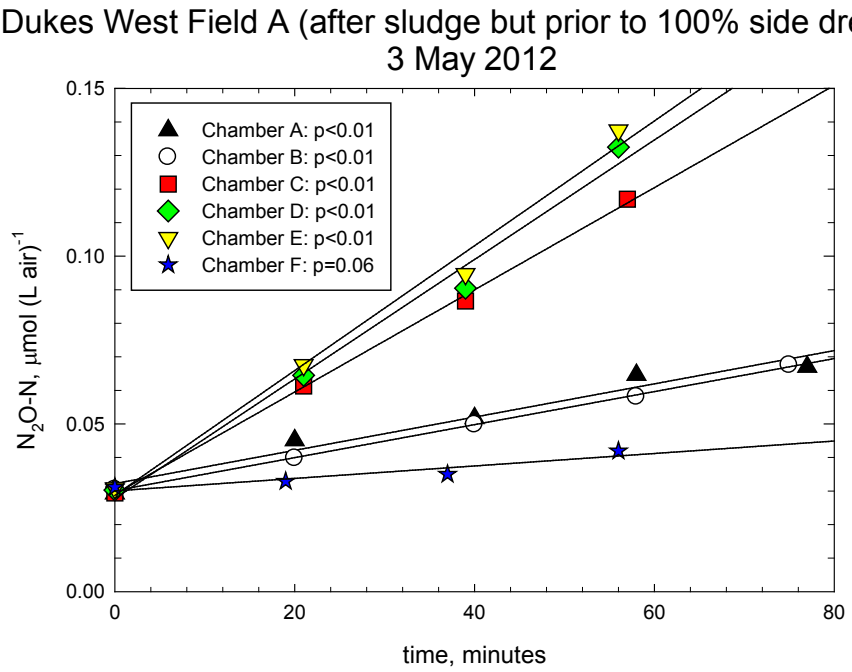

Figure 5. This is a preliminary data from Dr. Tom Fisher's research group. After sludge application, N_2O increases in time in the chamber headspace air, indicating a flux of N_2O from the soil to the atmosphere.

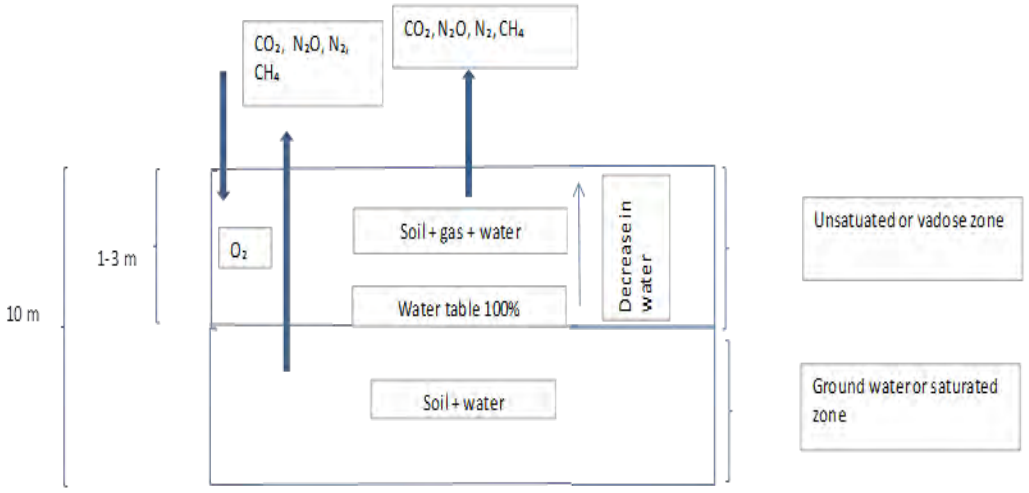

Figure 6. Carbon dioxide, nitrous oxide, nitrogen gas, and methane can flux from the unsaturated or vadose zone into the atmosphere. Carbon dioxide, nitrous oxide, nitrogen gas, and methane flux into the vadose zone from groundwater or the saturated zone. Water content increases through the vadose zone approaching the water table.

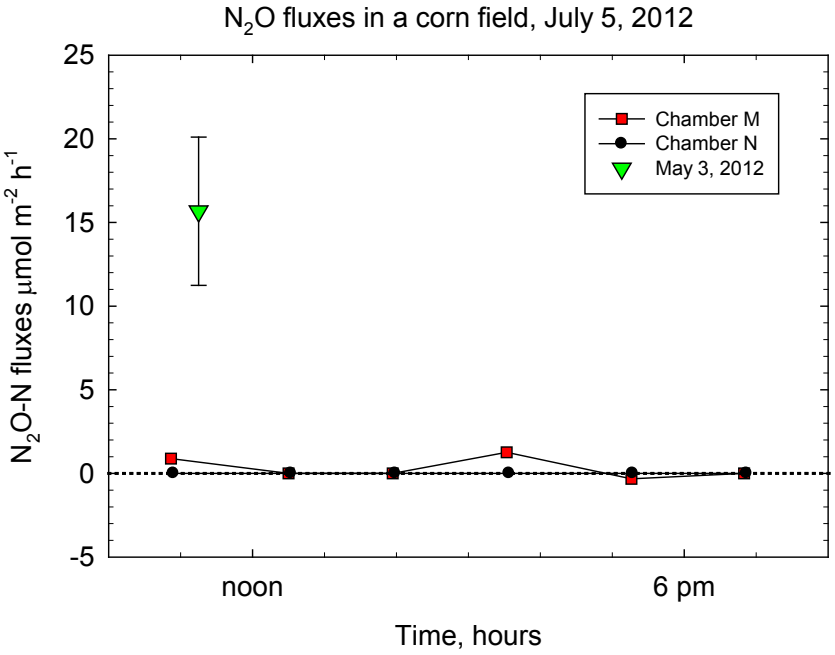

Figure 7. This graph shows the comparison between April 3, 2012 sampling of the fisher research group's and my July 24, 2012 10 hour sampling of nitrous oxide flux from a corn field.

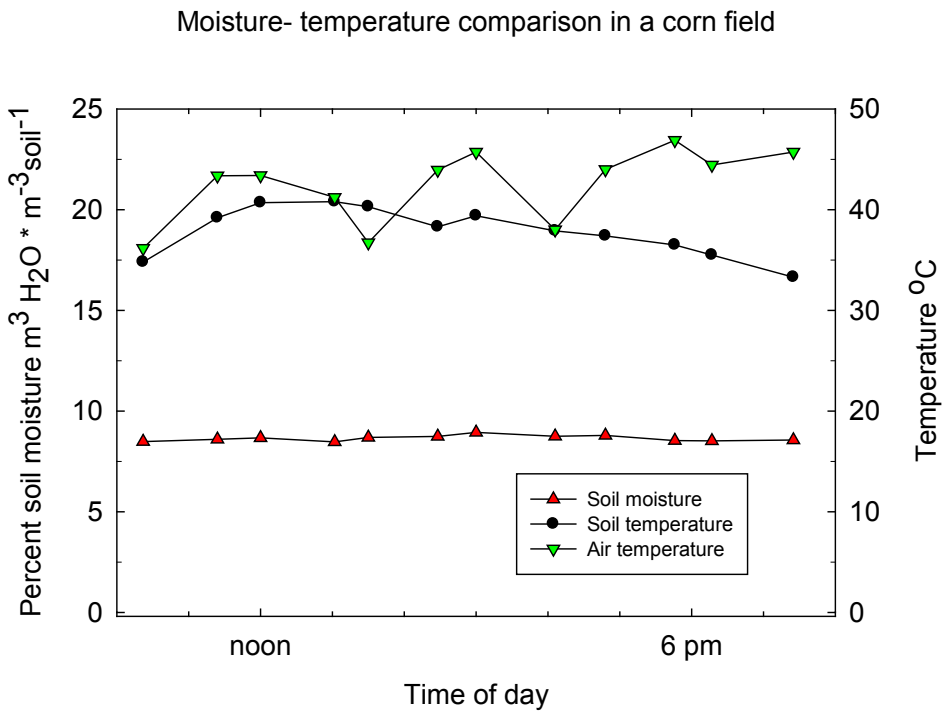

Figure 8. This graph shows my 10 hour sampling of percent moisture and temperature over time of day.

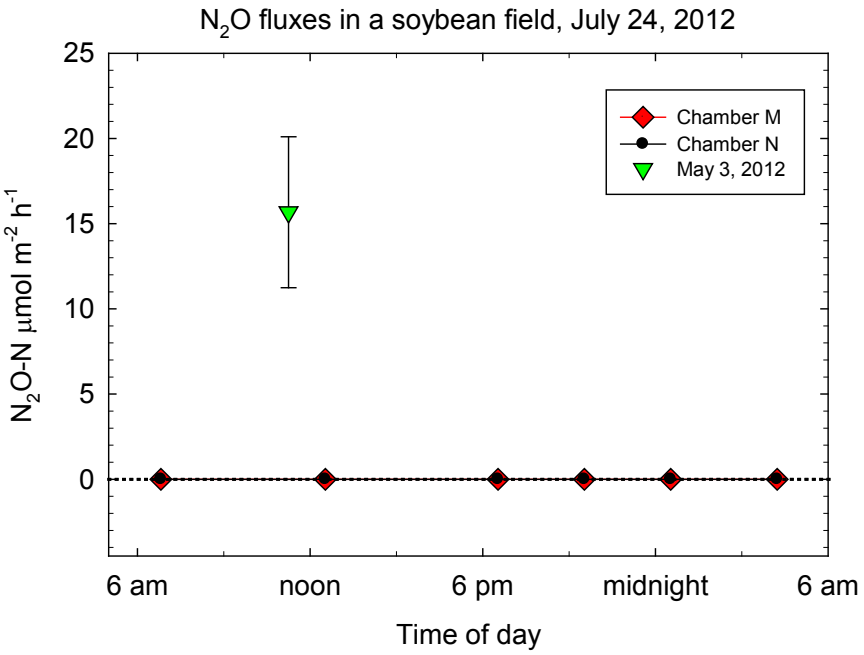

Figure 9. This graph shows the comparison between the Fisher research group's May 3, 2012 sampling from a soybean field and my July 24, 2012 24 hour sampling from a soybean field.

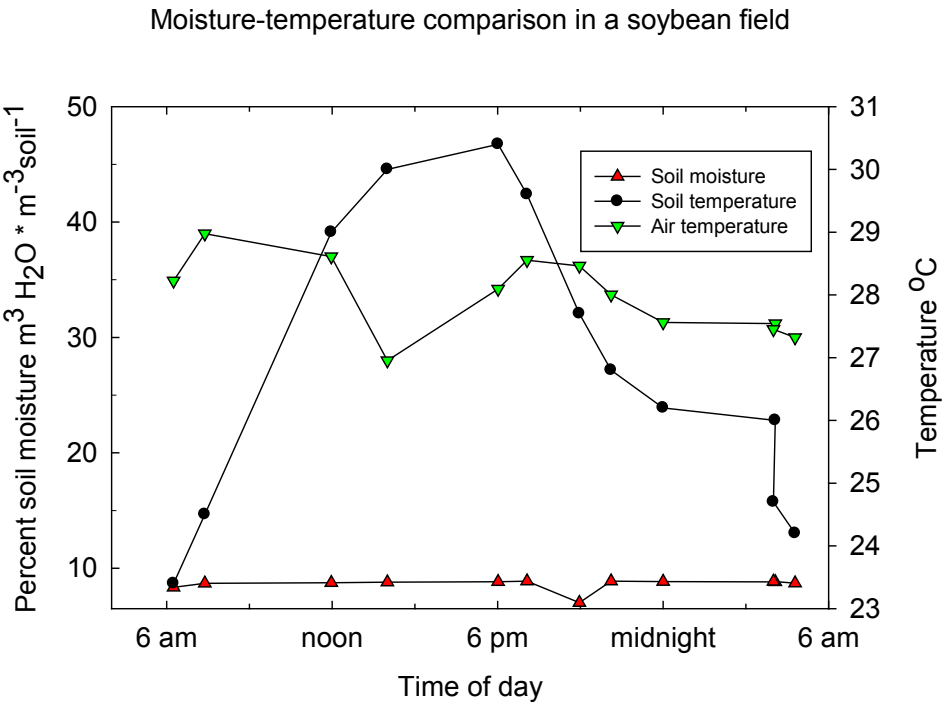

Figure 10. This graph shows the 24 hour sampling of percent moisture and temperature over time of the day.